PROGNOSTIC FACTORS AND NOVEL THERAPY IN UROTHELIAL CANCER

EDITED BY: Scott T. Tagawa and Sebastian Kobold
PUBLISHED IN: Frontiers in Oncology

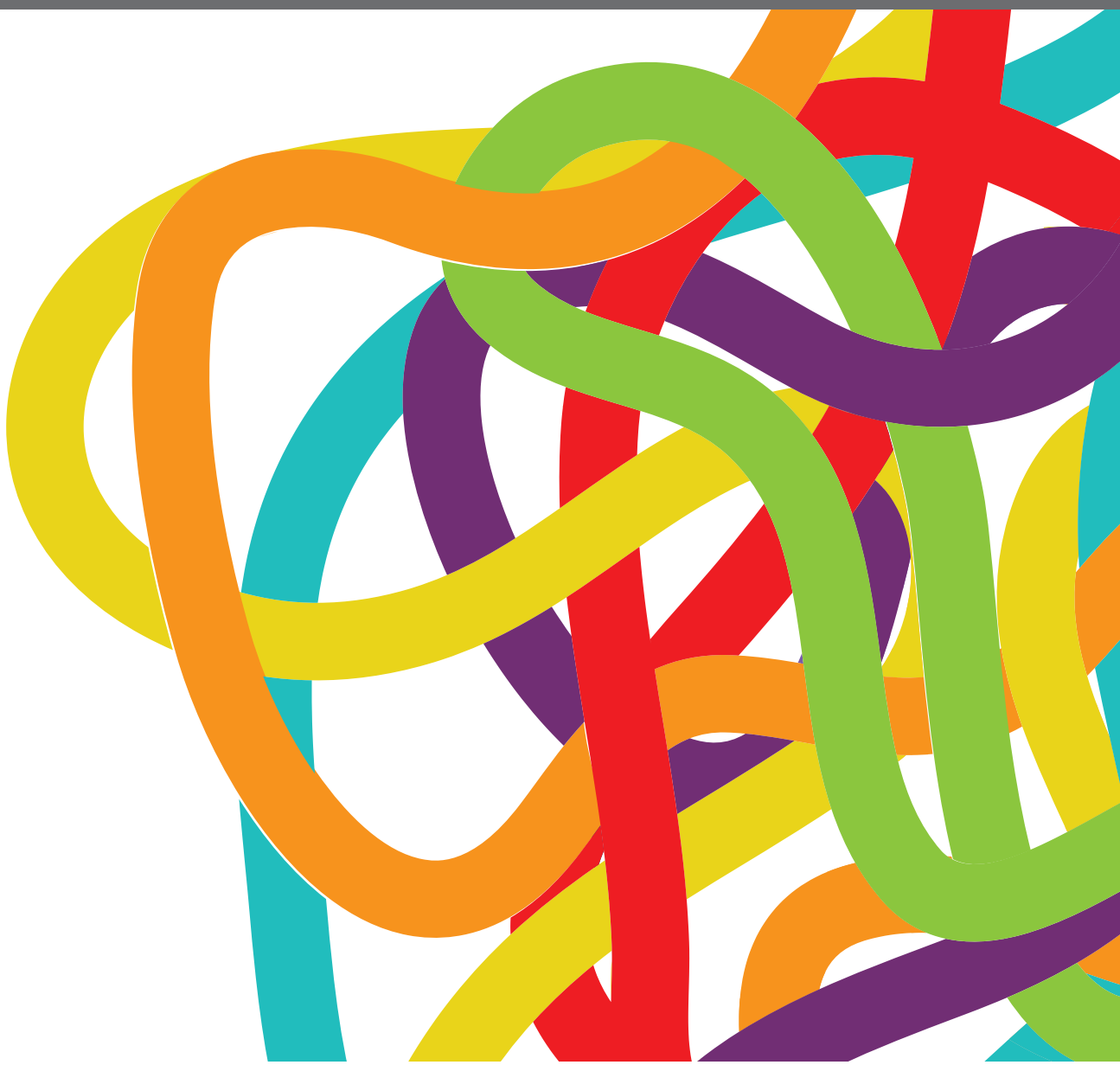

frontiers Research Topics

frontiers

ISSN 1664-8714
ISBN 978-2-88976-740-3
DOI 10.3389/978-2-88976-740-3

About Frontiers

Frontiers is more than just an open-access publisher of scholarly articles: it is a pioneering approach to the world of academia, radically improving the way scholarly research is managed. The grand vision of Frontiers is a world where all people have an equal opportunity to seek, share and generate knowledge. Frontiers provides immediate and permanent online open access to all its publications, but this alone is not enough to realize our grand goals.

Frontiers Journal Series

The Frontiers Journal Series is a multi-tier and interdisciplinary set of open-access, online journals, promising a paradigm shift from the current review, selection and dissemination processes in academic publishing. All Frontiers journals are driven by researchers for researchers; therefore, they constitute a service to the scholarly community. At the same time, the Frontiers Journal Series operates on a revolutionary invention, the tiered publishing system, initially addressing specific communities of scholars, and gradually climbing up to broader public understanding, thus serving the interests of the lay society, too.

Dedication to Quality

Each Frontiers article is a landmark of the highest quality, thanks to genuinely collaborative interactions between authors and review editors, who include some of the world's best academicians. Research must be certified by peers before entering a stream of knowledge that may eventually reach the public - and shape society; therefore, Frontiers only applies the most rigorous and unbiased reviews.
Frontiers revolutionizes research publishing by freely delivering the most outstanding research, evaluated with no bias from both the academic and social point of view. By applying the most advanced information technologies, Frontiers is catapulting scholarly publishing into a new generation.

What are Frontiers Research Topics?

Frontiers Research Topics are very popular trademarks of the Frontiers Journals Series: they are collections of at least ten articles, all centered on a particular subject. With their unique mix of varied contributions from Original Research to Review Articles, Frontiers Research Topics unify the most influential researchers, the latest key findings and historical advances in a hot research area! Find out more on how to host your own Frontiers Research Topic or contribute to one as an author by contacting the Frontiers Editorial Office: frontiersin.org/about/contact

PROGNOSTIC FACTORS AND NOVEL THERAPY IN UROTHELIAL CANCER

Topic Editors:
Scott T. Tagawa, Cornell University, United States
Sebastian Kobold, LMU Munich University Hospital, Germany

Citation: Tagawa, S. T., Kobold, S., eds. (2022). Prognostic Factors and Novel Therapy in Urothelial Cancer. Lausanne: Frontiers Media SA.
doi: 10.3389/978-2-88976-740-3

Table of Contents

05 ***The Prognostic Impact of Tumor Architecture for Upper Urinary Tract Urothelial Carcinoma: A Propensity Score-Weighted Analysis***
Hui-Ying Liu, Yen Ta Chen, Shun-Chen Huang, Hung-Jen Wang, Yuan-Tso Cheng, Chih Hsiung Kang, Wei Ching Lee, Yu-Li Su, Chun-Chieh Huang, Yin-Lun Chang, Yao-Chi Chuang, Hao Lun Luo and Po Hui Chiang

12 ***Case Report: Enfortumab Vedotin for Metastatic Urothelial Carcinoma: A Case Series on the Clinical and Histopathologic Spectrum of Adverse Cutaneous Reactions From Fatal Stevens-Johnson Syndrome/Toxic Epidermal Necrolysis to Dermal Hypersensitivity Reaction***
Paul V. Viscuse, Mario L. Marques-Piubelli, Meghan M. Heberton, Edwin Roger Parra, Amishi Y. Shah, Arlene Siefker-Radtke, Jianjun Gao, Sangeeta Goswami, Doina Ivan, Jonathan L. Curry and Matthew T. Campbell

20 ***Safety and Activity of Programmed Cell Death 1 Versus Programmed Cell Death Ligand 1 Inhibitors for Platinum-Resistant Urothelial Cancer: A Meta-Analysis of Published Clinical Trials***
Zaishang Li, Xueying Li, Wayne Lam, Yabing Cao, Hui Han, Xueqi Zhang, Jiequn Fang, Kefeng Xiao and Fangjian Zhou

30 ***Development of a Prognostic AI-Monitor for Metastatic Urothelial Cancer Patients Receiving Immunotherapy***
Stefano Trebeschi, Zuhir Bodalal, Nick van Dijk, Thierry N. Boellaard, Paul Apfaltrer, Teresa M. Tareco Bucho, Thi Dan Linh Nguyen-Kim, Michiel S. van der Heijden, Hugo J. W. L. Aerts and Regina G. H. Beets-Tan

42 ***FOXO3A Expression in Upper Tract Urothelial Carcinoma***
Guoyao Zhang, Wanping Shi, Enzhao Jia, Lei Zhang, Yongsheng Han, Ronald Rodriguez and Tianjiang Ma

49 ***Body Composition Parameters May Be Prognostic Factors in Upper Urinary Tract Urothelial Carcinoma Treated by Radical Nephroureterectomy***
Yulong Pan, Zeyu Chen, Lanqing Yang, Xingyuan Wang, Zeng Yi, Liang Zhou, Yongjiang Chen, Lu Yang, Hui Zhuo, Yige Bao and Qiang Wei

56 ***Impact of Androgen Suppression Therapy on the Risk and Prognosis of Bladder Cancer: A Systematic Review and Meta-Analysis***
Peng Xiang, Zhen Du, Yongxiu Hao, Di Guan, Dan Liu, Wei Yan, Mingdong Wang, Yutong Liu and Hao Ping

66 ***Identification of a Novel Tumor Microenvironment Prognostic Signature for Bladder Urothelial Carcinoma***
Chaojie Xu, Dongchen Pei, Yi Liu, Yang Yu, Jinhua Guo, Nan Liu and Zhengjun Kang

80 ***High Stromal SFRP2 Expression in Urothelial Carcinoma Confers an Unfavorable Prognosis***

Hong-Yue Lai, Chia-Chun Chiu, Yu-Hsuan Kuo, Hsin-Hwa Tsai, Li-Ching Wu, Wen-Hsin Tseng, Chien-Liang Liu, Chung-Hsi Hsing, Steven K. Huang and Chien-Feng Li

96 ***Preoperative Metabolic Syndrome and HDL-C Level Predict the Prognosis of Patients Following Radical Cystectomy: A Propensity Score Matching Study***

Zenan Liu, Hai Bi, Wei He, Xuehua Zhu, Jide He, Min Lu and Jian Lu

frontiers in Oncology

ORIGINAL RESEARCH
published: 25 February 2021
doi: 10.3389/fonc.2021.613696

The Prognostic Impact of Tumor Architecture for Upper Urinary Tract Urothelial Carcinoma: A Propensity Score-Weighted Analysis

Hui-Ying Liu[1], Yen Ta Chen[1], Shun-Chen Huang[2], Hung-Jen Wang[1], Yuan-Tso Cheng[1], Chih Hsiung Kang[1], Wei Ching Lee[1], Yu-Li Su[3], Chun-Chieh Huang[4], Yin-Lun Chang[1], Yao-Chi Chuang[1], Hao Lun Luo[1] and Po Hui Chiang[1]*

[1] Department of Urology, Kaohsiung Chang Gung Memorial Hospital and Chang Gung University College of Medicine, Kaohsiung, Taiwan, [2] Department of Pathology, Kaohsiung Chang Gung Memorial Hospital and Chang Gung University College of Medicine, Kaohsiung, Taiwan, [3] Department of Hematology and Oncology, Kaohsiung Chang Gung Memorial Hospital and Chang Gung University College of Medicine, Kaohsiung, Taiwan, [4] Department of Radiation Oncology, Kaohsiung Chang Gung Memorial Hospital and Chang Gung University College of Medicine, Kaohsiung, Taiwan

OPEN ACCESS

Edited by:
Marco Borghesi, University of Genoa, Italy

Reviewed by:
Ahmet Murat Aydin, Moffitt Cancer Center, United States
Julia Heinzelbecker, Saarland University Hospital, Germany

***Correspondence:**
Hao Lun Luo
alesy1980@gmail.com

Specialty section:
This article was submitted to Genitourinary Oncology, a section of the journal Frontiers in Oncology

Received: *03 October 2020*
Accepted: *04 January 2021*
Published: *25 February 2021*

Citation:
Liu H-Y, Chen YT, Huang S-C, Wang H-J, Cheng Y-T, Kang CH, Lee WC, Su Y-L, Huang C-C, Chang Y-L, Chuang Y-C, Luo HL and Chiang PH (2021) The Prognostic Impact of Tumor Architecture for Upper Urinary Tract Urothelial Carcinoma: A Propensity Score-Weighted Analysis. Front. Oncol. 11:613696. doi: 10.3389/fonc.2021.613696

Purpose: To assess the association of tumor architecture with cancer recurrence, metastasis, and cancer-specific survival (CSS) in patients treated with radical nephroureterectomy (RNU) for upper urinary tract urothelial carcinoma (UTUC) in Taiwan.

Materials and Methods: Data were collected from 857 patients treated with RNU between January 2005 and August 2016 in our hospital. Pathologic slides were reviewed by genitourinary pathologists. Propensity score weighting was performed for data analysis.

Results: Sessile growth pattern was observed in 212 patients (24.7%). Tumor architecture exhibited a significant association with bladder cancer history, chronic kidney disease (CKD), tumor stage, lymph node status, histological grade, lymphovascular invasion, concomitant carcinoma *in situ*, and the variant type [standardized mean difference (SMD) > 0.1 for all variables before weighting]. In the propensity score analysis, 424 papillary and sessile tumor architecture were analyzed to balance the baseline characteristics between the groups. Tumor architecture was an independent predictor of metastatic disease and CSS ($p = 0.033$ and $p = 0.002$, respectively). However, the associations of tumor architecture with bladder and contralateral recurrence were nonsignificant ($p = 0.956$ and $p = 0.844$, respectively).

Conclusions: Tumor architecture of UTUC after RNU is associated with established features of aggressive disease and predictors of metastasis and CSS. Assessment of tumor architecture may help identify patients who could benefit from close follow-up or early administration of systemic therapy after RNU. Tumor architecture should be included in UTUC staging after further confirmation.

Keywords: tumor architecture, papillary, sessile, upper urinary tract urothelial carcinoma, metastasis, cancer-specific survival

INTRODUCTION

Upper urinary tract urothelial carcinoma (UTUC), referred to as renal pelvic and ureteral tumors, comprises approximately 5% of all urothelial tumors and 10% of renal tumors (1–7). The incidence and biological behaviour of UTUC vary across ethnicities and geographic areas (8). Based on the Surveillance, Epidemiology and End Results database, the incidence of UTUC in the United States has been reported as low as 2.06 cases per 100,000 person-years (7). However, the incidence and disease presentation of UTUCs in the Asian population, particularly in Taiwan, differ from those in the Western population (9–12). First, UTUC accounts for 20%–30% of urothelial tumors and is more common in Asian than in Western populations (9, 12). Second, a high prevalence of non-organ confined (43%) and high-grade (82%) disease in Asiatic patients has been reported (10, 11). Third, UTUCs are more common in female than in male patients (9, 12, 13). Finally, in Asian countries, female patients with UTUC are less likely to develop late stage, large-sized tumor, and lymph node metastasis (LNM) than male patients, whereas this difference is not observed in Western countries (9).

Radical nephroureterectomy (RNU) with bladder cuff excision is the standard treatment for UTUC (1–7). For patients at high risk of treatment failure with RNU alone, adjuvant therapies are reasonable (6, 14). Of the total number of patients with UTUC, a substantial proportion of patients experience disease recurrence and 20%–55% may develop metastases and subsequently die from the disease (3, 6). The disease stage is the most important prognostic factor for UTUC (4). Identification of the clinical stage and prognosis are essential for accurate assessment and clinical decision-making for patients (1, 6).

Tumor stage, histologic grade, and LNM are the well-established and significant prognostic factors (1–3, 9). Several studies have evaluated the possible predictive factors for cancer recurrence and survival after RNU (1, 2, 6). The oncologic significance of other potentially relevant variables, such as tumor architecture, tumor site, tumor necrosis, lymphovascular invasion (LVI), and concomitant carcinoma *in situ* (CIS) remain to be confirmed (2, 6). The role of adjuvant chemotherapy was considered a new standard of care for patients with locally advanced UTUC to improve outcome (14). The sessile tumor architecture has been reported to be a predictor of poor outcomes in patients with bladder urothelial carcinoma (UC), and several studies have also investigated the significance of tumor architecture in patients with UTUC (3, 5, 6). Recognising these limitations, we report a large series from Taiwan, an endemic area of UTUC, to assess whether tumor architecture could be a valuable parameter for refining the prognosis of patients with UTUC.

MATERIALS AND METHODS

Study Population

Between January 2005 and December 2016, a total of 1,077 patients with localized upper urinary tract cancer were administered surgical intervention at our institution. Of the total, we excluded 178 patients who underwent nephron-sparing surgery and 42 patients with non-UC histology. Overall, we included 857 patients who underwent nephroureterectomy with bladder cuff excision at our institution to assess the prognostic significance of tumor architecture in the clinical course of localized UT-UC. All enrolled patients underwent cystoscopy or computed tomography (CT) to preoperatively observe the presence of concurrent bladder disease or distant metastasis. We performed lymph node dissection only when lymph node was larger than 1cm from pre-operative imaging or suspicious lesions during operation. The percentage of negative lymph nodes was defined as negative pathological findings after lymph node dissection or patient did not underwent lymph node dissection, which was 85.1% in the papillary tumor architecture group and 75.5% in the sessile tumor architecture group. Perioperative data, such as age, sex, smoking history, and bladder cancer history, were obtained through chart review. This study was approved by the Institutional Review Board of Kaohsiung Chang Gung Memorial Medical Center (IRB number: 202000185B0).

Pathological Evaluation

UC was histologically confirmed in all specimens, and specimens with variant histology were also included in this study. Genitourinary pathologists, who were blinded to the clinical outcomes, reviewed all slides according to identical strict criteria. Tumors were staged according to the American Joint Committee on Cancer tumor–node–metastasis (TNM) classification. Tumor grading was assessed according to the 2004 and 2016 World Health Organisation/International Society of Urologic Pathology consensus classification (15–18). Tumor architecture was defined by a uropathologist at our institution based on the predominant feature (3, 19). Tumor stage, architecture, grade, necrosis, and concomitant CIS were also assessed in every representative slide.

Follow-Up Protocol and Definition of Oncological Event

Our institutional follow-up protocol included postoperative cystoscopy every 3 months. CT was performed annually to assess lymph node status and local or regional recurrence of the tumor. Elective bone scans, chest CT, and magnetic resonance imaging were performed when clinically indicated. Metastasis was defined as local failure in the operative site or regional lymph nodes or distant metastasis. Bladder and contralateral recurrences were considered separately in the analysis of recurrence-free survival. Treating physicians determined the cause of death by using chart review or by inspecting death certificates. Cancer-specific death was defined as death event due to concurrent UC metastases or progressive disease.

Statistical Analysis

Descriptive statistical analysis results of continuous variables were reported as mean and standard deviation, and data for categorical variables in the study cohort were summarized as n (%). To address systematic differences between sessile and papillary groups (i.e., the confounding baseline parameter factor), we applied the average treatment effect for the treated (ATT) units weighting analysis (also called weighting by odds).

ATT, a form of propensity-score analysis, can be used in outcome analysis to estimate the average treatment effect for the treated units (individuals who actually received the treatment) by weighting the control group to the treated group. The propensity

score was calculated using logistic regression to model the tumor architecture in the baseline period by age at index date, sex, bladder cancer history, tumor location, chronic kidney disease (CKD) group, cancer stage, lymph node status, histology grade, lymphovascular invasion, CIS, tumor necrosis, variant type, and perioperative chemotherapy.

The algorithm combined weighted estimates across several parametric and nonparametric prediction modelling approaches based on the accuracy of predictions from the models to create an overall propensity score estimate, which increased the robustness of the analysis. Postweighting balance in covariates between treatment groups was evaluated using the standardised mean difference (SMD) approach. Imbalance was defined as a standardised mean difference (SMD) of >0.1.

Kaplan–Meier curves and log-rank tests were used to compare metastasis-free survival (MFS), cancer-specific survival (CSS), bladder recurrence-free survival, and contralateral recurrence-free survival between two tumor architecture groups with and without ATT weighting. All statistical tests were two-tailed and conducted at 5% significance level by using R version 3.6.3 and the IPW survival, tableone, survey, and hrIPW packages.

RESULTS

Association of Tumor Architecture With Clinical and Pathologic Characteristics

Table 1 shows the association of tumor architecture with clinical and pathologic characteristics before and after propensity score

TABLE 1 | Association of tumor architecture with clinical and pathologic characteristics in patients treated with radical nephroureterectomy for upper tract urothelial carcinoma before and after propensity-score analysis.

Characteristic	Before Weighting			After Weighting		
	Papillary (n = 645)	Sessile (n = 212)	SMD	Papillary (n = 212)	Sessile (n = 212)	SMD
Follow-up, month, [mean(SD)]	47.10 (35.19)	39.34 (35.31)				
Age, [mean (SD)]	66.80 (10.84)	67.18 (9.81)	0.036	66.89 (10.45)	67.18 (9.81)	0.028
Gender, n (%)			0.038			0.040
Men	295 (45.7%)	101 (47.6%)		105 (49.6%)	101 (47.6%)	
Women	350 (54.3%)	111 (52.4%)		107 (50.4%)	111 (52.4%)	
Bladder cancer history, n (%)			0.134			0.026
Negative	468 (72.6%)	166 (78.3%)		168 (79.4%)	166 (78.3%)	
Positive	177 (27.4%)	46 (21.7%)		44 (20.6%)	46 (21.7%)	
Cancer location, n (%)			0.049			0.003
Multifocal	175 (27.1%)	53 (25.0%)		53 (24.9%)	53 (25.0%)	
Unifocal	470 (72.9%)	159 (75.0%)		159 (75.1%)	159 (75.0%)	
CKD Group, n (%)			0.244			0.079
Stage 1	53 (8.2%)	20 (9.4%)		20 (9.6%)	20 (9.4%)	
Stage 2	147 (22.8%)	62 (29.2%)		68 (32.3%)	62 (29.2%)	
Stage 3	225 (34.9%)	80 (37.7%)		73 (34.4%)	80 (37.7%)	
Stage 4	72 (11.2%)	17 (8.0%)		18 (8.3%)	17 (8.0%)	
Stage 5	148 (22.9%)	33 (15.6%)		33 (15.4%)	33 (15.6%)	
Stage, n (%)			0.742			0.001
Localized	486 (75.3%)	87 (41.0%)		87 (41.0%)	87 (41.0%)	
Locally advanced	159 (24.7%)	125 (59.0%)		125 (59.0%)	125 (59.0%)	
LN status, n (%)			0.240			0.008
Negative	624 (96.7%)	193 (91.0%)		192 (90.8%)	193 (91.0%)	
Positive	21 (3.3%)	19 (9.0%)		20 (9.2%)	19 (9.0%)	
Histological grade, n (%)			0.250			0.006
Low	65 (10.1%)	8 (3.8%)		8 (3.7%)	8 (3.8%)	
High	580 (89.9%)	204 (96.2%)		204 (96.3%)	204 (96.2%)	
LVI, n (%)			0.522			0.027
Negative	529 (82.0%)	125 (59.0%)		128 (60.3%)	125 (59.0%)	
Positive	116 (18.0%)	87 (41.0%)		84 (39.7%)	87 (41.0%)	
Concomitant CIS, n (%)			0.149			0.007
Negative	403 (62.5%)	117 (55.2%)		116 (54.8%)	117 (55.2%)	
Positive	242 (37.5%)	95 (44.8%)		96 (45.2%)	95 (44.8%)	
Tumor necrosis, n (%)			0.055			0.001
Negative	409 (63.4%)	140 (66.0%)		140 (66.0%)	140 (66.0%)	
Positive	236 (36.6%)	72 (34.0%)		72 (34.0%)	72 (34.0%)	
Variant type, n (%)			0.128			0.038
Negative	435 (67.4%)	130 (61.3%)		126 (59.5%)	130 (61.3%)	
Positive	210 (32.6%)	82 (38.7%)		86 (40.5%)	82 (38.7%)	
Periop CT (ACT+NCT), n (%)			0.392			0.029
Negative	613 (95.0%)	176 (83.0%)		178 (84.1%)	176 (83.0%)	
Positive	32 (5.0%)	36 (17.0%)		34 (15.9%)	36 (17.0%)	

SMD, standardized mean difference; SD, standard deviation; CKD, chronic kidney disease; LN, lymph node; LVI, lymphovascular invasion; CIS, carcinoma in situ; CT, chemotherapy; ACT, adjuvant chemotherapy; NCT, neoadjuvant chemotherapy.

matching (PSM). Of 857 patients, sessile and papillary growth patterns were present in 212 (24.7%) and 645 (75.3%) patients, respectively. The mean follow-up period of sessile group and papillary group was 39.34 ± 35.31 months and 47.10 ± 35.19 months, respectively. Tumor architecture exhibited significant association with bladder cancer history, CKD group, tumor stage, lymph node status, histological grade, LVI, concomitant CIS, and variant type (SMD > 0.1 for all variables before weighting). In total, 32 (5.0%) patients with papillary growth pattern and 36 (17.0%) patients with sessile growth pattern had received either neoadjuvant or adjuvant perioperative chemotherapy. In the propensity score analysis, 424 papillary and sessile tumor architecture were analysed. The baseline characteristics in the weighted groups were well balanced.

Association of Tumor Architecture With Clinical Outcomes

Bladder Recurrence

Bladder and contralateral recurrences were considered separately for analysing the recurrence-free survival rate. The overall 2-, 5-, and 10-year bladder recurrence-free survival estimates in the papillary tumor architecture group were 76.6% (± 3.1%), 70.0% (± 3.9%), and 65.5% (± 5.4%), respectively. Similarly, the overall 2-, 5-, and 10-year estimates for bladder recurrence-free survival in the sessile tumor architecture group were 75.7% (± 3.2%), 71.7% (± 3.9%), and 61.1% (± 6.9%), respectively. No significant difference in bladder recurrence-free survival rate between the groups was found either after weighting (weighted log-rank test, p = 0.956, **Figure 1**) or before weighting (unweighted log-rank test, p = 0.353, **Supplement 1**).

Contralateral Recurrence

The overall 2-, 5-, and 10-year contralateral recurrence-free survival estimates in the papillary tumor architecture group were 97.2% (± 1.3%), 90.2% (± 3.0%), and 75.5% (± 8.8%), respectively. By contrast, the overall 2-, 5-, and 10-year contralateral recurrence-free survival estimates in the sessile tumor architecture group were 96.5% (± 1.4%), 90.9% (± 3.2%), and 83.6% (± 6.0%), respectively. No significant difference in contralateral recurrence-free survival rate between the groups was found (weighted log-rank test, p = 0.844, **Figure 2**). The difference between the groups before weighting was also nonsignificant (unweighted log-rank test, p = 0.453, **Supplement 2**).

Metastasis

The overall 2-, 5-, and 10-year MFS estimates in the papillary tumor architecture group were 68.1% (± 3.3%), 63.3% (± 3.7%), and 62.5% (± 3.8%), respectively. Nevertheless, the overall estimates in the sessile tumor architecture group at 2, 5, and 10 year were 63.0% (± 3.5%), 56.3% (± 3.9%), and 49.7% (± 5.0%), respectively. **Figure 3** demonstrates ATT weighted Kaplan–Meier estimates of MFS stratified by tumor architecture. The MFS rate was significantly lower in the sessile tumor architecture group both after (weighted log-rank test, p = 0.033) and before weighting (unweighted log-rank test, p < 0.001, **Supplement 3**).

Cancer-Specific Survival

The overall CSS estimates at 2, 5, and 10 years in the papillary tumor architecture group were 85.1% (± 2.6%), 73.9% (± 3.7%), and 71.7% (± 4.1%), respectively. Nevertheless, the overall estimates at 2, 5, and 10 years in the sessile tumor architecture group were 78.4% (± 3.0%), 63.6% (± 4.2%), and 58.0% (± 5.4%), respectively.

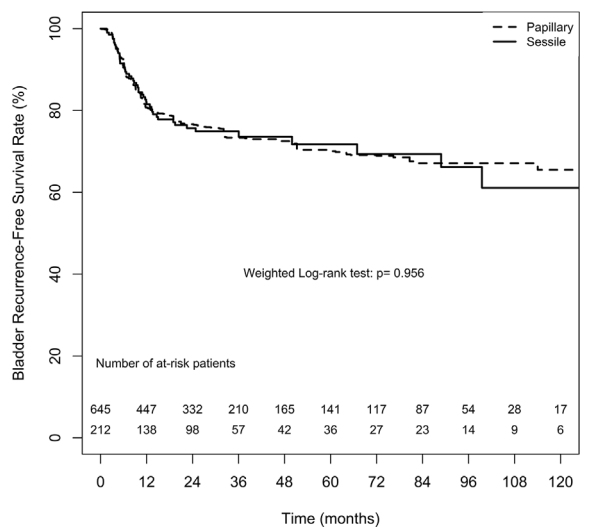

FIGURE 1 | Average treatment effect for the treated (ATT) weighting Kaplan-Meier estimates for bladder recurrence-free survival rate. Numbers along x axis are the numbers of patients remaining in the risk set at each time point.

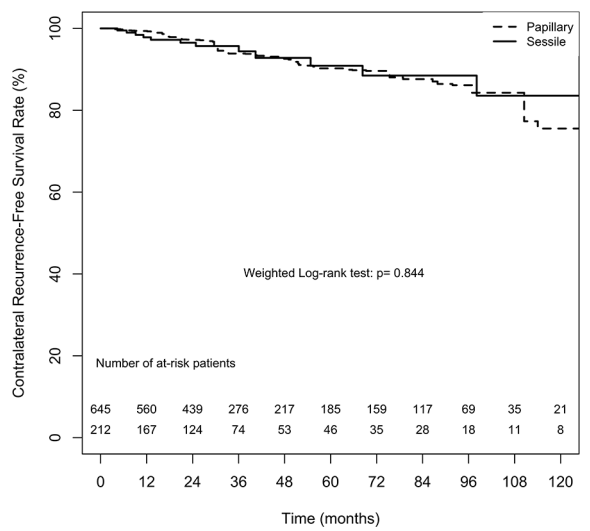

FIGURE 2 | Average treatment effect for the treated (ATT) weighting Kaplan-Meier estimates for contralateral recurrence-free survival rate. Numbers along x axis are the numbers of patients remaining in the risk set at each time point.

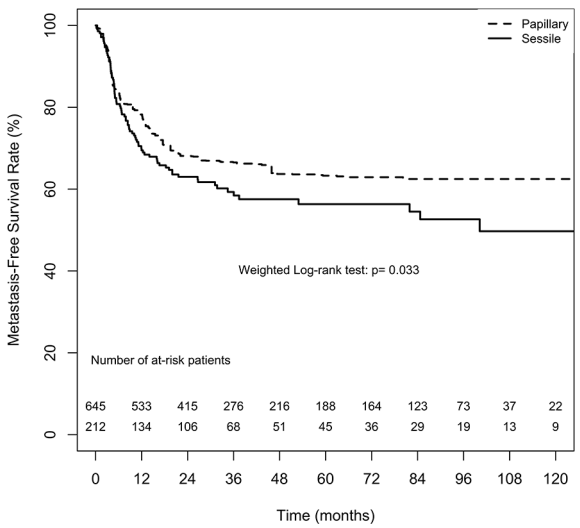

FIGURE 3 | Average treatment effect for the treated (ATT) weighting Kaplan-Meier estimates for metastasis-free survival rate. Numbers along x axis are the numbers of patients remaining in the risk set at each time point.

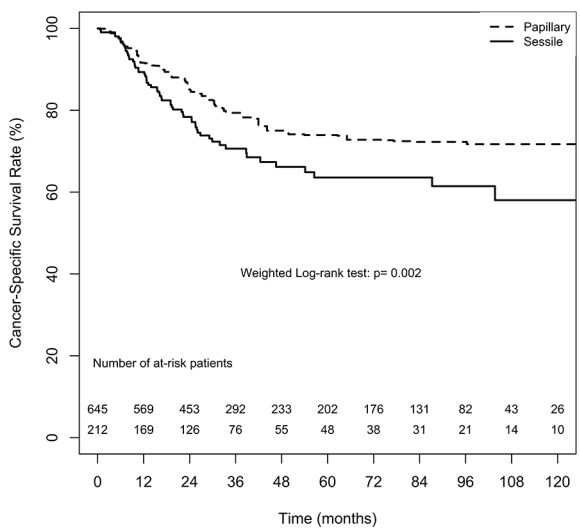

FIGURE 4 | Average treatment effect for the treated (ATT) weighting Kaplan-Meier estimates for cancer-specific survival. Numbers along x axis are the numbers of patients remaining in the risk set at each time point.

Figure 4 demonstrates ATT weighted Kaplan–Meier estimates of CSS stratified by tumor architecture. The survival rate was significantly lower in the sessile tumor architecture group (weighted log-rank test, $p = 0.002$). Additionally, the CSS rate was significantly lower in the sessile tumor architecture group before weighting (unweighted log-rank test, $p < 0.001$, **Supplement 4**).

DISCUSSION

First, this retrospective study supports the role of radical surgery for patients with localized UTUC. In our study, the 5-year bladder recurrence-free survival rate was 70% and 71.7% in papillary and sessile tumor architecture groups, respectively. The 5-year CSS rates in the papillary and sessile groups were 73.9% and 63.6%, respectively. Oncologic outcomes reported in our study were similar to those reported in other studies. In these studies, the recurrence rates in the bladder varied from 15% to 50% (20), and the 5-year CSS after RNU conducted in a 3-single-centre series ranged between 61% and 76% (2). Nevertheless, some patients experienced metastasis and cancer-related deaths after RNU. Therefore, we attempted to identify predictive factors for adverse outcomes and further develop the optimal therapeutic options.

The present study demonstrated that factors associated with the probability of tumor recurrence and death among patients with UTUC include pathological stage, histological grade, tumor architecture, lymphovascular invasion (LVI), and lymph node status (2, 3, 8, 9, 21). Additionally, neoadjuvant or adjuvant chemotherapy may influence the survival rate in this group of patients (2, 14). Consistent with previous studies, our data indicate the association of sessile tumor architecture with established features of biologically aggressive UTUC, such as advanced stage, high tumor grade, metastases to lymph nodes, and LVI (3, 5, 9). We also found a correlation of tumor architecture with bladder cancer history, CKD group, concomitant CIS, and the variant type. Notably, sessile tumor architecture was found to be associated with poor prognosis (3, 9, 22). We used propensity score weighting by ATT method to minimize the effect of confounding variables between two tumor architecture groups to precisely interpret the outcomes.

Approximately 24.7% of patients in our series exhibited sessile tumor growth pattern, whereas sessile architecture have been reported in 20%–28% of patients treated with RNU in other studies (2, 5). The rate of recurrence in the bladder after primary UTUC treatment has been reported to be 15%–50% (20). However, results indicating the association of tumor growth pattern with tumor recurrence are controversial. Some studies have concluded that tumor architecture is independently associated with disease recurrence (2–4, 23). Fan et al. reported a significantly lower recurrence-free survival (RFS) in patients with sessile architecture compared with those with papillary architecture, and the univariate and multivariate analyses have indicated that tumor architecture is an independent prognostic factor for RFS (6). Conversely, Fajkovic et al. (24) and Favaretto et al. (25) have not been able to establish the tumor architecture as a significant predictor for disease recurrence.

Several confounding factors, including patient-specific, tumor-specific, treatment-specific, and prognostic biomarkers have been shown to contribute to disease recurrence after RNU (6). The nonspecific relationships between tumor architecture and disease recurrence might account for negative findings in our study. In accordance with previous studies, we found that tumor architecture is significantly associated with

the development of metastatic disease and an independent prognostic marker of CSS after RNU (2–4, 22). Indeed, tumor cell infiltration is a crucial step in tumor dissemination that facilitates further metastasis to distant organs (1). Similar to these studies, we found a strong association of tumor architecture with metastasis and CSS, indicating that sessile UTUC is more aggressive than papillary UTUC. Early diagnosis of these patients would allow a selective administration of adjuvant chemotherapy.

Studies have reported death of nearly 30% of patients with UTUC from metastasis within 5 years of RNU administration (2, 5). Early identification of patients at high risk of disease progression could therefore help tailor the follow-up protocols after surgery. In addition to well-known prognostic factors, such as stage, lymph node status, and grade, the tumor architecture may be a useful predictor for RNU outcomes. Moreover, the greatest advantage of this feature is that it can be accessed macroscopically during endoscopic examination. In a large multicentre series of more than 1,300 UTUC patients treated with RNU, Remzi et al. showed that macroscopic sessile architecture was independently associated with oncologic outcome. In a recent systemic review, sessile tumor architecture was considered to be a valuable biomarker for predicting prognoses of UTUC patients (3, 5, 26). Adequate risk-stratification is necessary for treatment selection, planning the follow-up, and enrolling patients into clinical trials for adjuvant therapy.

Our study has several limitations. First, because this was a retrospective, single-centre analysis, it has inherent limitations. Second, patients who had not received surgery were excluded. Third, the treatment of each patient by different physicians might have introduced differences despite the evaluation of specimens by pathologists specialized in urology; however, our findings are applicable because differences in practice patterns among the physicians in our study were reflective to those used in the real world. Finally, this study lacked the record of the number of lymph nodes removed and the operative method used. Furthermore, not all of the patients received lymph node dissection during surgery.

In conclusion, the tumor architecture of UTUC after RNU is associated with established features of aggressive disease and predictors of metastasis and CSS; however, it is not an independent risk factor for bladder or contralateral disease recurrence. For better appraisal of the course of UTUC, tumor architecture should be considered in a predictive model for disease progression and as a useful factor to identify patients who might benefit from close follow-up or early administration of systemic therapy. To reach any definitive conclusion regarding the prognostic value of tumor architecture, further confirmation using adequately designed prospective trials with larger sample sizes is required.

DATA AVAILABILITY STATEMENT

The raw data supporting the conclusions of this article will be made available by the authors, without undue reservation.

AUTHOR CONTRIBUTIONS

H-YL: acquisition of data, analysis and interpretation of data, drafting the manuscript, and statistical analysis. YTC: administrative, technical, and material support. S-CH: administrative, technical, and material support. H-JW: administrative, technical, and material support. YTC: administrative, technical, and material support. CK: administrative, technical, and material support. WL: administrative, technical, and material support. YS: administrative, technical, and material support. CH: administrative, technical, and material support. YLC: administrative, technical, and material support. YCC: administrative, technical, and material support. HL: conception and design and supervision. PC: conception and design and supervision. All authors contributed to the article and approved the submitted version.

FUNDING

This study is funded by the project of Kaohsiung Chang Gung Memorial Hospital (CMRPG8J0921).

ACKNOWLEDGMENTS

We are grateful to the Biostatistics Center at Kaohsiung Chang Gung Memorial Hospital for assistance with statistical analysis.

SUPPLEMENTARY MATERIAL

The Supplementary Material for this article can be found online at: https://www.frontiersin.org/articles/10.3389/fonc.2021.613696/full#supplementary-material

REFERENCES

1. Kikuchi E, Margulis V, Karakiewicz PI, Roscigno M, Mikami S, Lotan Y, et al. Lymphovascular invasion predicts clinical outcomes in patients with node-negative upper tract urothelial carcinoma. *J Clin Oncol* (2009) 27:612–8. doi: 10.1200/JCO.2008.17.2361
2. Margulis V, Shariat SF, Matin SF, Kamat AM, Zigeuner R, Kikuchi E, et al. Outcomes of radical nephroureterectomy: a series from the Upper Tract Urothelial Carcinoma Collaboration. *Cancer* (2009) 115:1224–33. doi: 10.1002/cncr.24135
3. Remzi M, Haitel A, Margulis V, Karakiewicz P, Montorsi F, Kikuchi E, et al. Tumour architecture is an independent predictor of outcomes after nephroureterectomy: a multi-institutional analysis of 1363 patients. *BJU Int* (2009) 103:307–11. doi: 10.1111/j.1464-410X.2008.08003.x
4. Verhoest G, Shariat SF, Chromecki TF, Raman JD, Margulis V, Novara G, et al. Predictive factors of recurrence and survival of upper tract

urothelial carcinomas. *World J Urol* (2011) 29:495–501. doi: 10.1007/s00345-011-0710-3
5. Fritsche HM, Novara G, Burger M, Gupta A, Matsumoto K, Kassouf W, et al. Macroscopic sessile tumor architecture is a pathologic feature of biologically aggressive upper tract urothelial carcinoma. *Urol Oncol* (2012) 30:666–72. doi: 10.1016/j.urolonc.2010.07.010
6. Fan B, Hu B, Yuan Q, Wen S, Liu T, Bai S, et al. Impact of tumor architecture on disease recurrence and cancer-specific mortality of upper tract urothelial carcinoma treated with radical nephroureterectomy. *Tumour Biol* (2017) 39:1010428317710822. doi: 10.1177/1010428317710822
7. Huang CC, Su YL, Luo HL, Chen YT, Sio TT, Hsu HC, et al. Gender Is a Significant Prognostic Factor for Upper Tract Urothelial Carcinoma: A Large Hospital-Based Cancer Registry Study in an Endemic Area. *Front Oncol* (2019) 9:157. doi: 10.3389/fonc.2019.00157
8. Matsumoto K, Novara G, Gupta A, Margulis V, Walton TJ, Roscigno M, et al. Racial differences in the outcome of patients with urothelial carcinoma of the upper urinary tract: an international study. *BJU Int* (2011) 108:E304–9. doi: 10.1111/j.1464-410X.2011.10188.x
9. Chen XP, Xiong GY, Li XS, Matin SF, Garcia M, Fang D, et al. Predictive factors for worse pathological outcomes of upper tract urothelial carcinoma: experience from a nationwide high-volume centre in China. *BJU Int* (2013) 112:917–24. doi: 10.1111/bju.12238
10. Kang CH, Yu TJ, Hsieh HH, Yang JW, Shu K, Huang CC, et al. The development of bladder tumors and contralateral upper urinary tract tumors after primary transitional cell carcinoma of the upper urinary tract. *Cancer* (2003) 98:1620–6. doi: 10.1002/cncr.11691
11. Li C-C, Chang T-H, Wu W-J, Ke H-L, Huang S-P, Tsai P-C, et al. Significant Predictive Factors for Prognosis of Primary Upper Urinary Tract Cancer after Radical Nephroureterectomy in Taiwanese Patients. *Eur Urol* (2008) 54:1127–35. doi: 10.1016/j.eururo.2008.01.054
12. Chou YH, Huang CH. Unusual clinical presentation of upper urothelial carcinoma in Taiwan. *Cancer* (1999) 85:1342–4. doi: 10.1002/(SICI)1097-0142(19990315)85:6<1342::AID-CNCR17>3.0.CO;2-B
13. Yang M-H, Chen K-K, Yen C-C, Wang W-S, Chang Y-H, Huang WJ-S, et al. Unusually high incidence of upper urinary tract urothelial carcinoma in Taiwan. *Urology* (2002) 59:681–7. doi: 10.1016/S0090-4295(02)01529-7
14. Birtle A, Johnson M, Chester J, Jones R, Dolling D, Bryan RT, et al. Adjuvant chemotherapy in upper tract urothelial carcinoma (the POUT trial): a phase 3, open-label, randomised controlled trial. *Lancet* (2020) 395:1268–77. doi: 10.1016/S0140-6736(20)30415-3
15. al. EJSGEJe. *World Health Organization Classification of Tumours: Pathology and Genetics of Tumours of the Urinary System and Male Genital Organs Lyon*. France: IARC Press (2004).
16. Miyamoto H, Miller JS, Fajardo DA, Lee TK, Netto GJ, Epstein JI. Non-invasive papillary urothelial neoplasms: the 2004 WHO/ISUP classification system. *Pathol Int* (2010) 60:1–8. doi: 10.1111/j.1440-1827.2009.02477.x
17. Humphrey PA, Moch H, Cubilla AL, Ulbright TM, Reuter VE. The 2016 WHO Classification of Tumours of the Urinary System and Male Genital Organs-Part B: Prostate and Bladder Tumours. *Eur Urol* (2016) 70:106–19. doi: 10.1016/j.eururo.2016.02.028
18. Moch H, Cubilla AL, Humphrey PA, Reuter VE, Ulbright TM. The 2016 WHO Classification of Tumours of the Urinary System and Male Genital Organs-Part A: Renal, Penile, and Testicular Tumours. *Eur Urol* (2016) 70:93–105. doi: 10.1016/j.eururo.2016.02.029
19. Epstein JI, Amin MB, Reuter VR, Mostofi FKCommittee TBCC. The World Health Organization/International Society of Urological Pathology Consensus Classification of Urothelial (Transitional Cell) Neoplasms of the Urinary Bladder. *Am J Surg Pathol* (1998) 22:1435–48. doi: 10.1097/00000478-199812000-00001
20. Ishioka J, Saito K, Kijima T, Nakanishi Y, Yoshida S, Yokoyama M, et al. Risk stratification for bladder recurrence of upper urinary tract urothelial carcinoma after radical nephroureterectomy. *BJU Int* (2015) 115:705–12. doi: 10.1111/bju.12707
21. Shao Y, Li W, Wang D, Wu B. Prognostic value of preoperative lymphocyte-related systemic inflammatory biomarkers in upper tract urothelial carcinoma patients treated with radical nephroureterectomy: a systematic review and meta-analysis. *World J Surg Oncol* (2020) 18:273–. doi: 10.1186/s12957-020-02048-7
22. Langner C, Hutterer G, Chromecki T, Rehak P, Zigeuner R. Patterns of invasion and histological growth as prognostic indicators in urothelial carcinoma of the upper urinary tract. *Virchows Arch* (2006) 448:604–11. doi: 10.1007/s00428-006-0150-4
23. Margulis V, Youssef RF, Karakiewicz PI, Lotan Y, Wood CG, Zigeuner R, et al. Preoperative multivariable prognostic model for prediction of nonorgan confined urothelial carcinoma of the upper urinary tract. *J Urol* (2010) 184:453–8. doi: 10.1016/j.juro.2010.03.142
24. Fajkovic H, Cha EK, Jeldres C, Donner G, Chromecki TF, Margulis V, et al. Prognostic Value of Extranodal Extension and Other Lymph Node Parameters in Patients With Upper Tract Urothelial Carcinoma. *J Urol* (2012) 187:845–51. doi: 10.1016/j.juro.2011.10.158
25. Favaretto RL, Bahadori A, Mathieu R, Haitel A, Grubmüller B, Margulis V, et al. Prognostic role of decreased E-cadherin expression in patients with upper tract urothelial carcinoma: a multi-institutional study. *World J Urol* (2017) 35:113–20. doi: 10.1007/s00345-016-1835-1
26. Zhao H, Zhang L, Wu B, Zha Z, Yuan J, Jiang Y, et al. The prognostic value of tumor architecture in patients with upper tract urothelial carcinoma treated with radical nephroureterectomy: A systematic review and meta-analysis. *Med (Baltimore)* (2020) 99:e22176–e. doi: 10.1097/MD.0000000000022176

Conflict of Interest: The authors declare that the research was conducted in the absence of any commercial or financial relationships that could be construed as a potential conflict of interest.

frontiers in Oncology

CASE REPORT
published: 04 March 2021
doi: 10.3389/fonc.2021.621591

Case Report: Enfortumab Vedotin for Metastatic Urothelial Carcinoma: A Case Series on the Clinical and Histopathologic Spectrum of Adverse Cutaneous Reactions From Fatal Stevens-Johnson Syndrome/Toxic Epidermal Necrolysis to Dermal Hypersensitivity Reaction

Paul V. Viscuse[1†], Mario L. Marques-Piubelli[2†], Meghan M. Heberton[3], Edwin Roger Parra[2], Amishi Y. Shah[4], Arlene Siefker-Radtke[4], Jianjun Gao[4], Sangeeta Goswami[4], Doina Ivan[5], Jonathan L. Curry[2,5‡] and Matthew T. Campbell[4‡]*

[1] Division of Cancer Medicine-Hematology/Oncology Fellowship Program, The University of Texas MD Anderson Cancer Center, Houston, TX, United States, [2] Department of Translational Molecular Pathology, The University of Texas MD Anderson Cancer Center, Houston, TX, United States, [3] Department of Dermatology, The University of Texas MD Anderson Cancer Center, Houston, TX, United States, [4] Department of Genitourinary Medical Oncology, The University of Texas MD Anderson Cancer Center, Houston, TX, United States, [5] Department of Pathology, The University of Texas MD Anderson Cancer Center, Houston, TX, United States

Enfortumab vedotin is a Nectin-4 directed antibody-drug conjugate approved in metastatic urothelial carcinoma following progression on a platinum-containing chemotherapy and immune checkpoint blockade. On-target dermatologic toxicity may occur from Nectin-4 expression in the skin. We highlight a case of Stevens-Johnson Syndrome/Toxic Epidermal Necrolysis following enfortumab infusions that was ultimately fatal. The second case describes an erythema multiforme-like rash with interface dermatitis related to enfortumab. Dermatologic findings, immunohistochemistry studies, and immune profiling are detailed. These cases demonstrate the potentially catastrophic outcomes in some patients treated with enfortumab. Patients must be monitored for cutaneous toxicities with early involvement of dermatology and dermatopathology.

Keywords: bladder cancer, enfortumab vedotin, SJS/TEN, urothelial cancer, adverse (side) effects, erythema multiform

OPEN ACCESS

Edited by:
Scott T. Tagawa,
Cornell University, United States

Reviewed by:
Ajjai Alva,
University of Michigan, United States
Ignacio Duran,
Marqués de Valdecilla University Hospital, Spain

***Correspondence:**
Matthew T. Campbell
Mcampbell3@mdanderson.org

†These authors have contributed equally to this work

‡These authors have contributed equally to this work

Specialty section:
This article was submitted to Genitourinary Oncology, a section of the journal Frontiers in Oncology

Received: *26 October 2020*
Accepted: *07 January 2021*
Published: *04 March 2021*

Citation:
Viscuse PV, Marques-Piubelli ML, Heberton MM, Parra ER, Shah AY, Siefker-Radtke A, Gao J, Goswami S, Ivan D, Curry JL and Campbell MT (2021) Case Report: Enfortumab Vedotin for Metastatic Urothelial Carcinoma: A Case Series on the Clinical and Histopathologic Spectrum of Adverse Cutaneous Reactions From Fatal Stevens-Johnson Syndrome/Toxic Epidermal Necrolysis to Dermal Hypersensitivity Reaction. Front. Oncol. 11:621591. doi: 10.3389/fonc.2021.621591

INTRODUCTION

Enfortumab vedotin (EV) is an antibody-drug conjugate approved by the Food and Drug Administration in locally advanced or metastatic urothelial carcinoma following progression on platinum-containing chemotherapy and programmed death receptor-1 (PD-1) or programmed death-ligand 1 inhibitor (PD-L1). The antibody is directed at Nectin-4 and is linked to monomethyl

auristatin E (MMAE), a potent antimitotic payload that blocks tubulin polymerization. The approval was based on a phase II study showing an overall response rate of 44% and median duration of response of 7.6 months (1). Preliminary results from the ongoing phase III EV-301 trial comparing EV to chemotherapy in previously treated patients with urothelial carcinoma have the primary end point of overall survival benefit (2). Dermatologic adverse events have been cited due to on-target toxicity from Nectin-4 expression in normal skin (3). Details of these events are not available, and the specific pathologic and immunologic findings have not been described.

We present our experience with enfortumab by describing a case of rapidly progressing Stevens-Johnson Syndrome/Toxic Epidermal Necrolysis (SJS/TEN) and a case of an erythema multiforme (EM)-like rash with histopathologic features of interface dermatitis related to EV.

CASE DESCRIPTION

Patient 1

A 71-year-old male developed painless gross hematuria that persisted for a month. His past medical history was notable for compensated liver cirrhosis secondary to non-alcoholic fatty liver disease with portal hypertension, atrial fibrillation, and hypertension. Non-oncologic medications included aspirin, propranolol, and losartan. A contrast-enhanced CT of the abdomen and pelvis revealed a left kidney mass (4.6 × 5.9 × 4.0 cm) with a small (0.8 cm) left paracolic lymph node and several sub centimeter bibasilar solid pulmonary nodules.

A CT-guided biopsy of the left kidney mass revealed high-grade urothelial carcinoma with invasion into the adjacent renal parenchyma. The lung nodules were suspicious for metastases, so he was started on cisplatin-based chemotherapy. He had a partial response after four cycles of treatment. He then received pembrolizumab IV 200 mg every 3 weeks and received a total of five cycles before discontinuation for disease progression. The patient enrolled on a clinical protocol with the combination of PD-1 antibody and an oral small molecule tyrosine kinase inhibitor targeting VEGFR2, KIT, TYRO3, AXL, and MER. Within one month, he developed grade IV pancreatitis which completely resolved with corticosteroid taper and cessation of therapy. He did not have any documented skin toxicity during this time. He initiated EV seven weeks from the last dose of immunotherapy and five weeks from the last dose of targeted therapy (**Figure 1**).

He received EV 1.25 mg/kg on days 1 and 8 of the first cycle. Within 24 h of the day 8 infusion, he experienced diffuse pruritus. Four days after the infusion, he presented to the emergency department with fevers to 101°F and mouth pain but was otherwise hemodynamically stable with unremarkable cardiac and pulmonary exams. His dermatologic exam on admission revealed a small ulceration on the right lateral upper lip, well-demarcated erythema of the inferior tongue tip, and tender erythema of the axillae, flanks, inguinal region, and soles of feet (**Figures 2A, B**). He had flaccid ruptured bullae with approximately 11% of body surface area involvement that included the right heel, right posterior upper arm, and left forearm with positive Nikolsky sign. Eosinophil count and liver function tests were within normal limits. He was admitted and

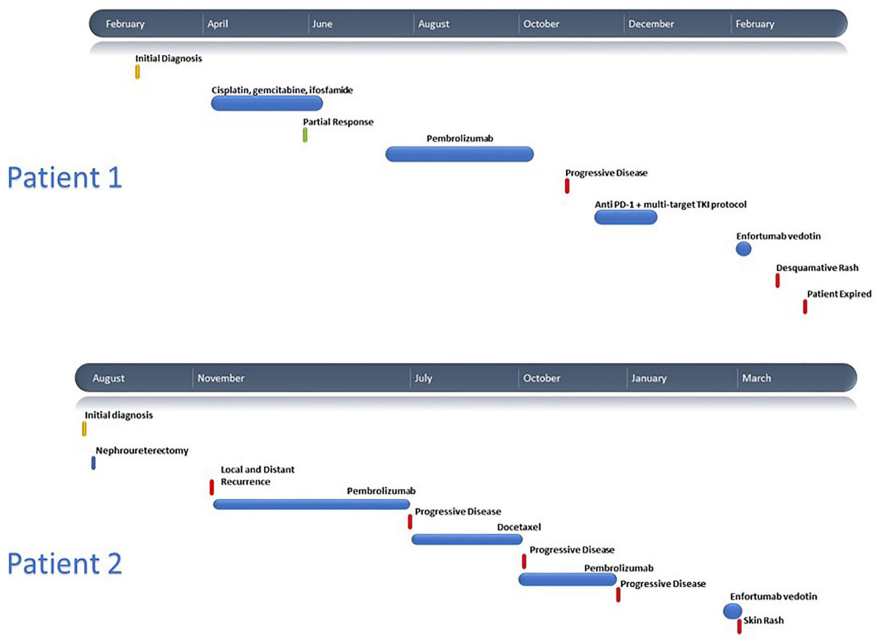

FIGURE 1 | Clinical timelines for Patient 1 and Patient 2.

initiated on systemic steroids. Twelve days after treatment and 4 days after symptom onset, a punch biopsy of the left axillae confirmed subepidermal bulla with detached epidermis with scattered dyskeratotic cells and mixed dermal inflammatory infiltrate composed of lymphocytes, neutrophils, eosinophils, and macrophages (**Figure 2C**). The clinical and histologic findings were compatible with early changes of SJS/TEN.

The inflammatory infiltrate was composed of CD4+ and CD8+ T-cells admixed with MPO+ neutrophils and scattered CD68+ macrophages with absence of CD20+ B-cells (**Figures 2D, E**). Immune profiling with Vectra 3.0 spectral multiplex immunofluorescence (mIF) imaging system (PerkinElmer) and InForm 2.4.8 image analysis software were performed on the SJS/TEN skin biopsy utilizing a panel of antibodies to evaluate for the T-cell density (anti-CD3 and anti-CD4) and T helper (Th) cell immune response (Th1, anti-TBet; Th2, anti-Gata3; Th17, anti-RORγT; Tregs, anti-FoxP3). The density of skin infiltrating lymphocytes was composed predominantly of CD4+ T-cells with a subset of CD8+ T-cells (**Figures 2F, G**). There was absence of skin infiltrating lymphocytes in the epidermis. The Th immune profile consisted primarily of Th2 (Gata3+ cells) and Tregs (FoxP3+ cells) lymphocytes. A subset of CD4+ T-cells were Th17 (RORγT+ cells) and a minor population was Th1 (anti-TBet+ cells) (**Figure 3**).

ICU transfer with IV methylprednisolone treatment was initiated on day 3 for involvement of 18% total body surface area and high SCORETEN of 7. Antimicrobial therapy included cefepime, acyclovir, and mupirocin. He developed hypotension with a worsening rash, acute kidney injury, atrial fibrillation with rapid ventricular rate, hyponatremia, hyperglycemia, and anion-gap metabolic acidosis. Full thickness ulcers developed on the left upper arm, bilateral axillae, posterior ankles, right forearm, and scrotum with positive Nikolsky sign. He subsequently was transferred to the burn unit at a nearby hospital, but the patient expired several days later.

Patient 2

A 77-year-old male presented with gross hematuria and flank pain in the setting of a left renal mass and underwent left nephroureterectomy with pathology confirming high grade papillary urothelial carcinoma. Two months later, he was found to have recurrence in the left nephrectomy bed, liver, lungs, lymph nodes, and bones with cisplatin ineligibility. He had recently progressed following treatment with docetaxel and, more recently, pembrolizumab which was discontinued approximately 2 months prior to his visit with no adverse effects (**Figure 1**). He was initiated on EV and subsequently developed a rash 2 days after his third infusion with tender erythema in the axillae, scrotum, and inguinal folds. Pruritic papules and vesicles of the chest and back, and bullae on the dorsal 2nd and 3rd digits of the left foot were observed (**Figure 4A**). Eighteen days after his first infusion, skin biopsy of chest (**Figure 4B**) and inguinal fold (**Figure 4H**) revealed bullous formation and interface dermatitis with dyskeratosis respectively. There were associated eosinophils and some neutrophils. The clinical and pathologic findings were compatible with EV-associated drug toxicity.

Immunohistochemical studies revealed perivascular dermal infiltrates with CD4+ and CD8+ T-cells (**Figures 4C, D, I, J**) and scattered CD68+ macrophages with few MPO+ neutrophils in the blister cavity and an absence of CD20+ B-cells. mIF studies revealed primarily CD4+ T-cell lymphocyte density with Tregs (FoxP3+ cells) in both lesions (**Figures 4E, F, K, L**). The interface dermatitis toxicity in the inguinal fold biopsy (lesion 1) exhibited a higher density of CD8+ lymphocytes compared to the bullous toxicity in the chest biopsy (lesion 2). There was also higher density Th17 (RORγT+ cells) in lesion 1 compared to lesion 2. The Th1 subset (TBet+ cells) of lymphocytes comprised of a small population of skin infiltrating lymphocytes with higher density of Th1 subset in the interface dermatitis toxicity (lesion 1) compared to bullous toxicity (lesion 2). In contrast, the density of Th2 lymphocytes (Gata3+ cells) was greater in lesion 2 compared to the lesion 1 (**Figure 3**).

Eosinophils were within normal limits. Alanine aminotransferase (ALT) and aspartate aminotransferase (AST) were elevated to 89 U/L and 99 U/L respectively. He had significant improvement in his rash and liver enzyme levels following 24–48 h of treatment with silver sulfadiazine cream, triamcinolone 0.1% ointment TID, and prednisone 60 mg daily. He continues EV without further complications.

DISCUSSION

Metastatic urothelial carcinoma has a poor prognosis with a median overall survival of less than 12 months. Approximately half of patients respond to first-line platinum-based chemotherapy and many patients are platinum-ineligible due to comorbidities (4, 5). Anti-PD-1/L1 therapy has been approved post-platinum with objective response rates up to 21% in the second-line setting and 24% in the first-line setting for platinum-ineligible patients (6, 7). Some patients who progress following chemotherapy and immunotherapy and demonstrate an FGFR alteration have the option to receive the FGFR 1-4 inhibitor erdafitinib (8). For the vast majority of patients, no standard therapeutic options remain outside of EV. EV is a fully human monoclonal antibody conjugated to a microtubule-disrupting agent monomethyl auristatin E (MMAE). It targets Nectin-4 which is a transmembrane protein involved in oncogenesis and is highly expressed in urothelial carcinoma. It received accelerated approval by the Food and Drug Administration in December 2019 based on results from the phase II EV201 study (1).

Of note, Nectin-4 is weakly to moderately expressed in skin with rashes occurring as an on-target toxicity. EV201 noted dermatologic adverse events in 48% of patients (25% grade 3 or higher) with onset typically seen in the first treatment cycle, consisting of weekly dosing on day 1, day 8, and day 15 out of 28 days. Most were described as "low grade", "maculopapular", and "diffuse". Events were typically manageable with topical corticosteroids, oral antihistamines, systemic corticosteroids, and/or dose reductions/delays. However, one patient experienced a grade 3 rash reported as SJS 4 days after the initial dose with resolution after EV discontinuation and steroid treatment. There were no drug related deaths reported (1). Application of the Naranjo algorithm indicates probable

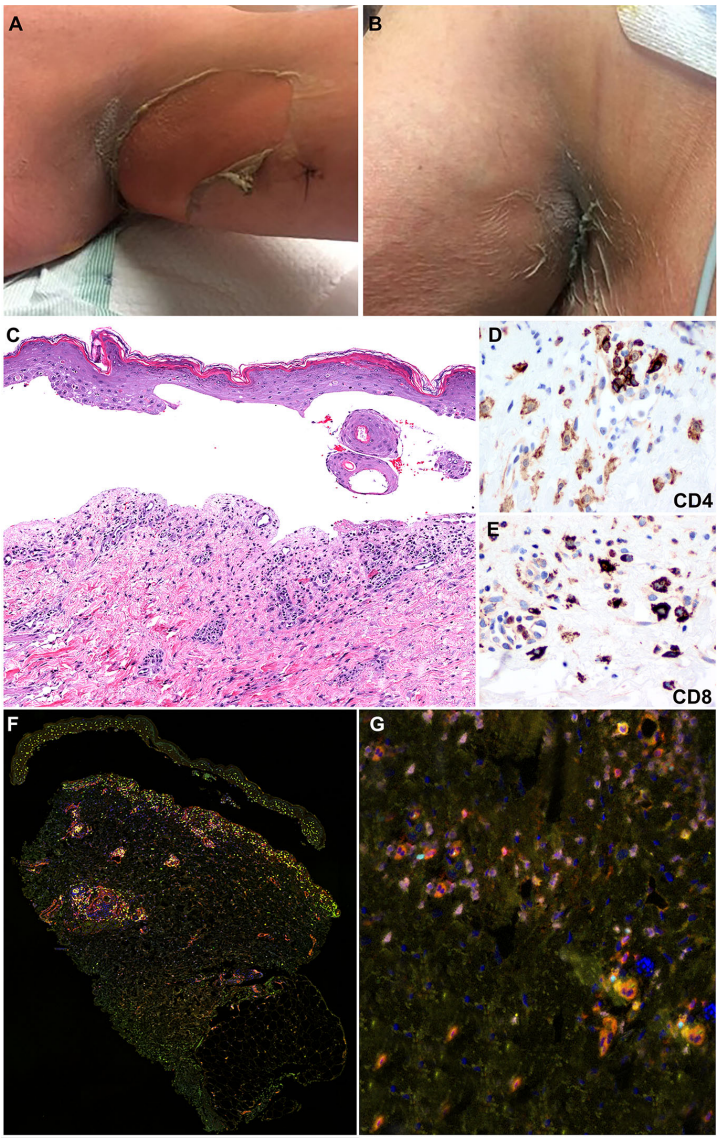

FIGURE 2 | Clinicopathologic illustration of Patient 1. **(A, B)** Dusky erythematous patches and detachment of skin of the axillary vaults. **(C)** Patient 1 skin biopsy with epidermal detachment and blister cavity with scattered necrotic epidermal keratinocytes. An associated dermal superficial dermis shows interstitial and perivascular lymphohistiocytic infiltrate and few eosinophils and neutrophils (hematoxylin and eosin, original magnification, 40x). **(D, E)** Immunohistochemical studies show that the inflammatory infiltrates are composed of CD4+ T-cells with a subset of CD8+ T-cells (Immunohistochemistry, anti-CD4 and anti-CD8 x400). **(F, G)** Multiplex immunofluorescence (mIF) studies with immune-oncology toxicity panel of anti-CD3, anti-CD8, anti-FoxP3, anti-TBet, anti-Gata3, and anti-RORγT antibodies for patient 1. Stevens-Johnson syndrome/toxic epidermal necrolysis lesion shows inflammatory infiltrate in superficial dermis composed of CD3+ T-cells (orange) admixed with CD8+ T-cells (red). The infiltrate consists of increased numbers of Gata3+ cells (pink) and Th2 immunophenotype. Rare subsets of cells are positive for FoxP3 (cyan) and RORγT (green) corresponding to Tregs and Th17 immunophenotype, respectively.

causality and relationship of skin toxicity to EV in our cases (9). The proposed mechanism is targeting of Nectin-4 by EV with delivery of the MMAE payload to the skin resulting in the observed keratinocyte apoptosis. Alternatively, the dermatologic sequalae observed could be attributed solely to the MMAE payload without Nectin-4 direction. This is supported by the common occurrence of skin rash as an adverse event in trials evaluating other antibody-drug conjugates that incorporate MMAE, occurring in 31% of patients with classical Hodgkin lymphoma treated with brentuximab vedotin monotherapy, 44% of patients treated with glemutumumab vedotin, and 13–31% of patients treated with polatuzumab vedotin (10). Lastly, dermatologic toxicities from prior immune checkpoint inhibitor treatment cannot be entirely ruled out as delayed onset of SJS/TEN >8 weeks following exposure have been cited (11, 12). The

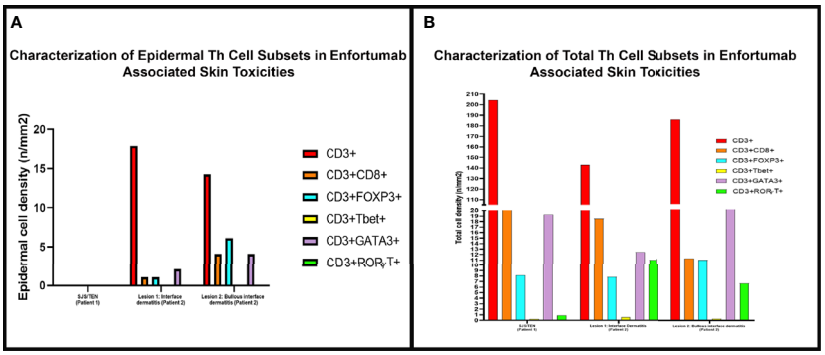

FIGURE 3 | The density of skin infiltrating lymphocytes in the epidermis and skin biopsy by multiplex immunofluorescence (mIF) in patient 1 with Stevens-Johnson syndrome/toxic epidermal necrolysis SJS/TEN and patient 2 interface dermatitis toxicity (lesion 1) and bullous toxicity (lesion 2). **(A)** Skin infiltrating lymphocytes were absent in the epidermis in patient 1 with SJS/TEN. In patient 2, the interface dermatitis toxicity (lesion 1) and the bullous toxicity (lesion 2) exhibited CD3+ T-cells with variable density of CD8+ T-cells and Tregs and Th2 positive cells. **(B)** Examination of the total density of skin infiltrating lymphocytes by mIF analysis revealed that all three (SJS/TEN, interface dermatitis toxicity, and bullous toxicity) lesions analyzed consisted of CD3+ T-cells with a subset of CD8+ T-cells. All three lesions exhibited similar density of FoxP3+ cells and a minor population of TBet+ cells. The lesions from patient 2 exhibited higher density of RORγT+ cells compared to SJS/TEN lesion from patient 1.

histomorphologic features exhibit interface dermatitis with dyskeratosis (3). The extent of damage to the DEJ and subsequent blister formation and clinical manifestation of SJS/TEN appear variable between patients and among lesions biopsied in a patient (*e.g.*, patient 2). The composition of the immune infiltrate also appears variable among lesions though conclusions from this small sample size are limited. All lesions were composed of Th2 lymphocytes with a subset of Tregs and Th17 cells. All biopsies exhibited a subset of Th17 cells, which have been reported in peripheral blood and skin biopsies of patients with SJS/TEN, EM, and drug induced hypersensitivity reactions (13). *Ex vivo* expansion of skin infiltrating lymphocytes in patients with SJS/TEN, EM, and drug induced dermal hypersensitivity reaction (DHR) revealed the dynamic production of IL-17 with maximum concentration of IL-17 cells at 21 days after onset of skin reaction (13). Furthermore, increased Th17 cells in the peripheral blood and blister fluid of patients with SJS/TEN has been observed (14). Collectively, the composition of the immune infiltrate and Th17 cell subset may have a role in EV associated skin toxicities. The extent of skin infiltrating Th17 cells may be related to the timing of biopsy, onset of toxicity, and disease course.

SJS/TEN represent a spectrum of febrile mucocutaneous drug reactions (15). Categories are delineated based on BSA involvement: 1) SJS <10% BSA; 2) SJS/TEN overlap >10 to <30% BSA; 3) TEN >30% BSA (16). Rashes tend to present as dusky, red skin macules and/or patches with progression to widespread bullae, skin sloughing, and mucosal erosions with positive Nikolsky sign and associated fevers. A skin biopsy can help differentiate from other possible entities though it mainly represents a clinical diagnosis. Most cases are associated with medications, typically antibiotics, but also with allopurinol and anticonvulsants (17). More recently, RAF and immune checkpoint inhibition may be associated with SJS/TEN (18). Lesions typically occur 7-21 days after drug exposure but can occur within 2 days upon re-exposure. Management requires discontinuation of the offending agent. Supportive care with fluid resuscitation, electrolyte replacement, and nutrition should be provided in an intensive care setting. Use of non-adherent dressings provides topical skin care. There is otherwise limited evidence for other therapeutic interventions such as IVIG, IV cyclosporine, IV corticosteroids, and/or TNF-α antagonist such as etanercept (19–22). Survival often results in sequelae of scarring, pigmentation changes, and ocular complications. There is a high mortality rate of 0–9% in SJS, 3.9–19.4% in SJS/TEN, and 15-23% for TEN (23, 24). The SCORTEN score within 24 hours of admission and again on day 3 of hospitalization can aid prognostication. The score ranges from 0 to 7 with one point for each of the following: 1) Age 40 y or older; 2) pulse 120 bpm or more; 3) comorbid malignancy; 4) 10% or more body surface involvement; 5) serum urea >28 mg/dl; 6) serum glucose >252 mg/dl; 7) serum bicarbonate <20 mEq/L (25).

CONCLUSION

With limited therapeutic options for patients with urothelial carcinoma following progression on platinum-based chemotherapy and immune checkpoint blockade, EV will see increased use. In patients with co-morbidities, low performance status, and laboratory values not acceptable for clinical trials, toxicity may be enhanced as compared to clinical trial participants. Since Nectin-4 is expressed in the skin, it is plausible that we will see increased skin toxicity from EV. Though it is not entirely clear if the catastrophic outcomes described in patient 1 are due to EV, vigilance is warranted in this subset of patients. These patients must be monitored to characterize the type of cutaneous toxicity with early involvement of dermatology and dermatopathology.

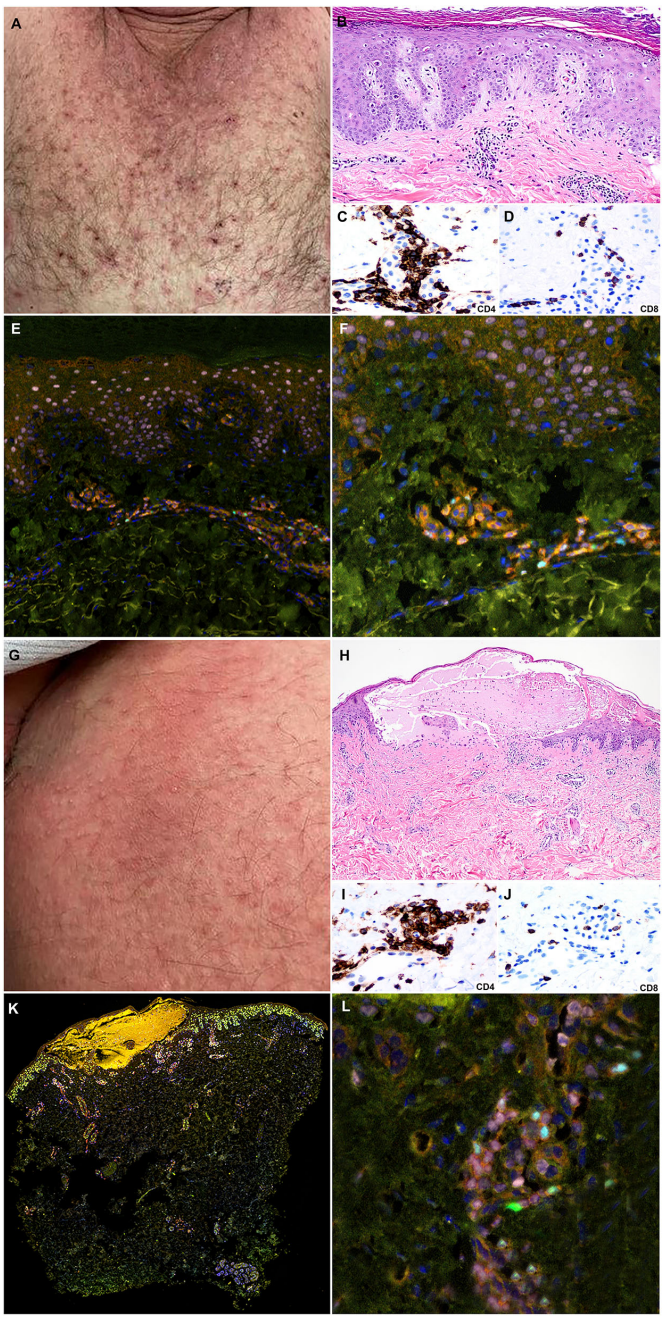

FIGURE 4 | Clinicopathologic illustration of Patient 2. **(A)** Crusted thin red papules on the chest. **(B)** Patient 2 skin biopsy with interface dermatitis toxicity (lesion 1) with scattered dyskeratotic cells and the superficial perivascular dermal inflammatory infiltrate with eosinophils (hematoxylin and eosin, original magnification, 40x). **(C, D)** Immunohistochemical studies show that the inflammatory infiltrates are composed of CD4+ T-cells with a subset of CD8+ T-cells (Immunohistochemistry, anti-CD4 and anti-CD8, x400). **(E, F)** Multiplex immunofluorescence (mIF) studies with immune-oncology toxicity panel of anti-CD3, anti-CD8, anti-FoxP3, anti-TBet, anti-Gata3, and anti-RORγT antibodies. Patient 2, interface dermatitis toxicity (lesion 1) shows dermal inflammatory infiltrate that exhibits Th2 immunophenotype with Gata3+ cells (pink). There is a subset of Tregs, Foxp3+ cells (cyan), and Th17, RORγT positive cells (green) in the inflammatory infiltrate. **(G)** Erythematous patches on the abdomen. **(H)** Patient 2 skin biopsy with bullous toxicity (lesion 2) with scattered dyskeratotic cells (white arrows) and the superficial perivascular dermal inflammatory infiltrate with eosinophils and few neutrophils [hematoxylin and eosin (H&E), original magnification]. **(I, J)** Immunohistochemical studies show that the inflammatory infiltrates are composed of CD4+ T-cells with a subset of CD8+ T-cells (immunohistochemistry, anti-CD4 and anti-CD8, x400). **(K, L)** Multiplex immunofluorescence (mIF) studies with immune-oncology toxicity panel for patient 2; bullous toxicity (lesion 2) shows similar Th2 immunophenotype with Gata3+ cells (pink) and subsets of Tregs, Foxp3+ cells (cyan), and Th17, RORγT positive cells (green) [Vectra 3.0 spectral multiplex immunofluorescence (mIF) imaging system (PerkinElmer) and InForm 2.4.8 image analysis software Colors: Blue, DAPI; Red, CD3; Orange, CD8; Cyan, FOXP3; Yellow, TBet; Pink, GATA3; Green, RORγT].

DATA AVAILABILITY STATEMENT

The raw data supporting the conclusions of this article will be made available by the authors, without undue reservation.

ETHICS STATEMENT

Written informed consent was not obtained from the individual(s) for the publication of any potentially identifiable images or data included in this article.

AUTHOR CONTRIBUTIONS

PV and MM-P contributed equally to development of the manuscript. JC and MC contributed equally and provided expert oversight for the completion of the manuscript. MH provided dermatology input on manuscript and images. EP performed tissue studies for figures. AS, AS-R, JG, DI, and SG provided input on preparation of manuscript. All authors contributed to the article and approved the submitted version.

REFERENCES

1. Rosenberg JE, O'Donnell PH, Balar AV, McGregor BA, Heath EI, Yu EY, et al. Pivotal Trial of Enfortumab Vedotin in Urothelial Carcinoma After Platinum and Anti-Programmed Death 1/Programmed Death Ligand 1 Therapy. *J Clin Oncol* (2019) 37(29):2592–600. doi: 10.1200/JCO.19.01140
2. Seattle Genetics and Astellas Announce PADCEV® (enfortumab vedotin-ejfv) Significantly Improved Overall Survival in Phase 3 Trial in Previously Treated Locally Advanced or Metastatic Urothelial Cancer [news release]. Bothell, Washington and Tokyo. Available at: https://www.businesswire.com/news/home/20200918005101/en/Seattle-Genetics-and-Astellas-Announce-PADCEV%C2%AE-enfortumab-vedotin-ejfv-Significantly-Improved-Overall-Survival-in-Phase-3-Trial-in-Previously-Treated-Locally-Advanced-or-Metastatic-Urothelial-Cancer (Accessed September 18, 2020). Published September 18, 2020.
3. Wu S, Adamson AS. Cutaneous toxicity associated with enfortumab vedotin treatment of metastatic urothelial carcinoma. *Dermatol Online J* (2019) 25 (2):13030.
4. Bellmunt J, von der Maase H, Mead GM, Skoneczna I, De Santis M, Daugaard G, et al. Randomized phase III study comparing paclitaxel/cisplatin/gemcitabine and gemcitabine/cisplatin in patients with locally advanced or metastatic urothelial cancer without prior systemic therapy: EORTC Intergroup Study 30987. *J Clin Oncol* (2012) 30(10):1107–13. doi: 10.1200/JCO.2011.38.6979
5. von der Maase H, Hansen SW, Roberts JT, Dogliotti L, Oliver T, Moore MJ, et al. Gemcitabine and cisplatin versus methotrexate, vinblastine, doxorubicin, and cisplatin in advanced or metastatic bladder cancer: results of a large, randomized, multinational, multicenter, phase III study. *J Clin Oncol* (2000) 18(17):3068–77. doi: 10.1200/JCO.2000.18.17.3068
6. Balar AV, Castellano D, O'Donnell PH, Grivas P, Vuky J, Powles T, et al. First-line pembrolizumab in cisplatin-ineligible patients with locally advanced and unresectable or metastatic urothelial cancer (KEYNOTE-052): a multicentre, single-arm, phase 2 study. *Lancet Oncol* (2017) 18 (11):1483–92. doi: 10.1016/S1470-2045(17)30616-2
7. Bellmunt J, de Wit R, Vaughn DJ, Fradet Y, Lee JL, Fong L, et al. Pembrolizumab as Second-Line Therapy for Advanced Urothelial Carcinoma. *N Engl J Med* (2017) 376(11):1015–26. doi: 10.1056/NEJMoa1613683
8. Loriot Y, Necchi A, Park SH, Garcia-Donas J, Huddart R, Burgess E, et al. Erdafitinib in Locally Advanced or Metastatic Urothelial Carcinoma. *N Engl J Med* (2019) 381(4):338–48. doi: 10.1056/NEJMoa1817323
9. Naranjo CA, Busto U, Sellers EM, Sandor P, Ruiz I, Roberts EA, et al. A method for estimating the probability of adverse drug reactions. *Clin Pharmacol Ther* (1981) 309(2):239–45. doi: 10.1038/clpt.1981.154
10. Chang E, Weinstock C, Zhang L, Charlab R, Dorff SE, Gong Y, et al. FDA Approval Summary: Enfortumab Vedotin for Locally Advanced or Metastatic Urothelial Carcinoma. *Clin Cancer Res* (2020). doi: 10.1158/1078-0432.CCR-20-2275
11. Hwang A, Iskandar A, Dasanu CA. Stevens-Johnson syndrome manifesting late in the course of pembrolizumab therapy. *J Oncol Pharm Pract* (2019) 25 (6):1520–2. doi: 10.1177/1078155218791314
12. Maloney NJ, Ravi V, Cheng K, Bach DQ, Worswick S. Stevens-Johnson syndrome and toxic epidermal necrolysis-like reactions to checkpoint inhibitors: a systematic review. *Int J Dermatol* (2020) 59(6):e183–e8. doi: 10.1111/ijd.14811
13. Fujiyama T, Kawakami C, Sugita K, Kubo-Kabashima R, Sawada Y, Hino R, et al. Increased frequencies of Th17 cells in drug eruptions. *J Dermatol Sci* (2014) 73(1):85–8. doi: 10.1016/j.jdermsci.2013.08.008
14. Teraki Y, Kawabe M, Izaki S. Possible role of TH17 cells in the pathogenesis of Stevens-Johnson syndrome and toxic epidermal necrolysis. *J Allergy Clin Immunol* (2013) 131(3):907–9. doi: 10.1016/j.jaci.2012.08.042
15. Lerch M, Mainetti C, Terziroli Beretta-Piccoli B, Harr T. Current Perspectives on Stevens-Johnson Syndrome and Toxic Epidermal Necrolysis. *Clin Rev Allergy Immunol* (2018) 54(1):147–76. doi: 10.1007/s12016-017-8654-z
16. Bastuji-Garin S, Rzany B, Stern RS, Shear NH, Naldi L, Roujeau JC. Clinical classification of cases of toxic epidermal necrolysis, Stevens-Johnson syndrome, and erythema multiforme. *Arch Dermatol* (1993) 129(1):92–6. doi: 10.1001/archderm.129.1.92
17. Kohanim S, Palioura S, Saeed HN, Akpek EK, Amescua G, Basu S, et al. Stevens-Johnson Syndrome/Toxic Epidermal Necrolysis–A Comprehensive Review and Guide to Therapy. I. Systemic Disease. *Ocul Surf* (2016) 14(1):2–19. doi: 10.1016/j.jtos.2015.10.002
18. Robinson S, Saleh J, Curry JL, Mudaliar K. Pembrolizumab-Induced Stevens-Johnson Syndrome/Toxic Epidermal Necrolysis in a Patient With Metastatic Cervical Squamous Cell Carcinoma: A Case Report. *Am J Dermatopathol* (2020) 42(4):292–6. doi: 10.1097/DAD.0000000000001527
19. Ng QX, De Deyn M, Venkatanarayanan N, Ho CYX, Yeo WS. A meta-analysis of cyclosporine treatment for Stevens-Johnson syndrome/toxic epidermal necrolysis. *J Inflam, Res* (2018) 11:135–42. doi: 10.2147/JIR.S160964
20. Wang R, Zhong S, Tu P, Li R, Wang M. Rapid remission of Stevens-Johnson syndrome by combination therapy using etanercept and intravenous immunoglobulin and a review of the literature. *Dermatol Ther* (2019) 32(4): e12832. doi: 10.1111/dth.12832
21. Ye LP, Zhang C, Zhu QX. The Effect of Intravenous Immunoglobulin Combined with Corticosteroid on the Progression of Stevens-Johnson Syndrome and Toxic Epidermal Necrolysis: A Meta-Analysis. *PloS One* (2016) 11(11):e0167120. doi: 10.1371/journal.pone.0167120
22. Zimmermann S, Sekula P, Venhoff M, Motschall E, Knaus J, Schumacher M, et al. Systemic Immunomodulating Therapies for Stevens-Johnson Syndrome and Toxic Epidermal Necrolysis: A Systematic Review and Meta-analysis. *JAMA Dermatol* (2017) 153(6):514–22. doi: 10.1001/jamadermatol.2016.5668
23. Finkelstein Y, Macdonald EM, Li P, Hutson JR, Juurlink DN. Recurrence and Mortality Following Severe Cutaneous Adverse Reactions. *JAMA* (2014) 311 (21):2231–2. doi: 10.1001/jama.2014.839
24. Hsu DY, Brieva J, Silverberg NB, Silverberg JI. Morbidity and Mortality of Stevens-Johnson Syndrome and Toxic Epidermal Necrolysis in United States Adults. *J Invest Dermatol* (2016) 136(7):1387–97. doi: 10.1016/j.jid.2016.03.023
25. Bastuji-Garin S, Fouchard N, Bertocchi M, Roujeau JC, Revuz J, Wolkenstein P. SCORTEN: a severity-of-illness score for toxic epidermal necrolysis. *J Invest Dermatol* (2000) 115(2):149–53. doi: 10.1046/j.1523-1747.2000.00061.x

Conflict of Interest: MC: Advisory Board/Honorarium: Seattle Genetics, Astellas, Eisai, AstraZeneca, Exelixis, EMD Serono, Pfizer Education grants: Roche, Bristol Myers Squibb, Pfizer Research grants: AstraZeneca, Exelixis, Janssen, Pfizer, EMD Serono.

The remaining authors declare that the research was conducted in the absence of any commercial or financial relationships that could be construed as a potential conflict of interest.

frontiers in Oncology

SYSTEMATIC REVIEW
published: 01 April 2021
doi: 10.3389/fonc.2021.629646

Safety and Activity of Programmed Cell Death 1 Versus Programmed Cell Death Ligand 1 Inhibitors for Platinum-Resistant Urothelial Cancer: A Meta-Analysis of Published Clinical Trials

Zaishang Li[1,2,3†], Xueying Li[4†], Wayne Lam[5], Yabing Cao[6], Hui Han[7,8,9], Xueqi Zhang[1,2,3], Jiequn Fang[1,2,3], Kefeng Xiao[1,2,3] and Fangjian Zhou[7,8,9*]*

[1] Department of Urology, Shenzhen People's Hospital, The Second Clinic Medical College of Jinan University, Shenzhen, China, [2] Department of Urology, First Affiliated Hospital of Southern University of Science and Technology, Shenzhen, China, [3] Department of Urology, Minimally Invasive Urology of Shenzhen Research and Development Center of Medical Engineering and Technology, Shenzhen, China, [4] Department of Oncology, The Seventh Affiliated Hospital of Sun Yat-sen University, Shenzhen, China, [5] Division of Urology, Department of Surgery, Queen Mary Hospital, The University of Hong Kong, Hong Kong, Hong Kong, [6] Department of Oncology, Hospital Kiang Wu, Macau, Macau, [7] Department of Urology, Sun Yat-sen University Cancer Center, Guangzhou, China, [8] Department of Urology, State Key Laboratory of Oncology in South China, Guangzhou, China, [9] Department of Urology, Collaborative Innovation Center of Cancer Medicine, Guangzhou, China

Background: Programmed death 1/ligand 1 (PD-1/L1) inhibitors have acceptable antitumor activity in patients with platinum-resistant urothelial cancer (UC). However, the reliability and comparability of the antitumor activity, safety profiles and survival outcomes of different immune checkpoint inhibitors are unknown. Our objective was to compare the clinical efficacy and safety of anti–PD-1/PD-L1 therapies in platinum-resistant UC patients.

Methods: We reviewed the published trials from the PubMed, Embase and Cochrane Library databases up to August 2020. A well-designed mirror principle strategy to screen and pair trial characteristics was used to justify indirect comparisons. The primary end point was the objective response rate (ORR). The safety profile and survival outcomes were also evaluated. The restricted mean survival time (RMST) up to 12 months was calculated.

Results: Eight studies including 1,666 advanced or metastatic UC patients (1,021 patients with anti–PD-L1 treatment and 645 patients with anti–PD-1 treatment) met the study criteria. The ORRs of anti–PD-1 and PD-L1 therapy were 22% (95% CI, 18%–25%) and 15% (95% CI, 13%–17%) with all studies combined. The proportions of the treated population with a confirmed objective response (I^2 = 0; P = 0.966; HR, 1.60; 95% CI, 1.23–2.07; P < 0.001) and disease control (I^2 = 30.6%; P = 0.229; HR, 1.35; 95% CI, 1.10–1.66; P = 0.004) were higher with anti–PD-1 therapy than with anti–PD-L1 therapy. The treatment-related adverse events (AEs) (I^2 = 78.3%; P = 0.003; OR, 1.09; 95% CI, 0.65–1.84; P = 0.741) and grade 3–5 treatment-related AEs (I^2 = 68.5%; P = 0.023; OR,

OPEN ACCESS

Edited by:
Camillo Porta,
Fondazione Ospedale San Matteo (IRCCS), Italy

Reviewed by:
Yüksel Ürün,
Ankara University, Turkey
Melissa A. Reimers,
Washington University in St. Louis, United States

***Correspondence:**
Fangjian Zhou
zhoufj@ sysucc.org.cn
Kefeng Xiao
kevin5510315@qq.com

[†]These authors have contributed equally to this work

Specialty section:
This article was submitted to Genitourinary Oncology, a section of the journal Frontiers in Oncology

Received: 15 December 2020
Accepted: 09 March 2021
Published: 01 April 2021

Citation:
Li Z, Li X, Lam W, Cao Y, Han H, Zhang X, Fang J, Xiao K and Zhou F (2021) Safety and Activity of Programmed Cell Death 1 Versus Programmed Cell Death Ligand 1 Inhibitors for Platinum-Resistant Urothelial Cancer: A Meta-Analysis of Published Clinical Trials. Front. Oncol. 11:629646. doi: 10.3389/fonc.2021.629646

1.69; 95% CI, 0.95–3.01; $P = 0.074$) of anti–PD-1 therapy were comparable to those of anti–PD-L1 therapy. The RMST values at the 12-month follow-up were 9.4 months (95% CI,: 8.8–10.0) for anti–PD-1 therapy and 9.3 months (95% CI, 8.8–9.7) for anti–PD-L1 therapy (z = 0.26, $P = 0.794$). There was no significant difference between patients in the anti–PD-1 and anti–PD-L1 groups (12-month overall survival (OS): 43% versus 42%, $P = 0.765$. $I^2 = 0$; $P = 0.999$; HR, 0.95; 95% CI, 0.83–1.09; $P = 0.474$).

Conclusions: The results of our systematic comparison suggest that anti–PD-1 therapy exhibits better antitumor activity than anti–PD-L1 therapy, with comparable safety profiles and survival outcomes. These findings may contribute to enhanced treatment awareness in patients with platinum-resistant UC.

Keywords: immunotherapy, urologic neoplasms, review, programmed cell death 1 receptor, programmed cell death 1 ligand

INTRODUCTION

Advanced or metastatic urothelial cancer (UC) patients have a poor prognosis (1, 2), and platinum-based first-line chemotherapy is the standard treatment option for these patients (1, 3–5). However, the median overall survival (OS) of UC patients who benefit from combination chemotherapy regimens is only 14 to 15 months (1). When first-line chemotherapy resistance occurs, other regimens have limited efficacy, and these patients have an OS of approximately 6 months (3, 6, 7).

Immune checkpoint inhibitors including programmed death 1 (PD-1) and programmed death 1 programmed death ligand 1 (PD-L1) treatment represent a breakthrough in the treatment of advanced or metastatic UC (8, 9), and the safety and activity of anti–PD-1/PD-L1 therapy for advanced or metastatic UC patients have been confirmed (1). In a multicenter, phase 3 randomized trial (KEYNOTE-045), pembrolizumab showed encouraging survival benefits over chemotherapy in advanced/metastatic, platinum-refractory UC (10, 11). Atezolizumab was also confirmed to have a clinical benefit, as the survival of the immunotherapy group was higher than that of the chemotherapy group (12–15).

Studies have confirmed that the mechanism divergence in the inhibitory pathway influences the clinical effects of PD-1 and PD-L1 therapy (16–18). However, the differences between anti–PD-1 and anti–PD-L1 in advanced or metastatic UC patients have raised uncertainties. A network meta-analysis that compared the survival of patients with PD-1 versus PD-L1 blockade included only two studies, limiting the amount of data available for analysis (19).

In this meta-analysis, we used a well-designed mirror principle strategy that included screening and pairing trial characteristics to adjust for indirect comparisons (20). The durable response rates, survival, and tolerability of anti–PD-1/PD-L1 therapy in patients with platinum-resistant UC were strictly assessed.

Abbreviations: AE, adverse event; CI, confidence interval; CR, complete remission; DCR, disease control rate; HR, hazard ratio; OR, odds ratios; ORR, objective response rate; OS, overall survival; PD, progressive disease; PD-1/L1, programmed death 1/ligand 1; PFS, progression-free survival; RMST, restricted mean survival time; PR, partial response; SD, stable disease; UC, urothelial cancer.

METHODS

Search Strategy

Literature Search Strategy

Following the Preferred Reporting Items for Systematic Review and Meta- Analyses (PRISMA) statement, the strategy of the study was determined in advance and uploaded to the PROSPERO online platform. PubMed, Embase, and the Cochrane Library were searched for studies published up to August 2020. The following medical subject heading (MeSH) terms and their combinations were searched in the [Title/Abstract] field: PD-1, PD-L1, programmed death receptor 1, programmed death receptor ligand 1, immune checkpoint inhibitors, and urothelial carcinoma.

Inclusion and Exclusion Criteria

Eligible studies included the following: (1) patients with advanced or metastatic UC; (2) anti–PD-1/PD-L1 treatment; (3) patients with platinum-resistant disease; (4) clinical trials (phase I, II or III); (5) ≥20 patients who reported responses; and (6) published in the English language. Studies including anti–PD-/PD-L1 treatment with other immunotherapies, anti–PD-/PD-L1 neoadjuvant treatment, and anti–PD-/PD-L1 as maintenance treatment and retrospective studies were excluded. For duplicate publications, only the most recent and complete publication was included.

Data Extraction

Xueying Li and Zaishang Li independently extracted and summarized the information. A senior researcher (Hui Han) served as the adjudication author and resolved any disagreements. Disagreements among all authors were resolved *via* discussion. The following information was extracted from the studies: first author, year of publication, phase of trials, National Clinical Trial number, clinical trial name, treatments, number of patients, sex, age, physical condition score, follow-up time, objective response rate (ORR), progression-free survival (PFS), OS, and adverse events (AEs). The level of evidence for the evaluated studies was assessed according to the Grading of Recommendations Assessment, Development and Evaluation (GRADE) system and the Oxford system (21, 22).

Statistical Analysis

The mirror principle was applied to compare anti–PD-1 and anti–PD-L1 therapies (20). The studies were matched based on characteristics including immunotherapy drugs, therapeutic schedule, clinical trial phase, previous treatments, lines of treatment, PD-L1 expression level, Eastern Cooperative Oncology Group (ECOG) performance status, and sex ratio. Studies lacking a relevant variable, for example, the IMvigor130 trial, were also eligible for this study. Only successfully matched studies were further analyzed.

The primary outcome was the ORR. The secondary outcomes were the disease control rate (DCR), AEs, and OS. The AEs were evaluated according to human body systems. Survival data were reconstructed with Engauge software for direct comparisons (19, 23). Reconstructed survival data meta-analysis methods were used to estimate the restricted mean survival time (RMST) up to 12 months and assessed using the method described by Grambsch and Therneau (24–26). RMST analyses were conducted with R software (survRM2 and metafor packages).

The survival rate of affected patients was expressed as the hazard ratio (HR), and the presence of lymph node metastasis was expressed as an odds ratios (OR) (27). Stata version 12 (Stata Corp, College Station, TX, USA) was used for comparisons of the HR or OR and their 95% confidence intervals (CIs). Specified subgroup analyses were conducted for studies that included immune checkpoint inhibitors and other lines of treatment. Statistical heterogeneity between studies was assessed using the chi-square test with a random-effects model if the *P* value was <0.10; otherwise, a fixed-effects model was used. Sensitivity analyses were performed for high-quality studies. Funnel plots, and Begg's and Egger's tests were used to screen for potential publication bias.

RESULTS

Study Selection and Characteristics

Eight studies including 1,666 advanced or metastatic UC patients (1,021 patients with anti–PD-L1 treatment and 645 patients with anti–PD-1 treatment) met the inclusion criteria (**Figure 1**). Detailed characteristics are summarized in **Table 1**. The JAVELIN Solid trial (dose-expansion cohort) (34), in which 90% of patients with ≥1% PD-L1 expression were given avelumab, was matched with the KEYNOTE-012 trial (30). The level of evidence according to the GRADE and Oxford systems for the evaluated studies is shown in **Table 1**. **Table 2** shows the matched outcomes using the mirror principle (32).

The studies included two anti–PD-1 drugs (two studies on pembrolizumab and two studies on nivolumab) and three anti–PD-1 trials (two studies on atezolizumab, one study on avelumab, and one study on durvalumab). The sensitivity analysis, Begg's test and Egger's test showed that no bias existed in the selected studies.

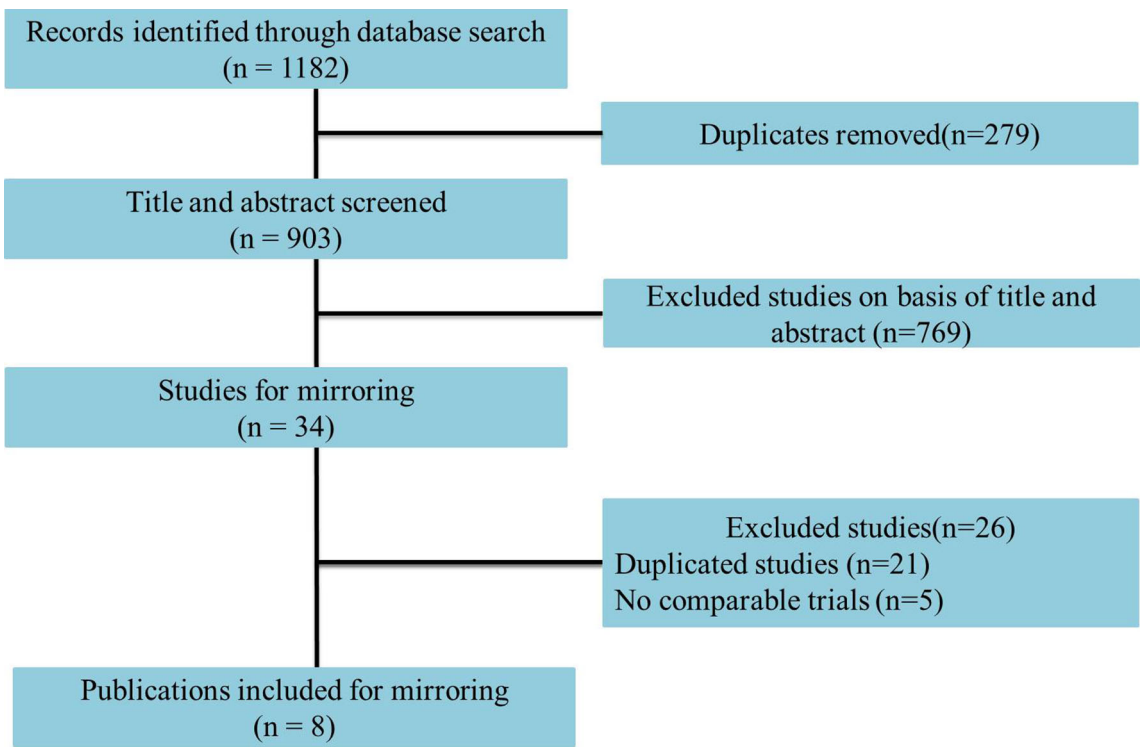

FIGURE 1 | Flowchart of study selection.

TABLE 1 | The characteristics of included trials.

Author	Year	NCT Number	RCT name	Clinical Trial Phase	Intervention	Total (n)	Median Age (range)	Male n(%)	ECOGPS=0 n(%)	MPs Median, months (95% CI)	mOS Median, months (95% CI)	Follow-up (month) Median, months (range or IQR)	Level of evidence according to the GRADE system	Level of evidence according to the Oxford System
Fradet et al. (11)	2019	NCT02256436	KEYNOTE-045	III	Pembrolizumab	270	67 (29–88)	200 (74)	119 (44)	2.1 (2.0–2.2)	10.1 (8.0–12.3)	27.7 (median)	Grade 1	1b
Powles et al. (28)	2018	NCT02302807	IMvigor211	III	Atezolizumab	467	67 (43–88)	81 (70)	61 (53)	NA	8.6 (7.8–9.6)	17.3 (range, 0–24·5)	Grade 1	1b
Ohyama et al. (29)	2019	NCT 02387996	CheckMate 275	II	Nivolumab	270	66 (38–90)	211 (78)	145 (54)	1.9 (1.9–2.3)	8.6 (6.1–11.3)	33.7 (minimum)	Grade 2	2b
Rosenberg et al. (30)	2016	NCT02108652	IMvigor210 (Cohort 2)	II	Atezolizumab	310	66 (32–91)	241 (78)	117 (38)	2.7 (2.1–3.9)	7.9 (6.6–9.3)	11.7 (IQR, 11·4–12·2)	Grade 2	2b
Sharma et al. (31)	2016	NCT01928394	CheckMate 032	I/II	Nivolumab	78	66 (31–85)	54 (69)	42 (54)	NA	9.7 (7.3–16.2)	15.2 (IQR, 12·9–16·8)	Grade 2	2b
Powles et al. (32)	2017	NCT01693562	Study 1108	I/II	Durvalumab	191	67 (34–88)	136 (71)	64 (34)	1.5 (1.4–1.9)	18.2 (8.1-NE)	5.8 (range, 0.4–25.9)	Grade 2	2b
Plimack et al. (33)	2017	NCT01848834	KEYNOTE-012	Ib	Pembrolizumab	33	70 (44–85)	23 (70)	9 (27)	2 (2–4)	13 (5–20)	13 (IQR, 5–23)	Grade 2	2b
Apolo et al. (34)	2017	NCT01772004	JAVELIN Solid (dose-expansion cohort)	Ib	Avelumab	44	68 (63–73)	30 (68)	19 (43)	2.9 (1.5–4.4)	13.7 (8.5-NE)	16.5 (IQR, 15.8–16.7)	Grade 2	2b

IQR, interquartile range; HR, hazard ratio; NA, not available, ICI, immune checkpoint inhibitor; Ctl, control.

Antitumor Activity

The ORR of anti–PD-L1 therapy was 15% (95% CI, 13%–17%) for all studies combined (**Figure 2A**). The combined ORR of anti–PD-1 therapy was 22% (95% CI, 18%–25%) (**Figure 2B**).

After matching, the proportion of the treated population with a confirmed objective response was higher with anti–PD-1 therapy than with anti–PD-L1 therapy (I^2 = 0; P = 0.966; HR, 1.60; 95% CI, 1.23–2.07; P < 0.001) among advanced or metastatic UC patients after progression on platinum-based chemotherapy (**Figure 3A**). According to the subgroup analysis, the ORR was also higher with anti–PD-1 therapy than with anti–PD-L1 therapy in studies with a sample size >50 (I^2 = 0%; P = 0.875; HR, 1.60; 95% CI, 1.22–2.08; P < 0.001).

The DCR was also higher with anti–PD-1 therapy than with anti–PD-L1 therapy in all included studies (I^2 = 30.6%; P = 0.229; HR, 1.35; 95% CI, 1.10–1.66; P = 0.004. **Figure 3B**) and in studies with a sample size >50 (I^2 = 0%; P = 0.404; HR, 1.40; 95% CI, 1.13–1.72; P = 0.002).

However, the progressive disease rate of the anti–PD-1 group was comparable to that of the anti–PD-L1 group (I^2 = 41.7%; P = 0.162; HR, 0.82; 95% CI, 0.62–1.10; P = 0.189). The investigator-assessed antitumor activity and median duration of response are shown in **Table 3**.

Safety Analysis

The treatment-related AEs (I^2 = 78.3%; P = 0.003; OR, 1.09; 95% CI, 0.65–1.84; P = 0.741) and grade 3–5 treatment-related AEs (I^2 = 68.5%; P = 0.023; OR, 1.69; 95% CI, 0.95–3.01; P = 0.074) associated with anti–PD-1 therapy were comparable to those of anti–PD-L1 therapy. Various AEs are shown in **Figure 4** and **Table 3**.

No significant difference was found among treatment-related AEs leading to treatment discontinuation (I^2 = 58.1%; P = 0.067; OR, 1.59; 95% CI, 0.70–3.60; P = 0.264) and AEs leading to death (I^2 = 0; P = 0.524; OR, 2.27; 95% CI, 0.80–6.50; P = 0.127), as shown in **Figure 4A**. Among AEs with an incidence ≥1%, there were no AEs that occurred more frequently in the PD-1 group (**Figure 4B**).

Survival

The median OS times of patients with anti–PD-L1 therapy and anti–PD-1 therapy were 8.4 months (95% CI, 7.7–9.2), and 9.8 months (95% CI, 8.3–11.4), respectively, in all studies combined.

In an analysis that considered time separately, the number of anti–PD-1–treated patients at risk of death was similar to that of the anti–PD-L1-treated group at 6 months (I^2 = 91.2%; P = 0; OR, 1.65; 95% CI, 0.76–3.57; P = 0.204). At 12 months, the number of anti–PD-1–treated patients at risk of death was higher than that of anti–PD-L1–treated patients (I^2 = 87.8%; P = 0; OR, 2.17; 95% CI, 1.04–4.44; P = 0.033).

However, the RMST values at the 12-month follow-up were 9.4 months (95% CI, 8.8–10.0) for anti–PD-1 therapy and 9.3 months (95% CI, 8.8–9.7) for anti–PD-L1 therapy (z = 0.26, P = 0.794).

The reconstructed survival data were highly consistent with the published data. The Kaplan-Meier (KM) curves of patients in

TABLE 2 | The indirect comparison of selected studies based on the mirror principle.

Matched groups	RCT name	Immunotherapy drug	Therapeutic schedule	Clinical trial Phase	Therapeutic schedule	Lines of Treatment	PD-L1 status	ECOG-PS	Male (%) ± 2%
1	KEYNOTE-045	PD-L1	Pembrolizumab	III	Platinum-based chemotherapy	≤3	All	0–1**	72% (+2%)
	IMvigor211	PD-1	Atezolizumab	III	Platinum-based chemotherapy	≤3	All	0–1	72% (–2%)
2	CheckMate 275	PD-L1	Nivolumab	II	Platinum-based chemotherapy	2	All	0–1***	78% (0)
	IMvigor210 (Cohort 2)	PD-1	Atezolizumab	II	Platinum-based chemotherapy	2	All	0–1	78% (0)
3	CheckMate 032	PD-L1	Nivolumab	I/II	Platinum-based chemotherapy	2	All	0–1	70% (–1%)
	Study 1108	PD-1	Durvalumab	I/II	Platinum-based chemotherapy	2	All	0–1	70% (+1%)
4	KEYNOTE-012	PD-L1	Pembrolizumab	Ib	Previous treatment, including platinum-based therapy	≥1	≥1% PD-L1 expression	0–1	69% (+1%)
	JAVELIN Solid (dose-expansion cohort)	PD-1	Avelumab	Ib	Platinum-based chemotherapy	≥1	≥1% PD-L1 expression*	0-1	69% (-1%)

**90% patients with ≥1% PD-L1 expression; **only 2 (0.7%) patients with ECOG performance status of 2; ***only one (0.4%) patient had ECOGperformance status of 3.*

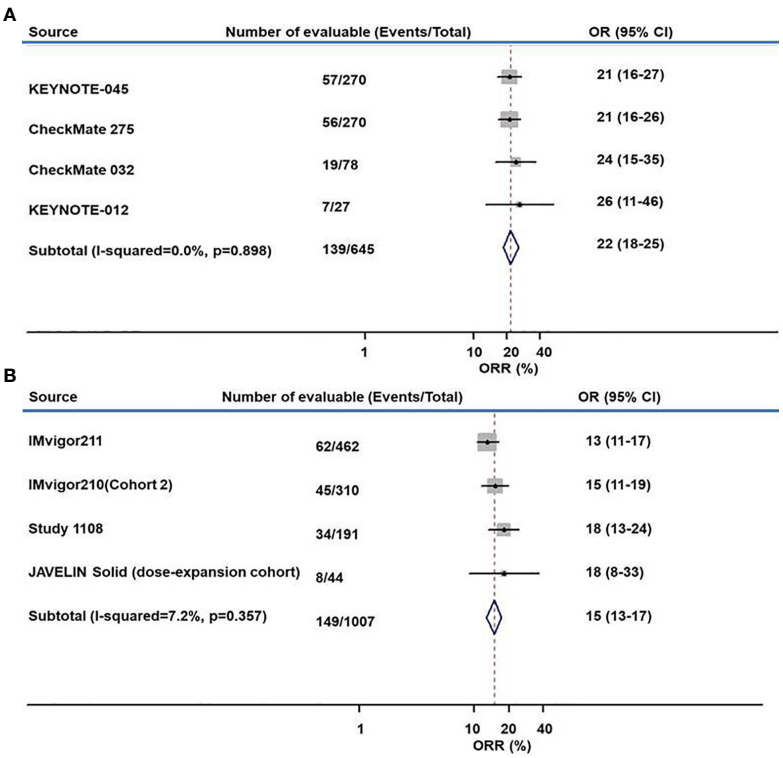

FIGURE 2 | Meta-analysis of pooled odds ratios of an objective response to anti–PD-1 and anti–PD-L1 therapy. **(A)** anti–PD-1, **(B)** anti–PD-L1.

the anti–PD-1 and anti–PD-L1 groups were reconstructed at the common maximum follow-up time (12 months) for direct comparison (**Figure 5A**). No significant difference was observed between patients in the anti–PD-1 and anti–PD-L1 groups (12-month OS: 43% versus 42%, $P = 0.765$. $I^2 = 0$; $P = 0.999$; HR, 0.95; 95% CI, 0.83–1.09; $P = 0.474$, **Figure 5B**).

DISCUSSION

In this study, we first used a well-designed mirror principle strategy that involved screening and pairing trial characteristics to minimize the potential bias in patients with platinum-resistant UC (20). The systematic review and meta-analysis was first

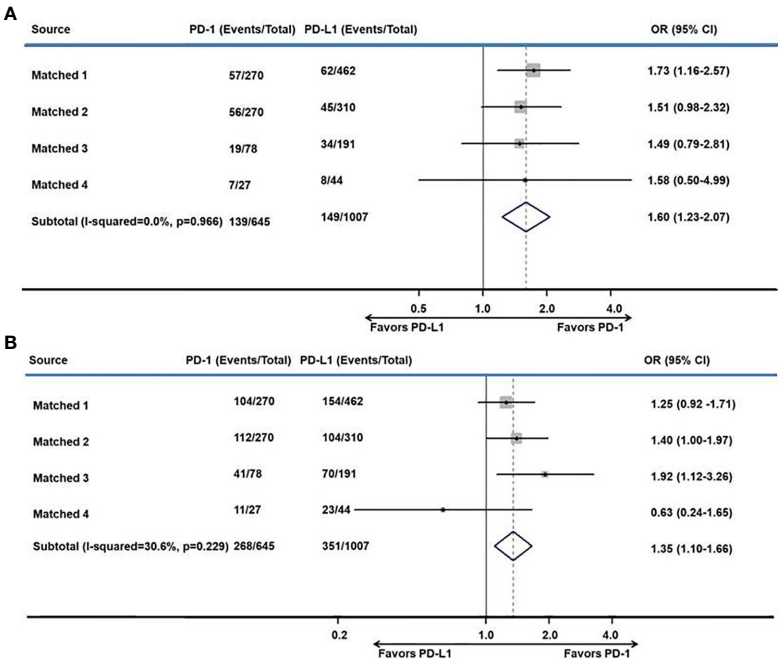

FIGURE 3 | Meta-analysis of pooled odds ratios of a tumor response to anti–PD-1 versus anti–PD-L1 therapy. **(A)** ORR, **(B)** DCR.

adjusted for direct comparisons of anti–PD-1 and anti–PD-L1 therapy. The results suggested that anti–PD-1 therapy exhibited better antitumor activity than anti–PD-L1 therapy, with an acceptable safety profile.

Immune checkpoint inhibitors have remarkable clinical effects after progression with platinum-based chemotherapy (13, 33, 34). A meta-analysis showed that the ORR of immune-checkpoint inhibitors was 17.7% (*95% CI, 16%–20%*) (35). In another meta-analysis, the ORR of second-line or later treatment with immune checkpoint inhibitors was 18% (*95%* CI, 15%–22%) (8). Due to lack of head-to-head research or appropriate statistical methods, the difference in ORRs between patients treated with anti–PD-1 and anti–PD-L1 therapy has not been examined. Our results showed that the ORR of anti–PD-L1 therapy was 15% (95% CI, 15%–17%), and the ORR of anti–PD-1 therapy was 22% (95% CI, 18%–25%). Patient characteristics were matched using the mirror principle to minimize potential bias, and this method has been shown to be effective (20). With the mirror principle, the overall results showed that anti–PD-1 therapy exhibited better antitumor activity than anti–PD-L1 therapy in terms of the ORR and DCR.

The safety profiles of both therapies were acceptable. These immune checkpoint inhibitors were well tolerated in previous trials (13, 28, 31, 36). Grade 1–2 AEs were the most frequent treatment-related AEs and were manageable with expectant treatment (1, 15). In this analysis, the treatment-related AEs of anti–PD-1 therapy were comparable to those of anti–PD-L1 therapy. A network meta-analysis that included only two studies showed that pembrolizumab had advantages over atezolizumab in terms of serious AEs (9). However, we found that the incidence of treatment-related AEs and grade 3–5 treatment-related AEs associated with anti–PD-1 therapy were comparable to those of anti–PD-1 therapy.

In a previous study, immunotherapies had more obvious survival benefits than chemotherapy (9, 35). Even for monotherapy, immune checkpoint inhibitors also has delightful prognosis. The IMvigor130 trail provided evidence to support that anti–PD-L1 therapy plus chemotherapy can prolong the PFS of urothelial carcinoma patients (15). The Keynote-045 and IMvigor211 studies also demonstrated that the OS rate for pembrolizumab treatment was higher than that of chemotherapy in patients with platinum-resistant UC (11, 29). There were only two trials, which had insufficient power, that indicated no significant differences between PD-1 and PD-L1 blockade (19, 20). Using the same statistical methods, the median OS times with anti–PD-L/PD-L1 therapy were 8.4 months and 9.8 months, respectively, in all studies combined. At the common maximum follow-up time (12 months), although the rate of death of anti–PD-1–treated patients was lower, the OS of anti–PD-1–treated patients was comparable to that of anti–PD-L1–treated patients.

Differences exist in the mechanism of action between PD-1 and PD-L1 (16, 37, 38), which might explain the clinical differences in theory. PD-1 antibodies can bind to PD-1 to its ligands (PD-L1 and PD-L2), however, the interaction of PD-1 and PD-L2 remains intact, which may inhibit activation of T cells in PD-L1 antibodies (20). Therefore, the tumor might escape antitumor immune response through the PD-1/PD-L2 axis when

TABLE 3 | Adverse events that occurred during the trial period.

Variable	Matched 1		Matched 2		Matched 3		Matched 4	
	anti–PD-L1	anti–PD-1	anti–PD-L1	anti–PD-1	anti–PD-L1	anti–PD-1	anti–PD-L1	anti–PD-1
Objective response								
No. objective response (n/N)	62/462	57/270	45/310	56/270	34/191	19/78	8/44	7/27
ORR (%)	13 (11–17)	21 (16–27)	15 (11–19)	21 (16–26)	18 (13–24)	24 (15–35)	18 (8–33)	26 (11–46)
DCR n (%)	154 (33)	104 (39)	104 (34)	112 (42)	70 (37)	41 (53)	23 (52)	11 (41)
CR n (%)	16 (3)	25 (9)	15 (5)	18 (7)	7 (4)	5 (6)	5 (11)	3 (1)
PR n (%)	46 (10)	32 (12)	30 (10)	38 (14)	27 (14)	14 (18)	3 (7)	4 (2)
SD n (%)	92 (20)	47 (17)	59 (19)	56 (21)	36 (19)	22 (28)	15 (34)	4 (2)
PD n (%)	240 (52)	131 (49)	159 (51)	111 (41)	88 (46)	30 (38)	15 (34)	14 (52)
Median duration of response	21.7 (13.0–21.7)	NE (1.6–30.0)	NE (2.0–13.7)	20.3 (11.5-31.3)	NE (0.9-19.9)	9.4 (5.7–12.5)	NE (3-NE)	10 (4–22)
Adverse events								
Treatment-related AEs	319 (69)	165 (62)	215 (69)	187 (69)	116 (61)	63 (81)	29 (66)	20 (61)
Treatment-related AEs (3–5 grade)	91 (20)	44 (17)	50 (16)	67 (25)	13 (7)	17 (22)	3 (7)	5 (15)
Treatment-related serious AEs	72 (16)	32 (12)	34 (11)	NA	9 (5)	8 (10)	2 (5)	3 (9)
Treatment-related AEs leading to treatment discontinuation	16 (3)	18 (7)	11 (4)	27 (10)	9 (5)	2 (3)	4 (9)	2 (6)
Treatment-related AEs lead to death	4 (1)	4 (2)	0	3 (1)	2 (1)	1 (1)	0	0
AEs with incidence ≥1%								
Asthenia	51 (43)	17 (5)	21 (8)	19 (6)	0	0	5 (11)	0
Circulatory	0	0	8 (3)	0	3 (2)	0	0	0
Decreased appetite	56 (18)	25 (9)	36 (13)	26 (8)	18 (9)	0	2 (5)	0
Fatigue	116 (25)	37 (14)	93 (34)	52 (17)	37 (19)	28 (36)	9 (20)	6 (18)
Pyrexia	40 (9)	0	28 (10)	17 (5)	15 (8)	0	0	0
Dermatological	120 (26)	84 (32)	54 (20)	120 (39)	33 (17)	39 (50)	8 (18)	2 (6)
Endocrine	53 (45)	19 (5)	0	46 (15)	9 (5)	5 (6)	4 (9)	0
Gastrointestinal	161 (35)	78 (29)	87 (32)	106 (34)	29 (15)	11 (14)	9 (20)	0
Hematogenous	29 (15)	8 (10)	9 (3)	30 (10)	8 (4)	27 (35)	10 (23)	1 (3)
Hepatic	0	0	10 (4)	15 (5)	25 (13)	5 (6)	3 (7)	2 (6)
Renal	0	0	0	5 (2)	1 (1)	1 (1)	0	0
Respiratory	35 (11)	8 (3)	17 (6)	14 (5)	0	7 (9)	1 (2)	0
Others	49 (11)	36 (14)	0	0	11 (6)	10 (13)	0	10 (30)

(1) Circulatory: atrial fibrillation, cardiorespiratory arrest, hypertension, hypotension, myocarditis (2); dermatological: alopecia, dermatitis acneiform, dry mouth, maculopapular, mucosal inflammation, skin reactions, pruritus, rash, stomatitis, tumor flare, uveitis (3); endocrine:adrenal disorder, diabetes, hypothyroidism, hypophysitis, hyperthyroidism, hypersensitivity, hyperglycemia, pituitary disorder, rheumatoid arthritis, thyroid disorder; (4) gastrointestinal: abdominal pain, colitis, constipation, diarrhea, intestinal perforation, increased amylase, nausea, pancreatitis, vomiting (5); hematogenous: anemia, blood alkaline phosphatase increased, creatine phosphokinase, dehydration, hyponatremia, increased blood ALP level, Infusion-related reaction, leukocyte count decreased, lipase elevated, lymphocyte count decreased, neutropenia, thrombocytopenia (6); hepatic: alanine aminotransferase increased, amylase increased, aspartate aminotransferase increased, blood bilirubin increased, hepatitis (7); renal: nephritis, renal failure, urinary tract obstruction (8); respiratory: cough, dyspnea, interstitial lung disease, pneumonitis, respiratory tract infection, respiratory failure, wheezing (9); others: arthralgia, dysgeusia, edema peripheral, muscle spasms, myalgia, myositis, neuromyopathy, pain, paresthesia, peripheral sensory neuropathy, peripheral sensory neuropathy, rhabdomyolysis, toxic encephalopathy.

being treated with anti–PD-L1, which may explain why patients receiving anti–PD-1 therapy had a better response rate than anti–PD-L1 therapy. Studies are ongoing and some patients had subsequent therapies that impact on survival outcomes. The results of this study may provide a reference for clinical studies that contributes to enhancing treatment awareness in patients with platinum-resistant UC.

Several limitations of this study should be noted. 1) Due to the lack of clinical trials, the trials included in this study were relatively limited after matching. However, this illustrates the importance and necessity of this research. 2) Because the details of all studies are not available, the study lacks individual patient data creates an important handicap when comparing and matching. The method used was an indirect comparison. However, the statistical methods were also confirmed (19, 20, 25). This study screened the research through the mirror matching method, which led to the inability of matching analysis of some cancer data. All analyses may be considered exploratory rather than hypothesis-tested in our study. 3) We could not distinguish the differences among various types of drugs. 4) Some information was incomplete. For example, AEs were classified into different systems instead of being analyzed individually. However, the main endpoint of ORR was a better comparison of the outcome than AEs in this study. For a few studies, a subgroup analysis of metastases or PD-L1 expression was not performed. We suggest that subgroup analyses including metastases or PD-L1 expression will provide information for future studies.

CONCLUSION

In summary, the results of our systematic comparison suggest that anti–PD-1 therapy exhibits better antitumor activity than PD-L1 therapy in patients with platinum-resistant UC. The safety profiles and survival outcomes for PD-1 and PD-L1 treatment were comparable. These findings may contribute to enhancing treatment awareness in patients with platinum-resistant UC treatment.

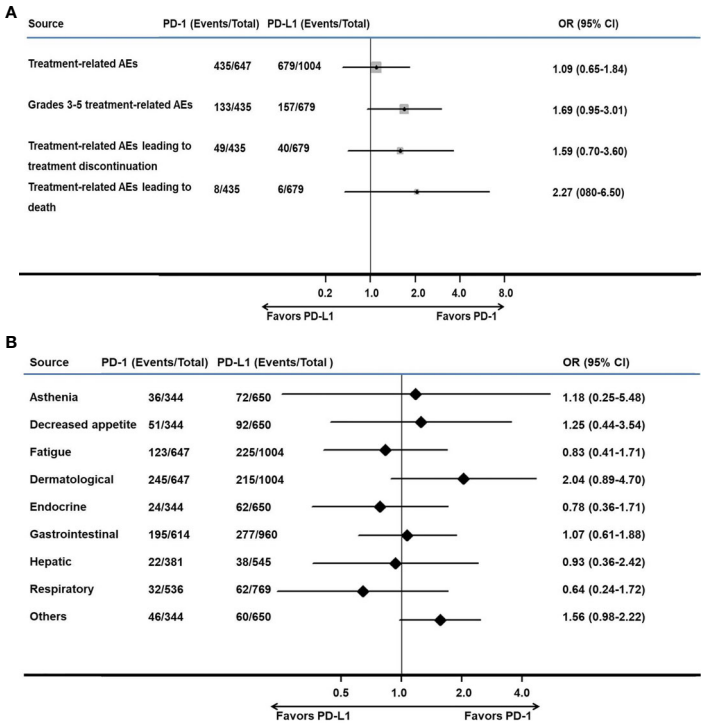

FIGURE 4 | Meta-analysis of pooled odds ratios of adverse events of anti–PD-1 versus anti–PD-L1 therapy. **(A)** adverse events with anti–PD-1 versus anti–PD-L1 therapy, **(B)** adverse events with an incidence ≥1% for anti–PD-1 versus anti–PD-L1 therapy.

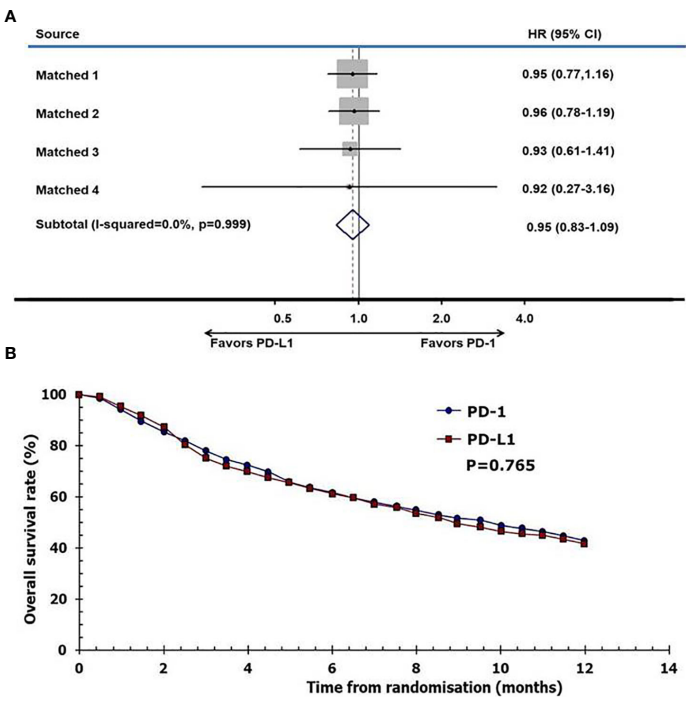

FIGURE 5 | Pooled hazard ratio of survival. **(A)** meta-analysis of pooled hazard ratios of overall survival outcomes of anti–PD-1 versus anti–PD-L1 therapy, **(B)** overall survival of patients with immune checkpoint inhibitors using reconstructed survival data.

DATA AVAILABILITY STATEMENT

The raw data supporting the conclusions of this article will be made available by the authors, without undue reservation.

AUTHOR CONTRIBUTIONS

FZ and KX had full access to all the data in the study and take responsibility for the integrity of the data and the accuracy of the data analysis. Study conception and design: ZL, XL, HH, and FZ. Acquisition of data: ZL, XL, and HH. Analysis and interpretation of data: all authors. Drafting of the manuscript: ZL and XL. Critical revision of the manuscript for important intellectual content: all authors. Statistical analysis: ZL, XL, FZ, and HH. Obtaining funding: ZL. Administrative, technical, or material support: FZ. Supervision: FZ. All authors contributed to the article and approved the submitted version.

FUNDING

This work was supported by the National Natural Science Foundation of China (Grant No. 81902610) and Science and Technology Planning Project of Shenzhen Municipality (CN) (JCYJ20190807145409328).

ACKNOWLEDGMENTS

We are grateful to the authors of the trials, the enrolled patients, their families, and the referring physicians.

REFERENCES

1. Flaig TW, Spiess PE, Agarwal N, Bangs R, Boorjian SA, Buyyounouski MK, et al. Bladder Cancer, Version 3.2020, NCCN Clinical Practice Guidelines in Oncology. *J Natl Compr Canc Netw* (2020) 18(3):329–54. doi: 10.6004/jnccn.2020.0011
2. Nakagawa T, Taguchi S, Kanatani A, Kawai T, Ikeda M, Urakami S, et al. Oncologic Outcome of Metastasectomy for Urothelial Carcinoma: Who Is the Best Candidate? *Ann Surg Oncol* (2017) 24(9):2794–800. doi: 10.1245/s10434-017-5970-8
3. Kaufman D, Raghavan D, Carducci M, Levine EG, Murphy B, Aisner J, et al. Phase II trial of gemcitabine plus cisplatin in patients with metastatic urothelial cancer. *J Clin Oncol Off J Am Soc Clin Oncol* (2000) 18(9):1921–7. doi: 10.1200/JCO.2000.18.9.1921
4. Loehrer PJ Sr, Einhorn LH, Elson PJ, Crawford ED, Kuebler P, Tannock I, et al. A randomized comparison of cisplatin alone or in combination with methotrexate, vinblastine, and doxorubicin in patients with metastatic urothelial carcinoma: a cooperative group study. *J Clin Oncol Off J Am Soc Clin Oncol* (1992) 10(7):1066–73. doi: 10.1200/JCO.1992.10.7.1066
5. Scher HI. A randomized comparison of cisplatin alone or in combination with methotrexate, vinblastine, and doxorubicin in patients with metastatic urothelial carcinoma: a cooperative group study. *J Urol* (1992) 148(5):1625–6.
6. Galsky MD, Mironov S, Iasonos A, Scattergood J, Boyle MG, Bajorin DF. Phase II trial of pemetrexed as second-line therapy in patients with metastatic urothelial carcinoma. *Invest New Drugs* (2007) 25(3):265–70. doi: 10.1007/s10637-006-9020-9
7. Vaughn DJ, Broome CM, Hussain M, Gutheil JC, Markowitz AB. Phase II trial of weekly paclitaxel in patients with previously treated advanced urothelial cancer. *J Clin Oncol Off J Am Soc Clin Oncol* (2002) 20(4):937–40. doi: 10.1200/JCO.2002.20.4.937
8. Tafuri A, Smith DD, Cacciamani GE, Cole S, Shakir A, Sadeghi S, et al. Programmed Death 1 and Programmed Death Ligand 1 Inhibitors in Advanced and Recurrent Urothelial Carcinoma: Meta-analysis of Single-Agent Studies. *Clin Genitourin Cancer* (2020) 351–60. doi: 10.1016/j.clgc.2020.01.004
9. Wang H, Liu J, Fang K, Ke C, Jiang Y, Wang G, et al. Second-line treatment strategy for urothelial cancer patients who progress or are unfit for cisplatin therapy: a network meta-analysis. *BMC Urol* (2019) 19(1):125. doi: 10.1186/s12894-019-0560-7
10. Vaughn DJ, Bellmunt J, Fradet Y, Lee JL, Fong L, Vogelzang NJ, et al. Health-Related Quality-of-Life Analysis From KEYNOTE-045: A Phase III Study of Pembrolizumab Versus Chemotherapy for Previously Treated Advanced Urothelial Cancer. *J Clin Oncol Off J Am Soc Clin Oncol* (2018) 36(16):1579–87. doi: 10.1200/JCO.2017.76.9562
11. Fradet Y, Bellmunt J, Vaughn DJ, Lee JL, Fong L, Vogelzang NJ, et al. Randomized phase III KEYNOTE-045 trial of pembrolizumab versus paclitaxel, docetaxel, or vinflunine in recurrent advanced urothelial cancer: results of >2 years of follow-up. *Ann Oncol* (2019) 30(6):970–6. doi: 10.1093/annonc/mdz127
12. Petrylak DP, Powles T, Bellmunt J, Braiteh F, Loriot Y, Morales-Barrera R, et al. Atezolizumab (MPDL3280A) Monotherapy for Patients With Metastatic Urothelial Cancer: Long-term Outcomes From a Phase 1 Study. *JAMA Oncol* (2018) 4(4):537–44. doi: 10.1001/jamaoncol.2017.5440
13. Pal SK, Hoffman-Censits J, Zheng H, Kaiser C, Tayama D, Bellmunt J. Atezolizumab in Platinum-treated Locally Advanced or Metastatic Urothelial Carcinoma: Clinical Experience from an Expanded Access Study in the United States. *Eur Urol* (2018) 73(5):800–6. doi: 10.1016/j.eururo.2018.02.010
14. Perez-Gracia JL, Loriot Y, Rosenberg JE, Powles T, Necchi A, Hussain SA, et al. Atezolizumab in Platinum-treated Locally Advanced or Metastatic Urothelial Carcinoma: Outcomes by Prior Number of Regimens. *Eur Urol* (2018) 73(3):462–8. doi: 10.1016/j.eururo.2017.11.023
15. Galsky MD, Arija JAA, Bamias A, Davis ID, De Santis M, Kikuchi E, et al. Atezolizumab with or without chemotherapy in metastatic urothelial cancer (IMvigor130): a multicentre, randomised, placebo-controlled phase 3 trial. *Lancet* (2020) 395(10236):1547–57. doi: 10.1016/S0140-6736(20)30230-0
16. Butte MJ, Keir ME, Phamduy TB, Sharpe AH, Freeman GJ. Programmed death-1 ligand 1 interacts specifically with the B7-1 costimulatory molecule to inhibit T cell responses. *Immunity* (2007) 27(1):111–22. doi: 10.1016/j.immuni.2007.05.016
17. Chen L, Han X. Anti-PD-1/PD-L1 therapy of human cancer: past, present, and future. *J Clin Invest* (2015) 125(9):3384–91. doi: 10.1172/JCI80011
18. Yearley JH, Gibson C, Yu N, Moon C, Murphy E, Juco J, et al. PD-L2 Expression in Human Tumors: Relevance to Anti-PD-1 Therapy in Cancer. *Clin Cancer Res* (2017) 23(12):3158–67. doi: 10.1158/1078-0432.CCR-16-1761
19. Niglio SA, Jia R, Ji J, Ruder S, Patel VG, Martini A, et al. Programmed Death-1 or Programmed Death Ligand-1 Blockade in Patients with Platinum-resistant Metastatic Urothelial Cancer: A Systematic Review and Meta-analysis. *Eur Urol* (2019) 76(6):782–9. doi: 10.1016/j.eururo.2019.05.037
20. Duan J, Cui L, Zhao X, Bai H, Cai S, Wang G, et al. Use of Immunotherapy With Programmed Cell Death 1 vs Programmed Cell Death Ligand 1 Inhibitors in Patients With Cancer: A Systematic Review and Meta-analysis. *JAMA Oncol* (2019) 375–84. doi: 10.1001/jamaoncol.2019.5367
21. Atkins D, Best D, Briss PA, Eccles M, Falck-Ytter Y, Flottorp S, et al. Grading quality of evidence and strength of recommendations. *BMJ* (2004) 328(7454):1490. doi: 10.1136/bmj.328.7454.1490
22. Schunemann HJ, Oxman AD, Brozek J, Glasziou P, Jaeschke R, Vist GE, et al. Grading quality of evidence and strength of recommendations for diagnostic tests and strategies. *BMJ* (2008) 336(7653):1106–10. doi: 10.1136/bmj.39500.677199.AE

23. Tierney JF, Stewart LA, Ghersi D, Burdett S, Sydes MR. Practical methods for incorporating summary time-to-event data into meta-analysis. *Trials* (2007) 8:16. doi: 10.1186/1745-6215-8-16
24. Grambsch P, Therneau TM. Proportional hazards tests and diagnostics based on weighted residuals. *Biometrika* (1994) 81(3):515–26. doi: 10.2307/2337123
25. Le CT, Grambsch PM, Louis TA. Association between survival time and ordinal covariates. *Biometrics* (1994) 50(1):213–9.
26. Smith CT, Williamson PR, Marson AG. Investigating heterogeneity in an individual patient data meta-analysis of time to event outcomes. *Stat Med* (2005) 24(9):1307–19. doi: 10.1002/sim.2050
27. Hartung J, Knapp G, Sinha BK. *Statistical Meta-analysis With Applications*. Hoboken, NJ: John Wiley & Sons (2008). doi: 10.1002/9780470386347
28. Powles T, O'Donnell PH, Massard C, Arkenau HT, Friedlander TW, Hoimes CJ, et al. Efficacy and Safety of Durvalumab in Locally Advanced or Metastatic Urothelial Carcinoma: Updated Results From a Phase 1/2 Open-label Study. *JAMA Oncol* (2017) 3(9):e172411. doi: 10.1001/jamaoncol.2017.2411
29. Ohyama C, Kojima T, Kondo T, Naya Y, Inoue T, Tomiya Y, et al. Nivolumab in patients with unresectable locally advanced or metastatic urothelial carcinoma: CheckMate 275 2-year global and Japanese patient population analyses. *Int J Clin Oncol* (2019) 24(9):1089–98. doi: 10.1007/s10147-019-01450-w
30. Rosenberg JE, Hoffman-Censits J, Powles T, van der Heijden MS, Balar AV, Necchi A, et al. Atezolizumab in patients with locally advanced and metastatic urothelial carcinoma who have progressed following treatment with platinum-based chemotherapy: a single-arm, multicentre, phase 2 trial. *Lancet* (2016) 387(10031):1029–20. doi: 10.1016/S0140-6736(16)00561-4
31. Sharma P, Callahan MK, Bono P, Kim J, Spiliopoulou P, Calvo E, et al. Nivolumab monotherapy in recurrent metastatic urothelial carcinoma (CheckMate 032): a multicentre, open-label, two-stage, multi-arm, phase 1/2 trial. *Lancet Oncol* (2016) 17(11):1590–8. doi: 10.1016/S1470-2045(16)30496-X
32. Powles T, Duran I, van der Heijden MS, Loriot Y, Vogelzang NJ, De Giorgi U, et al. Atezolizumab versus chemotherapy in patients with platinum-treated locally advanced or metastatic urothelial carcinoma (IMvigor211): a multicentre, open-label, phase 3 randomised controlled trial. *Lancet* (2018) 391(10122):748–57. doi: 10.1016/S0140-6736(17)33297-X
33. Plimack ER, Bellmunt J, Gupta S, Berger R, Chow LQ, Juco J, et al. Safety and activity of pembrolizumab in patients with locally advanced or metastatic urothelial cancer (KEYNOTE-012): a non-randomised, open-label, phase 1b study. *Lancet Oncol* (2017) 18(2):212–20. doi: 10.1016/S1470-2045(17)30007-4
34. Apolo AB, Infante JR, Balmanoukian A, Patel MR, Wang D, Kelly K, et al. Avelumab, an Anti-Programmed Death-Ligand 1 Antibody, In Patients With Refractory Metastatic Urothelial Carcinoma: Results From a Multicenter, Phase Ib Study. *J Clin Oncol Off J Am Soc Clin Oncol* (2017) 35(19):2117–24. doi: 10.1200/JCO.2016.71.6795
35. Sternberg CN, Loriot Y, James N, Choy E, Castellano D, Lopez-Rios F, et al. a Multinational Single-arm Safety Study of Atezolizumab Therapy for Locally Advanced or Metastatic Urothelial or Nonurothelial Carcinoma of the Urinary Tract. *Eur Urol* (2019) 76(1):73–81. doi: 10.1016/j.eururo.2019.03.015
36. Chang SS. Re: Atezolizumab in Patients with Locally Advanced and Metastatic Urothelial Carcinoma Who Have Progressed following Treatment with Platinum-Based Chemotherapy: A Single-Arm, Multicentre, Phase 2 Trial. *J Urol* (2016) 196(6):1637–8. doi: 10.1016/j.juro.2016.09.025
37. Di Nunno V, De Luca E, Buttigliero C, Tucci M, Vignani F, Gatto L, et al. Immune-checkpoint inhibitors in previously treated patients with advanced or metastatic urothelial carcinoma: A systematic review and meta-analysis. *Crit Rev Oncol Hematol* (2018) 129:124–32. doi: 10.1016/j.critrevonc.2018.07.004
38. Galsky MD, Saci A, Szabo PM, Han GC, Grossfeld G, Collette S, et al. Nivolumab in Patients with Advanced Platinum-resistant Urothelial Carcinoma: Efficacy, Safety, and Biomarker Analyses with Extended Follow-up from CheckMate 275. *Clin Cancer Res* (2020) 5120–8. doi: 10.1158/1078-0432.CCR-19-4162
39. Fessas P, Lee H, Ikemizu S. Janowitz T. A molecular and preclinical comparison of the PD-1-targeted T-cell checkpoint inhibitors nivolumab and pembrolizumab. *Semin Oncol* (2017) 44(2):136–40. doi: 10.1053/j.seminoncol.2017.06.002
40. Alsaab HO, Sau S, Alzhrani R, Tatiparti K, Bhise K, Kashaw SK, et al. PD-1 and PD-L1 Checkpoint Signaling Inhibition for Cancer Immunotherapy: Mechanism, Combinations, and Clinical Outcome. *Front Pharmacol* (2017) 8:561. doi: 10.3389/fphar.2017.00561

Conflict of Interest: The authors declare that the research was conducted in the absence of any commercial or financial relationships that could be construed as a potential conflict of interest.

frontiers in Oncology

ORIGINAL RESEARCH
published: 06 April 2021
doi: 10.3389/fonc.2021.637804

Development of a Prognostic AI-Monitor for Metastatic Urothelial Cancer Patients Receiving Immunotherapy

Stefano Trebeschi[1,2,3], *Zuhir Bodalal*[1,2], *Nick van Dijk*[4], *Thierry N. Boellaard*[1], *Paul Apfaltrer*[1,5], *Teresa M. Tareco Bucho*[1,2], *Thi Dan Linh Nguyen-Kim*[1,2,6], *Michiel S. van der Heijden*[4,7], *Hugo J. W. L. Aerts*[1,2,3,8] and *Regina G. H. Beets-Tan*[1,2,9*]

[1] Department of Radiology, The Netherlands Cancer Institute — Antoni van Leeuwenhoek Hospital, Amsterdam, Netherlands, [2] GROW School for Oncology and Developmental Biology, Maastricht University, Maastricht, Netherlands, [3] Artificial Intelligence in Medicine (AIM) Program, Mass General Brigham, Harvard Medical School, Boston, MA, United States, [4] Department of Medical Oncology, The Netherlands Cancer Institute — Antoni van Leeuwenhoek Hospital, Amsterdam, Netherlands, [5] Department of Biomedical Imaging and Image-guided Therapy, Medical University of Vienna, Vienna, Austria, [6] Institute for Diagnostic and Interventional Radiology, University Hospital of Zurich, Zurich, Switzerland, [7] Department of Molecular Carcinogenesis, The Netherlands Cancer Institute — Antoni van Leeuwenhoek Hospital, Amsterdam, Netherlands, [8] Radiology and Nuclear Medicine, Maastricht University, Maastricht, Netherlands, [9] Institute of Regional Health Research, University of Southern Denmark, Odense, Denmark

OPEN ACCESS

Edited by:
Sebastian Kobold,
LMU Munich University Hospital, Germany

Reviewed by:
Guru Sonpavde,
Dana–Farber Cancer Institute, United States
Tingying Peng,
Helmholtz-Gemeinschaft Deutscher Forschungszentren (HZ), Germany

***Correspondence:**
Regina G. H. Beets-Tan
r.beetstan@nki.nl

Specialty section:
This article was submitted to Genitourinary Oncology, a section of the journal Frontiers in Oncology

Received: 04 December 2020
Accepted: 22 February 2021
Published: 06 April 2021

Citation:
Trebeschi S, Bodalal Z, van Dijk N, Boellaard TN, Apfaltrer P, Tareco Bucho TM, Nguyen-Kim TDL, van der Heijden MS, Aerts HJWL and Beets-Tan RGH (2021) Development of a Prognostic AI-Monitor for Metastatic Urothelial Cancer Patients Receiving Immunotherapy. Front. Oncol. 11:637804. doi: 10.3389/fonc.2021.637804

Background: Immune checkpoint inhibitor efficacy in advanced cancer patients remains difficult to predict. Imaging is the only technique available that can non-invasively provide whole body information of a patient's response to treatment. We hypothesize that quantitative whole-body prognostic information can be extracted by leveraging artificial intelligence (AI) for treatment monitoring, superior and complementary to the current response evaluation methods.

Methods: To test this, a cohort of 74 stage-IV urothelial cancer patients (37 in the discovery set, 37 in the independent test, 1087 CTs), who received anti-PD1 or anti-PDL1 were retrospectively collected. We designed an AI system [named prognostic AI-monitor (PAM)] able to identify morphological changes in chest and abdominal CT scans acquired during follow-up, and link them to survival.

Results: Our findings showed significant performance of PAM in the independent test set to predict 1-year overall survival from the date of image acquisition, with an average area under the curve (AUC) of 0.73 ($p < 0.001$) for abdominal imaging, and 0.67 AUC ($p < 0.001$) for chest imaging. Subanalysis revealed higher accuracy of abdominal imaging around and in the first 6 months of treatment, reaching an AUC of 0.82 ($p < 0.001$). Similar accuracy was found by chest imaging, 5–11 months after start of treatment. Univariate comparison with current monitoring methods (laboratory results and radiological assessments) revealed higher or similar prognostic performance. In multivariate analysis, PAM remained significant against all other methods ($p < 0.001$), suggesting its complementary value in current clinical settings.

Conclusions: Our study demonstrates that a comprehensive AI-based method such as PAM, can provide prognostic information in advanced urothelial cancer patients receiving

immunotherapy, leveraging morphological changes not only in tumor lesions, but also tumor spread, and side-effects. Further investigations should focus beyond anatomical imaging. Prospective studies are warranted to test and validate our findings.

Keywords: artificial intelligence, immunotherapy, checkpoint inhibitors, urothelial cancer, treatment monitoring, imaging - computed tomography, response assessment, prognostication

INTRODUCTION

Durable clinical benefit to immune checkpoint inhibitors in metastatic setting led to approval in several malignancies (1–3). Unlike traditional cancer treatments, such as chemotherapy and radiotherapy, which are administered for a predefined amount of time, immunotherapy is generally administered until there are tangible clinical benefits or until progressive disease/adverse events deem it unsuitable—for a maximum of 2 years. To achieve this, an accurate treatment evaluation method is required.

Whole-body Computed Tomography (CT) provides information on the full-picture of the patient. Beyond tumor size dynamics, CT imaging allows assessment of immune-related side-effects and/or disease-related complications.

Therapy response evaluation following CT is measured according to the *response evaluation criteria in solid tumor* (RECIST) (4), or iRECIST, adapted for immunotherapy (5). This involves prospective tracking of preselected lesions by measuring 2-dimensional diameters. Various immune-related toxicities and cancer-related complications that inform clinical practice may also be identified on CT scans, but are not accounted for in current RECIST criteria. So far, a comprehensive quantitative approach that involves quantitative response evaluation and clinically relevant conditions is lacking.

Quantitative approaches, such as radiomics, have been explored in the past (6, 7). While these led to satisfactory results in the field of prognostication, these rely mostly on manual segmentations, which are time-consuming and prone to human operator error. A comprehensive non-invasive method that comprises the assessment of tumor size dynamics and side-effects or other cancer-induced conditions, in an automatic and precise quantitative manner, would be preferable.

Novel techniques of computational imaging and artificial intelligence (AI) can be the basis for quantitative methods for treatment monitoring (8). Specifically, AI algorithms can be seen as methods to capture, measure, and quantify complex highly-variable anatomical phenomena for prognostic purposes, in a robust and time-efficient manner. To this end, we have developed an AI algorithm that performs automated tracking and quantification of morphological changes based on longitudinal CT imaging in immunotherapy treated patients, allowing correlations with overall survival. We term our AI system the *Prognostic AI-monitor* (PAM). Recently, a similar pilot approach was tested in a study on chest imaging of a NSCLC cohort (8), demonstrating accurate response prediction and a correlation with overall survival. In this study, we aim to extend the model to thoracoabdominal imaging, and validate it on a cohort of metastatic urothelial cancer patients treated with anti-PD1/PDL1. The model accuracy will be assessed at various time points within the treatment timeline, and the explicability through qualitative investigation of AI-generated prognostic heatmaps.

MATERIALS AND METHODS

Study Cohort

We retrospectively included stage-IV urothelial cancer patients treated with anti-PDL1 or anti-PD1 monotherapy that had started follow-up imaging at the Netherlands Cancer Institute - Antoni van Leeuwenhoek hospital (NKI-AVL, Amsterdam, The Netherlands) between 07-2014 and 06-2018. Response evaluation was done using regular contrast-enhanced CT scans of the abdomen, chest, or both. For all patients, CT imaging scans acquired between 6 months prior to the start of immunotherapy, up to 2 years after, were collected. Inclusion criteria were high-resolution images (slice thickness $\leq$ 5 mm), and the presence of at least thorax or abdomen in the scan field. As we aim to use AI to track changes across follow-up, patients with $<$ 2 scans, at two different time points, could not be included. These criteria were verified automatically via the DICOM tag, or via the automatic localization algorithm proposed by Zhang et al. (9), respectively. For each patient, we recorded age at start of treatment, date of start of treatment, and date of death. Additionally, to compare PAM with current treatment monitoring standards, we collected parameters of radiological assessments (progression and response), as well as routine clinical blood analyses (hemoglobin, leukocyte count, thrombocyte count, and erythrocyte count). The entire dataset was divided into discovery and an independent test set based on the patients' ID (even IDs were assigned to the discovery set, odd IDs were assigned to the independent test set, creating a 50/50 split). The study was conducted at the NKI-AVL after approval of the local Institutional Review Board (IRBd19-083).

Data Harmonization

A data harmonization protocol was applied to mitigate heterogeneity from typical real-world imaging datasets. This consisted of isotropic linear resampling of the scans at 2 mm, clipping of the Hounsfield units between−120 (fat) and 300 (cancellous bone), and rescaling of the intensities between 0 and 1. All images were cropped and padded to 192 × 192 × 192 voxels (160 axial coordinate for chest imaging).

Prognostic AI-Monitor

PAM is composed of three AI-modules. The first module, termed *localizer*, consisted of a VGG-like convolutional network, tasked to crop out the chest and the abdomen in two separate images, each according to standardized anatomical locations. These were

defined as the space between the lower neck and the lower diaphragm, and the space between the upper diaphragm and the lower pelvis, respectively. The second and third modules, termed *tracker*s, consisted of two instances of the same convolutional network, one trained for chest imaging, and one for abdominal imaging, tasked to quantify morphological changes between pairs of images. We termed these modules the *chest* and *abdominal tracker*, respectively. Their architecture was based on radiological deep learning-based image-to-image registration. At its core, each tracker is tasked to match anatomical landmarks and shapes of two 3D radiological images. In doing so, the network learns to quantify anatomical differences between pairs of scans. We leveraged the tracker network knowledge (i.e., its *latent representation*) to extract quantitative imaging feature vectors representing morphological changes between follow-up scans of the same patient, and fed them into a classifier trained to predict survival. Time from start of treatment, and time between scans were also fed into the classifier, for temporal reference.

Localizer Module

The localizer module was designed following the research of Zhang et al. (9). The authors showed how a convnet trained to sort slices in a specific order (e.g., from head to toe) can be used for anatomical localization. The network followed a siamese learning scheme. It received a pair of CT slices from a single scan, and had to learn which of the two slices would be on top of the other in the original CT scan. The only way for the network to learn to perform this task would be for the network to assign to each anatomical location a number i that would increase from head to toe. Once the training was complete, we used the network to retrieve a specific location by searching for their assigned number (for example, in our case, the upper-most point of the diaphragm was always assigned to be around $i = 25$). This algorithm idea is particularly powerful, as the ground truth (i.e., the order of the slices) can be automatically extracted from the CT scan, and therefore it does not require any manual labeling.

Our localizer module was built largely based on Zhang's architecture design — the exact architecture we used is shown in **Figure 1A**. The network was trained following the same siamese learning scheme of the original research (9). Binary cross-entropy was the loss function chosen, the optimizer was Adam with an initial learning rate of 0.001, and the batch size was set to 8 (i.e., 8 random scans, one random pair of slices per scan). As it was difficult to set a number of epochs (considering it could be based either on the number of scans or on the number of slices), we chose to set a general number of iterations, namely 50,000. RANSAC regression (10) was used to model the relation between the network score and the actual slice number for each scan. We chose RANSAC for its robustness to irregularities provided by the localizer algorithm. **Figure 1B** shows the localizer network applied to a scan.

Tracker Module

The tracker module was designed following the research of Balakrishnan et al. (11) and Zhao et al. (12), as well as our previous work on chest imaging in NSCLC (8). The network receives two images as input (i.e., a moving and fixed one) concatenated along the channel axis. The architecture of the network processes the input in two subsequent parts. The first part, consisting of VGG-like convnet, parses the images through a series of five subsequent convolutional blocks and two fully connected layers, to regress the 12 parameters of the affine transform. This is used to give a linear pre-alignment between the input images, correcting for different patient positions. The second part of the network follows a U-Net architecture (13), where the inputs (i.e., the affine warped moving image and the fixed image) are processed together to regress a displacement field. The displacement field specifies for each voxel a 3D vector. The vector indicates where the voxel in that location of the moving image would be displaced to, in order to match the corresponding anatomical structure in the fixed image. This part of the network consisted of an encoder with four convolutional blocks downsampling the images by half the size via striding, a convolutional latent space with stride of one, and four deconvolutional blocks each upsampling the inputs by double the size via striding. Skip connections were implemented between encoding and decoding layers following the implementation in the original paper. Both affine and deformable parameters are applied to the moving image through a spatial transformation layer.

The network was trained to minimize the correlation coefficient loss (11, 12). Three penalties were also employed to mitigate for unlikely morphological deformations: two on the affine loss (weighted 1/10), and one on the deformable loss (weighted 1/100). We decided to decrease the weight on the deformable loss to give to the model more freedom in modeling abdominal changes. Adam optimizer was used during training, with an initial learning rate of 3×10^{-4}. A curriculum learning scheme was implemented during training, such that the loss would be computed on a decreasingly smoother version of the images. The smoothing was implemented via average pooling, starting with a kernel size of 9, and reduced by 3 at epochs 100, 150, and 175. Batch size was set to 2. To mitigate negative effects resulting from the small batch size, group normalization was employed instead of batch normalization (14). **Figure 2A** shows a detailed overview of the model and the loss used.

Both the localizer and trackers were unbiased toward both cancer and treatment, and could be trained on unlabeled data. Using The Cancer Imaging Archive (TCIA) (15), we collected[1] all available radiological images, and excluded scans with non-axial acquisition, low resolution ($>$ 5 mm), animals (e.g., mice, suine) and phantoms. Based on thorax-abdominal CT scans, we then trained the localizer module on a lymphadenopathy dataset and extracted abdomen slices from all archived CT scans. Next, the isolated set of abdominal CT scans (16–35) were employed to train the abdominal tracker PAM module. We kept a 10% hold out during training to control for overfitting (i.e., patients whose ID were multiples of 10 were held out). At each training iteration, we created a batch by randomly sampling pairs of TCIA's abdominal CT scans. This implies that the network learned, in principle, to register pairs (likely) composed of scans from different patients, or even different datasets. This auxiliary task

[1] Accessed on the 21st of April 2020.

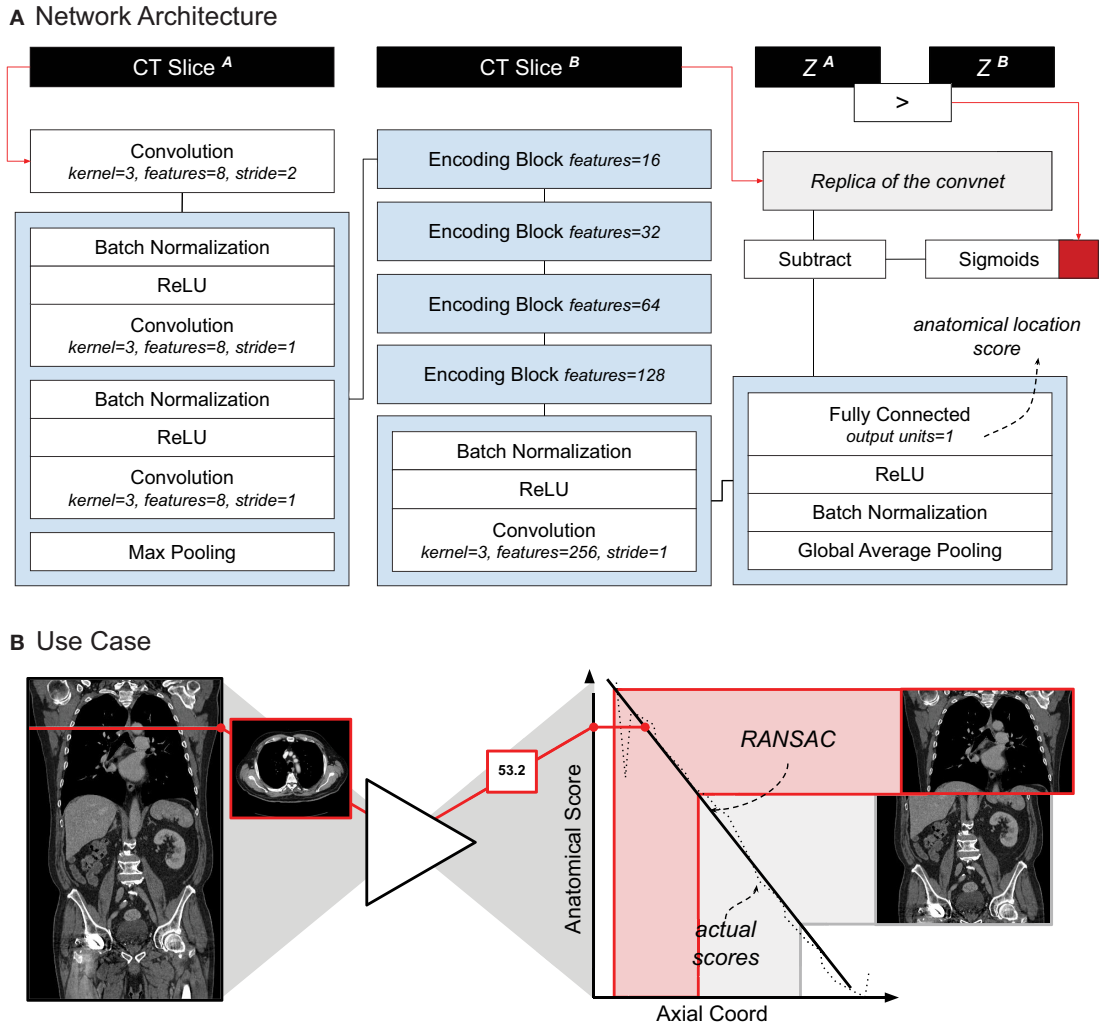

FIGURE 1 | (A) Schematic representation of the localizer architecture and its training. The CT slices in input are axial slices taken from the same CT scan. Z^1 and Z^2 are the axial coordinates of each input slice, respectively. The red square symbolizes the binary cross entropy loss function used during training. **(B)** A use-case of the localizer. Each axial slice is processed through the network to generate a score. A linear relation between the scores and the axial coordinate is estimated. Cropping of the thorax and abdomen is done based on the anatomical scores, and corresponding axial slice.

represents a more complex problem than the one of matching follow-up scans of the same patient. Our goal was for the AI to learn to match corresponding imaging landmarks, and to cover a large set of possible variations while, simultaneously, containing its scope (or *prior knowledge*) to landmarks in the abdominal area. For the chest AI tracker module, we leveraged the trained weights from the NSCLC study (8). The code of both tracker and localizer have been added to the department AI repository[2].

Association With Survival

In order to predict survival, we trained a logistic regression classifier based on the quantitative features extracted from the tracker. More specifically, we leveraged the feature maps in the deepest layer of the U-Net (this is shown in **Figure 2A**). To obtain a feature vector that can be used for the standard logistic classifier, we applied global average pooling. The resulting feature vector (96 entries or features) was fed into the logistic regression model to predict whether the patient would die within 1 year after the date of the latter scan, see **Figure 2B**. For simplicity, the higher resolution information flow in the skip layers and in the final deformation field were not utilized for prognostication. Time from start of treatment, and time between scans were also fed into the classifier, for temporal reference. For each patient, we employed any two scans that were at most 1 year apart from each other.

Comparison to Clinical Standards for Monitoring

We compared PAM against radiological assessments and blood values. For simplicity, we limited the analysis to PAM-scores

[2]Github: github.com/nki-radiology/PAM.

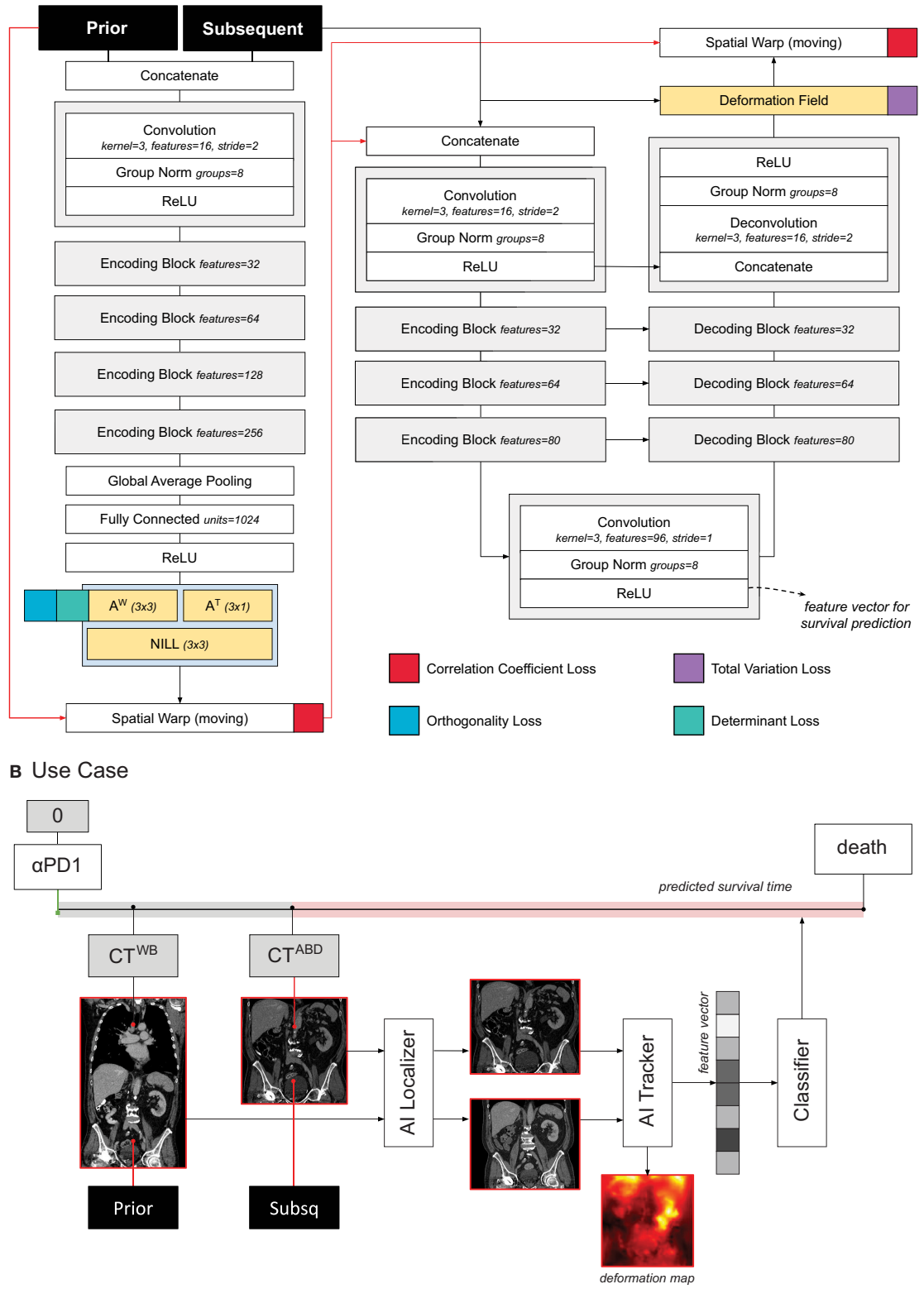

FIGURE 2 | (A) Schematic representation of the tracker architecture and its training. **(B)** Use case of the tracker within PAM.

of abdominal imaging. We employed both univariate and multivariate comparison. The large majority of scans included in the analysis of PAM did not have a corresponding radiological assessment, or blood exam done on the same day — in other words, there was no one-to-one matching for the majority of the cases. To overcome this limitation, we averaged the values of both radiological assessments and blood work over a window of 6 weeks, centered on the date of the CT scan analyzed by PAM. Since PAM leverages tracking of morphological changes, we applied the same principle to the blood values. Namely, we estimated the rate of change of each blood value over time, i.e., $(v_s - v_p)/dt$, where v_p and v_s is the blood values at prior and subsequent scan, respectively, and dt is the time in between.

Radiological progression and response were assessed based on an increase in diameter of 20% or decrease of 30% in diameter, respectively, according to RECIST standards. Diameters were derived using $d = \sqrt[3]{(6V/\pi)}$, where V is the tumor volume delineated by a radiologist (PA). As these assessments already represented longitudinal change, they were left untouched, allowing for the creation of two classes (i.e. "response" and "progression").

Prognostic Heatmaps

In order to interpret the results from PAM, we employed an occlusion sensitivity method (36). With this method, we occluded a section (or patch) of the image to the AI, by setting its voxel intensities to zero. We collected the prediction made by the AI on the occluded image, and compared it with the prediction on the original image. The importance of that patch was defined as the absolute difference between the predictions made on the occluded and the prediction made on the original image. A heatmap was generated by scrolling the occluded patch through the image, and collecting the relative importance of each patch. We termed the resulting visualization the prognostic heatmap. The pseudo-code of the algorithm is presented in **Algorithm 1**. A board-certified radiologist (TNB, specialized in thoracic and abdominal oncologic imaging, blinded to the outcome) was tasked to visually analyse the prognostic maps for a subcohort of the validation set. These were patients that had both thoracic and abdominal imaging. We chose the first available scan pair closest to the start of treatment — namely baseline and first follow-up. The radiologist was tasked to identify the location of highlights on the heatmaps, as well as pathologies/anomalies that were not highlighted, i.e., "hotspots" and "coldspots," respectively. Expert assessments were categorized based on whether they were hotspots or coldspots. This resulted in three classes of interest: hotspots on tumor lesions or therapy-related lesions, hotspots on seemingly healthy parenchyma, and coldspots on tumor or therapy-related lesions. Coldspots on healthy tissues are trivial, and therefore not accounted for.

Statistical Analysis

PAM aims to predict whether the patient will die within 1 year after the date of the latter scan. As this is done through a classification system, we evaluated the performance of the model using classical classification statistics. Namely, we assessed specificity, sensitivity, and area under the receiver operating curve (ROC-AUC). Statistical significance was assessed using the Mann-Whitney-U test. Confidence intervals were estimated via bootstrapping performed using sampling with replacement (1,000 times). Statistical comparison between ROC-AUC was performed via McNeils' test. Multiple hypothesis testing was corrected with the false discovery rate (FDR) method with alpha set at 10%. A generalized multivariate linear regression was employed to evaluate the significance of PAM against current clinical standards (radiology and blood work).

Algorithm 1 | A1. Generation of Heatmaps for Model Explainability.

Input (prior, subsequent, time_start, time_delta)	
1	Reference_score ← PAM(prior, subsequent, time_start, time_delta)
2	ROI ← (0:64, 0:64, 0:64) *[A]*
3	Occluded_prior, Occluded_subsequent ← copy (prior), copy (subsequent)
4	Occluded_prior[ROI], Occluded_subsequent[ROI] ← 0, 0
5	Occluded_score ← PAM(occluded_prior, occluded_subsequent, time_start, time_delta)
6	ROI_importance ← |occluded_score - reference_score|
7	Prognostic_map[ROI] ← maximum (prognostic_map[ROI], roi_importance) *[B]*
8	Move the ROI 8 voxels along one of the axis
9	If ROI has not scrolled through the whole image yet, go to Step 3
10	Return prognostic_map

[A] cube of 64 × 64 × 64 in the top left back corner, [B] since the ROI are overlapping, we chose to use the maximum function, which prevents erroneous overriding of previous estimation.

RESULTS

Study Cohort

A total of $N = 103$ patients were included in this study. Ten patients had only one scan available, making it impossible to model longitudinal changes, and therefore had to be excluded from the analysis. Nineteen patients did not have enough time between imaging date and censor date, and were excluded (see **Figure 3A**). The median age in this cohort was 65 years (IQR: 55 — 72). Upon stratification, $N = 37$ patients were assigned to the training set, and $N = 37$ in the validation set. In terms of overall survival, the median was reached in about 1 year (345 days).

Imaging-wise, we included a total of $N = 1{,}087$ CT scans between 6 months before start of treatment and up to 2 years after. These were used to create the scan pairs needed for PAM to model morphological changes. In total, we found $N = 2{,}339$ abdominal, and $N = 7{,}431$ chest scan pairs. We further excluded all scan pairs of living patients whose time between the latest scan and censor was < 1 year, and whose time between scans in the scan pair was more than 1 year. This resulted in $N = 1{,}209$ abdominal scan pairs, and $N = 3{,}701$ chest scan pairs in the discovery set and $N = 614$ and $N = 1{,}937$, in the validation set, respectively. We chose not to limit the analysis to only subsequent scans, as the time points of when they were taken, and the time interval between them might vary. We rather chose to include all feasible pairs, within a given time-interval.

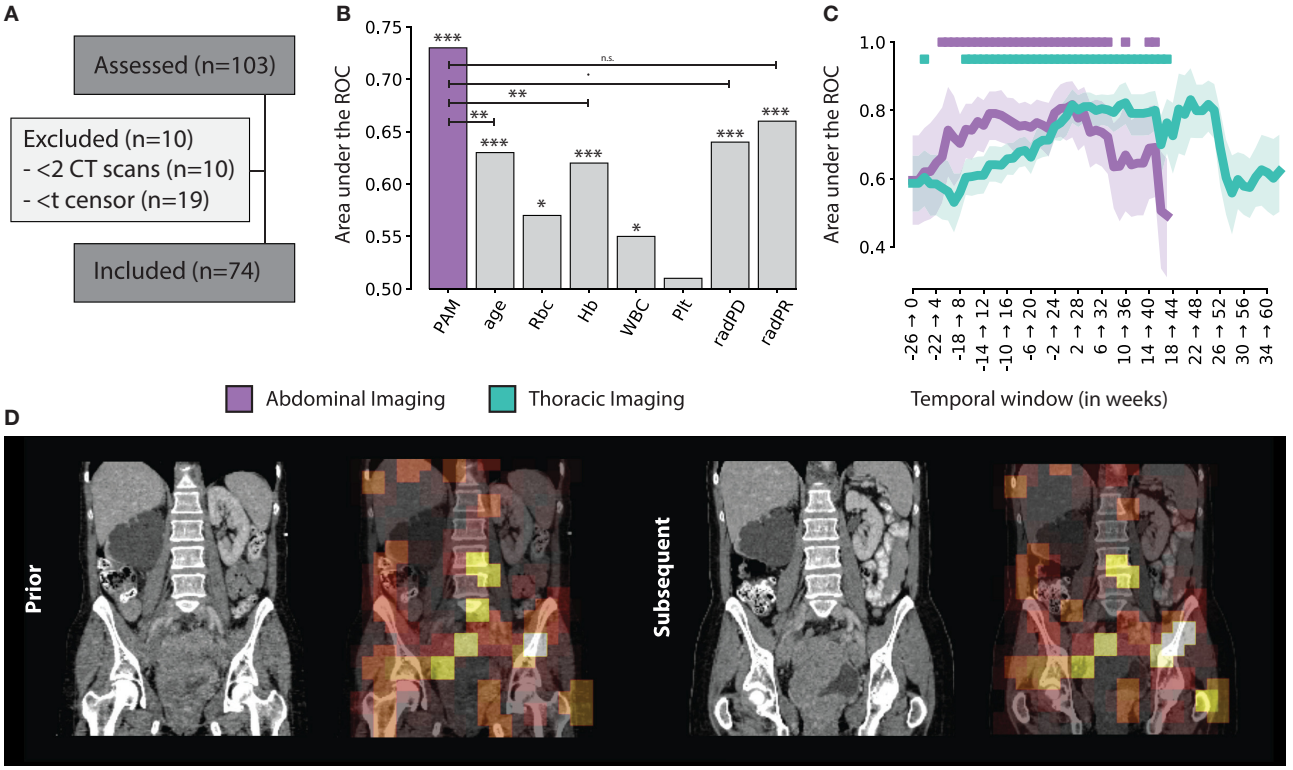

FIGURE 3 | (A) Consensus, **(B)** PAM Abdominal tracker performance compared to other standard factors used for treatment monitoring. Significance levels are reported for $p < 0.001$ (***), 0.01 (**), 0.05 (*), 0.1 (·) and n.s. for non-significant **(C)** PAM Abdominal and Thoracic monitoring performance, over time, with respect to the start of treatment, in weeks. The | indicates statistical significance after FDR correction **(D)** Example of the prognostic heat map overlaid on top of the original abdominal scan.

With respect to the unlabelled data used for training, we retrieved a total of $N = 37{,}573$ CT scans from TCIA. The localizer was trained first, on $N = 176$ thoracoabdominal CT scans from the lymphadenopathy dataset. The abdominal tracker was trained on $N = 3{,}137$ abdominal CT scans, resulting from the automatic inclusion procedure.

Prognostic Performance

We assessed the ability of the classifier (trained on the imaging features of the tracker module) to predict 1 year survival after the latter scan of the scan pair. Across all scan pairs and treatment course (up to 6 months before and 2 years after start of therapy), the overall performance on the independent validation set was 0.73 AUC (CI: 0.69–0.76, $p < 0.001$) for abdominal images, and 0.67 AUC (CI: 0.64–0.69, $p < 0.001$) for chest images. Specificity and sensitivity were 0.74 (CI: 0.69–0.80) and 0.60 (CI: 0.56–0.64) for abdominal images; and 0.71 (CI: 0.68–0.74) and 0.58 (0.56–0.60) for chest images, respectively.

This results gives us an overview of the performance of PAM, independently from the treatment time point or interval between follow-up scans. To gain additional insights in the performance of PAM at different treatment time points, we employed a temporal analysis of the performance on a 6-months moving window. Particularly, we estimated the performance of PAM for all pairs acquired between day d and $d + 6$ months, with d moving forward by 7 days at each step. The analysis was run on temporal windows with at least 10 positive and 10 negative samples to limit statistical noise. For abdominal scans, the highest prognostic performance was reached in the first 6 months of treatment (7–189 days), with an ROC-AUC of 0.82 (CI: 0.72–0.89, $P < 0.0001$). In general, the temporal windows around and up to the first 8 months of treatment seem to be the ones carrying the highest predictive value, staying significant after correction for multiple hypothesis testing. Similar results were obtained for chest scans. The highest prognostic performance was reached later than the abdominal model, around 5–11 months after start of treatment, with a ROC-AUC of 0.83 (CI: 0.71–0.92, $P = 0.0002$). Unlike abdominal scans, which were observed to have a prognostic value both around and during treatment, chest scans carried much higher prognostic value during treatment rather than around the start date. Detailed results of the prognostic performance over time are shown in **Figures 3B,C**.

To investigate PAM as a biomarker, we analyzed the scans taken before the start of treatment. Namely, we investigated the abdominal scan pairs whose scans were taken between 12 weeks prior and start of treatment. This resulted in 31 scan pairs of 26 patients in the external validation set. Four patients had multiple scan pairs. We aggregated multiple scan pairs per patient by taking the average PAM prediction. This resulted in an AUC of 0.70 (CI: 0.50–0.88, $p = 0.054$) for the prediction of 1

year survival from the moment of start of treatment. Specificity and sensitivity were 0.69 (CI: 0.50–0.87) and 0.82 (CI: 0.58–1.00), respectively. Further analysis on PAM predicted survival at baseline showed a significant difference of >464 days between low- and high-risk patients ($p = 0.012$, *log rank test*), with the high-risk group had a median survival of 266 days, and the low-risk group did not reach median survival within the first 2 years of treatment. Combination of the abdominal and thoracic scores (i.e., average) yielded a lower performance in terms of classification (0.65 AUC, CI: 0.46–0.83, $p = 0.118$), and virtually unchanged results for the survival analysis ($p = 0.012$, *log-rank test*). The limited number of patients did not allow to explore more advanced methods for score combinations.

Comparison With Current Monitoring Standards

Univariate analysis for current monitoring standards showed significant performance for both radiological assessments, as well as laboratory (hemoglobine, erythrocytes, leukocytes, and thrombocytes) results. Radiological progression and response reached an AUC of 0.64 (CI: 0.58–0.70, $p < 0.001$) and 0.66 (CI: 0.62–0.69, $p < 0.001$), respectively. In terms of blood markers, increases in erythrocyte counts (0.57 AUC, CI: 0.51–0.62, $p = 0.019$), hemoglobin (0.62 AUC, CI: 0.57–0.66, $p < 0.001$), and leukocyte counts (0.55 AUC, CI: 0.49–0.61, $p = 0.039$) were all significant. None of these markers performed better than PAM. PAM performance remained statistically significant against these other biomarkers using multivariate analysis. Other factors that retained significance were radiological progression ($p < 0.001$), leukocyte count ($p = 0.023$), and age ($p = 0.006$). Hemoglobin and erytrocyten were displayed with a high correlation (0.92) and were averaged together. Their average, along with radiological response and thrombocyte count were not significant. Results of both univariate and multivariate are presented in **Table 1** and **Figure 3B.**

Visual Analysis of Abdominal Heatmaps

Results from visual analysis were classified based on highlighted areas (hotspots), and whether they were cancer lesions, cancer-spread complications, therapy-induced complications, or seemingly healthy tissue. If cancer lesions and cancer-spread or therapy-induced complications were not covered by a hotspot, these were flagged as coldspots. In total, $N = 31$ cases were analyzed. **Table 2** shows a summary of the results. A heatmap example is shown in **Figure 3D**.

In the abdomen, primary bladder tumors ($N = 13$), involved lymph nodes ($N = 18$) and liver metastases ($N = 10$) were flagged as prognostic by the AI algorithm in most cases where they were present—namely, hotspots in 85, 83, and 80% of cases, respectively. Similar frequencies were observed for bone ($N = 7$) and peritoneal metastases ($N = 7$), having been flagged in 86 and 71% of cases. Rare occurrences of adrenal metastasis, as well as abdominal wall metastasis and a ureter mass were also found, both as hotspots and coldspots. Low occurrence was also observed for cancer spread-related complications. These were hydronephrosis ($N = 5$), ascites ($N = 3$) and pleural effusion ($N = 1$). Hydronephrosis and ascites were highlighted in 4 and 2 cases, respectively. Far more common were hotspots observed on seemingly healthy tissue, including the hip region ($N = 27$), pelvic bone ($N = 26$), spine ($N = 25$), liver and bowels ($N = 20$), kidneys ($N = 17$), and spleen ($N = 16$). It was further observed that, in the large majority of cases, only part of the tissue would be highlighted, but never the full organ.

Visual Analysis of Chest Heatmaps

In the thorax, 7 out of 11 lung lesions were highlighted (64%). The mediastinum, chest wall, and upper spine were the most common hotspots in seemingly healthy areas. Other lesion types, such as lymph node metastases and bone metastases, were also present but low in numbers. Observed cancer spread-related complications include pleural effusion (hotspot in 1 out of 2 cases), and ascites (coldspot). Pneumonitis and sarcoid-like disease were also present as therapy-related complication hotspots, but both as single cases. A summary of the results is shown in **Table 2**.

DISCUSSION

Advanced and non-invasive imaging methods for evaluation of treatment response, which would provide comprehensive and reliable information on how the patient responds to treatment, could improve accurate clinical decision making. Our aim was to assess the prognostic value of AI-enriched thoraco-abdominal CT response assessment in stage-IV urothelial cancer patients undergoing immune checkpoint inhibitors. We set up a fully-automatic AI-system that would track changes between follow-up thoraco-abdominal CT scans, and linked their quantitative descriptors to overall survival. We term this method *prognostic AI-monitor* (PAM).

Our findings showed that PAM reached significant predictive performance for both thoracic and abdominal CT, with AUCs of 0.67 and 0.73, respectively, for the prediction of 1-year overall survival from the moment of the scan. In-depth analysis revealed stark differences in the prognostic value of morphological changes depending on the time point of treatment, with the first 9 months of treatment being the most predictive and significant AUCs > 0.70, peaking to over 0.80 for both abdominal imaging, and thoracic imaging. Similar findings were observed in our previous study on NSCLC (8), where the changes recorded by the algorithm in the first 3 to 5 months of treatment were observed to have a higher prognostic value. In the present study, we extended the system to include both the thorax and abdomen, and trained with far larger datasets both in terms of pre-training as well as survival association. The AI algorithm designed in this study was significantly extended to a comprehensive AI-system (i.e., PAM), able to scan imaging data, identify the regions of interests, and analyze them for the purpose of monitoring and prognostication. By including abdominal images, we also showed that the previous system (8) can be extended to multiple parts of the human body.

To the best of our knowledge, this is one of the first studies employing artificial intelligence for prognostication in immunotherapy-treated urothelial cancer patients. In the study by Park et al. (37), the authors developed a radiomics model for the prediction of objective response and overall survival

TABLE 1 | Prognostic performance of PAM against current monitoring tools.

Univariate analysis					
	N. negative/positive	***p*-value**	**ROC AUC (95 CI)**	**Sensitivity**	**Specificity**
Erythrocyte count (Δ/dt)	358/110	**0.019**	0.57 (0.51–0.62)*	0.47 (0.43–0.52)	0.42 (0.34–0.49)
Hemoglobin (Δ/dt)	372/122	**< 0.001**	0.62 (0.57–0.66)*	0.47 (0.43–0.51)	0.38 (0.31–0.45)
Leukocyte count (Δ/dt)	366/116	**0.039**	0.55 (0.49–0.61)	0.52 (0.48–0.56)	0.56 (0.49–0.64)
Thrombocyte count (Δ/dt)	366/116	0.421	0.51 (0.45–0.56)	0.51 (0.47–0.56)	0.54 (0.46–0.61)
Radiological Progression	145/65	**< 0.001**	0.64 (0.58–0.70)	0.87 (0.82–0.91)	0.42 (0.31–0.52)
Radiological response	145/65	**< 0.001**	0.66 (0.62–0.69) *	0.69 (0.62–0.75)	0.00 (0.00–0.00)
AI-score (abdomen)	437/117	**< 0.001**	0.73 (0.69–0.76)	0.60 (0.56–0.64)	0.74 (0.69–0.80)
AI-score (thorax)	1,421/516	**< 0.001**	0.67 (0.64–0.69)	0.58 (0.56–0.60)	0.71 (0.68–0.74)
Multivariate analysis					
	Coefficient	**Standard deviation**	**95 Confidence interval**		***p*-value**
Intercept	−1.1010	3.213	−7.398	5.196	0.732
AI-score (abdomen)	−7.9394	1.683	−11.239	−4.640	**<0.001**
Age	−7.3906	2.699	−12.680	−2.101	**0.006**
Erythrocyte + hemoglobin (Δ/dt)	−0.2210	2.455	−5.034	4.592	0.928
Leukocyte count (Δ/dt)	10.9735	4.810	1.546	20.401	**0.023**
Thrombocyte count (Δ/dt)	−0.3935	2.022	−4.357	3.570	0.846
Radiological progression	−3.0030	0.693	−4.361	−1.645	**<0.001**
Radiological response	> 100	> 100	< −100	> 100	0.999

*AUC < 0.5 were inverted for readability, indicated by *.*

in a similar population. Machine learning was also employed on imaging (radiomics) features, however these were extracted via manually delineated lesions. The authors reported an AUC of 0.88 (CI: 0.65–0.97) for objective response prediction of bladder tumors in a cohort of $N = 21$ patients, with a significant difference in overall survival between (radiomics-identified) higher and lower risk groups. Our findings also showed significant differences in survival, but in contrast to the above study, we looked at the whole body changes, not only those of the tumoral lesions but also the non-tumoral treatment- or cancer-related changes (e.g., side-effects, organ compression, etc.). Our results are comparable to state-of-the-art methods based on time-consuming, error-prone, manual delineations (6, 7). Till now, single lesion analysis has allowed the field to develop, however, it has restricted the usage of the image only to selected areas-of-interest, accounting for <5% of the total data in the scan. While these methods have been refined to leverage known factors in cancer growth, including vascularity (38), oxygenation (39), and metabolic activity (40)—our approach is different. Not only do we offer a novel fully automatic procedure which completely eradicates the need of time-consuming segmentations, but it also makes use of the whole body image of the patient, to evaluate the patient's status and estimate survival.

We analyzed the PAM further, by means of visualization. More specifically, we employed a visualization method (36) to generate heatmaps, which highlighted regions of the image that carried higher predictive value, according to PAM. In our case, hotspots would correspond to gross morphological changes that the AI algorithm deemed of prognostic relevance. An expert radiologist was tasked to visually confirm these findings. Our findings show that changes in the primary tumor of the bladder, as well as metastases in lymph nodes, liver, peritoneum, and skeleton were among the most predictive for the algorithm.

Interestingly, there are similarities between our results, and the results from the NSCLC study (8). In both cases, the region of the primary tumor, as well as lymph nodes and bone lesions were closely inspected by the algorithm. Additionally, in the present study, the algorithm is also tracking changes in liver and peritoneal metastases. Unlike the present study however, the AI in the NSCLC cohort was working only on chest imaging, therefore unable to access the abdominal cavity.

There is evidence, in both studies, that bone lesions should be accounted for in imaging evaluation schedules. These are considered non-target lesions in the current response criteria and are notoriously difficult to assess (4, 5, 41). Both bladder and lung cancer generated evidence to support the further investigation for the inclusion of CT changes in the bone among the target lesions.

Generally speaking, these findings suggest an unequal effect of cancer lesions on survival. While this might seem trivial at first (e.g., brain metastases are known to have worse prognosis), all current imaging methods for response evaluation and prognostication [like the RECISTs (4, 5, 41)] do not distinguish between lesion types. RECIST methods are based on the change in the sum of diameters of a (limited) set of lesions. In other words, the growth of lesions in one organ is measured and weighed in the same way as the growth of another lesion in

TABLE 2 | Visual analysis of PAM generated prognostic maps.

	Rare (<10%)	10–25%	25–50%	Frequent (>50%)
		Abdominal imaging		
Hotspot tumor	Lung mets (3), adrenal mets (1), abdominal wall mets (1), ureter (1), recurrence (2), deposition (2)	Bone mets (6), peritoneal (5)	Bladder Ca (11), lymph nodes mets (16), liver mets (8)	
Hotspot tumor-related	Ascites (2)	Hydronephrosis (4)		
Hotspot therapy-related				
Hotspot healthy	Pelvis (2), genital (3), retroperitoneum (2)	Chest wall (7), pancreas (6)	Abdominal wall (14), stomach (13)	Bowel (21), liver (21), spleen (17), kidneys (18), spine (26), pelvic bone (27), hip region (28)
Coldspot tumor	Bladder Ca (2), lymph nodes mets (3), lung mets (1), bone mets (1), liver mets (2), peritoneal mets (2), abdominal wall mets (1), recurrence (1)			
Coldspot tumor-related	Pleural effusion (1), ascites (1), hydronephrosis (1)			
		Chest imaging		
Hotspot tumor	Lymph nodes mets (3), bone mets (2)	Lung mets (7), liver mets (4)		
Hotspot tumor-related	Pleural effusion (1)			
Hotspot therapy-related	Pneumonitis (1), sarcoid like (2)			
Hotspot healthy	Lung (2)			Mediastinum (25), chest wall (27), upper abdomen (22), spine (26)
Coldspot tumor	Lymph nodes mets (3), lung mets (4), bone mets (2), liver mets (1)			
Coldspot tumor-related	Pleural effusion (1), ascites (1)			

Ca, cancer; Mets, metastases. Number of cases between parenthesis (N).

a different organ—no distinction is made. Our results however suggest that these factors should be accounted for, which would therefore require a more comprehensive evaluation scheme.

In this study, we proposed a method that is based on image-to-image registration, leveraging the properties of this technique in finding corresponding anatomical landmarks in pairs of images, and therefore constructing a model able to track not only tumors but also tumor- and therapy induced changes, as well as seemingly healthy parenchyma. Our method does not preclude the usage of other techniques and methods. As we have observed, commonly used clinical response evaluation tools also retained significance when compared against PAM, suggesting PAM as a complementary value to the current clinical standards. An optimal approach to the utilization of PAM would be integration of this method with other diagnostic tools currently available (42).

The study was limited to whole-body CT, which is the workhorse in standard clinical practice. As brain imaging is not part of the standard whole-body CT protocol, anatomical and functional changes in the brain as captured on MRI and PET/CT are yet to be explored. We envision a more comprehensive usage of this technique, where all available imaging during follow-up is leveraged for prognostication purposes. It is also yet to be confirmed whether the PAM approach would extend to other treatments and cancer types, and to which extent survival associations would be interchangeable. Further development of PAM should also focus on pre-treatment scans. In this study, we analyzed scans acquired up to 6 months before the start of treatment. Some patients had to be excluded, as they lacked follow-ups. We acknowledge that this could have introduced a bias toward patients with extensive treatment history, or against patients with the worse survival outcomes. An extension of PAM to include more of the treatment history would be beneficial in this sense, but it would require PAM to deal with the plethora of all different treatments, and combinations thereof, that nowadays oncological patients receive, hence beyond the scope of this study.

Another limitation of the study is the monocentric nature of the analysis. While CT data is generally acknowledged to have higher level of reproducibility across vendors than MRI, it is yet to be seen whether this would hamper the association with survival, and to what extent. Nonetheless, we made sure

to train the tracker and localizer modules on large publicly-available datasets that would, in theory, provide a larger pool of variations in image acquisition protocols. Future studies should be focused on including a larger cohort of patients. This would allow not only to increase the number of features used in deformation modeling (now limited to 96), but also the machine learning classifier used for predicting survival, which could in turn increase the performance of the model.

Finally, the readers were, just like the algorithm, blinded to the patient's full-history. This did not allow them, for example, to perform a complete RECIST assessment, which would require the computation of a nadir. Further investigations should also focus on a full-comparison of PAM and RECIST criteria (and iRECIST), on whether they are complementary or mutually exclusive, and what are the benefits of using one or the other.

As a future outlook, we envision an extended PAM-like algorithm to be set up as a clinical decision support system in tumor boards, providing continuous monitoring and prognostication information, in order to assist physicians in the treatment decision process.

CONCLUSIONS

In this study, we investigated the prognostic information of AI-derived whole-body imaging monitoring markers in advanced urothelial cancer receiving checkpoint inhibitors. We hypothesized that quantitative AI-derived features describing morphological changes happening during the course of treatment could hold prognostic information. To this end, we designed and implemented a prognostic AI-monitor (PAM). Our findings demonstrate that PAM is complementary to existing monitoring methods, while reaching comparable or superior accuracy. We argue that this could be the result of PAM's ability to analyze the whole body, including non-target cancer lesions and non-cancer lesions. Further investigation should focus on the development of a comprehensive pipeline beyond anatomical imaging, as well as on external validations.

DATA AVAILABILITY STATEMENT

The datasets presented in this article are not readily available because local privacy regulation do not allow us to share CT scans publicly for this project. Feature sets are available on request. Requests to access the datasets should be directed to ST, s.trebeschi@nki.nl.

ETHICS STATEMENT

The studies involving human participants were reviewed and approved by Institutional Review Board, NKI-AVL. Written informed consent for participation was not required for this study in accordance with the national legislation and the institutional requirements.

AUTHOR CONTRIBUTIONS

ST: software development. ST, ZB, TB, TT, and TN-K: conceptualization and experimental design. ZB, TB, and ND: clinical results validation and interpretation. ST, ZB, TN-K, and ND: radiological and clinical data collection and curation. MH, HA, and RB-T: project supervision and resource acquisition. All authors: results, manuscript editing, and validation.

FUNDING

This work was also carried out on the Dutch national e-infrastructure with the support of SURF Cooperative. TN-K was funded by the Oncologic Imaging Fellowship Grant from the European Society of Radiology.

ACKNOWLEDGMENTS

The authors would also like to thank NVIDIA for their kind donation via the Academic GPU Grant Program as well as the Maurits en Anna de Kock Stichting for its financial support.

REFERENCES

1. Planchard D, Popat S, Kerr K, Novello S, Smit EF, Faivre-Finn C, et al. Metastatic non-small cell lung cancer: ESMO clinical practice guidelines for diagnosis, treatment and follow-up. *Ann Oncol.* (2018) 29:iv192–237. doi: 10.1093/annonc/mdy275
2. Michielin O, van Akkooi ACJ, Ascierto PA, Dummer R, Keilholz U. Cutaneous melanoma: ESMO Clinical Practice Guidelines for diagnosis, treatment and follow-up. *Ann Oncol.* (2019) 30:1884–901. doi: 10.1093/annonc/mdz411
3. Balar AV, Galsky MD, Rosenberg JE, Powles T, Petrylak DP, Bellmunt J, et al. Atezolizumab as first-line treatment in cisplatin-ineligible patients with locally advanced and metastatic urothelial carcinoma: a single-arm, multicentre, phase 2 trial. *Lancet.* (2017) 389:67–76. doi: 10.1016/S0140-6736(16)32455-2
4. Eisenhauer EA, Therasse P, Bogaerts J, Schwartz LH, Sargent D, Ford R, et al. New response evaluation criteria in solid tumours: revised RECIST guideline (version 1.1). *Eur J Cancer.* (2009) 45:228–47. doi: 10.1016/j.ejca.2008.10.026
5. Seymour L, Bogaerts J, Perrone A, Ford R, Schwartz LH, Mandrekar S, et al. iRECIST: guidelines for response criteria for use in trials testing immunotherapeutics. *Lancet Oncol.* (2017) 18:e143–52. doi: 10.1016/S1470-2045(17)30074-8
6. Trebeschi S, Drago SG, Birkbak NJ, Kurilova I, Călin AM, Delli Pizzi A, et al. Predicting response to cancer immunotherapy using noninvasive radiomic biomarkers. *Ann Oncol.* (2019) 30:998–1004. doi: 10.1093/annonc/mdz108
7. Sun R, Limkin EJ, Vakalopoulou M, Dercle L, Champiat S, Han SR, et al. A radiomics approach to assess tumour-infiltrating CD8 cells and response to anti-PD-1 or anti-PD-L1 immunotherapy: an imaging biomarker, retrospective multicohort study. *Lancet Oncol.* (2018) 19:1180–91. doi: 10.1016/S1470-2045(18)30413-3
8. Trebeschi S, Bodalal Z, Boellaard TN, Tareco Bucho TM, Drago SG, Kurilova I, et al. Prognostic value of deep learning mediated treatment monitoring in lung cancer patients receiving immunotherapy. *Front Oncol.* (2021) 11:9. doi: 10.3389/fonc.2021.609054
9. Zhang P, Wang F, Zheng Y. Self supervised deep representation learning for fine-grained body part recognition. In: *2017 IEEE 14th International Symposium on Biomedical Imaging.* Melbourne, (2017). p. 578–82 doi: 10.1109/ISBI.2017.7950587
10. Fischler MA, Bolles RC. Random sample consensus: a paradigm for model fitting with applications to image analysis and automated cartography. *Commun ACM.* (1981) 24:381–95. doi: 10.1145/358669.358692

11. Balakrishnan G, Zhao A, Sabuncu MR, Guttag J, Dalca AV. VoxelMorph: a learning framework for deformable medical image registration. *IEEE Trans Med Imaging.* (2019) 38:1788–800. doi: 10.1109/TMI.2019.2897538
12. Zhao S, Lau T, Luo J, Chang EI-C, Xu Y. Unsupervised 3D end-to-end medical image registration with volume tweening network. *IEEE J Biomed Health Inform.* (2019) 24:1394–404. doi: 10.1109/JBHI.2019.2951024
13. Ronneberger O, Fischer P, Brox T. U-net: convolutional networks for biomedical image segmentation. In: *Medical Image Computing and Computer-Assisted Intervention – MICCAI 2015.* Cham: Springer (2015). p. 234–41. doi: 10.1007/978-3-319-24574-4_28
14. Wu Y, He K. Group normalization. In: Ferrari V, Hebert M, Sminchisescu C, Weiss Y, editors. *15th European Conference, Munich, Germany, September 8-14, 2018, Proceedings* Cham: Springer International Publishing (2018). p. 3–19.
15. Clark K, Vendt B, Smith K, Freymann J, Kirby J, Koppel P, et al. The Cancer Imaging Archive (TCIA): maintaining and operating a public information repository. *J Digit Imaging.* (2013) 26:1045–1057. doi: 10.1007/s10278-013-9622-7
16. Smith KCK. Data from CT_COLONOGRAPHY. *Cancer Imaging Arch.* (2015). doi: 10.7937/K9/TCIA.2015.NWTESAY1
17. Beichel RR, Ulrich EJ, Bauer C, Wahle A, Brown B, Chang T, et al. Data From QIN-HEADNECK. *Cancer Imaging Arch.* (2015). doi: 10.7937/K9/TCIA.2015.K0F5CGLI
18. Kinahan P, Muzi M, Bialecki B, Herman B, Coombs L. Data from the ACRIN 6668 Trial NSCLC-FDG-PET. *Cancer Imaging Arch.* (2019). doi: 10.7937/TCIA.2019.30ILQFCL
19. Grossberg A, Elhalawani H, Mohamed A, Mulder S, Williams B, White AL, et al. *HNSCC* [Dataset]. The Cancer Imaging Archive (2020). doi: 10.7937/k9/tcia.2020.a8sh-7363
20. Heller N, Sathianathen N, Kalapara A, Walczak E, Moore K, Kaluzniak H, et al. *Data from C4KC-KiTS* [Data set]. The Cancer Imaging Archive (2019). doi: 10.7937/TCIA.2019.IX49E8NX
21. Kinahan P, Muzi M, Bialecki B, Coombs L. Data from ACRIN-FLT-Breast. *The Cancer Imaging Archive.* (2017). doi: 10.7937/K9/TCIA.2017.ol20zmxg
22. Bakr S, Gevaert O, Echegaray S, Ayers K, Zhou M. Shafiq M, et al. *Data for NSCLC Radiogenomics Collection.* The Cancer Imaging Archive (2017). doi: 10.7937/K9/TCIA.2017.7hs46erv
23. Roth H, Lu L, Seff A, Cherry KM, Hoffman J, Wang S, et al. A new 2.5 D representation for lymph node detection in CT. *Med Image Comput Comput Assist Interv.* (2015) 17:520–7 doi: 10.1007/978-3-319-10404-1_65
24. Bosch WR, Straube WL, Matthews JW, Purdy JA. *Data From Head-Neck_Cetuximab.* The Cancer Imaging Archive (2015). doi: 10.7937/K9/TCIA.2015.7AKGJUPZ
25. Madhavi P, Patel S, Tsao AS. *Data from Anti-PD-1 Immunotherapy Lung* [Data set]. The Cancer Imaging Archive (2019). doi: 10.7937/tcia.2019.zjjwb9ip
26. Patnana M, Patel S, Tsao A. *Anti-PD-1 Immunotherapy Melanoma Dataset* [Data set]. The Cancer Imaging Archive (2019). doi: 10.7937/tcia.2019.1ae0qtcu
27. Kurdziel KA, Apolo AB, Lindenberg L, Mena E, McKinney YY, Adler SS, et al. *Data From NaF_PROSTATE.* The Cancer Imaging Archive (2015). doi: 10.7937/K9/TCIA.2015.ISOQTHKO
28. Muzi P, Wanner M, and Kinahan P. *Data From RIDER Lung PET-CT.* The Cancer Imaging Archive (2015). doi: 10.7937/K9/TCIA.2015.OFIP7TVM
29. Vallières M, Freeman CR, Skamene SR, El Naqa I. A radiomics model from joint FDG-PET and MRI texture features for the prediction of lung metastases in soft-tissue sarcomas of the extremities. *Phys Med Biol.* (2015) 60:5471. doi: 10.1088/0031-9155/60/14/5471
30. Aerts HJWL, Rios Velazquez E, Leijenaar RTH, Parmar C, Grossmann P, Carvalho S, et al. *Data From NSCLC-Radiomics-Genomics.* The Cancer Imaging Archive (2015). doi: 10.7937/K9/TCIA.2015.L4FRET6Z
31. Wee L, Aerts HJL, Kalendralis P, Dekker A. *Data From NSCLC-Radiomics-Interobserver1* [Data set]. The Cancer Imaging Archive (2019). doi: 10.7937/tcia.2019.cwvlpd26
32. Bloch BN, Jain A, Jaffe CC. *Data From Breast-Diagnosis.* The Cancer Imaging Archive (2015). doi: 10.7937/K9/TCIA.2015.SDNRQXXR
33. Yorke AA, McDonald GC, Solis Jr D, Guerrero T. *Pelvic Reference Data.* The Cancer Imaging Archive (2019). doi: 10.7937/TCIA.2019.woskq5oo
34. Vallières M, Kay-Rivest E, Perrin LJ, Liem X, Furstoss C, Khaouam N, et al. (2017). *Data From Head-Neck-PET-CT.* The Cancer Imaging Archive (2019). doi: 10.7937/K9/TCIA.2017.8oje5q00
35. Aerts HJWL, Wee L, Rios Velazquez E, Leijenaar RTH, Parmar C, Grossmann P, et al. Data From NSCLC-Radiomics [Data set]. The Cancer Imaging Archive (2019). doi: 10.7937/K9/TCIA.2015.PF0M9REI
36. Zeiler MD, Fergus R. Visualizing and understanding convolutional networks. In: *Computer Vision – ECCV 2014.* Zurich: Springer International Publishing (2014). p. 818–33. doi: 10.1007/978-3-319-10590-1_53
37. Park KJ, Lee J-L, Yoon S-K, Heo C, Park BW, Kim JK. Radiomics-based prediction model for outcomes of PD-1/PD-L1 immunotherapy in metastatic urothelial carcinoma. *Eur Radiol.* (2020) 30:5392–403. doi: 10.1007/s00330-020-06847-0
38. Alilou M, Bera K, Vaidya P, Zagouras A, Patil P, Khorrami M, et al. Quantitative vessel tortuosity radiomics on baseline non-contrast lung CT predict response to immunotherapy and are prognostic of overall survival. *Med Imag Comp Aided Diagnosis.* (2019) 10950:109501F doi: 10.1117/12.2513648
39. Tunali I, Tan Y, Gray JE, Katsoulakis E, Eschrich SA, Saller J, et al. Hypoxia-related radiomics predict checkpoint blockade immunotherapy response of non-small cell lung cancer patients [abstract]. In: of the Annual Meeting of the American Association for Cancer Research 2020; 2020 Apr 27-28 and Jun 22-24. Philadelphia (PA): *AACR. Cancer Res.* (2020) 80(16 Suppl):5806
40. Mu W, Qi J, Lu H, Balagurunathan Y, Gillies RJ, Tunali I, et al. Radiomic biomarkers from PET/CT multi-modality fusion images for the prediction of immunotherapy response in advanced non-small cell lung cancer patients. *Med Imag Comp Aided Diagn.* (2018) 10575:105753S. doi: 10.1117/12.2293376
41. Schwartz LH, Litière S, de Vries E, Ford R, Gwyther S, Mandrekar S, et al. RECIST 1.1—Update and clarification: From the RECIST committee. *Eur J Cancer.* (2016) 62:132–7. doi: 10.1016/j.ejca.2016.03.081
42. Bodalal Z, Trebeschi S, Beets-Tan R. Radiomics: a critical step towards integrated healthcare. *Insights Imaging.* (2018) 9:911–4. doi: 10.1007/s13244-018-0669-3

Conflict of Interest: MH has consultancy agreements (paid to the institute) with Roche Genentech, BMS, Merck, and AstraZeneca; and grants (paid to the institute) from BMS, AstraZeneca, and Roche.

The remaining authors declare that the research was conducted in the absence of any commercial or financial relationships that could be construed as a potential conflict of interest.

frontiers in Oncology

ORIGINAL RESEARCH
published: 20 April 2021
doi: 10.3389/fonc.2021.603681

FOXO3A Expression in Upper Tract Urothelial Carcinoma

Guoyao Zhang[1†], Wanping Shi[2†], Enzhao Jia[3], Lei Zhang[1], Yongsheng Han[4], Ronald Rodriguez[5] and Tianjiang Ma[1]*

[1] Department of Oncology, Luohe Central Hospital, The First Affiliated Hospital of Luohe Medical College, Luohe, China, [2] Department of Oncology, The Second Affiliated Hospital, Chongqing Medical University, Chongqing, China, [3] Department of Pathology, Luohe Central Hospital, The First Affiliated Hospital of Luohe Medical College, Luohe, China, [4] Department of General Surgery, School of Medicine, Qinghai University, Xining, China, [5] Department of Urology, University of Texas Health Science Center San Antonio, San Antonio, TX, United States

Background: Epidemiological studies have reported various results regarding whether FOXO3A is related to various carcinomas. However, the prognostic significance of FOXO3A in upper tract urothelial carcinoma (UTUC) remains unclear. The purpose of this study was to validate the correlation between FOXO3A expression and oncological outcomes in UTUC.

Methods: The expression levels of FOXO3A in 107 UTUC patients were examined by immunohistochemistry (IHC). We examined the prognostic role of FOXO3A by using the Cox proportional hazard model.

Results: The results indicated that FOXO3A expression was notably decreased in UTUC tissue compared with control tissue. Decreased expression of FOXO3A was also related to advanced pathologic stage (P = 0.026), lymph node metastasis (P = 0.040), lymphovascular invasion (P < 0.001), and adjuvant therapy (P = 0.048). In addition, UTUC patients with low FOXO3A expression had a significantly shorter survival time, including both overall survival (OS) [hazard ratio (HR) 2.382, P = 0.004] and recurrence-free survival (RFS) (HR 2.385, P = 0.004), than those with high expression. Multivariate analyses showed that FOXO3A was a significant predictor for OS (HR 2.145, P = 0.014) and RFS (HR 2.227, P = 0.010) in UTUC patients.

Conclusion: Our results indicate that FOXO3A may be involved in the recurrence of UTUC and that it has certain clinical value in the therapeutic targeting and prognostic evaluation of UTUC.

Keywords: FOXO3A, prognosis, overall survival, recurrence-free survival, upper tract urothelial carcinoma

OPEN ACCESS

Edited by:
Ronald M. Bukowski, Cleveland Clinic, United States

Reviewed by:
Andrew Thomas Lenis, Memorial Sloan Kettering Cancer Center, United States
Alfredo Berruti, University of Brescia, Italy

****Correspondence:***
Guoyao Zhang
Guoyao_Zhang@163.com

[†]These authors have contributed equally to this work and share first authorship

Specialty section:
This article was submitted to Genitourinary Oncology, a section of the journal Frontiers in Oncology

Received: *01 October 2020*
Accepted: *22 March 2021*
Published: *20 April 2021*

Citation:
Zhang G, Shi W, Jia E, Zhang L, Han Y, Rodriguez R and Ma T (2021) FOXO3A Expression in Upper Tract Urothelial Carcinoma. Front. Oncol. 11:603681. doi: 10.3389/fonc.2021.603681

INTRODUCTION

Urothelial carcinoma (UC) is the most common malignancy of the urinary tract. However, upper tract (renal pelvis and ureter) tumors account for only 5% to 10% of all UCs, and almost 60% of upper tract UCs (UTUCs) are invasive at diagnosis (1, 2). Currently available prognostic tools that utilize clinical and pathological parameters are limited for UTUC. Through the analysis of

biomarkers in pathological specimens, we may strengthen the risk stratification and guide better prognostic evaluations for a more effective therapeutic strategy (3–5).

Forkhead box O 3a (FOXO3A) belongs to the FOXO protein family and is located on human chromosome 6q21 (6). FOXO3A activity and stability can be regulated by post–translational modifications, including phosphorylation, acetylation, ubiquitination and glycosylation, aside from its well-validated modifications in transcription (7). It has been highlighted as an important transcriptional regulator of crucial proteins participating in DNA damage repair (8), cell cycle regulation (9), apoptosis (10), angiogenesis (11), and cellular stress response (12). The function and detailed molecular mechanisms of FOXO3A in tumor progression remain elusive. FOXO3A is downregulated and functions as a tumor suppressor in several types of tumors, including urothelial carcinoma. Downregulation of FOXO3A expression promotes tumor occurrence, metastasis, and progression in breast cancer (13), gastric carcinoma (14), pancreatic ductal adenocarcinoma (15), cervical carcinoma (16), clear cell renal cell carcinoma (17), and urothelial carcinoma (18).

In contrast, it plays a more complex supportive role in various types of malignancies. For example, in glioblastoma multiforme, overexpression of FOXO3A is positively correlated with tumor progression and predicts a poor survival outcome (19). Some studies have reported that activation of FOXO3A can lead to the elimination of cancer stem cells (20–22). FOXO3A also enhances the invasive ability of tumor cells by regulating matrix metalloproteinases in a number of tumor cell types (23, 24). However, whether FOXO3A serves as a useful biomarker in UTUC has not been reported.

Herein, we first detected FOXO3A by immunohistochemical analysis of UTUC patients and then investigated any potential association between FOXO3A and clinicopathologic parameters in patients with UTUC. Moreover, we examined the prognostic role of FOXO3A and aimed to build a predictive model for UTUC.

METHODS

Patients

The present study was carried out at Luohe Central Hospital, Luohe, China. Ethical approval for this study was obtained from the Institutional Ethics Committee of the Department of Pathology, Luohe Central Hospital, Luohe, China.

We collected UTUC samples between November 2004 and December 2015 from the archives for immunohistochemical and survival analysis. Finally, 107 UTUC patients who underwent surgery in the pathology department of Luohe Central Hospital were selected. The inclusion criteria were as follows: 1) patients with a diagnosis of UTUC who underwent radical nephroureterectomy and had clinicopathological data, 2) patients for whom concomitant bladder cancer was excluded on cystoscopy, and 3) patients without any other malignancies or severe chronic disease.

Regular follow-up had no standard protocol due to the retrospective nature of the study. Patients received clinical and radiological follow-up in accordance with final pathology, guidelines at that time, and physician judgement. Clinical data were extracted from medical records, including tumor number, pathological stage, histology grade, depth of invasion, lymph node metastasis (LNM) status, lymphovascular invasion (LVI), histological differentiation, adjuvant therapy and neoadjuvant chemotherapy. The clinical features of the UTUC patients are listed in **Table 1**.

Immunohistochemistry

IHC staining for FOXO3a was performed following the manufacturer's recommendations. Tissue section blocks were cut into 4-μm-thick slides, dewaxed and rehydrated. The antigen was recovered, and endogenous peroxidase activity was blocked. The slides were then incubated with anti-FOXO3a antibody (1:100 dilution; Abcam, Cambridge, UK) for 1 hour. The

TABLE 1 | Association between FOXO3A expression and UTUC clinicopathological parameters.

Parameter	Overall	FOXO3A (Low expression)	FOXO3A (High expression)	*P*-value
Patients (n)	107	67	40	
Age, years				
< 65	49 (45.8)	30 (44.8)	19 (47.5)	0.842
≥ 65	58 (54.2)	37 (55.2)	21 (52.5)	
Gender				
Male	71 (66.4)	42 (62.7)	29 (72.5)	0.398
Female	36 (33.6)	25 (37.3)	11 (27.5)	
Multifocality				
Multifocal	22 (20.6)	12 (17.9)	10 (25.0)	0.460
Single	85 (79.4)	55 (82.1)	30 (75.0)	
Histologic grade				
Low	37 (34.6)	27 (40.3)	10 (25.0)	0.142
High	70 (65.4)	40 (59.7)	30 (75.0)	
pT stage				
Ta/T1	46 (43.0)	23 (34.3)	23 (57.5)	0.026
T2/T3/T4	61 (57.0)	44 (65.7)	17 (42.5)	
LNM				
No	66 (61.7)	36 (53.7)	30 (75.0)	0.040
Yes	41 (38.3)	31 (46.3)	10 (25.0)	
LVI				
Absent	53 (49.5)	23 (34.3)	30 (75.0)	<0.001
Present	54 (50.5)	44 (65.7)	10 (25.0)	
Histological differentiation				
Pure urothelial	89 (83.2)	57 (85.1)	32 (80.0)	0.595
Variant histology[a]	18 (16.8)	10 (14.9)	8 (20.0)	
Adjuvant therapy				
Yes	32 (29.9)	25 (37.3)	7 (17.5)	0.048
No	75 (70.1)	42 (62.7)	33 (82.5)	
Neoadjuvant chemotherapy				
Yes	15 (14.0)	9 (13.4)	6 (15.0)	1.000
No	92 (86.0)	58 (86.6)	34 (85.0)	

LNM, lymph node metastasis; LVI, lymphovascular invasion; pT, pathological tumor stage.
[a]Variant histology included micropapillary, plasmocytoid, sarcomatoid, and neuroendocrine types.

presence of brown chromophores in the nucleus and cytoplasm of target cells indicated positive immunoreactivity. Finally, the slide was examined by optical microscopy at 400× magnification. Negative and positive controls were scored to optimize staining.

Evaluation of the IHC Results

FOXO3A-positive cells were assessed irrespective of the intensity of staining, and intracytoplasmic staining of FOXO3A was subsequently evaluated. The methodology applied by Tian et al. (16) was used to evaluate the FOXO3A score.

The percentage of cells positive for FOXO3A in the tumor stroma was recorded by two observers (TJM and LZ) as 0 = no positive cells, 1 = 1–10% positive cells, 2 = 10–50% positive cells, 3 = 50–80% positive cells, and 4 = >80% positive cells. The same score obtained by more than two observers was counted as the final score. Each specimen received a score of 0, 1, 2, 3 or 4 according to the intensity of FOXO3A staining. The product of the intensity score and stained area percentage was added and used as the total score. The final scores ranged from 0 to 8 and were designated low (0–4) or high (5–8).

Statistical Analysis

The analysis of FOXO3A IHC staining between tumor tissue and adjacent normal tissues was assessed by the t-test or chi-square using GraphPad Prism 8 software. When FOXO3a IHC was deep sectioned, the tumor component of three of the 43 tumor tissues was lost, so the FOXO3a expression of these tumors could not be assessed; ultimately, these three tumor tissues were excluded from the analyses involving the tumor component expression. All 40 pairs of UTUC and adjacent normal tissues were considered in the remaining analyses.

The SPSS 26.0 software suite (SPSS Inc., Chicago, IL, USA) was utilized for all statistical analyses, and statistical significance was considered at $P < 0.05$. Associations between FOXO3A staining expression and clinicopathologic variables were estimated with Fisher's exact test. Overall survival (OS) was defined as tumor-related death, and recurrence-free survival (RFS) was defined as any local recurrence or distant recurrence, whichever occurred first. The difference in OS and RFS between the FOXO3A-high and FOXO3A-low groups was assessed in univariable and multivariable settings. Variables such as FOXO3A expression, pathological tumor stage, and histological differentiation were grouped into two groups: high expression vs low expression of FOXO3A, early stage (Ta-T1) vs late stage (T2-4), and pure urothelial vs variant histology.

RESULTS

Expression of FOXO3A Protein Is Decreased in UTUC Patients

Using the IHC staining method, the relative level of FOXO3A protein expression was assessed in 40 pairs of UTUC and adjacent normal tissues. Representative photographs of FOXO3A IHC are shown in **Figures 1A–C**. The scatter dot plot illustrated that the average immunoreactivity score of FOXO3A protein in 40 UTUC tissues was significantly downregulated compared with that of the 40 normal tissues (3.08 ± 0.43 VS 4.30 ± 0.44) (**Figure 1D**, $P < 0.001$). The expression of FOXO3A was lower in UTUC patients than in normal tissues (UTUC vs normal tissues: 13/40 vs. 22/40, $P < 0.001$).

FOXO3A Immunoexpression Is Associated With the Clinical Parameters of UTUC Patients

The correlations of the relative FOXO3A expression level with clinical criteria are shown in **Table 1**. The results showed that low expression of FOXO3A was significantly associated with aggressive pathological stage ($P = 0.026$), lymphovascular invasion ($P < 0.001$), lymph node metastasis ($P = 0.040$), and adjuvant therapy ($P = 0.048$).

Survival Analysis

In the Kaplan-Meier analyses, patients with low FOXO3A expression had markedly worse OS ($P = 0.003$; **Figure 2A**) and RFS ($P = 0.003$; **Figure 2B**) than those with high FOXO3A expression. Furthermore, log rank tests demonstrated a significant difference between the 5-year OS (83.6% in the high expression group vs. 60.7% in the low expression group) and RFS (83.5% in the high expression group vs. 61.4% in the low expression group) rates in these two groups.

Univariate analyses determined that pathological stage (both $P = 0.008$), lymph node metastasis (both $P < 0.001$), lymphovascular invasion (both $P = 0.028$), adjuvant therapy

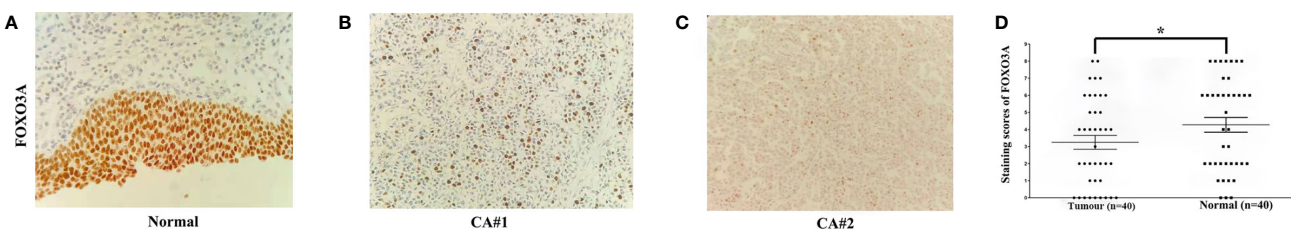

FIGURE 1 | FOXO3a expression in UTUC tissues determined by immunohistochemical staining (original magnification, 200×). **(A–C)** Representative FOXO3a expression in tumor and normal tissues, with positive expression located in the nucleus. **(D)** Scatter dot plot showing the staining score (mean ± SEM) of FOXO3a in tumor and normal tissues using the paired t-test. *P<0.001.

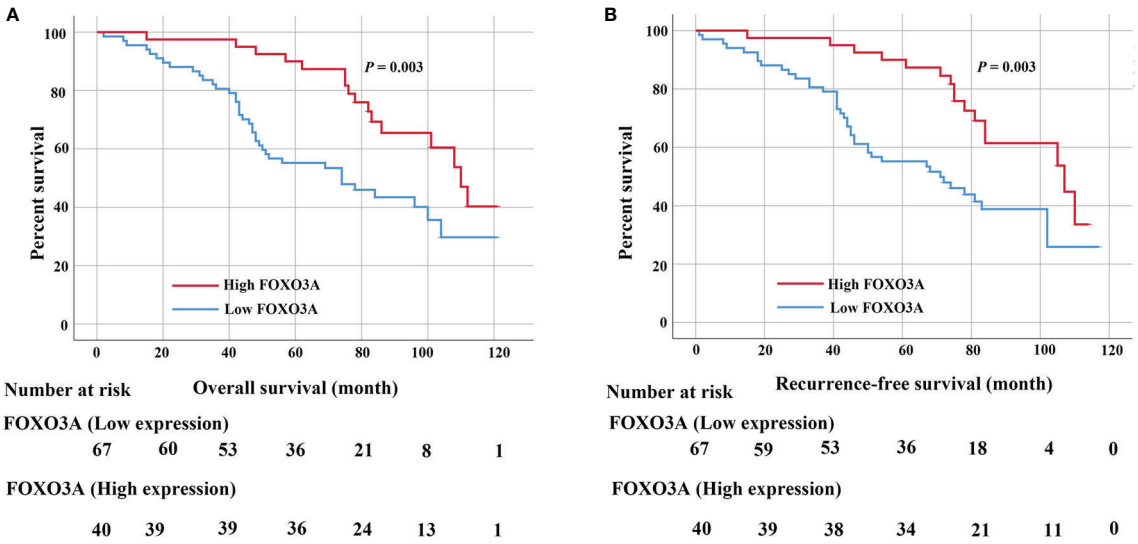

FIGURE 2 | **(A)** Kaplan–Meier curves for the 5-year OS rate of patients with UTUC and OS based on FOXO3a in UTUC patients. **(B)** Kaplan–Meier curves for the 5-year RFS rate of patients with UTUC and RFS based on FOXO3a in UTUC patients. Error bar = SEM.

($P = 0.025$ and $P = 0.015$) and FOXO3a protein (both $P = 0.004$) were significantly correlated with both OS and RFS. Histologic grade ($P = 0.049$) was also associated with OS (**Tables 2**, **3**). However, only pathological stage, lymph node metastasis and FOXO3A protein expression were ultimately determined to be predictors of the OS ($P = 0.031$, $P = 0.006$, $P = 0.014$) and RFS ($P = 0.022$, $P = 0.004$, $P = 0.010$) of UTUC patients in the multivariate analyses (**Tables 2**, **3**).

TABLE 2 | Univariate and multivariable analyses assessing the association between predictor variables and overall survival mortality among 107 patients for UTUC.

Characteristics	Univariate			Multivariate		
	Hazard Ratio	95%CI	*P-value*	Hazard Ratio	95%CI	*P-value*
Age, years						
≥ 65 *vs* < 65	1.110	0.649-1.894	0.704	0.875	0.482-1.588	0.660
Gender						
Male *vs* Female	0.699	0.404-1.207	0.199	0.754	0.428-1.328	0.329
Multifocal upper tract disease						
Multifocal *vs* Single	1.136	0.571-2.260	0.716	0.963	0.467-1.985	0.919
Histologic grade						
High *vs* Low	1.758	1.002-3.084	0.049	1.439	0.804-2.575	0.220
pT stage						
T2/T3/T4 *vs* Ta/T1	2.185	1.232-3.875	0.008	1.893	1.059-3.385	0.031
LNM						
Yes *vs* No	2.631	1.536-4.506	<0.001	2.152	1.245-3.721	0.006
LVI						
Present *vs* Absent	1.824	1.066-3.121	0.028	0.844	0.427-1.668	0.625
Histological differentiation						
Pure urothelial *vs* Variant histology[a]	1.017	0.497-2.081	0.963	0.870	0.406-1.867	0.721
Adjuvant therapy						
Yes *vs* No	1.887	1.084-3.282	0.025	1.203	0.662-2.187	0.543
Neoadjuvant chemotherapy						
Yes *vs* No	1.000	0.472-2.119	1.000	1.187	0.131-10.789	0.879
FOXO3A expression						
Low *vs* High	2.382	1.312-4.327	0.004	2.145	1.167-3.941	0.014

LNM, lymph node metastasis; LVI, lymphovascular invasion; pT, pathological tumor stage.

[a]*Variant histology included micropapillary, plasmocytoid, sarcomatoid, and neuroendocrine types.*

TABLE 3 | Univariate and multivariable analyses assessing the association between predictor variables and recurrence among 107 patients for UTUC.

Characteristics	Univariate			Multivariate		
	Hazard Ratio	95%CI	*P-value*	Hazard Ratio	95%CI	*P-value*
Age, years						
≥ 65 *vs* < 65	1.100	0.645-1.877	0.726	0.876	0.490-1.567	0.655
Gender						
Male *vs* Female	0.671	0.386-1.167	0.158	0.713	0.403-1.263	0.247
Multifocal upper tract disease						
Multifocal *vs* Single	1.189	0.598-2.367	0.621	0.971	0.470-2.005	0.913
Histologic grade						
High *vs* Low	1.708	0.975-2.993	0.062	1.298	0.715-2.356	0.391
pT stage						
T2/T3/T4 *vs* Ta/T1	2.181	1.229-3.871	0.008	1.971	1.102-3.527	0.022
LNM						
Yes *vs* No	2.708	1.580-4.643	<0.001	2.257	1.306-3.900	0.004
LVI						
Present vs Absent	1.834	1.069-3.144	0.028	0.844	0.426-1.670	0.626
Histological differentiation						
Pure urothelial *vs* Variant histology[a]	1.055	0.515-2.165	0.883	0.860	0.397-1.865	0.703
Adjuvant therapy						
Yes *vs* No	1.991	1.142-3.471	0.015	1.402	0.779-2.521	0.259
Neoadjuvant chemotherapy						
Yes *vs* No	1.039	0.488-2.209	0.922	1.144	0.125-10.491	0.906
FOXO3A expression						
Low *vs* High	2.385	1.314-4.329	0.004	2.227	1.209-4.101	0.010

LNM, lymph node metastasis; LVI, lymphovascular invasion; pT, pathological tumor stage.
[a]*Variant histology included micropapillary, plasmocytoid, sarcomatoid, and neuroendocrine types.*

DISCUSSION

Most recent studies have investigated whether FOXO3A plays a key role in UC. Shiota et al. (18) showed that FOXO3A inhibits UC invasiveness *via* Twist1, YB-1, and E-cadherin regulation. Zhuo et al. (25) reported that upregulation of CSTP1 expression suppresses IL-6 expression by regulating the Akt/FoxO3a signaling pathway in UC. Zhu et al. (26) showed that ATG7 overexpression promoted autophagic removal of FOXO3A in bladder carcinoma cells. Nevertheless, little is known about the prognostic role and clinicopathologic implications of FOXO3A in UTUC.

The results of our study reveal the following: (1) low FOXO3A expression predicts unfavorable survival and recurrence rates in UTUC patients; (2) FOXO3A expression is negatively associated with pathological stage, lymph node metastasis status, lymphovascular invasion, and adjuvant therapy in UTUC patients; and (3) FOXO3A expression is lower in UTUC tissue than in normal tissue. These findings indicate that FOXO3A is a prognostic factor for UTUC and that adjuvant therapy may be helpful in the high-risk subgroup of UTUC patients.

The biological mechanism of FOXO3A also illustrates its key role in the pathogenesis of UTUC. FOXO3A is part of a subfamily of winged-helix transcription factors, and its activity can be regulated by PI3K/AKT signaling (6). FOXO3A has been identified as a tumor suppressor because of its ability to promote cell cycle arrest (27) and DNA damage repair (28) and to inhibit tumor cell properties and tumorigenesis (22). Interestingly, several potential substrates for correlations between FOXO3A and tumor metastases have been described in previous studies (15, 29). In addition, FOXO3A has been implicated in epithelial mesenchymal transition, an important process during metastasis, and downregulation of FOXO3A promotes tumor cell migration and invasion (30–32).

This study is the first to evaluate the associations between FOXO3A expression and clinicopathological features and prognostic factors in UTUC by IHC. FOXO3A can be considered an anti-oncogene, and overexpression or pharmacological activation of FOXO3A inhibits tumor progression and improves prognosis. A previous study confirmed that downregulation of FOXO3a expression is associated with poor prognosis in bladder carcinoma patients by RT-PCR. Based on these data, we suggest that FOXO3A expression in UTUC tends to indicate a good prognosis.

However, there are still limitations to the study. 1) UTUC is rare, and the sample size was relatively small. 2) Determination of FOXO3A status is limited to IHC detection of the protein without integrated methodology or a scoring system. 3) The detailed molecular mechanism of FOXO3A in UTUC remains unknown. 4) Because this is a retrospective single-center study, potential bias exists and cannot avoid confounding factors and the absence of a standard for follow-up assessment. Therefore, larger patient groups are needed to further investigate the role of FOXO3A in UTUC and help us to better understand the molecular events involved in the pathogenesis of UTUC.

There is a complex crosstalk between FOXO3a/AKT signaling pathway and PD-L1 involved in tumorigenesis (26, 33). PD-L1 is a critical regulator in UC development and the level of functional PD-L1 plays a vital role in the effective immunotherapeutic treatments for UC (34, 35). Therefore, further exploration of the relationship between FOXO3a and PD-1 may have important implications for UTUC immunotherapy. FOXO3a activity is directly regulated by some miRNAs in UC (26, 36). This suggests that finding or synthesizing new chemotherapeutic

drugs targeting these miRNAs may also be a promising strategy for the treatment of UTUC.

In conclusion, our results showed that FOXO3A may be a potential biomarker for determining UTUC diagnosis and prognosis and may serve as a tumor-suppressing gene. Moreover, clarification of the underlying molecular mechanisms of FOXO3A in UTUC progression could aid in the development of targeted therapies for UTUC patients.

DATA AVAILABILITY STATEMENT

The original contributions presented in the study are included in the article/supplementary material. Further inquiries can be directed to the corresponding author.

ETHICS STATEMENT

The studies involving human participants were reviewed and approved by The Institutional Ethics Committee of Luohe Central Hospital, Luohe, China. The patients/participants provided their written informed consent to participate in this study.

AUTHOR CONTRIBUTIONS

GZ, EJ, and LZ: writing and figures. GZ, WS, YH, RR, and TM: concept and proof reading. All authors contributed to the article and approved the submitted version.

REFERENCES

1. Tay LJ, Chatterton K, Colemeadow J, Nair R, Bultitude M, Thomas K. Improving management of upper tract urothelial carcinoma. *BJU Int* (2020) 126:5–6. doi: 10.1111/bju.15068
2. Roupret M, Babjuk M, Burger M, Capoun O, Cohen D, Comperat EM, et al. European Association of Urology Guidelines on Upper Urinary Tract Urothelial Carcinoma: 2020 Update. *Eur Urol* (2021) 79:62–79. doi: 10.1016/j.eururo.2020.05.042
3. Roberts JL, Ghali F, Aganovic L, Bechis S, Healy K, Rivera-Sanfeliz G, et al. Diagnosis, management, and follow-up of upper tract urothelial carcinoma: an interdisciplinary collaboration between urology and radiology. *Abdom Radiol (NY)* (2019) 44:3893–905. doi: 10.1007/s00261-019-02293-9
4. Hassler MR, Bray F, Catto JWF, Grollman AP, Hartmann A, Margulis V, et al. Molecular Characterization of Upper Tract Urothelial Carcinoma in the Era of Next-generation Sequencing: A Systematic Review of the Current Literature. *Eur Urol* (2020) 78:209–20. doi: 10.1016/j.eururo.2020.05.039
5. Mori K, Janisch F, Mostafaei H, Lysenko I, Kimura S, Egawa S, et al. Prognostic value of preoperative blood-based biomarkers in upper tract urothelial carcinoma treated with nephroureterectomy: A systematic review and meta-analysis. *Urol Oncol* (2020) 38:315–33. doi: 10.1016/j.urolonc.2020.01.015
6. Alvarez B, Martinez AC, Burgering BM, Carrera AC. Forkhead transcription factors contribute to execution of the mitotic programme in mammals. *Nature* (2001) 413:744–7. doi: 10.1038/35099574
7. Kim CG, Lee H, Gupta N, Ramachandran S, Kaushik I, Srivastava S, et al. Role of Forkhead Box Class O proteins in cancer progression and metastasis. *Semin Cancer Biol* (2018) 50:142–51. doi: 10.1016/j.semcancer.2017.07.007
8. White RR, Maslov AY, Lee M, Wilner SE, Levy M, Vijg J. FOXO3a acts to suppress DNA double-strand break-induced mutations. *Aging Cell* (2020) 19: e13184. doi: 10.1111/acel.13184
9. Usami M, Kikuchi S, Takada K, Ono M, Sugama Y, Arihara Y, et al. FOXO3a Activation by HDAC Class IIa Inhibition Induces Cell Cycle Arrest in Pancreatic Cancer Cells. *Pancreas* (2020) 49:135–42. doi: 10.1097/MPA.0000000000001462
10. Lee N, Tilija Pun N, Jang WJ, Bae JW, Jeong CH. Pitavastatin induces apoptosis in oral squamous cell carcinoma through activation of FOXO3a. *J Cell Mol Med* (2020) 24:7055–66. doi: 10.1111/jcmm.15389
11. Sun Z, Li M, Bai L, Fu J, Lu J, Wu M, et al. Arsenic trioxide inhibits angiogenesis in vitro and in vivo by upregulating FoxO3a. *Toxicol Lett* (2019) 315:1–8. doi: 10.1016/j.toxlet.2019.08.009
12. Fasano C, Disciglio V, Bertora S, Lepore Signorile M, Simone C. FOXO3a from the Nucleus to the Mitochondria: A Round Trip in Cellular Stress Response. *Cells* (2019) 8:1110. doi: 10.3390/cells8091110
13. Pellegrino M, Rizza P, Dona A, Nigro A, Ricci E, Fiorillo M, et al. FoxO3a as a Positive Prognostic Marker and a Therapeutic Target in Tamoxifen-Resistant Breast Cancer. *Cancers (Basel)* (2019) 11:1858. doi: 10.3390/cancers11121858
14. Hu C, Ni Z, Li BS, Yong X, Yang X, Zhang JW, et al. hTERT promotes the invasion of gastric cancer cells by enhancing FOXO3a ubiquitination and subsequent ITGB1 upregulation. *Gut* (2017) 66:31–42. doi: 10.1136/gutjnl-2015-309322
15. Li J, Yang R, Dong Y, Chen M, Wang Y, Wang G. Knockdown of FOXO3a induces epithelial-mesenchymal transition and promotes metastasis of pancreatic ductal adenocarcinoma by activation of the beta-catenin/TCF4 pathway through SPRY2. *J Exp Clin Cancer Res* (2019) 38:38. doi: 10.1186/s13046-019-1046-x
16. Tian Y, Qi P, Hu X. Downregulated FOXO3a Associates With Poor Prognosis and Promotes Cell Invasion and Migration via WNT/beta-catenin Signaling in Cervical Carcinoma. *Front Oncol* (2020) 10:903. doi: 10.3389/fonc.2020.00903
17. Ni D, Ma X, Li HZ, Gao Y, Li XT, Zhang Y, et al. Downregulation of FOXO3a promotes tumor metastasis and is associated with metastasis-free survival of patients with clear cell renal cell carcinoma. *Clin Cancer Res* (2014) 20:1779–90. doi: 10.1158/1078-0432.CCR-13-1687
18. Shiota M, Song Y, Yokomizo A, Kiyoshima K, Tada Y, Uchino H, et al. Foxo3a suppression of urothelial cancer invasiveness through Twist1, Y-box-binding protein 1, and E-cadherin regulation. *Clin Cancer Res* (2010) 16:5654–63. doi: 10.1158/1078-0432.CCR-10-0376
19. Qian Z, Ren L, Wu D, Yang X, Zhou Z, Nie Q, et al. Overexpression of FoxO3a is associated with glioblastoma progression and predicts poor patient prognosis. *Int J Cancer* (2017) 140:2792–804. doi: 10.1002/ijc.30690
20. Chiu CF, Chang YW, Kuo KT, Shen YS, Liu CY, Yu YH, et al. NF-kappaB-driven suppression of FOXO3a contributes to EGFR mutation-independent gefitinib resistance. *Proc Natl Acad Sci U S A* (2016) 113:E2526–35. doi: 10.1073/pnas.1522612113
21. Sato A, Okada M, Shibuya K, Watanabe E, Seino S, Narita Y, et al. Pivotal role for ROS activation of p38 MAPK in the control of differentiation and tumor-initiating capacity of glioma-initiating cells. *Stem Cell Res* (2014) 12:119–31. doi: 10.1016/j.scr.2013.09.012
22. Liu H, Song Y, Qiu H, Liu Y, Luo K, Yi Y, et al. Downregulation of FOXO3a by DNMT1 promotes breast cancer stem cell properties and tumorigenesis. *Cell Death Differ* (2020) 27:966–83. doi: 10.1038/s41418-019-0389-3
23. Storz P, Doppler H, Copland JA, Simpson KJ, Toker A. FOXO3a promotes tumor cell invasion through the induction of matrix metalloproteinases. *Mol Cell Biol* (2009) 29:4906–17. doi: 10.1128/MCB.00077-09
24. Xu K, Pei H, Zhang Z, Dong S, Fu RJ, Wang WM, et al. FoxO3a mediates glioma cell invasion by regulating MMP9 expression. *Oncol Rep* (2016) 36:3044–50. doi: 10.3892/or.2016.5087
25. Zhuo D, Wu Y, Luo J, Deng L, Niu X. CSTP1 inhibits IL-6 expression through targeting Akt/FoxO3a signaling pathway in bladder cancer cells. *Exp Cell Res* (2019) 380:80–9. doi: 10.1016/j.yexcr.2019.04.019
26. Zhu J, Li Y, Luo Y, Xu J, Liufu H, Tian Z, et al. A Feedback Loop Formed by ATG7/Autophagy, FOXO3a/miR-145 and PD-L1 Regulates Stem-Like Properties and Invasion in Human Bladder Cancer. *Cancers (Basel)* (2019) 11:349. doi: 10.3390/cancers11030349

27. Liu Z, Shi Z, Lin J, Zhao S, Hao M, Xu J, et al. Piperlongumine-induced nuclear translocation of the FOXO3A transcription factor triggers BIM-mediated apoptosis in cancer cells. *Biochem Pharmacol* (2019) 163:101–10. doi: 10.1016/j.bcp.2019.02.012
28. Zhou Y, Chen E, Tang Y, Mao J, Shen J, Zheng X, et al. miR-223 overexpression inhibits doxorubicin-induced autophagy by targeting FOXO3a and reverses chemoresistance in hepatocellular carcinoma cells. *Cell Death Dis* (2019) 10:843. doi: 10.1038/s41419-019-2053-8
29. Li R, Quan Y, Xia W. SIRT3 inhibits prostate cancer metastasis through regulation of FOXO3A by suppressing Wnt/beta-catenin pathway. *Exp Cell Res* (2018) 364:143–51. doi: 10.1016/j.yexcr.2018.01.036
30. Liu H, Yin J, Wang H, Jiang G, Deng M, Zhang G, et al. FOXO3a modulates WNT/beta-catenin signaling and suppresses epithelial-to-mesenchymal transition in prostate cancer cells. *Cell Signal* (2015) 27:510–8. doi: 10.1016/j.cellsig.2015.01.001
31. Luo M, Wu C, Guo E, Peng S, Zhang L, Sun W, et al. FOXO3a knockdown promotes radioresistance in nasopharyngeal carcinoma by inducing epithelial-mesenchymal transition and the Wnt/beta-catenin signaling pathway. *Cancer Lett* (2019) 455:26–35. doi: 10.1016/j.canlet.2019.04.019
32. Bakir B, Chiarella AM, Pitarresi JR, Rustgi AK. EMT, MET, Plasticity, and Tumor Metastasis. *Trends Cell Biol* (2020) 30:764–76. doi: 10.1016/j.tcb.2020.07.003
33. Chen HN, Liang KH, Lai JK, Lan CH, Liao MY, Hung SH, et al. EpCAM Signaling Promotes Tumor Progression and Protein Stability of PD-L1 through the EGFR Pathway. *Cancer Res* (2020) 80:5035–50. doi: 10.1158/0008-5472.CAN-20-1264
34. Zhou TC, Sankin AI, Porcelli SA, Perlin DS, Schoenberg MP, Zang X. A review of the PD-1/PD-L1 checkpoint in bladder cancer: From mediator of immune escape to target for treatment. *Urol Oncol* (2017) 35:14–20. doi: 10.1016/j.urolonc.2016.10.004
35. Powles T, Eder JP, Fine GD, Braiteh FS, Loriot Y, Cruz C, et al. MPDL3280A (anti-PD-L1) treatment leads to clinical activity in metastatic bladder cancer. *Nature* (2014) 515:558–62. doi: 10.1038/nature13904
36. Chang Y, Jin H, Li H, Ma J, Zheng Z, Sun B, et al. MiRNA-516a promotes bladder cancer metastasis by inhibiting MMP9 protein degradation via the AKT/FOXO3A/SMURF1 axis. *Clin Transl Med* (2020) 10:e263. doi: 10.1002/ctm2.263s

Conflict of Interest: The authors declare that the research was conducted in the absence of any commercial or financial relationships that could be construed as a potential conflict of interest.

frontiers in Oncology

ORIGINAL RESEARCH
published: 24 May 2021
doi: 10.3389/fonc.2021.679158

Body Composition Parameters May Be Prognostic Factors in Upper Urinary Tract Urothelial Carcinoma Treated by Radical Nephroureterectomy

Yulong Pan[1,2], Zeyu Chen[1†], Lanqing Yang[1†], Xingyuan Wang[1], Zeng Yi[1], Liang Zhou[2], Yongjiang Chen[2], Lu Yang[1], Hui Zhuo[2], Yige Bao[1] and Qiang Wei[1*]*

[1] West China Hospital, Sichuan University, Chengdu, China, [2] Department of Urology, Chengdu Third People's Hospital, Chengdu, China

OPEN ACCESS

Edited by:
Antonio Augusto Ornellas, National Cancer Institute (INCA), Brazil

Reviewed by:
Gilda Alves Brown, Rio de Janeiro State University, Brazil
Lorenzo Bianchi, University of Bologna, Italy

***Correspondence:**
Yige Bao
baoyige@hotmail.com
Qiang Wei
weiqiang933@126.com

[†]These authors have contributed equally to this work

Specialty section:
This article was submitted to Genitourinary Oncology, a section of the journal Frontiers in Oncology

Received: 11 March 2021
Accepted: 28 April 2021
Published: 24 May 2021

Citation:
Pan Y, Chen Z, Yang L, Wang X, Yi Z, Zhou L, Chen Y, Yang L, Zhuo H, Bao Y and Wei Q (2021) Body Composition Parameters May Be Prognostic Factors in Upper Urinary Tract Urothelial Carcinoma Treated by Radical Nephroureterectomy. Front. Oncol. 11:679158. doi: 10.3389/fonc.2021.679158

Objective: This study assessed the association between body composition and prognosis of patients with upper urinary tract urothelial carcinoma (UTUC) patients treated by radical nephroureterectomy.

Methods: We retrospectively collected baseline data on age, sex, body mass index (BMI), hypertension, diabetes, and tumor-related factors. Computed tomography (CT) scans were performed to measure body composition parameters such as muscle attenuation (MA), total abdominal muscle area (TAMA), visceral fat area (VFA), intermuscular fat area (IMF), and lateral/posterior perirenal fat thickness (L/P PNF), visceral fat density (VD), and subcutaneous fat density (SD). Patient follow-up was conducted *via* telephone or in the clinic. The endpoints of follow-up were all-cause death, local progression or distant metastasis. Survival analysis was analyzed using the Kaplan-Meier method, and risk factors associated with prognosis were identified using univariate and multivariate Cox proportional hazard analyses.

Results: Among the 273 UTUC patients (median age, 68 years) enrolled in our study, 102 had a BMI > 24.0, 100 suffered from diabetes, and 120 had hypertension. A large proportion of patients (189) had high grade tumors. Across all patients, 1- and 3-year rates for overall survival were 86.45% and 75.55%; local progression-free survival, 92.11% and 89.67%; and distant metastasis-free survival, 85.23% and 80.17%. Based on the Cox regression analysis, MA, IMF, TAMA, TPA, TPT, APT, SMI and PMI significantly reduced the risk of local progression ($p < 0.05$), while PPNF = 1 point reduced the risk of distant metastasis ($p < 0.05$). Overall survival was significantly associated with MA, TAMA, and SMI ($p < 0.05$).

Conclusion: Our findings illustrate that body composition parameters can act as independent predictors of prognosis in UTUC patients who underwent RNU. These results can help improve stratification of patients and optimize postoperative treatment.

Keywords: upper urinary tract urothelial carcinoma, body composition parameters, prognostic factors, radical nephroureterectomy, computed tomography

INTRODUCTION

Urothelial cancer is an aggressive disease associated with high recurrence and progression rates (1). Upper urinary tract urothelial carcinoma (UTUC) accounts for approximately 10% of all renal tumors and 5-10% of all urothelial carcinomas; about 60% of UTUCs are invasive at diagnosis (1). The standard treatment for UTUC is radical nephroureterectomy (RNU) along with excision of the bladder cuff (1).

Body mass index (BMI) is an international indicator of body weight and thinness, as well as of an individual's health status. Studies have reported a strong correlation between BMI and prognosis in tumor patients (2, 3). However, individuals with the same BMI can have distinct body compositions, due to differences in body structure and functioning (4). The human body consists of lean tissue (i.e. muscle tissue), and adipose tissue, which stores fat. BMI is a relatively crude measure that does not take into account the individual effects of lean tissue, bones, and adipose tissue, nor does it describe the distribution of fat in the body (5–7). Studies have reported differences in BMI based on ethnicity (8), which therefore has confounded efforts to examine the association between BMI and prognosis. Additionally, muscles and adipose tissue are increasingly being recognized as separate organs, since they play important, but unique roles in the occurrence, progression, prognosis, and other aspects of diseases (5–7).

Apart from its effect on disease prognosis, body composition is also associated with risk of surgical complications, therapeutic efficacy, and treatment-related side effects (9). In this study, we retrospectively analyzed whether individual body composition parameters, including muscle and adipose tissue, are associated with prognosis of UTUC patients treated by RNU.

MATERIALS AND METHODS

Study Population

We retrospectively collected relevant data on UTUC patients registered in our hospital information system between January 2014 and June 2017. We included patients who received a pathological diagnosis of UTUC and had undergone RNU treatment at our hospital. We excluded patients who showed signs of other malignant neoplasms and those with metastatic tumors at local lymph nodes or distant organs at initial diagnosis. We collected data on baseline and clinical characteristics, including age, sex, weight, height, BMI, body composition parameters (see below), diagnosis of hypertension and diabetes, as well as various tumor characteristics (stage, primary site, laterality, grade, and maximum diameter). Due to the retrospective nature of this study, no information on alcohol intake, diet and exercises could be obtained, except for smoking

This study was approved by the Ethics Committee of our hospital.

Computed Tomography Scans and Body Composition Measurements

For each patient, results of computed tomography (CT) scan using a 64-slice multi detector CT scanner (Somatom Definition Flash, Siemens AG, Erlangen, Germany) was obtained from the database of our center, and conducted segmentation of the CT data using Volume. We followed previously described methods to measure body composition parameters.

We measured total abdominal muscle area (TAMA), which includes the rectus abdominis, intra-abdominal oblique, external oblique, transverse abdominis, paraspinal, and psoas muscles. We also measured total psoas muscle area (TPA), visceral fat area (VFA), subcutaneous fat area (SFA), visceral fat density (VD) and subcutaneous fat density (SD). Mean muscle attenuation (MA) and intermuscular fat tissue were measured at the level of the L3 inferior endplate, while the axial/transversal psoas thickness (APT/TPT) and subcutaneous fat thickness (SCF) were measured at the level of the umbilicus. Perirenal fat area (PFA) and lateral/posterior perirenal fat thickness (L/P PNF) were measured at the level of the renal vein (< 1 cm = 0 points, 1.1-1.9 cm = 1 point, > 2 cm = 2 points) (10). Tissue was defined as fat if its CT value fell within a range from -150 to -50 Hounsfield units, or as muscle if its CT value fell within a range from -29 to 150 Hounsfield units (10, 11).

Data Standardization and End Points of Study

Using data collected on fat and muscle area, we derived height-normalized indices (reported as cm^2/m^2) for subcutaneous fat (SFI), intermuscular fat (IFI), visceral fat (VFI), skeletal muscle (SMI), and psoas muscle (PMI) using data collected on fat and muscle area. Similarly, psoas muscle thickness, expressed as standardized APT and TPT, was normalized to height and reported as mm/m.

Based on previous literature, we calculated a VFA to SFA ratio (V/S) to provide a single measure of abdominal fat: an elevated V/S indicated higher visceral fat than subcutaneous fat content, and a V/S ≥ 0.4 was used to define visceral obesity (12). The endpoints of our study were overall survival (OS), defined as all-cause death; local progression (local metastasis or recurrence); and distant metastasis.

Patients Follow up

Follow-up was conducted based on the risk stratification of patients using EAU guidelines (1). Cystoscopy was conducted for low-risk patients at three months after RNU. If no reccurence was found in the bladder, subsequent cystoscopy was performed after one year and repeated annually. High-risk patients underwent cystoscopy and cytology every three months for the first two years, then every six months thereafter until five years, when checkups were done annually. In the case of high-risk patients, CT urograms and chest CTs were performed every six months for two years, then annually.

Statistical Analyses

All statistical analyses were performed using Empower 2.0. Differences in baseline characteristics were assessed using a chi-squared test. Continuous data were presented as median (min-max) and categorical data as frequency (%).Patient survival was analyzed using the Kaplan-Meier method. Further, a univariate Cox proportional hazard model was used to analyze OS, local progression-free survival (LPFS), and distant metastasis-free survival (DMFS). After adjusting for tumor stage, grade, tumor size (maximum diameter cut off at 3cm) and lymph node invasion, we included all significant variables ($p < 0.05$) in a multi-variate Cox proportional hazard analysis.

RESULTS

Baseline Characteristics

Among the 273 UTUC patients enrolled in this study, who were aged 30 to 92 years (median 68), 102 patients were considered as overweight (BMI > 24). Many of these patients also suffered from diabetes (n = 100) and hypertension (n = 120). A large proportion of these patients had tumors diagnosed as high-grade based on pathology (n = 189), including 90 patients with T3 tumors and 27 with T4 tumors. Further details on baseline characteristics are provided in **Table 1**.

Patient Survival

During follow-up, we found that 24 (9.56%) patients experienced local progression after RNU, 48 (19.13%) suffered distant metastasis, and 59 (23.51%) died. Kaplan-Meier analysis indicated OS rates of 86.45% at 1 year and 75.55% at 3 years (**Figure 1A**). The corresponding LPFS rates 92.11% and 89.67% (**Figure 1B**), while DMFS rates were 85.23% and 80.17% (**Figure 1C**).

Prognostic Factors

The uni-variate Cox proportional hazard analyses showed that higher values of MA, TAMA, TPT, SMI, and standardized TPT were associated with lower OS in patients ($p < 0.1$; **Table 2**). An increase in PMI, MA, TAMA, TPA, TPT, or APT was associated with lower incidence of local progression, while MA, TPA, PPNF =1 point, PMI, and standardized TPT was negatively associated with risk of distant metastasis.

TABLE 1 | Baseline characteristics of study cohort.

	Median (Min-Max)
Age	68.00 (30.00-92.00)
Muscle attenuation(MA)	30.70 (1.20-57.10)
IMF(intermuscular)	5.14 (0.62-17.65)
TAMA	53.87 (12.81-104.12)
TPA	8.50 (2.18-42.44)
VFA	58.48 (6.52-155.53)
SFA	55.09 (6.27-199.02)
Abdominal wall fat thickness	1.83 (0.31-4.43)
TPT	2.87 (1.45-5.56)
APT	3.90 (1.94-5.43)
LPNF	1.68 (0.10-5.05)
PPNF	1.17 (0.10-4.43)
PFA	7.51 (0.21-29.30)
SMI	20.63 (5.69-38.24)
PMI	3.24 (0.92-13.86)
SFA(standardized)	21.09 (2.30-70.51)
TPT(standardized)	2.39 (0.79-2570.18)
APT(standardized)	2.41 (1.21-3.28)
VFA/SFA	1.05 (0.22-2.89)
VFA(standardized)	22.84 (2.49-60.00)
(VFA+SFA+IFA)/TAMA	2.46 (0.24-6.34)
VD(visceral fat density)	-96.30 (-116.10–74.30)
SD(subcutaneous fat density)	-102.60 (-124.40–72.70)
	N (%)
Gender	
Male	148 (54.21%)
Female	125 (45.79%)
BMI	
<18.5	29 (10.78%)
18.5-23.9	138 (51.30%)
24-26.9	64 (23.79%)
27-29.9	35 (13.01%)
≥29.9	3 (1.12%)
IFG(≥ 5.6)or type 2 diabetes mellitus	
Yes	169 (62.83%)
No	100 (37.17%)
Hypertension(≥130/85mmHg)	
No	153 (56.04%)
Yes	120 (43.96%)
Hydronephrosis	
No	110 (41.35%)
Yes	156 (58.65%)
Primary site	
Renal pelvis	124 (45.59%)
Ureter	98 (36.03%)
T stage	
Tx, Ta, Tis	8 (2.96%)
T1	95 (35.19%)
T2	50 (18.52%)
T3	90 (33.33%)
T4	27 (10.00%)
Grade	
Low	80 (29.74%)
High	189 (70.26%)
Tumor size(maximum diameter)	
<3cm	82 (30.37%)
≥3cm	188 (69.63%)
Lymph-node invasion	
Without	252 (93.68%)
Identified	17 (6.32%)
Adjuvant therapy	
No	178 (77.06%)
Yes	53 (22.94%)

(Continued)

TABLE 1 | Continued

	Median (Min-Max)
Laterality	
Left	145 (53.11%)
Right	128 (46.89%)
LPNF(categorized)	
0	86 (40.95%)
1	82 (39.05%)
2	42 (20.00%)
PPNF(categorized)	
0	77 (36.84%)
1	95 (45.45%)
2	37 (17.70%)

After adjusting for confounding factors, the results of the adjusted model analysis showed that there was a significant association between MA, TAMA, SMI and OS (P<0.05). Additionally, MA, IMF, TAMA, TPA, TPT, APT, SMI and PMI were found to be inversely related to the risk of local progression, while PPNF = 1 point was associated with significantly lower risk of distant metastasis (**Table 3**).

DISCUSSION

Although both UTUC and bladder cancer involve malignant tumors in the urinary epithelium, UTUC has typically invaded the muscle layer by the time it is diagnosed. Therefore, UTUC patients have a significantly worse prognosis than those with bladder cancer, and they remain at high risk of tumor recurrence and metastasis even after RNU (1). Few studies have examined the combined prognostic effect of muscle and fat tissues, particularly in the Chinese population. To our knowledge, this is the first study examining the relationship of muscle and fat-related parameters with survival outcomes in UTUC patients treated with RNU. We found that muscle quality, muscle quantity, and perirenal fat thickness correlated significantly with survival of UTUC patients after RNU.

Studies involving UTUC patients have typically focused on various factors affecting disease prognosis, including tumor-related factors such as pathology stage and grade, or clinical factors such as physical status and smoking history (1). Age, tumor grade, location, T stage, growth pattern, lymphovascular invasion, and histological variation can affect the prognosis of UTUC patients treated with RNU (1). However, these factors depend on postoperative pathological examinations. Few large studies have examined preoperative factors that may help predict prognosis of UTUC patients.

Fat and muscle are two important components of the body that play distinct, yet significant roles in the management of diseases (2, 6). Clinical imaging has proved to be reliable for the assessment of the quantity and distribution of muscle and fat in the body (13, 14). The analysis of CT scans at the level of the third lumbar spine vertebra is considered the gold standard for measuring body composition parameters in muscle and adipose tissue. Among cancer patients undergoing chemotherapy, molecular-targeted therapy or immunotherapy (3, 9, 15), the loss of muscle mass or quality has been associated with decreased OS, increased incidence of surgical complications, as well as increased frequency and severity of adverse reactions. The prognostic effects of adipose tissue parameters vary based on the tumor type (2, 6).

Body composition parameters associated with skeletal mass (SMI and MA) have been identified as prognostic factors in lung cancer, esophageal cancer, gastric cancer, and pancreatic cancer (3, 9, 15, 16). MA is used to measure muscle quality, while SMI is used to measure body muscle mass (17, 18). However, it is unclear whether muscle mass (SMI) or quality (MA) is more suitable to understand disease prognosis in tumor patients (18). For example, in patients with non-small cell lung cancer and pancreatic cancer, only MA is a prognostic factor for OS. Low MA is associated with obesity, diabetes, loss of exercise and muscle atrophy. Studies have found that the attenuation density of skeletal muscle positively correlates with muscle quality and strength, and negatively correlates with muscle fiber fat content. Indeed, attenuation density of skeletal muscle varies inversely with the lipid drop content in muscle fibers (19). The mechanisms underlying these changes in muscle appear to affect its quality earlier, or more severely, than its quantity.

Based on the observed effects of muscle mass and quantity on prognosis, preoperative targeted intervention of muscle state may be an effective way to improve outcomes. Our results argue for preoperative efforts to improve muscle mass of

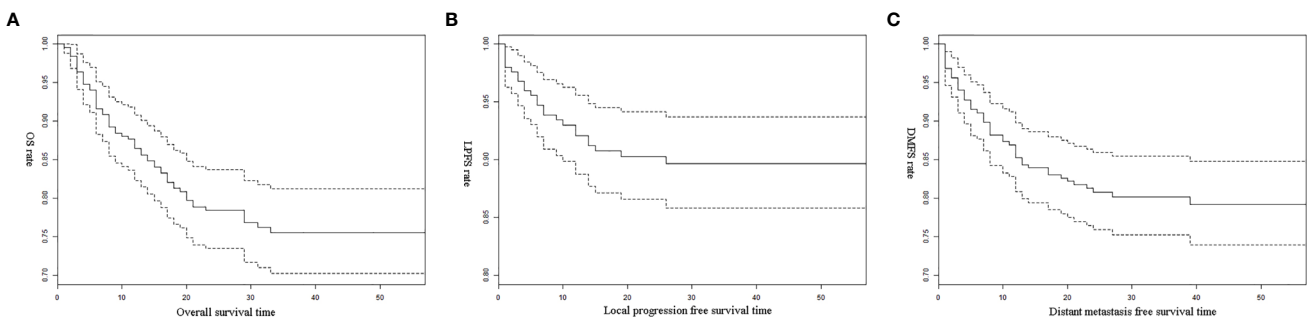

FIGURE 1 | **(A)** Overall survival of all patients; **(B)** Local progression free survival of all patients; **(C)** Distant metastasis free survival of all patients.

TABLE 2 | Univariate cox proportional hazard analysis for risk factors of patients' prognosis.

	OS HR (95%CI) p-value	LPS HR (95%CI) p-value	DM HR (95%CI) p-value
MA	0.96 (0.93, 0.98) 0.0015	0.96 (0.92, 1.00) 0.0587	0.96 (0.93, 0.99) 0.0051
IMF	1.05 (0.96, 1.14) 0.2946	0.88 (0.73, 1.06) 0.1638	1.02 (0.93, 1.12) 0.6566
TAMA	0.98 (0.97, 1.00) 0.0556	0.97 (0.95, 1.00) 0.0718	0.99 (0.97, 1.01) 0.2523
TPA	0.96 (0.90, 1.02) 0.1815	0.81 (0.69, 0.96) 0.0161	0.92 (0.84, 1.00) 0.0454
VFA	1.00 (0.99, 1.01) 0.7856	0.99 (0.98, 1.01) 0.3959	1.00 (0.99, 1.01) 0.6543
SFA	1.00 (0.99, 1.01) 0.5291	1.00 (0.98, 1.01) 0.5658	1.00 (0.99, 1.01) 0.7772
Abdominal wall fat thickness	1.23 (0.85, 1.78) 0.2781	1.31 (0.69, 2.49) 0.4015	1.03 (0.68, 1.57) 0.8775
TPT	0.62 (0.40, 0.96) 0.0339	0.36 (0.16, 0.83) 0.0162	0.84 (0.54, 1.32) 0.4491
APT	0.94 (0.61, 1.46) 0.7910	0.50 (0.24, 1.03) 0.0593	0.96 (0.60, 1.53) 0.8704
LPNF	0.94 (0.66, 1.33) 0.7189	0.78 (0.41, 1.49) 0.4598	0.99 (0.69, 1.42) 0.9478
PPNF	1.04 (0.69, 1.56) 0.8514	0.82 (0.38, 1.74) 0.5971	1.10 (0.72, 1.68) 0.6518
PFA	0.98 (0.92, 1.04) 0.4224	0.95 (0.86, 1.06) 0.3808	0.99 (0.93, 1.05) 0.7929
LPNF(categorized)			
0	1.0	1.0	1.0
1	0.83 (0.44, 1.57) 0.5641	0.63 (0.21, 1.93) 0.4188	0.71 (0.35, 1.43) 0.3365
2	0.75 (0.33, 1.69) 0.4862	0.48 (0.10, 2.26) 0.3528	0.94 (0.43, 2.08) 0.8848
PPNF(categorized)			
0	1.0	1.0	1.0
1	0.65 (0.34, 1.21) 0.1726	0.47 (0.15, 1.44) 0.1885	0.31 (0.14, 0.68) 0.0034
2	0.65 (0.27, 1.52) 0.3155	0.48 (0.10, 2.24) 0.3468	0.91 (0.43, 1.94) 0.8161
SMI	0.96 (0.91, 1.01) 0.0932	0.94 (0.86, 1.02) 0.1187	0.97 (0.92, 1.03) 0.3063
PMI	0.90 (0.76, 1.06) 0.2090	0.57 (0.36, 0.90) 0.0169	0.79 (0.62, 1.00) 0.0507
SFA(standardized)	1.00 (0.97, 1.02) 0.7228	0.99 (0.96, 1.04) 0.7899	1.00 (0.98, 1.03) 0.6957
TPT(standardized)	0.56 (0.29, 1.06) 0.0765	0.56 (0.17, 1.80) 0.3275	0.55 (0.28, 1.08) 0.0810
APT(standardized)	1.15 (0.51, 2.57) 0.7417	0.36 (0.10, 1.28) 0.1147	1.03 (0.44, 2.40) 0.9418
VFA/SFA	0.98 (0.53, 1.81) 0.9443	0.72 (0.24, 2.14) 0.5531	0.84 (0.42, 1.69) 0.6321
VFA(standardized)	1.00 (0.98, 1.02) 0.9998	0.99 (0.95, 1.03) 0.6399	1.01 (0.98, 1.03) 0.5012
(VFA+SFA+IFA)/TAMA	1.11 (0.88, 1.39) 0.3859	1.13 (0.76, 1.66) 0.5503	1.15 (0.90, 1.47) 0.2521
VD	1.02 (0.99, 1.05) 0.2256	1.03 (0.98, 1.09) 0.2880	1.00 (0.96, 1.04) 0.9838
SD	1.00 (0.97, 1.03) 0.8808	1.02 (0.97, 1.07) 0.3878	0.99 (0.96, 1.03) 0.6732

UTUC patients. Studies have reported that resistance training alone does not significantly improve musclemass (17). Further studies are necessary to identify approaches, perhaps combining exercise, nutrition, and drugs, that can effectively build muscle mass in UTUC patients.

Based on previous studies, we analyzed the prognostic effects of psoas muscle parameters (PMI and standardized TPT) on UTUC patients treated with RNU (20, 21). Patients with higher MA, TAMA and SMI values tended to be at lower risk of all-cause death. MA, IMF, TAMA, TPA, TPT, APT, SMI and PMI were associated with a reduction in local progression of the tumor; PPNF = 1 point was also associated with a reduced risk of distant metastasis. Our findings support the idea that psoas characteristics serve as markers of sarcopenia (20, 21).

Studies have reported that fat parameters (VFA, SFA, SCF, IFA, SD, VD) measured at the third lumbar vertebra were associated with prognosis of patients with adenoma-derived tumors, including renal cancer, colorectal cancer, or gastric carcinoma (11, 22). We found that these parameters had no effect on the prognosis of UTUC patients. This can be due to the small sample size in our study, or the differences between urothelial carcinoma and adenocarcinoma at the cellular level:

TABLE 3 | Multivariate cox proportional hazard analysis for risk factors of patients' prognosis.

	OS HR (95%CI) p-value	LPS HR (95%CI) p-value	DM HR (95%CI) p-value
MA	0.96 (0.94, 0.99) 0.0108	0.97 (0.94, 1.00) 0.0334	0.97 (0.94, 1.00) 0.0743
IMF	1.01 (0.91, 1.12) 0.8035	0.76 (0.58, 0.98) 0.0344	0.95 (0.84, 1.07) 0.3918
TAMA	0.97 (0.95, 0.99) 0.0065	0.96 (0.92, 0.99) 0.0155	0.98 (0.96, 1.00) 0.0603
TPA	0.97 (0.91, 1.04) 0.4234	0.75 (0.61, 0.92) 0.0059	0.92 (0.83, 1.02) 0.1159
TPT	0.78 (0.50, 1.22) 0.2757	0.35 (0.14, 0.85) 0.0206	0.95 (0.58, 1.55) 0.8379
APT	0.97 (0.59, 1.62) 0.9183	0.39 (0.16, 0.95) 0.0374	1.03 (0.59, 1.81) 0.9178
PPNF			
0	1.0	1.0	1.0
1	0.80 (0.41, 1.54) 0.5046	0.56 (0.18, 1.76) 0.3231	0.31 (0.13, 0.73) 0.0079
2	0.58 (0.23, 1.46) 0.2450	0.27 (0.03, 2.22) 0.2253	0.88 (0.38, 2.02) 0.7555
SMI	0.93 (0.87, 0.98) 0.0143	0.89 (0.80, 0.99) 0.0252	0.94 (0.88, 1.01) 0.0798
PMI	0.94 (0.79, 1.13) 0.5313	0.45 (0.26, 0.79) 0.0053	0.81 (0.60, 1.08) 0.1437

adenocarcinoma cells contain large amounts of lipid droplets, while urothelial carcinoma cells do not, and so lipid metabolism may not play a significant role in the latter cancer. Meanwhile, our results also suggest that perirenal or periureteral adipose tissue may significantly influence urothelial carcinoma invasion and progression.

Our results must be interpreted with caution in the light of certain limitations. The retrospective design of the study and the relatively small cohort are potential sources of bias. It was impossible to retrospectively obtain data on important diagnostic factors associated with sarcopenia, such as grip strength, walking speed, and patient self-report of the SARC-F questionnaire (23). Additionally, we did not have sufficient imaging data to compare changes in body composition before and after RNU treatment. Future work should focus on validating and extending these results.

CONCLUSION

Our findings show that preoperative assessment of body condition that is more finely grained than BMI can help predict prognosis of UTUC patients after RNU. We found that body composition parameters associated with muscle quality and muscle mass, can independently predict prognosis in such patients. Our results may help improve risk stratification of patients and their postoperative management.

DATA AVAILABILITY STATEMENT

The raw data supporting the conclusions of this article will be made available by the authors, without undue reservation.

ETHICS STATEMENT

The studies involving human participants were reviewed and approved by Ethics Committee on Biomedical Research, West China Hospital of Sichuan University. The patients/participants provided their written informed consent to participate in this study.

AUTHOR CONTRIBUTIONS

YP: data acquisition, investigation, writing - original draft, and formal analysis. ZC: conceptualization, data curation, formal analysis, software, validation, and writing - review & editing. LaY: software, visualization, and data acquisition. XW: data curation and software. ZY: formal analysis and investigation. LZ: visualization and data acquisition. YC: Writing - review & editing. LuY: software, investigation, and supervision. HZ: investigation and methodology. YB: supervision, validation, and project administration. QW: supervision, project administration, funding acquisition. All authors contributed to the article and approved the submitted version.

FUNDING

This work was supported by the National Natural Science Foundation of China (Grant number: 81500522) and Science & Technology Department of Sichuan Province (Grant number: 2020YFS0090, 2020YFS0046).

REFERENCES

1. Roupret M, Babjuk M, Comperat E, Zigeuner R, Sylvester RJ, Burger M, et al. European Association of Urology Guidelines on Upper Urinary Tract Urothelial Carcinoma: 2017 Update. *Eur Urol* (2018) 73(1):111–22. doi: 10.1016/j.eururo.2017.07.036
2. Caan BJ, Cespedes Feliciano EM, Kroenke CH. The Importance of Body Composition in Explaining the Overweight Paradox in Cancer-Counterpoint. *Cancer Res* (2018) 78(8):1906–12. doi: 10.1158/0008-5472.CAN-17-3287
3. Hacker UT, Hasenclever D, Linder N, Stocker G, Chung HC, Kang YK, et al. Prognostic Role of Body Composition Parameters in Gastric/Gastroesophageal Junction Cancer Patients From the EXPAND Trial. *J Cachexia Sarcopenia Muscle* (2020) 11(1):135–44. doi: 10.1002/jcsm.12484
4. Prado CM, Gonzalez MC, Heymsfield SB. Body Composition Phenotypes and Obesity Paradox. *Curr Opin Clin Nutr Metab Care* (2015) 18(6):535–51. doi: 10.1097/MCO.0000000000000216
5. Antonopoulos AS, Oikonomou EK, Antoniades C, Tousoulis D. From the BMI Paradox to the Obesity Paradox: The Obesity-Mortality Association in Coronary Heart Disease. *Obes Rev* (2016) 17(10):989–1000. doi: 10.1111/obr.12440
6. Brown JC, Cespedes Feliciano EM, Caan BJ. The Evolution of Body Composition in Oncology-Epidemiology, Clinical Trials, and the Future of Patient Care: Facts and Numbers. *J Cachexia Sarcopenia Muscle* (2018) 9(7):1200–8. doi: 10.1002/jcsm.12379
7. Goossens GH. The Metabolic Phenotype in Obesity: Fat Mass, Body Fat Distribution, and Adipose Tissue Function. *Obes Facts* (2017) 10(3):207–15. doi: 10.1159/000471488
8. Kokkinos P, Myers J, Faselis C, Doumas M, Kheirbek R, Nylen E. Bmi-Mortality Paradox and Fitness in African American and Caucasian Men With Type 2 Diabetes. *Diabetes Care* (2012) 35(5):1021–7. doi: 10.2337/dc11-2407
9. Linder N, Schaudinn A, Langenhan K, Krenzien F, Hau HM, Benzing C, et al. Power of Computed-Tomography-Defined Sarcopenia for Prediction of Morbidity After Pancreaticoduodenectomy. *BMC Med Imaging* (2019) 19(1):32. doi: 10.1186/s12880-019-0332-6
10. Kawamura N, Saito K, Inoue M, Ito M, Kijima T, Yoshida S, et al. Adherent Perinephric Fat in Asian Patients: Predictors and Impact on Perioperative Outcomes of Partial Nephrectomy. *Urol Int* (2018) 101(4):437–42. doi: 10.1159/000494068
11. Gill TS, Varghese BA, Hwang DH, Cen SY, Aron M, Aron M, et al. Juxtatumoral Perinephric Fat Analysis in Clear Cell Renal Cell Carcinoma. *Abdom Radiol (NY)* (2019) 44(4):1470–80. doi: 10.1007/s00261-018-1848-x
12. Clark W, Siegel EM, Chen YA, Zhao X, Parsons CM, Hernandez JM, et al. Quantitative Measures of Visceral Adiposity and Body Mass Index in Predicting Rectal Cancer Outcomes After Neoadjuvant Chemoradiation. *J Am Coll Surg* (2013) 216(6):1070–81. doi: 10.1016/j.jamcollsurg.2013.01.007
13. Henry Kvist BC, Ulla G, Ulf T, Lars S. Total and Visceral Adipose-Tissue Volumes Derived From Measurements With Computed Tomography in Adult Men and Women Predictive Equations. *Am J Clin Nutr* (1988) 48:11. doi: 10.1093/ajcn/48.6.1351
14. Mourtzakis M, Prado CM, Lieffers JR, Reiman T, McCargar LJ, Baracos VE. A Practical and Precise Approach to Quantification of Body Composition in Cancer Patients Using Computed Tomography Images Acquired During Routine Care. *Appl Physiol Nutr Metab* (2008) 33(5):997–1006. doi: 10.1139/H08-075

15. Huang X, Ma J, Li L, Zhu XD. Severe Muscle Loss During Radical Chemoradiotherapy for Non-Metastatic Nasopharyngeal Carcinoma Predicts Poor Survival. *Cancer Med* (2019) 8(15):6604–13. doi: 10.1002/cam4.2538
16. Cespedes EM, Feliciano WYC, Bradshaw PT, Prado CM, Alexeeff S, Albers KB, et al. Adipose Tissue Distribution and Cardiovascular Disease Risk Among Breast Cancer Survivors. *J Clin Oncol* (2019) 37(28):9. doi: 10.1200/JCO.19.00286
17. Goodpaster CLC BH, Visser M, Kelley DE, Scherzinger A, Harris TB, Stamm E, et al. Attenuation of Skeletal Muscle and Strength in the Elderly The Health ABC Study. *J Appl Physiol* (2001) 90:9. doi: 10.1152/jappl.2001.90.6.2157
18. Heymsfield SB, Gonzalez MC, Lu J, Jia G, Zheng J. Skeletal Muscle Mass and Quality: Evolution of Modern Measurement Concepts in the Context of Sarcopenia. *Proc Nutr Soc* (2015) 74(4):355–66. doi: 10.1017/S0029665115000129
19. Prado CMM, Lieffers JR, McCargar LJ, Reiman T, Sawyer MB, Martin L, et al. Prevalence and Clinical Implications of Sarcopenic Obesity in Patients With Solid Tumours of the Respiratory and Gastrointestinal Tracts: A Population-Based Study. *Lancet Oncol* (2008) 9(7):629–35. doi: 10.1016/S1470-2045(08)70153-0
20. Fukushima H, Nakanishi Y, Kataoka M, Tobisu K, Koga F. Prognostic Significance of Sarcopenia in Upper Tract Urothelial Carcinoma Patients Treated With Radical Nephroureterectomy. *Cancer Med* (2016) 5(9):2213–20. doi: 10.1002/cam4.795
21. Tsutsumi S, Kawahara T, Teranishi JI, Yao M, Uemura H. A Low Psoas Muscle Volume Predicts Longer Hospitalization and Cancer Recurrence in Upper Urinary Tract Urothelial Carcinoma. *Mol Clin Oncol* (2018) 8(2):320–2. doi: 10.3892/mco.2017.1537
22. Kapoor ND, Twining PK, Groot OQ, Pielkenrood BJ, Bongers MER, Newman ET, et al. Adipose Tissue Density on CT as a Prognostic Factor in Patients With Cancer: A Systematic Review. *Acta Oncol* (2020) 59(12):1–8. doi: 10.1080/0284186X.2020.1800087
23. Cruz-Jentoft AJ, Bahat G, Bauer J, Boirie Y, Bruyère O, Cederholm T, et al. Sarcopenia: Revised European Consensus on Definition and Diagnosis. *Age Ageing* (2019) 48(1):16–31. doi: 10.1093/ageing/afz046

Conflict of Interest: The authors declare that the research was conducted in the absence of any commercial or financial relationships that could be construed as a potential conflict of interest.

frontiers in Oncology

SYSTEMATIC REVIEW
published: 14 December 2021
doi: 10.3389/fonc.2021.784627

Impact of Androgen Suppression Therapy on the Risk and Prognosis of Bladder Cancer: A Systematic Review and Meta-Analysis

Peng Xiang[1,2†], Zhen Du[1†], Yongxiu Hao[3], Di Guan[1], Dan Liu[1], Wei Yan[1], Mingdong Wang[1], Yutong Liu[1] and Hao Ping[1,2]*

[1] Department of Urology, Beijing Tongren Hospital, Capital Medical University, Beijing, China, [2] Beijing Advanced Innovation Center for Big Data-Based Precision Medicine, Beihang University & Capital Medical University, Beijing Tongren Hospital, Beijing, China, [3] Department of Epidemiology and Biostatistics, School of Public Health, Peking University, Beijing, China

OPEN ACCESS

Edited by:
Scott T Tagawa, Cornell University, United States

Reviewed by:
Andrea Benedetto Galosi, Marche Polytechnic University, Italy
Ning Li, Fourth Affiliated Hospital of China Medical University, China

***Correspondence:**
Hao Ping
haopingcyh@163.com
orcid.org/0000-0002-0321-7921

[†]These authors have contributed equally to this work

Specialty section:
This article was submitted to Genitourinary Oncology, a section of the journal Frontiers in Oncology

Received: *28 September 2021*
Accepted: *24 November 2021*
Published: *14 December 2021*

Citation:
Xiang P, Du Z, Hao Y, Guan D, Liu D, Yan W, Wang M, Liu Y and Ping H (2021) Impact of Androgen Suppression Therapy on the Risk and Prognosis of Bladder Cancer: A Systematic Review and Meta-Analysis. Front. Oncol. 11:784627. doi: 10.3389/fonc.2021.784627

Purpose: The purpose of this study was to summarize the existing evidence and develop a comprehensive systematic review of the impact of androgen suppression therapy (AST) on the incidence or clinical outcomes of bladder cancer.

Methods: We systematically searched the PubMed and Embase databases from inception to June 20, 2021 to identify all observational studies examining the incidence or clinical outcomes of bladder cancer in patients who received AST. AST is defined as the use of 5-alpha reductase inhibitors (5-ARIs) or androgen deprivation therapy (ADT).

Results: A total of 18 observational studies were included. Our results showed that AST was not significantly associated with a reduced risk of BCa incidence (OR: 0.92, 95% CI: 0.68–1.24) compared with the lack of AST. The subgroup analysis revealed that finasteride use was significantly associated with a reduction in the risk of BCa incidence (OR: 0.75, 95% CI: 0.64–0.88). Recurrence-free survival (RFS) was improved among AST users compared with nonusers (HR: 0.68, 95% CI: 0.48–0.95), while no significant difference between AST users versus nonusers was identified for cancer-specific survival (CSS), overall survival (OS) or progression-free survival (PFS).

Conclusion: Current evidence indicates that therapy with finasteride may represent a potential strategy aimed at reducing BCa incidence. Moreover, AST has a beneficial effect on the recurrence of bladder cancer. Further well-designed randomized trials or cohort studies with better characterized study populations are needed to validate our preliminary findings.

Systematic Review Registration: International Prospective Register of Systematic Reviews database [https://www.crd.york.ac.uk/PROSPERO/], identifier CRD42021261685.

Keywords: androgen suppression therapy, bladder cancer, incidence, recurrence, meta-analysis

INTRODUCTION

Bladder cancer (BCa), predominantly urothelial carcinoma, is a common malignant genitourinary tumor (1, 2). Men are 3 to 4 times more frequently diagnosed with bladder cancer than women; however, women tend to be diagnosed with more advanced disease at presentation and have less favorable outcomes after treatment (1, 3–5). Female patients with urothelial carcinoma of the bladder have been shown to have worse cancer specific survival, overall survival and recurrence-free survival (5, 6). Recent studies question why there are differences, and the effects of sex hormones and its receptors, especially androgens, have become widely researched (1, 5–7).

Sex hormones and corresponding receptors are relevant modulators of cancer onset and progression in nonreproductive organs, particularly the lung, colorectal, bladder, stomach, kidney, pancreas, and thyroid gland (8). The excessive or reduced expression of these receptors, and the changes in their upstream or downstream pathways are closely related to the outcomes of BCa (8, 9). Numerous studies have focused on the role of androgen receptor (AR) and androgens in the development of bladder cancer. *In vitro* and *vivo* evidence highlights a crucial role for AR in BCa development, progression, recurrence and resistance to standard therapies such as chemotherapy, radiotherapy, and Bacillus Calmette Guerin (BCG) (2, 4, 8, 10–14). Emerging clinical evidence also suggests that the manipulation of androgen signaling may affect BCa behavior. Previous meta-analyses included limited clinical literature and some unreported relative risks in studies, suggesting that androgen suppression therapy (AST) consisting of 5-alpha reductase inhibitors (5-ARIs) or androgen deprivation therapy (ADT) can reduce BCa incidence, recurrence and specific mortality (15, 16). However, various results regarding the impact of AST on the incidence and recurrence of bladder cancer have been widely reported recently, and there are disputes among them. Therefore, with the increase in original research on this topic, an updated summary needs to be presented.

Herein, the aim of our study is to summarize the available evidence and develop a comprehensive systematic review of the effect of AST on the incidence of bladder cancer and the clinical outcomes of patients with bladder cancer.

METHODS

The protocol of this study has been registered in the International Prospective Register of Systematic Reviews database (CRD42021261685).

Search Strategy and Eligibility Criteria

The PubMed and Embase databases were searched from inception to June 20, 2021. The following search terms were used: "bladder cancer," "urothelial carcinoma," or "bladder neoplasms"; one of "androgen suppression therapy" or "5 alpha reductase inhibitor" or "5α-reductase" or "5ARI" or "finasteride" or "dutasteride " or "androgen deprivation therapy" or "anti-androgen" or "bicalutamide" or "enzalutamide" or "abiraterone" or "GnRH agonist" or "GnRH antagonist" or "castration" or "nilutamide" or "flutamide" or "apalutamide" or "darolutamide". The titles and abstracts of articles were screened initially to identify relevant studies. Then, the full texts of potentially relevant studies were carefully read to determine those that met the eligibility criteria. Retrospective and prospective studies evaluating the effect of AST (5-ARI or ADT) on BCa incidence, recurrence, or survival were included in the analysis. Articles that did not report AST in patients with BCa were excluded. Reviews, letters, editorials, replies from authors, case reports, conferences and articles not published in English were excluded. Two authors screened the search results and any disagreements were resolved.

Data Extraction and Quality Assessment

Data extracted from the eligible studies included study characteristics (e.g., study type, data source, study period, sample size,median of follow-up), patient characteristics (e.g., patient age, AST type), outcomes (e.g., BCa incidence, BCa recurrence), adjusted risk estimates with 95% confidence interval (CI) for outcomes, and potentially confounding factor adjustments (e.g., age, race, smoking, comorbidities tumor stage and grade, intravesical therapy). The main outcomes were ① incidence of BCa when AST was initiated before diagnosing BCa and ② recurrence-free survival (RFS), progression-free survival (PFS), overall survival (OS) or cancer-specific survival (CSS) when AST was initiated after diagnosing BCa. We used the Risk of Bias in Nonrandomized Studies of Interventions (ROBINS-I) tool to assess methodological quality and summarized the results in **Supplementary Table 1**.

Statistical Analysis

The meta-analysis was performed by the Review Manager Version 5.3 software. Due to the observational nature of the included studies, we extracted adjusted hazard ratios (HRs) and odds ratios (ORs) with 95% CIs from the multivariate logistic regression analysis to calculate the cumulative effect size (17). Moreover, HRs and incidence density ratios can be regarded as relative risks (RRs) directly (18, 19). Additionally, ORs are close to RRs because of the low incidence of outcome (<10%) (20). The Cochrane Q test and I^2 were used to determine the level of heterogeneity among studies. In the case of heterogeneity ($p < 0.10$ or $I^2 > 50\%$), the random effects model was used; otherwise, a fixed effects model was used. A p value < 0.05 was considered statistically significant. In addition, according to the type of AST, we performed a subgroup analysis of the effect of AST on BC incidence. Finally, publication bias was assessed by using a funnel plot when there were more than 10 studies that reported a specific outcome.

RESULTS

Characteristics of Included Studies and Patients

Overall, according to the screening criteria, the systematic review and meta-analysis included 18 studies with a total of 414 007 male patients (21–38) (**Figure 1**). Eight studies evaluated the effect of AST on bladder cancer incidence (22, 27, 28, 30, 32–34, 38).

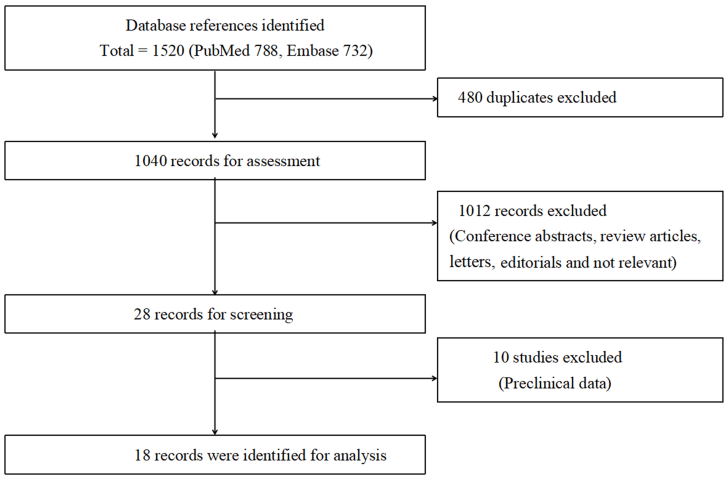

FIGURE 1 | Flow diagram of the study.

Ten studies examined the effect of AST on bladder cancer recurrence, progression and survival (21, 23–26, 29, 31, 35–37). The characteristics of the selected studies were summarized in **Table 1**. The search strategy was presented in **Supplementary Table 2**.

Effect of AST on Bladder Cancer Incidence

Eight studies with 393 907 participants evaluated whether AST reduced the incidence of bladder cancer diagnosis. The results from these studies are summarized in **Table 2**. Three studies reported a protective effect of AST on bladder cancer incidence, four reported no association, and one reported an increased risk. The meta-analysis of studies revealed a nonsignificant reduction in BCa incidence (OR: 0.92, 95% CI: 0.68–1.24) (**Figure 2**). Evidence of statistically significant heterogeneity was found in selected studies (I^2 = 90%, p < 0.001). When stratified by the type of AST, we found a statistically lower incidence of bladder cancer among men with finasteride (OR: 0.75, 95% CI: 0.64–0.88), while no statistically significant effect was seen with ADT (OR: 1.00, 95% CI: 0.46–2.15) vs. nonusers. In particular, Chen et al. (22) showed that only patients who received finasteride > 6 months had a lower risk of BCa. In the study of Morales et al. (27), the risk reduction was only observed in well-differentiated and moderately differentiated tumors, while the diagnosis of poorly differentiated or undifferentiated tumors was not reduced. Zhu et al. (38) indicated that the use of finasteride was associated with significant reductions in the risk of high-grade BCa and non-muscle invasive BCa. In addition, a decrease in the risk of BCa was shown only in Caucasians and Hispanics but not among African Americans.

Effect of AST on Bladder Cancer Recurrence and Progression

Ten studies including 20 100 participants reported the impact of AST on patients diagnosed with bladder cancer (**Table 3**). Five studies evaluated patients with non-muscle-invasive bladder cancer (NMIBC), and five included all patients with bladder cancer. The manipulation of the androgen signaling pathway involved the use of 5-ARIs in 4263 patients and ADT in 233 patients. For the analysis of RFS, a meta-analysis of seven studies with corresponding HRs was conducted. Compared with nonusers, AST users had significantly improved RFS (HR: 0.68, 95% CI: 0.48–0.95) (**Figure 3A**). The pooled analysis for RFS detected significant heterogeneity (I^2 = 90%, p < 0.001). Similarly, Kufukihara et al. (24) revealed that the rate of bladder tumor recurrence was significantly lower in the ADT group than in the counterpart (p = 0.027). However, McMartin et al. (26) failed to find a significant difference in RFS between patients undergoing therapy with 5-ARIs and controls.

For the analysis of CSS, a meta-analysis of three studies was conducted. Pooled data for CSS confirmed a nonsignificant difference in patients undergoing therapy with 5-ARIs compared to controls (HR: 0.89, 95% CI: 0.73–1.09) (**Figure 3B**). The pooled analysis found significant heterogeneity (I^2 = 78%, p = 0.01). Similarly, in the study by McMartin et al. (26), there was no significant difference in CSS between patients undergoing therapy with 5-ARIs and controls. Two studies reported OS in patients with 5-ARIs treatment after diagnosing BCa; there was no significant reduction in OS in these patients (HR: 0.69, 95% CI: 0.27–1.73) (**Figure 3C**). High heterogeneity for OS was observed (I^2 = 84%, p = 0.01). Owing to a paucity of HR data from PFS, we performed a descriptive analysis. PFS was investigated in 4 studies, and no differences between AST users and nonusers were found (21, 24, 31, 37).

DISCUSSION

In this comprehensive meta-analysis, we did not find evidence to support the previous hypothesis that the AST is associated with a lower incidence of bladder cancer. Interestingly, subgroup analysis in patients receiving finasteride showed a decreased

TABLE 1 | Characteristics of the included studies.

Study, year, country	Study type	Date source	Study period	Sample size	Comparisons	Participants	Age (yr), mean	Key inclusion criteria	Follow-up (yr)	Outcome measures
Al-Hogbani, 2020, Canada (21)	Retrospective cohort	Chart review	2013-2018	206	5-ARIs No 5-ARIs	39 167	74 68	NMIBC treated with BCG	3.3	Bladder cancer recurrence and progression-free survival
Chen, 2018, Taiwan (22)	Case control	Administrative database	2002-2013	33586	Bladder cancer No bladder cancer	16784 16784	68.6 ± 13.0 68.6 ± 13.0	Diagnosis of patients with bladder cancer or without bladder cancer	6	Effect of 5-ARIs on bladder cancer incidence
Izumi, 2014, Japan (23)	Retrospective cohort	Chart review	1991-2013	162	ADT No ADT	86 76	74 (59-88) 71.5 (54-92)	Diagnosis of bladder and prostate cancer	5.2	Bladder cancer recurrence
Kufukihara, 2021, Japan (24)	Retrospective cohort	Chart review	1999-2017	48	ADT No ADT	29 19	NA NA	Diagnosis of NMIBC and prostate cancer	5	Bladder tumor recurrence
Mäkelä, 2018, Finland (25)	Retrospective cohort	Administrative database	1997-2012	10702	5-ARIs No 5-ARIs	1328 5090	78 (72-83) 70 (61-78)	Diagnosis of bladder cancer	4.2	Bladder cancer specific survival; The risk of multiple TURB procedures
McMartin, 2019, Canada (26)	Retrospective cohort	Chart review	2009-2017	338	5-ARIs No 5-ARIs	48 290	72.5 68.7	Patients with urothelial carcinoma undergo radical cystectomy	1.8	Bladder cancer survival,such as OS, CSS and RFS; Pathological features assessment including LVI and PNI
Morales, 2016, America (27)	Retrospective cohort	Trial database	1993-2001	72370	5-ARIs No 5-ARIs	6069 66 301	63 (55-78) 62 (49-78)	PLCO screening trial participants	13	Incidence of bladder cancer
Moschini, 2019, America (28)	Retrospective cohort	Administrative database	2000-2009	196914	ADT No ADT	68421 128493	75 (70-79) 71 (68-76)	Diagnosis of localized prostate cancer	4.9	Incidence of bladder cancer
Pastore, 2019, Italy (29)	Retrospective cohort	Chart review	2015-2017	312	5-ARIs No 5-ARIs	165 147	75.2 ± 10.5 75.1 ± 9.3	Diagnosis of NMIBC	2.5	Bladder tumor recurrence and survival
Sathianathen, 2018, America (30)	Retrospective cohort	Trial database	1992-1998	2700	5-ARIs No 5-ARIs	1216 1484	62.6 ± 7.2 62.6 ± 7.4	MTOPS LUTS study participants	6	Incidence of bladder cancer
Shiota, 2017, Japan (31)	Retrospective cohort	Chart review	2010-2013	228	AST No AST	32 196	72 (66-78) 70 (62-77)	Diagnosis of NMIBC	3.6	Bladder tumor recurrence and survival
Shiota, 2015, Japan (32)	Retrospective cohort	Chart review	2000-2012	1334	ADT No ADT: RT Surgery	266 631 437	74 (69-78) 70 (65-74) 65 (60-69)	Diagnosis of prostate cancer	3.8	Incidence of bladder cancer
Van Hemelrijck, 2014, Switzerland (33)	Retrospective cohort	Trial database	1980-2010	20559	PCa with SPT PCa without SPT	1718 18841	71.4 ± 7.7 71.7 ± 9.3	Diagnosis of prostate cancer	5	Incidence of bladder cancer
Wallner, 2013, America (34)	Retrospective cohort	Administrative database	1998-2007	24038	PCa with SPT PCa without SPT	1359 22679	60-80 60-80	Diagnosed of localized prostate cancer	5.5	Incidence of bladder cancer
Wang, 2020, Taiwan (35)	Retrospective cohort	Administrative database	1998-2010	5214	5-ARIs No 5-ARIs	474 4740	76.5 ± 7.9 76.6 ± 8.5	Diagnosis of bladder cancer	3	Bladder cancer mortality and recurrence
Wissing, 2021, Canada (36)	Retrospective cohort	Administrative database	2000-2015	2822	5-ARIs No 5-ARIs	284 2538	74 (70-79) 70 (64-76)	Diagnosis of bladder cancer	7.7	Bladder tumor recurrence and survival
Wu, 2019, America (37)	Retrospective cohort	Chart review	2001-2017	274	AST No AST	36 238	68.3 68.3	NMIBC	3.1	Bladder tumor recurrence and survival
Zhu, 2021, America (38)	Retrospective cohort	Administrative database	2000-2016	42406	5-ARIs No 5-ARIs	5698 36708	70 ± 10.9 66.3 ± 13	Diagnosis of BPH	6.1	Incidence of bladder cancer

5-ARIs, 5-alpha reductase inhibitors; AST, Androgen suppression therapy; ADT, Androgen deprivation therapy; NMIBC, Non-muscle-invasive bladder cancer; BCG, Bacille Calmette-Guerin; NA, Not available; LUTS, Lower urinary tract symptoms; TURB, Transurethral resection of bladder; OS, Overall survival; RFS, Recurrence-free survival; CSS, Cancer-specific survival; LVI, Lymphovascular invasion; PNI, Perineural invasion; MTOPS, Medical Treatment of Prostate Symptoms; RT, Radiotherapy; SPT, Second primary tumor; BPH, Benign prostatic hyperplasia; PLCO, Prostate, Lung, Colon, Ovarian.

TABLE 2 | The effect of androgen suppression therapy on bladder cancer incidence.

Study, year, country	AST	AST duration	Bladder cancer cases (n)	Risk estimate for bladder cancer diagnosis	Notes
Chen, 2018, Taiwan (22)	Finasteride	< 6 months > 6 months	16784	1-179 cDDD OR 0.93 (95% CI: 0.79-1.09). ≥180 cDDD OR 0.84 (95% CI: 0.70-0.99)*	Adjusted for comorbidities (diabetes mellitus, cerebrovascular disease, chronic kidney disease, hypertension and hyperlipidemia), socioeconomic status (low, moderate and high), geographic region (northern, central, southern and eastern)
Morales, 2016, America (27)	Finasteride	>12 months	1031	HR 0.733 (95% CI: 0.552-0.974)*	Adjusted for age, smoking status, body mass index at baseline, race, family history of BCa, randomization arm, colon comorbidity, prostatitis, duration smoked cigarettes, and education
Moschini, 2019, America (28)	ADT	59 months	2495	HR 0.93 (95% CI: 0.85-1.02)	Adjusted for age, race, PCa clinical tumor stage, PCa biopsy Gleason score, as well as marital, socio-economic status and ever-smoker status, and competing-risk mortality
Sathianathen, 2018, America (30)	Finasteride	72 months	18	0.74% with Finasteride vs. 0.61% with control. OR 1.22 (95% CI: 0.48-3.09)	No adjustment of variables due to few events
Shiota, 2015, Japan (32)	ADT	45.5 months	19	0 with ADT vs.1.1% with surgery. OR 0.15 (95% CI: 0.01-2.68)	No adjustment of variables due to few events
Van Hemelrijck, 2014,Switzerland (33)	ADT	60 months	197	SIR 2.54 (95% CI: 1.91-3.33)*	The SIR is defined as the ratio of the observed numbers of primary tumors to the expected numbers
Wallner, 2013, America (34)	GnRH agonist	66 months	132	HR 0.53 (95% CI: 0.26-1.06)	Adjusted for age, race, year of prostate cancer diagnosis, healthcare visits, stage, Gleason score, and radiation therapy
Zhu, 2021, America (38)	Finasteride	73.6 months	846	HR 0.64 (95% CI: 0.51-0.80)*	Adjustment for age, race/ethnicity (Caucasian, African American, Hispanic and other) as well as smoking history

*ADT, Androgen deprivation therapy; AST, Androgen suppression therapy; GnRH, Gonadotropin-releasing hormone; BCa, Bladder cancer; cDDD, Cumulative defined daily dose; CI, Confidence interval; SIR, Standardized incidence ratio; HR, Hazard ratio; OR, Odds ratio; PCa, Prostate cancer. *p < 0.05.*

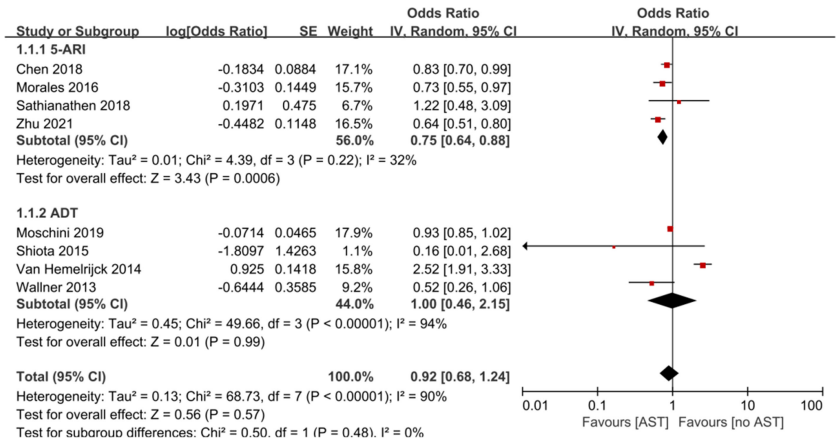

FIGURE 2 | Forest plots showing the effect of AST on bladder cancer incidence. AST, Androgen suppression therapy; 5-ARI, 5-alpha reductase inhibitor; ADT, Androgen deprivation therapy.

risk of BCa incidence (OR: 0.75, 95% CI: 0.64–0.88), while ADT had no effect on reducing BCa incidence. In addition, AST significantly reduced RFS in patients with bladder cancer but had no significant effect on CSS, OS or PFS.

Contrary to results of a previous meta-analysis (16), the clinical evidence in this review shows that there is no significant difference in the incidence of BCa between patients with AST and patients without AST. The earlier systematic review and meta-analysis included only three retrospective cohort studies to evaluate the impact of AST on bladder cancer incidence. Obviously, earlier conclusions are easily influenced by the results of newly published studies. In the subgroup analysis based on the type of AST, 5-ARIs exposure was significantly correlated with a decreased risk of subsequent BCa; however, ADT was not significantly correlated with the risk of subsequent BCa. Thus, it seems that suppressing the AR axis more effectively will not yield greater benefits. Nonetheless, we believe that more studies are needed to better evaluate the true benefits of ADT, as this treatment may only affect patients whose BCa does express AR (28). Notably, only a study from Van Hemelrijck et al. (33) indicated an increased risk of bladder cancer associated with ADT use. The authors calculated standardized incidence rates comparing the incidence of second primary malignancies (including bladder cancer) in the prostate cancer (PCa) patient group vs. the general male population in Zurich. However, compared with the general male population, patients with PCa may be monitored more carefully and contact doctors more frequently, thereby increasing the detection rate of bladder cancer and leading to detection bias (39). In our review, bicalutamide was not fully investigated due to limited use of included studies.

The pooled data for RFS in this review show that the risk of BCa recurrence is significantly reduced in patients undergoing hormonal manipulation with AST, which is consistent with the results of previous meta-analyses (15, 16). Creta et al. (15) and Kourbanhoussen et al. (2) indicated that low-grade and low-risk NMIBC may benefit more from the use of AST. This benefit was well reflected in studies including only NMIBC or studies with a high proportion of NMIBC and low-grade patients (23, 29, 31, 37). However, the pooled data for CSS, OS and PFS do not support a protective role of ADT and/or 5-ARIs in terms of BCa progression and survival in the subjects evaluated. Interestingly, Wu et al. (37) indicated that therapy with ADT or 5-ARIs may be associated with lower progression rates in patients with low/intermediate-risk BCa but not in their high-risk counterparts. The negative finding for PFS may be due to the small sample size and the number of events during follow-up, rather than a true lack of correlation. Moreover, the included studies contained many high-risk NMIBC and MIBC patients. It has been reported that these tumor types can reduce dependence on the AR signaling pathway, which may partly explain the lack of association between AST and BCa progression (37, 40–42). As expected, given the prevalence of urinary symptoms in older men, most studies have investigated the role of 5-ARIs in BCa, and only a few studies have investigated the role of ADT in BCa. Because the number of individual studies is insufficient for comparison, it is not clear whether more effective inhibition of the AR axis will yield greater benefits.

Zhu et al. (38) first demonstrated that after using finasteride, although Hispanic men have a similar reduced risk of bladder cancer compared with Caucasian men, African-American men do not. A possible biological explanation for this observation might be the structural variations in the AR protein across different races. African Americans are more likely to contain polymorphisms in AR, which causes their AR to become active and independent of DHT binding (38). The role of AST is not limited to the androgen axis. Clinically, 5-ARIs can increase serum estrogen levels (43, 44). With more effective anti-androgens, the reflex of estrogen increases even higher (2, 45, 46). Estrogens play important roles in BCa development and progression by exerting both stimulatory and inhibitory actions *via* estrogen receptor α (ERα) and ERβ (2, 8). Overall, it appears that estrogens may protect against or inhibit BCa development, but later—at more advanced stages—they might support tumor

TABLE 3 | The effect of androgen suppression therapy on bladder cancer recurrence and progression.

Study, year, country	AST	AST duration	Outcome	Risk estimate	Adjusted for covariates
Al-Hogbani, 2020, Canada (21)	Finasteride or Dutasteride	> 6 months	RFS PFS	HR 1.00 (95% CI: 0.55-1.79) 5-yr PFS with vs. without AST: 97.4% vs 98.2%	Adjusted for age, stage, grade, number of tumors, smoking history, tumor size, presence of CIS, and intravesical treatment
Izumi, 2014, Japan (23)	ADT	62 months	RFS	HR 0.29 (95% CI: 0.19-0.45)*	Adjusted for age. stage, grade, tumor number, tumor size, presence of CIS, and intravesical treatment
Kufukihara, 2021, Japan (24)	ADT	60 months	RFS PFS	5-yr RFS with vs. without ADT: 43.7% vs 27.7% (p = 0.027)* 5-yr PFS with vs. without ADT: p = 0.52	No adjustment of variables due to few events
Mäkelä, 2018, Finland (25)	Finasteride or Dutasteride	24 months	CSS Multiple TURB	Pre-diagnostic 5-ARI use: HR 0.85 (95% CI:0.74-0.97)* Post-diagnostic 5-ARI use: HR 0.78 (95% CI:0.68-0.89)* ≥2 resections: OR 0.89 (95% CI:0.74-1.07) ≥ 5 resections: OR 0.82 (95% CI:0.58-1.16)	Adjusted for age, gender, co-morbidities, primary bladder cancer treatment (surgery vs. other) and tumor extent at diagnosis (localized vs metastatic)
McMartin, 2019, Canada (26)	Finasteride or Dutasteride	22.1 months	OS RFS; CSS LVI; PM; PNI	HR: 0.40 (95% CI: 0.19-0.83)* No significant difference; No significant difference OR: 0.49 (95% CI: 0.2-1.00)*; NS; NS	Adjusted for age, use of neoadjuvant chemotherapy and pathologic stage
Pastore, 2019, Italy (29)	Dutasteride	>12 months	RFS	HR: 0.67 (95% CI: 0.52-0.85)*	Adjusted for age, stage, grade, number of tumors, smoking history, presence of CIS, and intravesical treatment
Shiota, 2017, Japan (31)	GnRH-agonist or Bicalutamide or Dutasteride	28 months	RFS PFS	HR: 0.36 (95% CI: 0.11-0.89)* PFS with vs. without AST: 100% vs 96.9%	Adjusted for stage, number of tumors, size of tumor, smoking status, and intravesical therapy
Wang, 2020, Taiwan (35)	5-ARIs	≥1 months	CSS RFS	OR 0.835 (95% CI: 0.71–0.98)* OR 0.956 (95% CI: 0.82–1.11)	Adjusted for age, and comorbidities including diabetes mellitus, hypertension, chronic kidney disease and hyperlipidemia
Wissing, 2021, Canada (36)	Finasteride or Dutasteride	24 months	OS CSS RFS	HR 1.03 (95% CI: 0.88–1.21) HR 1.12 (95% CI: 0.92–1.36) HR 1.19 (95% CI: 0.99–1.42)	Adjusted for age, region of residence, Charlson's comorbidity index, year of surgery, driving distance to the hospital, hospital type, annual radical cystectomy volume of the hospital and lead surgeon, type of bladder diversion, and administration of neoadjuvant chemotherapy
Wu, 2019, America (37)	GnRH-agonist or Anti-androgen or 5-ARIs	20 months	RFS PFS	HR: 0.53 (95% CI: 0.30–0.88)* 5-yr PFS with vs without AST: 80% vs 63% (p = 0.23)	Smoking history, risk group (low/intermediate or high), and postoperative chemotherapy use

*5-ARIs, 5-alpha reductase inhibitors; ADT, Androgen deprivation therapy; AST, Androgen suppression therapy; GnRH, Gonadotropin-releasing hormone; BCG, Bacille Calmette-Guerin; PFS, Progression-free survival; CIS, Carcinoma in situ; TURB, Transurethral resection of bladder; OS, Overall survival; RFS, Recurrence-free survival; CSS, Cancer-specific survival; LVI, Lymphovascular invasion; PM, Positive margins; PNI, Perineural invasion; CI, Confidence interval; OR, Odds ratio; HR, Hazard ratio; NS, No significance. *p < 0.05.*

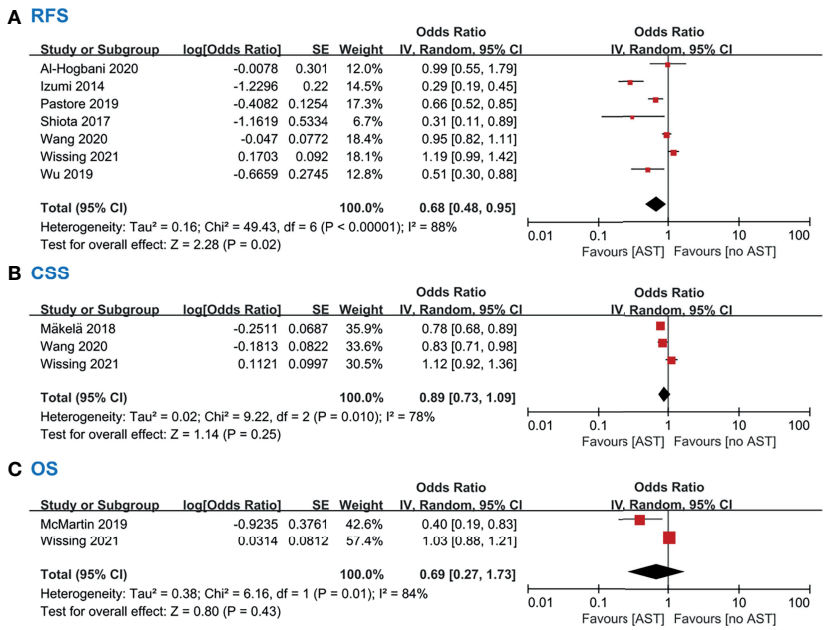

FIGURE 3 | **(A)** Forest plots showing the effect of AST on RFS in bladder cancer. **(B)** Forest plots showing the effect of AST on CSS in bladder cancer. **(C)** Forest plots showing the effect of AST on OS in bladder cancer. AST, Androgen suppression therapy; RFS, Recurrence-free survival; CSS, Cancer-specific survival; OS, Overall survival.

progression (8). The estrogen-signaling pathway during AST may still partially explain the observed effects in AST.

The number of included studies for meta-analysis was too small to fully assess the publication bias of the effects of AST on incidence or recurrence. Some of heterogeneities were too high. We speculate that several observational studies included in the present meta-analysis did not adjust for potential confounders such as age, race/ethnicity and smoking history, which may bias the pooled effect estimate and may affect heterogeneity. Moreover, differences in AST type, AST exposure time, follow-up duration and demographic characteristics of the included studies are also important reasons for the heterogeneity of results. The proportion of participants receiving 5-ARIs in the currently included studies is obviously higher than that of participants receiving ADT, making the overall effect of outcomes of AST more inclined to 5-ARIs. In most of the included studies, the average age of participants in the AST group was slightly higher than that in the non-AST group. The AST exposure time and follow-up duration of the included literature vary, although it was mostly longer than 2 years. Compared with a duration of less than 6 months, it seems that the use of 5ARIs for greater than 6 months can lead to more significant benefits (22), but the benefits have not been accumulated with years of 5-ARIs use (25). Most of the original studies did not mention the detailed characteristics of BCa, including grade, stage, and cancer cell type, which further limited the pooled analysis. We still do not know very clearly which types of BCa have a lower incidence and which types of BCa have a low recurrence rate after AST. Although the available preclinical evidence demonstrates that AST can interfere with the sensitivity of BCa to BCG or other therapies, its benefit is not observable when given in clinical studies (2, 15, 21). Further research is needed to better evaluate the role of androgen suppression in specific subgroups of BCa patients, to compare the effects of 5-ARIs and ADT and to better clarify androgen manipulation strategies for patients with BCa undergoing BCG, radiation or chemotherapy.

CONCLUSION

Our systematic review and meta-analysis identified 18 studies that evaluated androgen suppression on clinical outcomes in BCa patients. AST was not associated with a lower risk of BCa incidence, but a subgroup analysis showed that patients receiving 5-ARIs had a reduced risk of BCa incidence. In addition, AST has a beneficial effect on the recurrence rates of bladder cancer. We did not observe any significant differences in AST on CSS, OS or PFS when compared with the control. Further well-designed prospective studies adjusted for the major and common confounding factors are needed to validate our findings.

DATA AVAILABILITY STATEMENT

The raw data supporting the conclusions of this article will be made available by the authors, without undue reservation.

AUTHOR CONTRIBUTIONS

Conceptualization: PX, HP, and ZD. Data curation: YH, DG, DL, and PX. Formal analysis: WY, MW, PX, ZD, and YL. Project administration: HP. Resources: HP and ZD. Software: PX and YH. Supervision: HP. Validation: PX and HP. Visualization: PX. Writing - original draft: PX. Writing - review & editing: all authors. All authors contributed to the article and approved the submitted version.

FUNDING

This work was supported by the National Natural Science Foundation of China (Grant No. 81772698 and 82072833 to HP) and the Open Research Fund from Beijing Advanced Innovation Center for Big Data-Based Precision Medicine, Beijing Tongren Hospital, Beihang University & Capital Medical University (Grant No. BHTR-KFJJ-202005 to HP).

ACKNOWLEDGMENTS

The authors are very grateful to the urology department of Beijing Tongren Hospital for their selfless help in this work.

SUPPLEMENTARY MATERIAL

The Supplementary Material for this article can be found online at: https://www.frontiersin.org/articles/10.3389/fonc.2021.784627/full#supplementary-material

REFERENCES

1. Lenis AT, Lec PM, Chamie K, Mshs MD. Bladder Cancer: A Review. *JAMA* (2020) 324(19):1980–91. doi: 10.1001/jama.2020.17598
2. Kourbanhoussen K, McMartin C, Lodde M, Zlotta A, Bryan RT, Toren P. Switching Cancers: A Systematic Review Assessing the Role of Androgen Suppressive Therapy in Bladder Cancer. *Eur Urol Focus* (2020) 7(5):1044–51. doi: 10.1016/j.euf.2020.10.002
3. Dobruch J, Daneshmand S, Fisch M, Lotan Y, Noon AP, Resnick MJ, et al. Gender and Bladder Cancer: A Collaborative Review of Etiology, Biology, and Outcomes. *Eur Urol* (2016) 69(2):300–10. doi: 10.1016/j.eururo.2015.08.037
4. Ide H, Miyamoto H. Sex Hormone Receptor Signaling in Bladder Cancer: A Potential Target for Enhancing the Efficacy of Conventional Non-Surgical Therapy. *Cells* (2021) 10(5):1169. doi: 10.3390/cells10051169
5. Mori K, Mostafaei H, Enikeev DV, Lysenko I, Quhal F, Kimura S, et al. Differential Effect of Sex on Outcomes After Radical Surgery for Upper Tract and Bladder Urothelial Carcinoma: A Systematic Review and Meta-Analysis. *J Urol* (2020) 204(1):58–62. doi: 10.1097/JU.0000000000000788
6. Uhlig A, Strauss A, Seif Amir Hosseini A, Lotz J, Trojan L, Schmid M, et al. Gender-Specific Differences in Recurrence of Non-Muscle-Invasive Bladder Cancer: A Systematic Review and Meta-Analysis. *Eur Urol Focus* (2018) 4(6):924–36. doi: 10.1016/j.euf.2017.08.007
7. Martinez-Rojo E, Berumen LC, Garcia-Alcocer G, Escobar-Cabrera J. The Role of Androgens and Androgen Receptor in Human Bladder Cancer. *Biomolecules* (2021) 11(4):594. doi: 10.3390/biom11040594
8. Costa AR, Lanca de Oliveira M, Cruz I, Goncalves I, Cascalheira JF, Santos CRA. The Sex Bias of Cancer. *Trends Endocrinol Metab* (2020) 31(10):785–99. doi: 10.1016/j.tem.2020.07.002
9. Moorthy HK, Prabhu GGL, Venugopal P. Clinical and Therapeutic Implications of Sex Steroid Hormone Receptor Status in Urothelial Bladder Cancer. *Indian J Urol* (2020) 36(3):171–8. doi: 10.4103/iju.IJU_320_19
10. Koti M, Ingersoll MA, Gupta S, Lam CM, Li X, Kamat AM, et al. Sex Differences in Bladder Cancer Immunobiology and Outcomes: A Collaborative Review With Implications for Treatment. *Eur Urol Oncol* (2020) 3(5):622–30. doi: 10.1016/j.euo.2020.08.013
11. Luna-Velez MV, Dijkstra JJ, Heuschkel MA, Smit FP, van de Zande G, Smeets D, et al. Androgen Receptor Signalling Confers Clonogenic and Migratory Advantages in Urothelial Cell Carcinoma of the Bladder. *Mol Oncol* (2021) 15(7):1882–900. doi: 10.1002/1878-0261.12957
12. Deng G, Wang R, Sun Y, Huang CP, Yeh S, You B, et al. Targeting Androgen Receptor (AR) With Antiandrogen Enzalutamide Increases Prostate Cancer Cell Invasion Yet Decreases Bladder Cancer Cell Invasion *via* Differentially Altering the AR/CircRNA-ARC1/MiR-125b-2-3p or Mir-4736/Ppargamma/MMP-9 Signals. *Cell Death Differ* (2021) 28(7):2145–59. doi: 10.1038/s41418-021-00743-w
13. Ide H, Inoue S, Mizushima T, Jiang G, Chuang KH, Oya M, et al. Androgen Receptor Signaling Reduces Radiosensitivity in Bladder Cancer. *Mol Cancer Ther* (2018) 17(7):1566–74. doi: 10.1158/1535-7163.Mct-17-1061
14. Tripathi A, Gupta S. Androgen Receptor in Bladder Cancer: A Promising Therapeutic Target. *Asian J Urol* (2020) 7(3):284–90. doi: 10.1016/j.ajur.2020.05.011
15. Creta M, Celentano G, Napolitano L, La Rocca R, Capece M, Califano G, et al. Inhibition of Androgen Signalling Improves the Outcomes of Therapies for Bladder Cancer: Results From a Systematic Review of Preclinical and Clinical Evidence and Meta-Analysis of Clinical Studies. *Diagn (Basel)* (2021) 11(2):351. doi: 10.3390/diagnostics11020351
16. Kim A, Kim MS, Ahn JH, Choi WS, Park HK, Kim HG, et al. Clinical Significance of 5-Alpha Reductase Inhibitor and Androgen Deprivation Therapy in Bladder Cancer Incidence, Recurrence, and Survival: A Meta-Analysis and Systemic Review. *Aging Male* (2020) 23(5):971–8. doi: 10.1080/13685538.2019.1646238
17. Tellini R, Mari A, Muto G, Cacciamani GE, Ferro M, Stangl-Kremser J, et al. Impact of Smoking Habit on Perioperative Morbidity in Patients Treated With Radical Cystectomy for Urothelial Bladder Cancer: A Systematic Review and Meta-Analysis. *Eur Urol Oncol* (2020) 4(4):580–93. doi: 10.1016/j.euo.2020.10.006
18. Ronksley PE, Brien SE, Turner BJ, Mukamal KJ, Ghali WA. Association of Alcohol Consumption With Selected Cardiovascular Disease Outcomes: A Systematic Review and Meta-Analysis. *BMJ* (2011) 342:d671. doi: 10.1136/bmj.d671
19. Siristatidis C, Sergentanis TN, Kanavidis P, Trivella M, Sotiraki M, Mavromatis I, et al. Controlled Ovarian Hyperstimulation for IVF: Impact on Ovarian, Endometrial and Cervical Cancer–a Systematic Review and Meta-Analysis. *Hum Reprod Update* (2013) 19(2):105–23. doi: 10.1093/humupd/dms051
20. Zhang J, Yu KF. What's the Relative Risk? A Method of Correcting the Odds Ratio in Cohort Studies of Common Outcomes. *JAMA* (1998) 280(19):1690–1. doi: 10.1001/jama.280.19.1690
21. Al-Hogbani M, Gilbert S, Lodde M, Fradet Y, Toren P. Does 5-Alpha Reductase Inhibitor Use Improve the Efficacy of Intravesical Bacille Calmette-Guérin (BCG) for Non-Muscle Invasive Bladder Cancer? *Bladder Cancer* (2020) 6(1):63–9. doi: 10.3233/blc-190262
22. Chen CC, Huang CP, Tsai YT, Hseih TF, Shyr CR. The Genomic Alterations of 5alpha-Reductases and Their Inhibitor Finasteride's Effect in Bladder Cancer. *Anticancer Res* (2017) 37(12):6893–8. doi: 10.21873/anticanres.12152
23. Izumi K, Taguri M, Miyamoto H, Hara Y, Kishida T, Chiba K, et al. Androgen Deprivation Therapy Prevents Bladder Cancer Recurrence. *Oncotarget* (2014) 5(24):12665–74. doi: 10.18632/oncotarget.2851
24. Kufukihara R, Kikuchi E, Ogihara K, Shigeta K, Yanai Y, Takamatsu K, et al. Role of Previous Malignancy History in Clinical Outcomes in Patients With

Initially Diagnosed Non-Muscle Invasive Bladder Cancer. *Ann Surg Oncol* (2021) 28(9):5349–59. doi: 10.1245/s10434-021-09750-0
25. Makela VJ, Kotsar A, Tammela TLJ, Murtola TJ. Bladder Cancer Survival of Men Receiving 5alpha-Reductase Inhibitors. *J Urol* (2018) 200(4):743–8. doi: 10.1016/j.juro.2018.04.082
26. McMartin C, Lacombe L, Fradet V, Fradet Y, Lodde M, Toren P. Receipt of 5-Alpha Reductase Inhibitors Before Radical Cystectomy: Do They Render High-Grade Bladder Tumors Less Aggressive? *Clin Genitourin Cancer* (2019) 17(6):e1122–8. doi: 10.1016/j.clgc.2019.07.016
27. Morales EE, Grill S, Svatek RS, Kaushik D, Thompson IMJr., Ankerst DP, et al. Finasteride Reduces Risk of Bladder Cancer in a Large Prospective Screening Study. *Eur Urol* (2016) 69(3):407–10. doi: 10.1016/j.eururo.2015.08.029
28. Moschini M, Zaffuto E, Karakiewicz P, Mattei A, Gandaglia G, Fossati N, et al. The Effect of Androgen Deprivation Treatment on Subsequent Risk of Bladder Cancer Diagnosis in Male Patients Treated for Prostate Cancer. *World J Urol* (2019) 37(6):1127–35. doi: 10.1007/s00345-018-2504-3
29. Pastore AL, Fuschi A, De Nunzio C, Balzarro M, Al Salhi Y, Velotti G, et al. Possible Role of 5-Alpha Reductase Inhibitors in Non-Invasive Bladder Urothelial Neoplasm: Multicentre Study. *Minerva Urol Nefrol* (2019). doi: 10.23736/S0393-2249.19.03563-X
30. Sathianathen NJ, Fan Y, Jarosek SL, Lawrentschuk NL, Konety BR. Finasteride Does Not Prevent Bladder Cancer: A Secondary Analysis of the Medical Therapy for Prostatic Symptoms Study. *Urol Oncol* (2018) 36(7):338.e13–338.e17. doi: 10.1016/j.urolonc.2018.03.020
31. Shiota M, Kiyoshima K, Yokomizo A, Takeuchi A, Kashiwagi E, Dejima T, et al. Suppressed Recurrent Bladder Cancer After Androgen Suppression With Androgen Deprivation Therapy or 5alpha-Reductase Inhibitor. *J Urol* (2017) 197(2):308–13. doi: 10.1016/j.juro.2016.08.006
32. Shiota M, Yokomizo A, Takeuchi A, Imada K, Kiyoshima K, Inokuchi J, et al. Secondary Bladder Cancer After Anticancer Therapy for Prostate Cancer: Reduced Comorbidity After Androgen-Deprivation Therapy. *Oncotarget* (2015) 6(16):14710–9. doi: 10.18632/oncotarget.3817
33. Van Hemelrijck M, Feller A, Garmo H, Valeri F, Korol D, Dehler S, et al. Incidence of Second Malignancies for Prostate Cancer. *PLoS One* (2014) 9(7): e102596. doi: 10.1371/journal.pone.0102596
34. Wallner LP, Wang R, Jacobsen SJ, Haque R. Androgen Deprivation Therapy for Treatment of Localized Prostate Cancer and Risk of Second Primary Malignancies. *Cancer Epidemiol Biomarkers Prev* (2013) 22(2):313–6. doi: 10.1158/1055-9965.EPI-12-1137
35. Wang CS, Li CC, Juan YS, Wu WJ, Lee HY. 5alpha-Reductase Inhibitors Impact Prognosis of Urothelial Carcinoma. *BMC Cancer* (2020) 20(1):872. doi: 10.1186/s12885-020-07373-4
36. Wissing MD, O'Flaherty A, Dragomir A, Tanguay S, Kassouf W, Aprikian AG. The Use of 5-Alpha Reductase Inhibitors and Alpha-1 Blockers Does Not Improve Clinical Outcome in Male Patients Undergoing Radical Cystectomy for Bladder Cancer in Quebec, Canada. *Clin Genitourin Cancer* (2021) 19 (4):371–371.e9. doi: 10.1016/j.clgc.2021.01.007
37. Wu SC, Kwon D, Jue JS, Chen FV, Velasquez Escobar MC, Punnen S, et al. Androgen Suppression Therapy Is Associated With Lower Recurrence of Non-Muscle-Invasive Bladder Cancer. *Eur Urol Focus* (2021) 7(1):142–7. doi: 10.1016/j.euf.2019.04.021
38. Zhu D, Srivastava A, Agalliu I, Fram E, Kovac EZ, Aboumohamed A, et al. Finasteride Use and Risk of Bladder Cancer in a Multiethnic Population. *J Urol* (2021) 206(1):15–21. doi: 10.1097/JU.0000000000001694
39. Santella C, Rouette J, Brundage MD, Filion KB, Azoulay L. Androgen Deprivation Therapy for Prostate Cancer and the Risk of Bladder Cancer: A Systematic Review of Observational Studies. *Urol Oncol* (2020) 38(11):816–25. doi: 10.1016/j.urolonc.2020.04.028
40. Miyamoto H, Yao JL, Chaux A, Zheng Y, Hsu I, Izumi K, et al. Expression of Androgen and Oestrogen Receptors and Its Prognostic Significance in Urothelial Neoplasm of the Urinary Bladder. *BJU Int* (2012) 109(11):1716–26. doi: 10.1111/j.1464-410X.2011.10706.x
41. Sikic D, Breyer J, Hartmann A, Burger M, Erben P, Denzinger S, et al. High Androgen Receptor mRNA Expression Is Independently Associated With Prolonged Cancer-Specific and Recurrence-Free Survival in Stage T1 Bladder Cancer. *Transl Oncol* (2017) 10(3):340–5. doi: 10.1016/j.tranon.2017.01.013
42. Boorjian S, Ugras S, Mongan NP, Gudas LJ, You X, Tickoo SK, et al. Androgen Receptor Expression Is Inversely Correlated With Pathologic Tumor Stage in Bladder Cancer. *Urology* (2004) 64(2):383–8. doi: 10.1016/j.urology.2004.03.025
43. Lee YR, Im E, Kim H, Lew BL, Sim WY, Lee J, et al. Untargeted Metabolomics and Steroid Signatures in Urine of Male Pattern Baldness Patients After Finasteride Treatment for a Year. *Metabolites* (2020) 10(4):131. doi: 10.3390/metabo10040131
44. Kristal AR, Till C, Tangen CM, Goodman PJ, Neuhouser ML, Stanczyk FZ, et al. Associations of Serum Sex Steroid Hormone and 5alpha-Androstane-3alpha,17beta-Diol Glucuronide Concentrations With Prostate Cancer Risk Among Men Treated With Finasteride. *Cancer Epidemiol Biomarkers Prev* (2012) 21(10):1823–32. doi: 10.1158/1055-9965.EPI-12-0695
45. Wadhwa VK, Weston R, Parr NJ. Bicalutamide Monotherapy Preserves Bone Mineral Density, Muscle Strength and has Significant Health-Related Quality of Life Benefits for Osteoporotic Men With Prostate Cancer. *BJU Int* (2011) 107(12):1923–9. doi: 10.1111/j.1464-410X.2010.09726.x
46. Liang Z, Cao J, Tian L, Shen Y, Yang X, Lin Q, et al. Aromatase-Induced Endogenous Estrogen Promotes Tumour Metastasis Through Estrogen Receptor-Alpha/Matrix Metalloproteinase 12 Axis Activation in Castration-Resistant Prostate Cancer. *Cancer Lett* (2019) 467:72–84. doi: 10.1016/j.canlet.2019.09.001

Conflict of Interest: The authors declare that the research was conducted in the absence of any commercial or financial relationships that could be construed as a potential conflict of interest.

Publisher's Note: All claims expressed in this article are solely those of the authors and do not necessarily represent those of their affiliated organizations, or those of the publisher, the editors and the reviewers. Any product that may be evaluated in this article, or claim that may be made by its manufacturer, is not guaranteed or endorsed by the publisher.

frontiers in Oncology

ORIGINAL RESEARCH
published: 01 March 2022
doi: 10.3389/fonc.2022.818860

Identification of a Novel Tumor Microenvironment Prognostic Signature for Bladder Urothelial Carcinoma

*Chaojie Xu†, Dongchen Pei†, Yi Liu, Yang Yu, Jinhua Guo, Nan Liu and Zhengjun Kang**

Department of Urology, The Fifth Affiliated Hospital of Zhengzhou University, Zhengzhou University, Zhengzhou, China

Background: The tumor microenvironment (TME) regulates the proliferation and metastasis of solid tumors and the effectiveness of immunotherapy against them. We investigated the prognostic role of TME-related genes based on transcriptomic data of bladder urothelial carcinoma (BLCA) and formulated a prediction model of TME-related signatures.

Methods: Molecular subtypes were identified using the non-negative matrix factorization (NMF) algorithm based on TME-related genes from the TCGA database. TME-related genes with prognostic significance were screened with univariate Cox regression analysis and lasso regression. Nomogram was developed based on risk genes. Receiver operating characteristic (ROC) curve and decision curve analysis (DCA) were used for inner and outer validation of the model. Risk scores (RS) of patients were calculated and divided into high-risk group (HRG) and low-risk group (LRG) to compare the differences in clinical characteristics and PD-L1 treatment responsiveness between HRG and LRG.

Results: We identified two molecular subtypes (C1 and C2) according to the NMF algorithm. There were significant differences in overall survival (OS) ($p<0.05$), progression-free survival (PFS) ($p<0.05$), and immune cell infiltration between the two subtypes. A total of eight TME-associated genes (*CABP4*, *ZNF432*, *BLOC1S3*, *CXCL11*, *ANO9*, *OAS1*, *FBN2*, *CEMIP*) with independent prognostic significance were screened to build prognostic risk models. Age ($p<0.001$), grade ($p<0.001$), and RS ($p<0.001$) were independent predictors of survival in BLCA patients. The developed RS nomogram was able to predict the prognosis of BLCA patients at 1, 3, and 5 years more potentially than the models of other investigators according to ROC and DCA. RS showed significantly higher values ($p = 0.047$) in patients with stable disease (SD)/progressive disease (PD) compared to patients with complete response (CR)/partial response (PR).

Conclusions: We successfully clustered and constructed predictive models for TME-associated genes and helped guide immunotherapy strategies.

Keywords: tumor microenvironment, prognosis, bladder urothelial carcinoma, immunotherapy, non-negative matrix factorization

OPEN ACCESS

Edited by:
Scott T. Tagawa,
Cornell University, United States

Reviewed by:
Ali Amin,
Rhode Island Hospital, United States
Mehmet Asim Bilen,
Emory University, United States

***Correspondence:**
Zhengjun Kang
kzj7153@sina.com

†These authors have contributed equally to this work

Specialty section:
This article was submitted to Genitourinary Oncology, a section of the journal Frontiers in Oncology

Received: *20 November 2021*
Accepted: *26 January 2022*
Published: *01 March 2022*

Citation:
Xu C, Pei D, Liu Y, Yu Y, Guo J, Liu N and Kang Z (2022) Identification of a Novel Tumor Microenvironment Prognostic Signature for Bladder Urothelial Carcinoma. Front. Oncol. 12:818860. doi: 10.3389/fonc.2022.818860

INTRODUCTION

Bladder urothelial carcinoma (BLCA) is the pathological type of bladder cancer with the highest percentage, about 90% (1). There were globally approximately 550,000 new patients and 200,000 deaths in 2018 (2). Despite significant advances in the treatment of BLCA with radiotherapy, surgery, and targeted therapy, the prognosis of BCLA patients remains poor, with 30% of them having muscle-invasive bladder cancer (MIBC) at initial consultation (3). However, patients with MIBC are characterized by rapid disease progression and low survival, with a 5-year tumor-specific mortality rate of >50% (4). Therefore, a validated prognostic risk model can help guide individualized treatment of BLCA patients to improve their prognosis.

At present, the 8th edition of the TNM staging method published by the Union International Center of Cancer (UICC) is one of the most valuable indicators to determine the prognosis of patients with BLCA (5). However, due to the heterogeneity of BLCA, the prognosis of patients with the same TNM stage may vary considerably (6–8). In addition, multiple comprehensive BLCA molecular typing based on genetic analysis can forecast the overall survival (OS) of individuals, such as ferroptosis-associated gene signature (9), autophagy-associated gene signature (10), and RNA binding protein-associated gene signature (11). Therefore, we considered the use of gene signatures as biomarkers that could predict individual prognosis and drug responsiveness, thus improving clinical outcomes in BLCA patients.

The tumor microenvironment (TME) includes solid tumor cells, vascular network, extracellular matrix, secreted factors (cytokines, chemokines), and distantly recruited cells such as activated B cells and macrophages (12). Overall, this homeostatic system supports the progression and recurrence of malignancies and has important implications in chemoresistance and immunotherapy (13, 14). Mesenchymal cells such as fibroblasts within TME are associated with the T-cell efflux phenotype in bladder cancer (15). In addition, the non-immune cellular components of TME also influence the therapeutic response, for example, the secretion of TGF-β by fibroblasts can lead to efflux of immune cells or resistance to chemotherapeutic agents, and therefore the therapeutic effect of the tumor varies with the degree of stromal cell infiltration (16). Therefore, tumor tissue gene expression profiles can reflect the relationship between TME and patient prognosis.

In summary, TME-associated gene signature can enhance the reliability of forecasting patient prognosis. Therefore, we aimed to design a prediction model combining TME-related gene signatures and patient clinical characteristics and develop a nomogram to forecast the prognosis of BLCA patients at 1, 3, and 5 years.

Abbreviations: TME, Tumor microenvironment; BLCA, bladder urothelial carcinoma; NMF, non-negative matrix factorization; K-M, Kaplan-Meier; ROC, receiver operating characteristic; DCA, decision curve analysis; RS, Risk score; HRG, high-risk group; LRG, low-risk group; MIBC, muscle-invasive bladder cancer; UICC, Union International Center of Cancer; OS, overall survival; PFS, Progression-free survival; GEO, Gene-Expression Omnibus; TCGA-BLCA, The Cancer Genome Atlas-Bladder Cancer; CNV, copy number variation; RSS, sum of squared residuals; MCP, Microenvironment Cell Populations; TMB, tumor mutation burden; RMS, restricted mean survival; CR, complete response; PR, partial response; SD, stable disease; PD, progressive disease; GSEA, Gene set enrichment analysis; PD-L1, programmed death ligand 1; HR, hazard ratio; NES, normalized enrichment score; EMT, epithelial-mesenchymal transition.

MATERIALS AND METHODS

Data Download and Preprocessing

We downloaded transcriptome data and clinical annotations from the Genomic Data Commons. The TCGA-BLCA (The Cancer Genome Atlas-Bladder Cancer) cohort consisted of 433 RNA sequencing samples, including 19 normal profiles and 414 tumor profiles. We removed samples without clinical follow-up information and microdissection from the TCGA-BLCA cohort, resulting in the inclusion of a total of 359 samples. We also downloaded the simple nucleotide variation data in the TCGA database for further analysis of copy number variation (CNV).

Moreover, for external validation, data for the cohort of GSE31684 were obtained from the GEO database. The microarray data of GSE31684 from Affymetrix Human Genome U133 Plus 2.0 Array, we downloaded the normalized matrix file directly. All dates contain survival information.

TME-related genes were obtained from published studies (17–23), and a total of 4061 genes were included (**Table S1**). We used the UCSC Xena (https://xenabrowser.net/) to download the TCGA-GDC pan-cancer data.

Screening for TME-Related Differentially Expressed Genes

The differentially expressed TME-associated genes in BLCA tissues and adjacent tissues were screened, and the screened differential genes and their expression were organized into a gene expression matrix with a corrected $p<0.05$ and the absolute value of differential expression multiplicity >1 (FDR<0.05 and $|\log2\text{Fold Change}|>1$) was set as the threshold value.

Identification of Molecular Subtypes Using Non-Negative Matrix Factorization (NMF) Algorithm

Fifty iterations of the sample were performed using NMF for extracting biological correlation coefficients and predicting the inner feature structure in gene expression matrices (24). We observed performance for the number of clusters k between two and ten.

Comparison of Immune Scores Between Clusters

Microenvironment Cell Populations (MCP) counters allow quantification of the absolute abundance of eight immune cells and two stromal cells from transcriptomic data (24). We evaluated infiltrating cell scores between clusters, which included neutrophils, NK cells, and myeloid dendritic cells, among others. Then we evaluated the infiltrating cells between clusters.

Univariate Cox Regression Analysis and Lasso Regression Analysis

At the ratio of 7:3, 359 samples were divided into the training set and validation set with no one as the control. TME-related

differentially expressed genes were subjected to univariate Cox analysis to get the prognostic genes. The lasso method prevents model overfitting by building a penalized feature to build a more refined model. We then applied lasso Cox regression to minimize the amounts of genes in the prognostic modeling. The results of the lasso regression analysis on the variables affecting the outcome of individuals with BLCA were incorporated into multivariate Cox regression analysis.

Construction of a Nomogram Combined With Risk Score (RS) and Clinical Features

The TCGA cohort was used to build a nomogram to forecast the prognosis of individuals with BLCA, with variables including RS and clinical characteristics. RS was calculated according to the expression of differential genes and regression analysis coefficient values. The formula is shown below:

$$riskscore = \sum_{i=1}^{n}(coefi * Xi)$$

We classify the cases into high-risk group (HRG) and low-risk group (LRG) according to the median RS. The receiver operating characteristic (ROC) curve was utilized to assess the predictive value of RS for prognosis. Kaplan-Meier (K-M) curves were drawn and the Log-rank method was used to evaluate OS.

Prediction Model Evaluation

ROC, calibration curve (bootstrap 1000), and decision curve analysis (DCA) were applied to assess the confidence validity of the model. Our RS nomogram was also compared with those of other established models. RMS time was used to assess the prognostic accuracy of the models beyond 60 months of patient survival.

Gene Set Enrichment Analysis (GSEA)

The c2.cp.kegg.v7.4.symbols and c5.go.v7.4.symbols collection were used to explore the function annotation in HRG and LRG by GSEA software. Gene sets with FDR < 0.05 were was considered statistically significant.

Immunotherapy Prediction

We selected patients with urologic tumors in the IMvigor210 cohort who had received programmed death-ligand 1 (PD-L1) blockade treatment to predict response to immunotherapy. This cohort had a total of 348 cases, containing 232 death samples and 116 censored, all of which contained survival data. BLCA patients who received anti-PD-L1 therapy could be classified into the following categories according to the patient's response: complete response (CR), partial response (PR), stable disease (SD), and progressive disease (PD). Among them, CR and PR are recognized as patients who respond to immunotherapy. SD and PD are recognized as patients who do not respond to immunotherapy. We computed RS for each case and classified them as HRG and LRG based on the median value of RS.

Statistical Analysis

Statistical analysis and graphical work were finished in the R environment (version 4.1.1). Volcano maps were drawn using the "ggplot2" package. Violin plots were drawn with "ggpubr" package. Cox regression analyses were performed by the "survival" package. We used the Chi-square test or Fisher's exact test to measure the difference between training and validating sets and the relationship between clinical data and RS. K-M survival curves with log-rank tests were plotted by the "survminer" package. The ROC curves were depicted by the "timeROC" package. Calibration curves were derived from the "rms" package. The restricted mean survival (RMS) package was for computing the C-index for each of the models. $p < 0.05$ is considered to have statistical difference.

RESULTS

Patient Characteristics and Analysis of Differentially Expressed Genes Associated With TME in BLAC Patients

The TCGA-BLCA cohort consisted of 433 RNA sequencing samples, including 19 normal samples and 414 tumor samples. The characteristics of the cases enrolled in this study were shown in **Table 1** after pre-processing. In total, there were 1014 TME-associated genes (FDR<0.05 and $|\log_2 FC|>1$) differentiated in expression between BLCA patients and regular bladder tissue. The top 50 up-regulated and down-regulated genes with differential expression were plotted as volcanoes (**Figure 1A**).

Molecular Subtypes of TME-Related Genes According to the NMF Algorithm

We clustered genes based on the differential expression TME-related genes by the NMF algorithm. When k=2, C1 and C2 were formed based on covariance and RSS (**Figures 1B–D**). Survival results showed that cases in the C1 cluster had better OS and PFS than those in the C2 cluster (**Figures 1E, F**). There were differences in immune scores between C1 and C2 for nine cell types, including CD8+ T cells ($p<0.05$), cytotoxic lymphocytes ($p<0.05$), B cells ($p<0.05$), neutrophils ($p = 0.023$), monocytes ($p<0.05$), endothelial cells ($p<0.05$), fibroblasts ($p<0.05$), NK cells ($p<0.05$), and myeloid dendritic cells ($p = 0.014$) (**Figures 2A–I**). The international transcriptomic immune typology of solid tumors has established six immune subtypes, including wound healing (Immune C1), IFN-gamma dominant (Immune C2), inflammatory (Immune C3), lymphocyte depleted (Immune C4), immunologically quiet (Immune C5), and TGF-beta dominant (Immune C6). Our molecular subtyping results were compared with the former and the results are shown in **Figure 1G**.

Developing an RS Prediction Model for TME-Related Genes

At the ratio of 7:3, 359 samples were randomly divided into a training set (n = 252) and validation set (n = 107) (**Table 2**). Baseline features of the patients demonstrated no obvious distinction between them in terms of gender, age, pathological grade, treatment history, and TNM stage ($p>0.05$). Univariate Cox analysis was performed on the training cohort with 173 differentially TME-associated genes ($p < 0.05$) (**Table S2**).

TABLE 1 | Clinicopathological characteristics of BLCA patients from the TCGA and GEO databases.

Characteristics	TCGA-BLCA cohort N = 359	GSE31684 N = 93
Age		
<=65	141 (39.28%)	28 (39.41%)
>65	218 (60.72%)	65 (60.59%)
Gender		
Female	99 (27.58%)	25 (26.88%)
Male	260 (72.42%)	68 (73.12%)
Grade		
High	342 (95.26%)	87 (93.50%)
Low	14 (3.9%)	6 (6.50%)
Unknow	3 (0.84%)	0 (0.00%)
Stage		
I-II	113 (31.48%)	74 (79.57%)
III-IV	244 (67.97%)	11 (11.83%)
Unknow	2 (0.56%)	8 (8.60%)
T		
T0-T2	107 (29.81%)	NA
T3-T4	223 (62.12%)	NA
Unknow	29 (8.08%)	NA
M		
M0	164 (45.68%)	NA
M1	11 (3.06%)	NA
Unknow		NA
N	184 (51.25%)	
N0-N1	251 (69.92%)	NA
N2-N3	72 (20.06%)	NA
Unknow	36 (10.03%)	NA
Neoadjuvant therapy		
Yes	10 (2.79%)	NA
No	349 (97.21%)	NA
Radiotherapy		
Yes	15 (4.18%)	NA
No	243 (67.69%)	NA
Unknow	101 (28.13%)	NA
Survival status		
Alive	201 (55.99%)	28 (30.11%)
Dead	158 (44.01%)	65 (69.89%)
The median follow-up time (year)	5.19	2.57

Lasso regression was applied to achieve reduction in the number of genes while remaining highly accurate. The traces of independent variables showed a gradual increase in the number of independent coefficients that converge to zero as λ decreases (**Figure 3A**). We selected 11 genes as candidate genes according to the best value of λ (**Figure 3B**). Then TME-related genes with significant differences were screened according to a multifactorial Cox proportional risk model. Finally, eight genes were obtained, constructing the following equation:

$$\begin{aligned} risk\ score\ (RS) = &-(0.2823 \times CABP4) - (0.2536 \times ZNF432) \\ &- (0.4745 \times BLOC1S3) - (0.1731 \times CXCL11) \\ &- (0.2813 \times AN09) - (0.2149 \times OAS1) \\ &+ (0.1846 \times FBN2) + (0.2785 \times CEMIP) \end{aligned}$$

ROC was utilized to evaluate the accuracy of the RS model in our training set. As shown in **Figure 3C**, the area under curve (AUC) for the model were 0.818, 0.776, and 0.771 for 1-, 3-, and 5- years, respectively. We used the median value of RS as the boundary to classify the samples into HRG and LRG. K-M survival analysis showed that LRG had a better prognosis than HRG (**Figure 4C**).

We performed survival analyses in the TCGA test set, all TCGA set, and the GEO cohort. HRG had a significantly worse prognosis than LRG (**Figure 4D–F**). In the three validation sets, the 1-year AUC was 0.761, 0.664, and 0.589, respectively (**Figures 3D–F**). In the GEO cohort, the low AUC values at 1, 3, and 5 years were partly due to the short median follow-up time of patients.

Construction of a Nomogram Containing RS for TME-Related Genes

We used univariate and multivariate Cox regression to examine the relationship between potential variables and OS, which included RS, TNM stage, pathological grade, age, and sex (**Table 3**). The results showed that RS (HR: 1.045, 95% CI: 1.019–1.071, p<0.001), TNM stage(HR: 2.127, 95% CI: 1.416–3.196, p<0.001), and age (HR: 1.034, 95% CI: 1.017–1.052, p<0.001) were independent risk factors. Next, we constructed a nomogram including RS and clinical features (**Figure 4A**). Individualized 1-year, 3-year, and 5-year survival rates can be visualized based on the nomogram. For example, a 63-year-

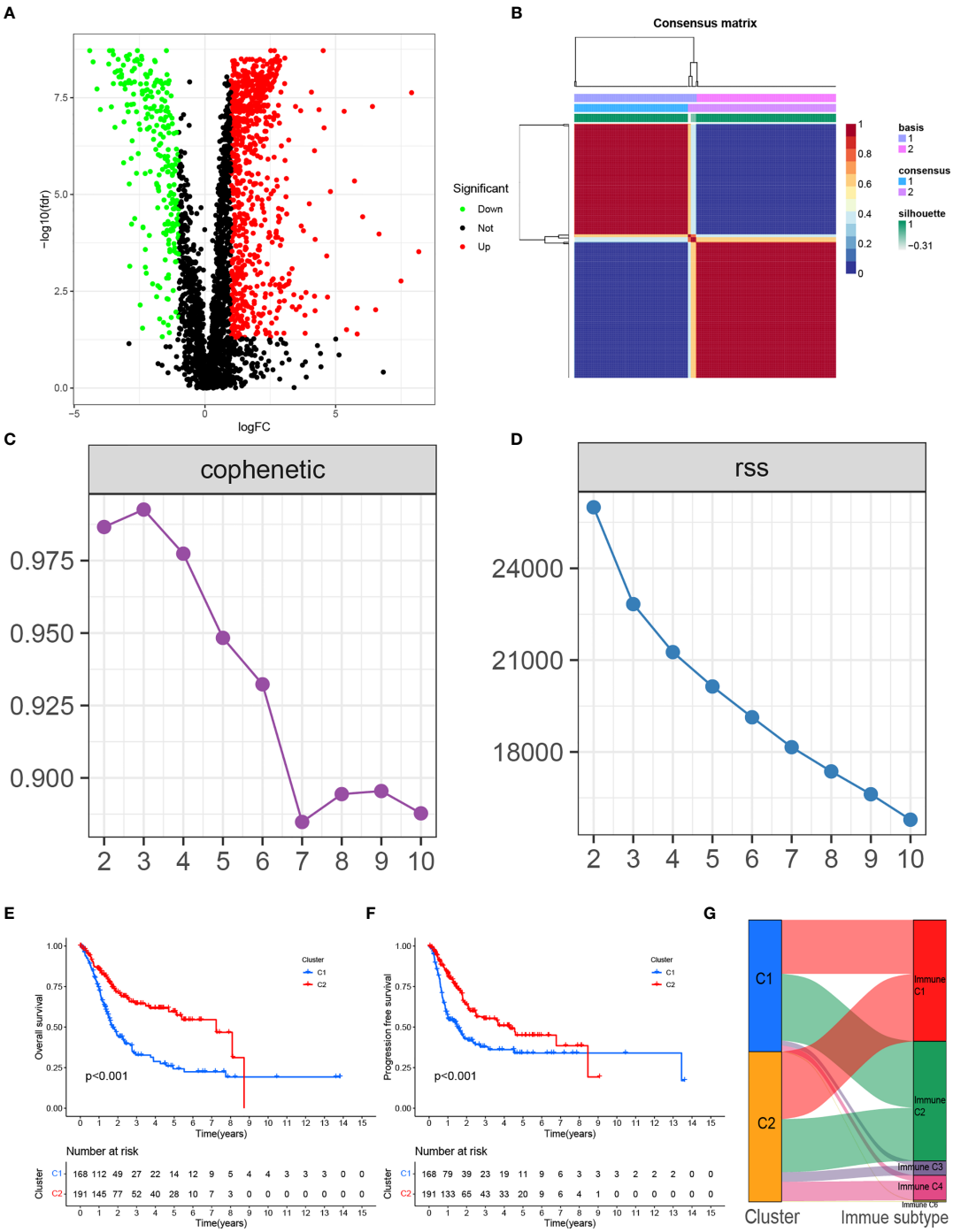

FIGURE 1 | **(A)** Volcano plot of differentially expressed genes in BLCA from the TCGA database. **(B)** Consensus map clustered *via* the non-negative matrix factorization (NMF) algorithm. **(C)** The cophenetic correlation coefficient is used to reflect the stability of the cluster obtained from NMF. **(D)** RSS is used to reflect the clustering performance of the model. **(E)** Overall survival (OS) showed significant differences between C1 and C2. **(F)** Progression-free survival (PFS) showed significant differences between C1 and C2. **(G)** Alluvial plot showing the percentage of C1 and C2 between molecular subtypes.

old male patient diagnosed with BLCA has clinical features of T3M0N0, high pathological grading, and low RS. The clinician can then calculate the corresponding scores for the variables, with a final total score of 442. Thus, the patient's 1-year, 3-year, and 5-year survival rates can be inferred to be 0.944,0.797, and 0.685, respectively. The results showed a significant impact of RS on survival prediction. We drew calibration graphs of 1-year, 3-year, and 5-year OS in the training sets to demonstrate the consensus of

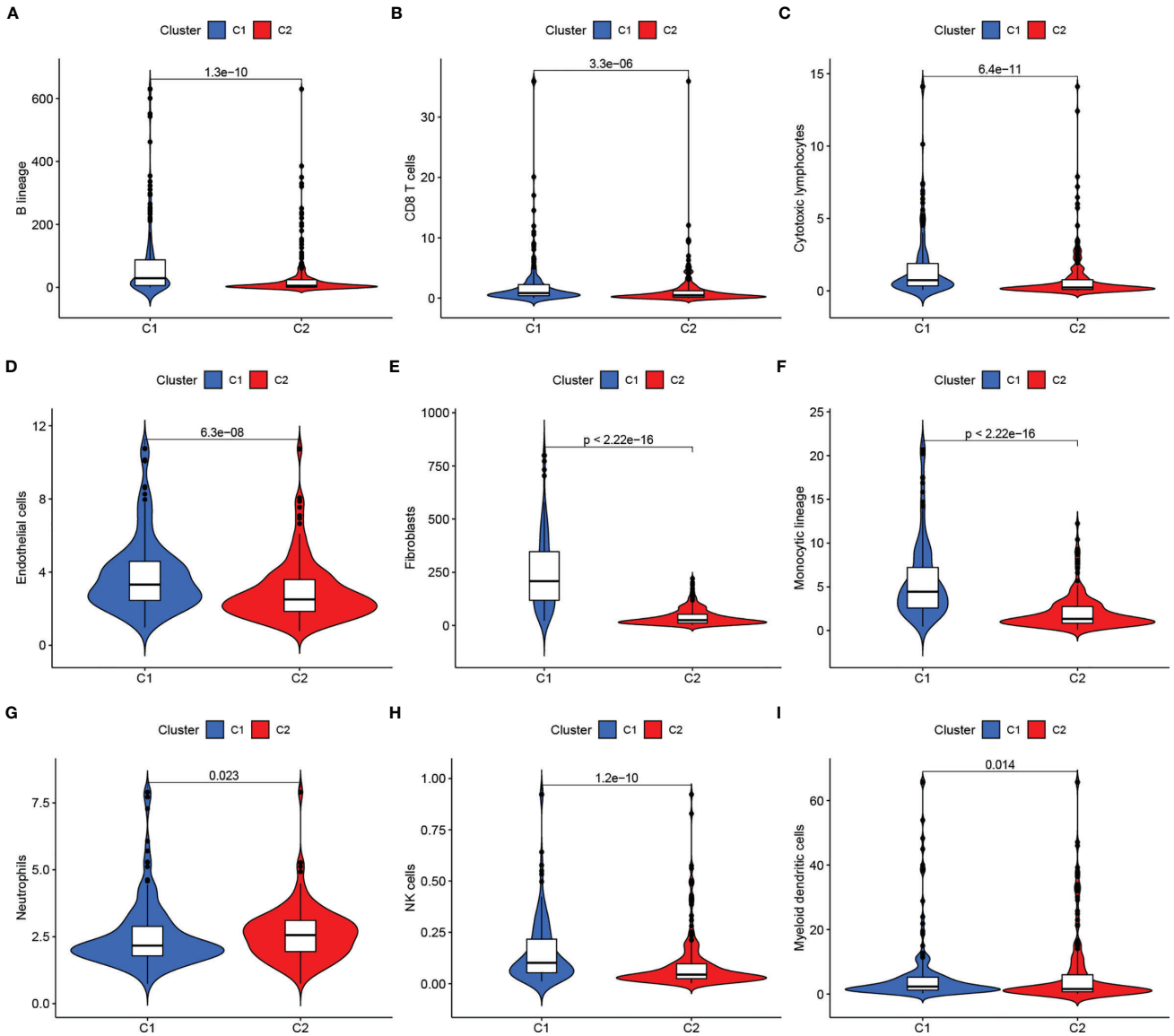

FIGURE 2 | **(A–I)** Immune scores of cells of the tumor microenvironment (TME) showed significant differences.

our model with the real results (**Figure 4B**). The AUC of the model was higher than the other impact factors in the 3-year and 5-year ROC curve (**Figures 5B, C**). However, the RS was higher than the AUC of the nomogram at 1-year ROC curve, which was the highest of all factors (**Figure 5A**). Finally, DCA to assess the clinical utility of nomograms. Both nomogram and RS showed good consistency in forecasting OS at 1, 3, and 5 years compared with a singular prognostic factor (**Figures 5D–F**).

Comparison of the Eight-Gene Signature Risk Model With Other Models

We compared the prediction models of our eight-gene signature with other models to demonstrate the predictive performance of our model, including models of the identified 3-gene (25), 5-gene (26), and 7-gene signature (27). We also computed RS for every sample by multivariate Cox regression analysis. We evaluated the ROC of the four models according to the corresponding genes. The cases were then classified into HRG and LRG based on the median RS value. In all four models, there was a significant difference in survival time between patients in the HRG and LRG groups, with patients in LRH having a better prognosis than those in HRG (**Figures 6E–H**). However, the ROC of the previous models showed lower AUCs and, therefore, the other three models have worse predictions compared to our nomogram. (**Figures 6A–D**).

We calculated the C-index of the four models and found that our model has the highest C-index with 0.695 (**Figure 6I**). RMS time was used to estimate the forecasting effectiveness of the

TABLE 2 | Comparison of TCGA training and testing cohort.

Characteristics	TCGA Testing Cohort N = 107	TCGA Training Cohort N = 252	*p*-Value
Age			0.5587
<=65	45 (42.06%)	96 (38.1%)	
>65	62 (57.94%)	156 (61.9%)	
Gender			0.1973
Female	35 (32.71%)	64 (25.4%)	
Male	72 (67.29%)	188 (74.6%)	
Grade			1
High	103 (96.26%)	239 (94.84%)	
Low	4 (3.74%)	10 (3.97%)	
Unknow	0 (0%)	3 (1.19%)	
Stage			0.5564
I-II	31 (28.97%)	82 (32.54%)	
III-IV	76 (71.03%)	168 (66.67%)	
Unknow	0 (0%)	2 (0.79%)	
T			0.806
T0-T2	30 (28.04%)	77 (30.56%)	
T3-T4	67 (62.62%)	156 (61.9%)	
Unknow	10 (9.35%)	19 (7.54%)	
M			1
M0	46 (42.99%)	118 (46.83%)	
M1	3 (2.8%)	8 (3.17%)	
Unknow	58 (54.21%)	126 (50%)	
N			0.254
N0-N1	79 (73.83%)	172 (68.25%)	
N2-N3	17 (15.89%)	55 (21.83%)	
Unknow	11 (10.28%)	25 (9.92%)	
Neoadjuvant therapy			0.7362
Yes	2 (1.87%)	8 (3.17%)	
No	105 (98.13%)	244 (96.83%)	
Radiotherapy			0.9045
Yes	4 (3.74%)	11 (4.37%)	
No	77 (71.96%)	166 (65.87%)	
Unknow	26 (24.3%)	75 (29.76%)	

model at different time points. Our model was found to outperform the other two gene signatures at > 60 months except for Zhou signature. This demonstrates that our nomogram has an advantage over the other models in predicting both patient survival up to 5 years and patient survival beyond 60 months (**Figure 6J**).

Functional Analysis of Genes Between HRG and LRG

We ran GSEA on samples within the HRG and LRG. We identified the following pathways with associated normalized enrichment score (NES) and the adjusted p-value (q-value) enriched in the HRG (**Figures 7A, D**): *KEGG_FOCAL_ADHESION* (NES =2.1496, q =1.57E-08), *KEGG_ECM_RECEPTOR_INTERACTION* (NES =2.2856, q =4.50E-07), *KEGG_REGULATION_OF_ACTIN_CYTOSKELETON* (NES =2.0206, q =1.25E-06), *KEGG_SYSTEMIC_LUPUS_ERYTHEMATOSUS* (NES =2.0084, q =4.96E-05), *KEGG_PATHWAYS_IN_CANCER* (NES =1.7137, q =0.0003), *GOBP_CELLULAR_ION_HOMEOSTASIS* (NES =1.9040, q =1.71E-08), *GOBP_CIRCULATORY_SYSTEM_PROCESS* (NES =2.0543, q =1.71E-08), *GOBP_CORNIFICATION* (NES =2.5951, q =1.71E-08), *GOBP_EPIDERMAL_CELL_DIFFERENTIATION* (NES =2.6868, q =1.71E-08), *GOBP_EPIDERMIS_DEVELOPMENT* (NES =2.5372, q =1.71E-08).

Classical pathways in tumors include immune checkpoints, DNA duplication, mismatch repair, and epithelial-mesenchymal transition (EMT). The correlation of RS with target genes was analyzed by extracting the expression of the relevant pathway target genes from the samples. The results showed that RS was positively correlated with EMT-related genes (*F-AP*, *TAGLN*, and *LOXL2*) (**Figure 7C**).

We computed the immune cell fraction for every sample of the TCGA-BLCA set using an MCP counter and then compared their correlation with RS. As shown in **Figure 7F**, RS was positively correlated with CD8+ T cells ($p<0.05$), endothelial cells ($p<0.05$), and fibroblasts ($p<0.05$). In addition, we evaluated the correlation between RS, TMB, and infiltrating cells by MCP counter with the results shown in **Figure 7B**.

Our analysis showed that there were also differences in RS between clinical subgroups of BLCA patients. More specifically, patients older than 65 years, with no history of radiotherapy, female, and with high TNM stage had higher RS (**Figures 8A–E**). The K-M survival curves of patients in both stage I-II and III-IV subgroups also proved our results (**Figures 8F–H**). In addition, the K-M survival curves of patients in both MIBC and NMIBC subgroups also proved our results (**Figures 8H, I**).

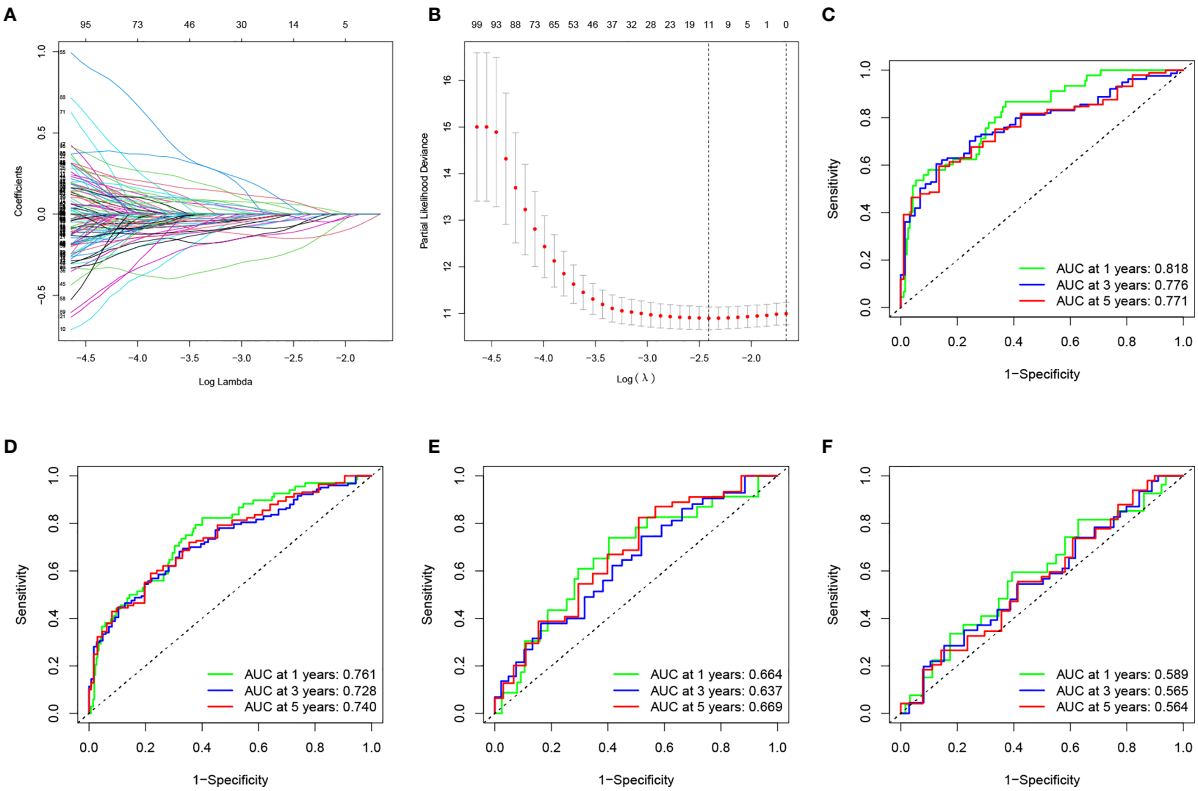

FIGURE 3 | **(A)** Changing the trajectory of each independent variable (the abscissa represents the corrected lambda and the ordinate represents the coefficient of the independent variable). **(B)** log value of the independent variable lambda (the abscissa represents the CI of each lambda, and the ordinate represents errors in cross-validation). **(C–F)** Construction and validation of the TME-related eight-gene risk score (RS) for BLCA with 1-, 3- and 5-year receiver operating characteristic (ROC) within different cohorts: **(C)** TCGA training cohort; **(D)** entire TCGA cohort; **(E)** TCGA testing cohort; **(F)** GEO cohort.

Prediction of Response to Immunotherapy Based on RS Model

We selected patients with urologic tumors in the IMvigor210 cohort who had received PD-L1 blockade therapy to observe the effectiveness against immunotherapy. We calculated the RS for each sample and classified them into HRG and LRG based on the median RS value. the RS showed significantly higher values ($p = 0.047$) in patients with SD/PD compared to patients with CR/PR (**Figure 7E**). This suggests that our RS model may be useful in predicting patient response to PD-L1 blocking therapy.

DISCUSSION

The major discovery of our work was a prediction model according to the TME - associated gene signature of BLCA. TME heterogeneity has an essential role in patient prognosis and in predicting the effectiveness of targeted therapies (28–30). 4061 TME-related genes and 359 BLCA samples of TCGA were evaluated in this work. We applied the NMF method to distinguish two molecular clusters, which is a promising novel clustering method. There were differences in immune scores for TME-infiltrating cell types between C1 and C2. In addition, correlation analysis with prognostic indicators OS and PFS also showed differences between C1 and C2. These results demonstrate the heterogeneity of TME.

We found that our prognostic model based on eight TME-related genes (*CABP4*, *ZNF432*, *BLOC1S3*, *CXCL11*, *ANO9*, *OAS1*, *FBN2*, *CEMIP*) was able to accurately forecast the probability of survival in individuals with BLCA. Prior researches have examined several genes included in our signature under a variety of tumors. For instance, *CXCL11* has an important role in the production of chemokines. First, these mediators can trigger the accumulation of CD8+ T cells that can contribute to the elimination of the tumor. Secondly, the production of these chemokines by tumor tissue may trigger the migration and activation of immune cells including myeloid-derived suppressor cells and regulatory T cells, which act in favor of the tumor and its progress (31). *FBN2* is highly expressed in lung cancer tissues, and as an oncogene, it affects the pathogenesis of lung cancer (32). In addition, Chen Y (33) found that *CEMIP* can promote a variety of tumor processes by affecting tumor proliferation, dedifferentiation, and the tumor microenvironment. In terms of molecular mechanisms, existing

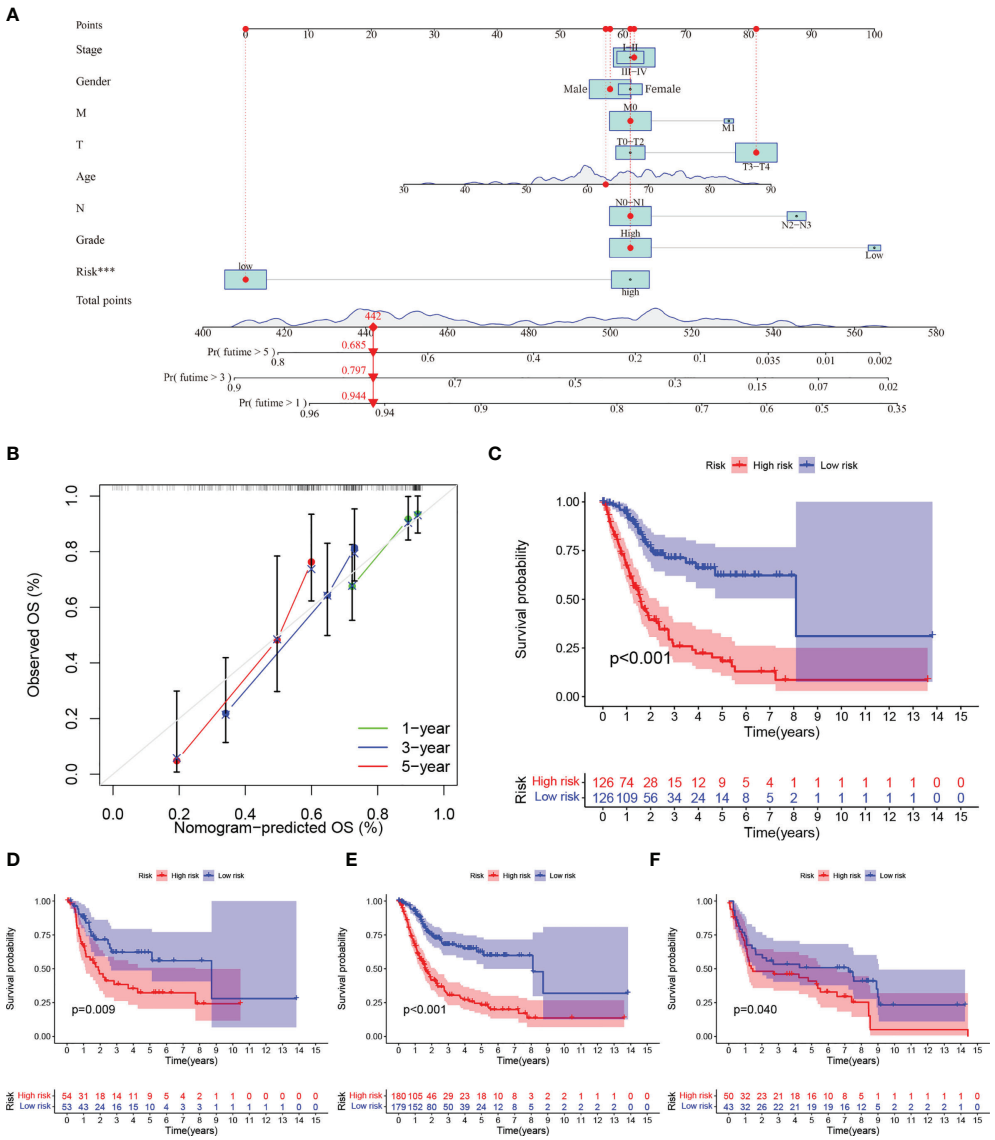

FIGURE 4 | **(A–C) (A)** Nomogram predicting the 1-, 3- and 5-year OS for patients. The points identified on the point scale of each variable are totaled. Finally, beneath the total points, the probability of 1-, 3- or 5-year survival is projected on the scales below. **(B)** Calibration curves for the nomogram predicted 1-, 3- and 5-year OS for patients in relation to actual survival. **(C–F)** Construction and validation of the TME-related eight-gene risk score (RS) for BLCA with Kaplan–Meier (KM) curves within different cohorts: **(C)** TCGA training cohort; **(D)** TCGA testing cohort; **(E)** entire TCGA cohort; **(F)** GEO cohort.

TABLE 3 | Univariable and multivariable Cox regression to analyze the relationship between the RS and clinical prognosis.

Variables	Univariable Analysis			Multivariable Analysis		
	HR	95%*CI*	*P*-Value	HR	95%*CI*	*P*-Value
Age	1.038	1.021–1.056	<0.001	1.034	1.017–1.052	<0.001
Gender	0.891	0.632–1.257	0.511	~	~	~
Grade	1.779	0.438–7.227	0.421	~	~	~
Stage	2.330	1.555–3.492	<0.001	2.127	1.416–3.196	<0.001
Risk Score	1.057	1.032–1.083	<0.001	1.045	1.019–1.071	<0.001

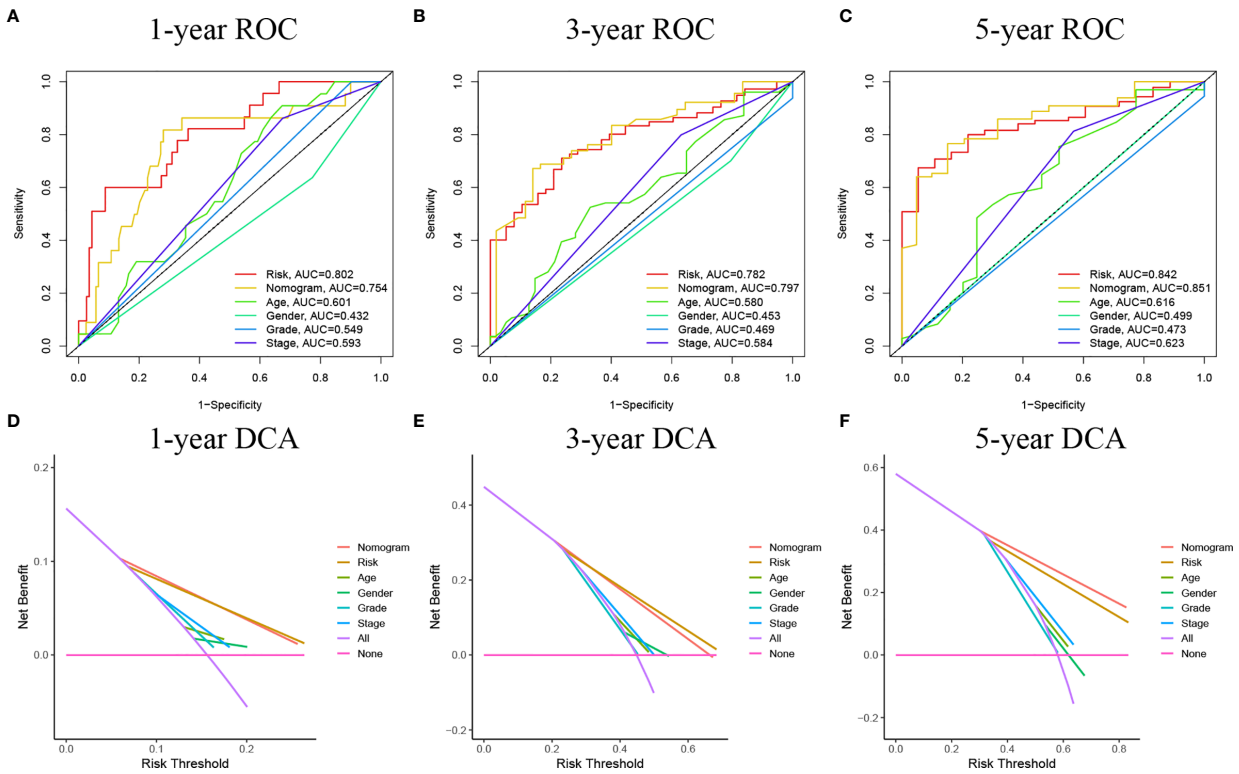

FIGURE 5 | **(A–C)** ROC curves of the nomograms compared with other clinical variables. **(D–F)** Decision curve analysis (DCA) curves can evaluate the clinical benefit of the nomograms and their potential scope of application. None indicates that all samples are negative and none are treated, therefore the net benefit is zero. All indicates that all samples are positive and all are treated. The x-axis represents the threshold probability.

research has shown that *CEMIP* mainly affects the WNT and EGFR signaling pathways.

Multivariate Cox regression analysis revealed RS (HR =1.045, 95% CI: 1.019-1.071) as an independent risk factor, which was validated in both the internal and external sets. We then defined HRG and LRG in the TCGA cohort based on the median RS value. For example, we found that RS was positively correlated with EMT-related genes. In general, a greater degree of immune infiltration could explain a more immune defense in LRG, and thus a more favorable prognosis. Conversely, positively correlated EMT genes may lead to a higher propensity for metastasis and a poorer outcome for BLCA patients in HRG. In addition, RS differs between clinical subgroups of BLCA patients, with a worse prognosis in the elderly, women, and patients with high TNM staging. Thus, our results suggest that RS can provide resilient risk stratification for BLCA patients.

Nomograms are a well-recognized statistical method for visualizing and predicting the probability of survival of patients (34–36). We innovatively constructed an advanced nomogram for the prognosis of BLCA patients according to TME-RS. The ROC and DCA proved that they can exactly assess the outcome of patients. When we compared our nomogram with three other predictive genes signatures by Wang et al. (27), Zhou et al. (25), and Li et al. (26). Our nomogram showed the highest C-index. These findings suggest that the clinical utility of our constructed nomogram is outperformed by other models. Next, our team will transfer this RS model to other urological tumors such as renal clear cell carcinoma to demonstrate the potential pan-cancer usability of the model.

Of course, there were still some deficiencies in our research. First of all, all our data come from the TCGA database and GEO database, and the sample size was not large enough, which may lead to the bias of the results. Secondly, our conclusions were also lack experimental verification. Therefore, it was necessary to conduct multicenter, large sample, prospective double-blind trials for further verification in the future.

CONCLUSIONS

In conclusion, our eight TME-associated gene signatures combined with clinical features may more accurately predict

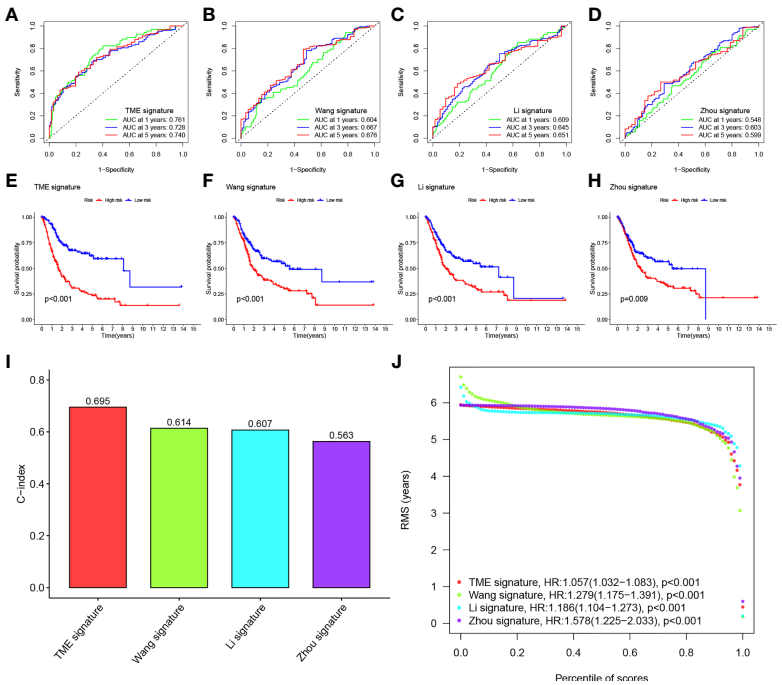

FIGURE 6 | **(A–D)** ROC of three other published gene signatures. **(E–H)** KM curves of three other published gene signatures. **(I)** Concordance index (C-index) of the four prognostic risk models including our model, which has the highest C-index. **(J)** Restricted mean survival (RMS) time curve of all five prognostic risk models, revealing an overlap of 60 months.

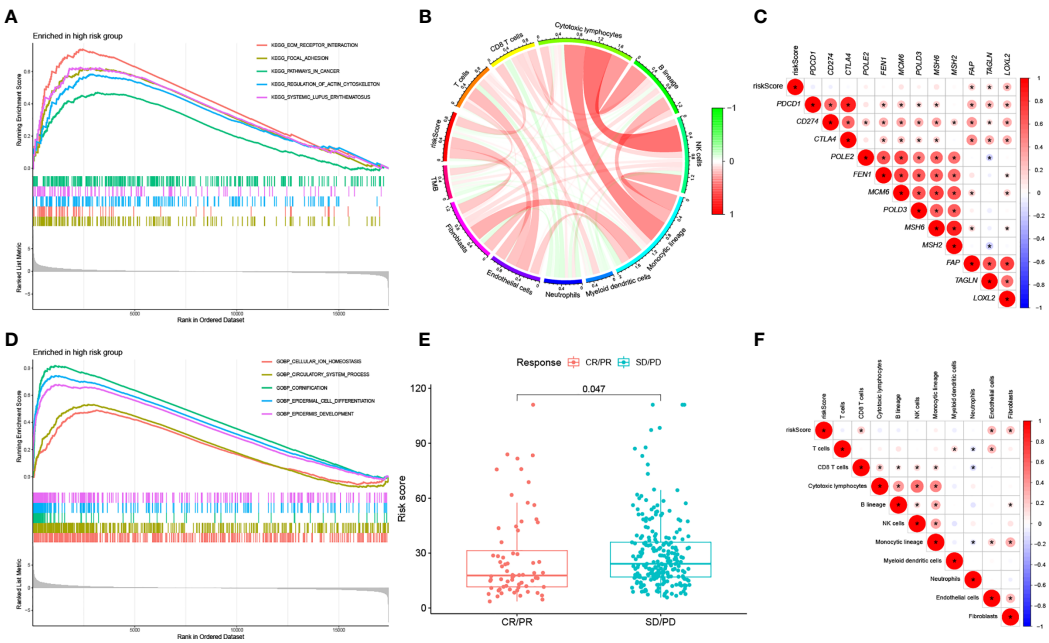

FIGURE 7 | **(A)** KEGG analysis of our signature in the HRG. **(B)** Correlation between RS, immune cell score and TMB. **(C)** Correlation between RS of BLCA samples and expression of representative genes for generic pathway targets in oncology. **(D)** GO analysis of our signature in the HRG. **(E)** RS according to the effectiveness of immunotherapy expressed as complete response (CR), partial response (PR), stable disease (SD), or progressive disease (PD). **(F)** Correlation between RS of BLCA samples and immune scores.

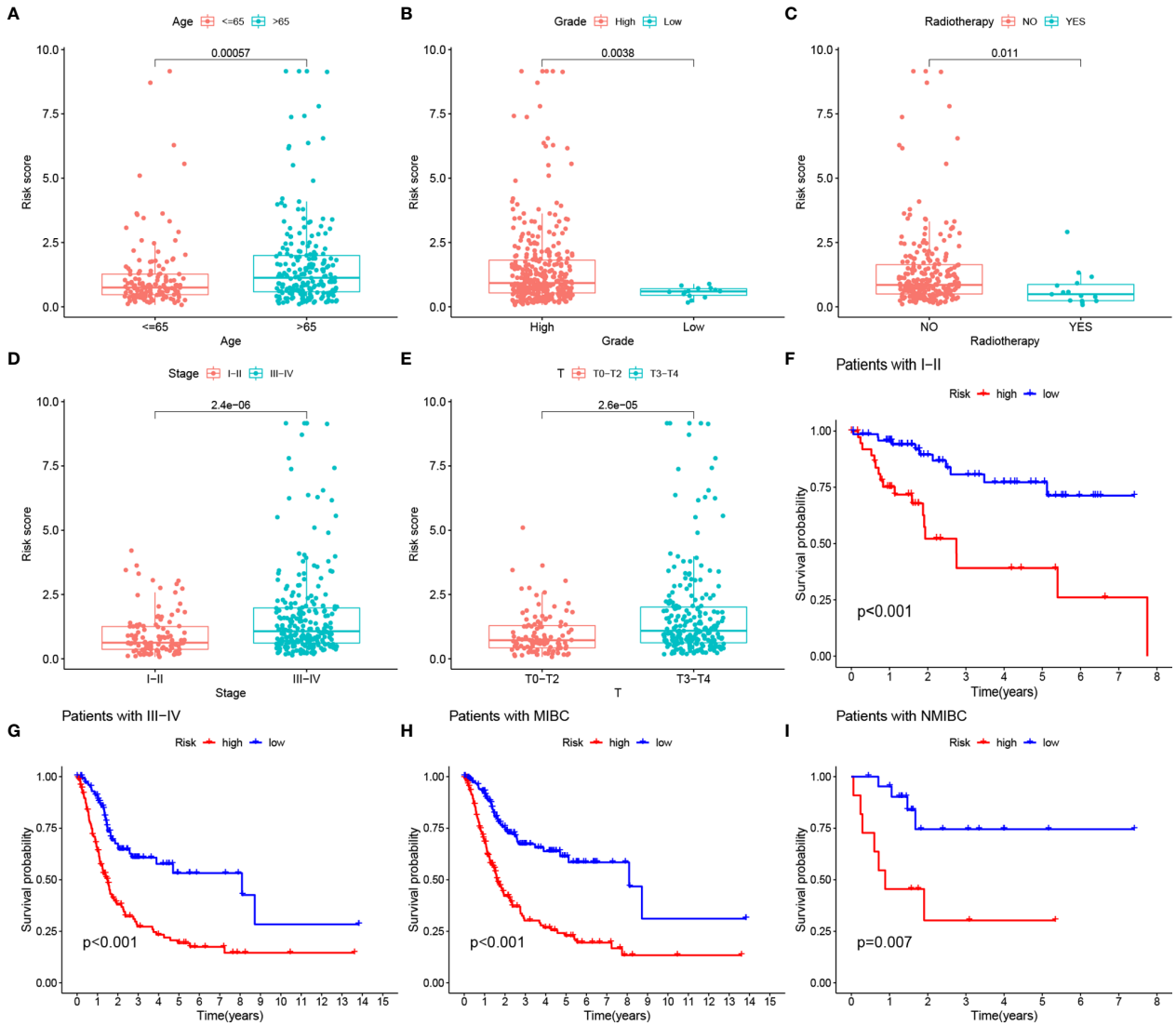

FIGURE 8 | **(A–E)** RS comparison of clinical information of BLCA samples. **(F, G)** Evaluation of the eight-gene risk model in different stage groups with OS KM curves comparing HRG and LRG. **(H, I)** Evaluation of the eight-gene risk model in different degree of tumor infiltration groups with OS KM curves comparing HRG and LRG.

patient survival at 1, 3, and 5 years. Both external and internal validation were able to have the ability to verify the forecasting capability of the model. RS can be promising to predict the response to immunotherapy of BLCA individuals with PD-L1 blocking therapy.

DATA AVAILABILITY STATEMENT

The datasets presented in this study can be found in online repositories. The names of the repository/repositories and accession number(s) can be found in the article/ **Supplementary Material**.

AUTHOR CONTRIBUTIONS

CX, ZK, and DP designed this work. YL analyzed the data. CX and DP wrote this manuscript. ZK edited and revised the manuscript. JG, NL and YY did a lot of work in revising the paper, including re-screening the data, analyzing the data, plotting the figures and the layout of the figures. YY embellished the language of the paper. All authors approved this manuscript.

FUNDING

This study was funded by the Health Care Commission of Henan Province (201403125, LHGJ20190422) and the Department of Education of Henan Province (21A320037).

SUPPLEMENTARY MATERIAL

The Supplementary Material for this article can be found online at: https://www.frontiersin.org/articles/10.3389/fonc.2022.818860/full#supplementary-material

REFERENCES

1. Zhang M, Zhang X, Yu M, Zhang W, Zhang D, Zeng S, et al. A Novel Ferroptosis-Related Gene Model for Overall Survival Predictions of Bladder Urothelial Carcinoma Patients. *Front Oncol* (2021) 11:698856. doi: 10.3389/fonc.2021.698856
2. Bray F, Ferlay J, Soerjomataram I, Siegel R, Torre L, Jemal A. Global Cancer Statistics 2018: GLOBOCAN Estimates of Incidence and Mortality Worldwide for 36 Cancers in 185 Countries. *CA: Cancer J Clin* (2018) 68:394–424. doi: 10.3322/caac.21492
3. Witjes J, Bruins H, Cathomas R, Compérat E, Cowan N, Gakis G, et al. European Association of Urology Guidelines on Muscle-Invasive and Metastatic Bladder Cancer: Summary of the 2020 Guidelines. *Eur Urol* (2021) 79:82–104. doi: 10.1016/j.eururo.2020.03.055
4. van den Bosch S, Alfred Witjes J. Long-Term Cancer-Specific Survival in Patients With High-Risk, Non-Muscle-Invasive Bladder Cancer and Tumour Progression: A Systematic Review. *Eur Urol* (2011) 60:493–500. doi: 10.1016/j.eururo.2011.05.045
5. Magers M, Lopez-Beltran A, Montironi R, Williamson S, Kaimakliotis H, Cheng LJH. Staging of Bladder Cancer. *Histopathology* (2019) 74:112–34. doi: 10.1111/his.13734
6. Barton M. High Morbidity and Mortality Found for High-Risk, Non-Muscle-Invasive Bladder Cancer. *CA: Cancer J Clin* (2013) 63:371–2. doi: 10.3322/caac.21201
7. Chedgy E, Black P. Radical Cystectomy and the Multidisciplinary Management of Muscle-Invasive Bladder Cancer. *JAMA Oncol* (2016) 2:855–6. doi: 10.1001/jamaoncol.2016.0149
8. Jain P, Kathuria H, Momin M. Clinical Therapies and Nano Drug Delivery Systems for Urinary Bladder Cancer. *Biomed Pharmacother* (2021) 226:107871. doi: 10.1016/j.pharmthera.2021.107871
9. Liang Y, Ye F, Xu C, Zou L, Hu Y, Hu J, et al. A Novel Survival Model Based on a Ferroptosis-Related Gene Signature for Predicting Overall Survival in Bladder Cancer. *Front Oncol* (2021) 21:943. doi: 10.1186/s12885-021-08687-7
10. Cao R, Ma B, Wang G, Xiong Y, Tian Y, Yuan L, et al. Identification of Autophagy-Related Genes Signature Predicts Chemotherapeutic and Immunotherapeutic Efficiency in Bladder Cancer (BLCA). *J Cell Mol Med* (2021) 25:5417–33. doi: 10.1111/jcmm.16552
11. Chen F, Wang Q, Zhou Y. The Construction and Validation of an RNA Binding Protein-Related Prognostic Model for Bladder Cancer. *BMC Cancer* (2021) 21:244. doi: 10.1186/s12885-021-07930-5
12. Ren F, Zhao Q, Zhao M, Zhu S, Liu B, Bukhari I, et al. Immune Infiltration Profiling in Gastric Cancer and Their Clinical Implications. *Cancer Sci* (2021) 112(9):3569–84. doi: 10.1111/cas.15057
13. Hui L, Chen Y. Tumor Microenvironment: Sanctuary of the Devil. *Cancer Lett* (2015) 368:7–13. doi: 10.1016/j.canlet.2015.07.039
14. Whiteside TJO. The Tumor Microenvironment and Its Role in Promoting Tumor Growth. *Oncogene* (2008) 27:5904–12. doi: 10.1038/onc.2008.271
15. Mariathasan S, Turley S, Nickles D, Castiglioni A, Yuen K, Wang Y, et al. Tgfβ Attenuates Tumour Response to PD-L1 Blockade by Contributing to Exclusion of T Cells. *Nature* (2018) 554:544–8. doi: 10.1038/nature25501
16. Wang Y, Chen L, Yu M, Fang Y, Qian K, Wang G, et al. Immune-Related Signature Predicts the Prognosis and Immunotherapy Benefit in Bladder Cancer. *Cancer Med* (2020) 9:7729–41. doi: 10.1002/cam4.3400
17. Aran D, Hu Z, Butte AJ. Xcell: Digitally Portraying the Tissue Cellular Heterogeneity Landscape. *Genome Biol* (2017) 18:220. doi: 10.1186/s13059-017-1349-1
18. Becht E, Giraldo NA, Lacroix L, Buttard B, Elarouci N, Petitprez F, et al. Estimating the Population Abundance of Tissue-Infiltrating Immune and Stromal Cell Populations Using Gene Expression. *Genome Biol* (2016) 17:218. doi: 10.1186/s13059-016-1070-5
19. Chifman J, Pullikuth A, Chou JW, Bedognetti D, Miller LD. Conservation of Immune Gene Signatures in Solid Tumors and Prognostic Implications. *BMC Cancer* (2016) 16:911. doi: 10.1186/s12885-016-2948-z
20. Li B, Severson E, Pignon J-C, Zhao H, Li T, Novak J, et al. Comprehensive Analyses of Tumor Immunity: Implications for Cancer Immunotherapy. *Genome Biol* (2016) 17:174. doi: 10.1186/s13059-016-1028-7
21. Newman AM, Liu CL, Green MR, Gentles AJ, Feng W, Xu Y, et al. Robust Enumeration of Cell Subsets From Tissue Expression Profiles. *Nat Methods* (2015) 12:453–7. doi: 10.1038/nmeth.3337
22. Rooney M, Shukla S, Wu C, Getz G, Hacohen NJC. Molecular and Genetic Properties of Tumors Associated With Local Immune Cytolytic Activity. *Cell* (2015) 160:48–61. doi: 10.1016/j.cell.2014.12.033
23. Tirosh I, Izar B, Prakadan SM, Wadsworth MH, Treacy D, Trombetta JJ, et al. Dissecting the Multicellular Ecosystem of Metastatic Melanoma by Single-Cell RNA-Seq. *Science* (2016) 352:189–96. doi: 10.1126/science.aad0501
24. Gaujoux R, Seoighe C. A Flexible R Package for Nonnegative Matrix Factorization. *BMC Bioinf* (2010) 11:367. doi: 10.1186/1471-2105-11-367
25. Li F, Teng H, Liu M, Liu B, Zhang D, Xu Z, et al. Prognostic Value of Immune-Related Genes in the Tumor Microenvironment of Bladder Cancer. *Front Oncol* (2020) 10:1302. doi: 10.3389/fonc.2020.01302
26. Li X, Feng J, Sun Y, Li X. An Exploration of the Tumor Microenvironment Identified a Novel Five-Gene Model for Predicting Outcomes in Bladder Cancer. *Front Oncol* (2021) 11:642527. doi: 10.3389/fonc.2021.642527
27. Wang Z, Tu L, Chen M, Tong S. Identification of a Tumor Microenvironment-Related Seven-Gene Signature for Predicting Prognosis in Bladder Cancer. *BMC Cancer* (2021) 21:692. doi: 10.1186/s12885-021-08447-7
28. Hanahan D, Coussens L. Accessories to the Crime: Functions of Cells Recruited to the Tumor Microenvironment. *Cancer Cell* (2012) 21:309–22. doi: 10.1016/j.ccr.2012.02.022
29. Hanahan D, Weinberg RJC. Hallmarks of Cancer: The Next Generation. *Cell* (2011) 144:646–74. doi: 10.1016/j.cell.2011.02.013
30. Schulz M, Salamero-Boix A, Niesel K, Alekseeva T, Sevenich L. Microenvironmental Regulation of Tumor Progression and Therapeutic Response in Brain Metastasis. *Front Immunol* (2019) 10:1713. doi: 10.3389/fimmu.2019.01713
31. Nazari A, Ahmadi Z, Hassanshahi G, Abbasifard M, Taghipour Z, Falahati-Pour SK, et al. Effective Treatments for Bladder Cancer Affecting CXCL9/CXCL10/CXCL11/CXCR3 Axis: A Review. *Oman Med J* (2020) 35:e103. doi: 10.5001/omj.2020.21
32. Hong Q, Li R, Zhang Y, Gu KJCm. biology. Fibrillin 2 Gene Knockdown Inhibits Invasion and Migration of Lung Cancer Cells. *Cell Mol Biol* (2020) 66:190–6. doi: 10.14715/cmb/2020.66.7.29
33. Chen Y, Zhou H, Jiang W, Wang J, Tian Y, Jiang Y, et al. The Role of CEMIP in Tumors: An Update Based on Cellular and Molecular Insights. *Biomed Pharmacother* (2021) 146:112504. doi: 10.1016/j.biopha.2021.112504
34. Fakhry C, Zhang Q, Nguyen-Tân P, Rosenthal D, Weber R, Lambert L, et al. Development and Validation of Nomograms Predictive of Overall and Progression-Free Survival in Patients With Oropharyngeal Cancer. *J Clin Oncol* (2017) 35:4057–65. doi: 10.1200/JCO.2016.72.0748
35. Previs R, Bevis K, Huh W, Tillmanns T, Perry L, Moore K, et al. A Prognostic Nomogram to Predict Overall Survival in Women With Recurrent Ovarian Cancer Treated With Bevacizumab and Chemotherapy. *Gynecol Oncol* (2014) 132:531–6. doi: 10.1016/j.ygyno.2014.01.036
36. Wang S, Fuller C, Kim J, Sittig D, Thomas C, Ravdin P. Prediction Model for Estimating the Survival Benefit of Adjuvant Radiotherapy for Gallbladder Cancer. *J Clin Oncol* (2008) 26:2112–7. doi: 10.1200/JCO.2007.14.7934

Conflict of Interest: The authors declare that the research was conducted in the absence of any commercial or financial relationships that could be construed as a potential conflict of interest.

this article, or claim that may be made by its manufacturer, is not guaranteed or endorsed by the publisher.

frontiers in Oncology

ORIGINAL RESEARCH
published: 16 March 2022
doi: 10.3389/fonc.2022.834249

High Stromal SFRP2 Expression in Urothelial Carcinoma Confers an Unfavorable Prognosis

Hong-Yue Lai[1,2], Chia-Chun Chiu[3], Yu-Hsuan Kuo[4], Hsin-Hwa Tsai[1,2], Li-Ching Wu[1], Wen-Hsin Tseng[5], Chien-Liang Liu[5,6], Chung-Hsi Hsing[2,7,8], Steven K. Huang[5,9] and Chien-Feng Li[1,2,10,11,12,13]**

[1] Center for Precision Medicine, Chi Mei Medical Center, Tainan, Taiwan, [2] Department of Medical Research, Chi Mei Medical Center, Tainan, Taiwan, [3] Genetics Generation Advancement Corp., Taipei, Taiwan, [4] Division of Hematology and Oncology, Department of Internal Medicine, Chi Mei Medical Center, Tainan, Taiwan, [5] Division of Urology, Department of Surgery, Chi Mei Medical Center, Tainan, Taiwan, [6] Division of Uro-Oncology, Department of Surgery, Chi Mei Medical Center, Tainan, Taiwan, [7] Department of Anesthesiology, Chi Mei Medical Center, Tainan, Taiwan, [8] Department of Anesthesiology, College of Medicine, Taipei Medical University, Taipei, Taiwan, [9] Department of Medical Science Industries, College of Health Sciences, Chang Jung Christian University, Tainan, Taiwan, [10] Department of Clinical Pathology, Chi Mei Medical Center, Tainan, Taiwan, [11] National Institute of Cancer Research, National Health Research Institutes, Tainan, Taiwan, [12] Institute of Precision Medicine, National Sun Yat-Sen University, Kaohsiung, Taiwan, [13] Department of Pathology, School of Medicine, College of Medicine, Kaohsiung Medical University, Kaohsiung, Taiwan

OPEN ACCESS

Edited by:
Francesca Sanguedolce, University of Foggia, Italy

Reviewed by:
Jian Lu, Peking University Third Hospital, China
Maolake Aerken, University at Buffalo, United States

***Correspondence:**
Chien-Feng Li
angelo.p@yahoo.com.tw
Steven K. Huang
7224837@gmail.com

Specialty section:
This article was submitted to Genitourinary Oncology, a section of the journal Frontiers in Oncology

Received: *13 December 2021*
Accepted: *22 February 2022*
Published: *16 March 2022*

Citation:
Lai H-Y, Chiu C-C, Kuo Y-H, Tsai H-H, Wu L-C, Tseng W-H, Liu C-L, Hsing C-H, Huang SK and Li C-F (2022) High Stromal SFRP2 Expression in Urothelial Carcinoma Confers an Unfavorable Prognosis. Front. Oncol. 12:834249. doi: 10.3389/fonc.2022.834249

Background: Urothelial carcinoma (UC) patients often bear clinical and genetic heterogeneity, which may differ in management and prognosis. Especially, patients with advanced/metastatic UC generally have a poor prognosis and survive for only few months. The Wnt/β-catenin signaling is found to be highly activated in several cancers, including UC. However, accumulated evidence has shown discordance between the Wnt/β-catenin signaling and UC carcinogenesis. Accordingly, we aim to get a better understanding of the molecular characterization of UC, focusing on the Wnt signaling, which may add value to guiding management more precisely.

Patients and Methods: Clinical data and pathological features were retrospectively surveyed. The correlations of secreted Frizzled-related protein 2 (SFRP2) immunoexpression with clinicopathological features were analyzed by Pearson's chi-square test. The Kaplan–Meier method with a log-rank test was employed to plot survival curves. All significant features from the univariate analysis were incorporated into the Cox regression model for multivariate analysis.

Results: Following data mining on a transcriptome dataset (GSE31684), we identified that 8 transcripts in relation to the Wnt signaling pathway (GO: 0016055) were significantly upregulated in advanced/metastatic bladder tumors. Among these transcripts, the *SFRP2* level showed the most significant upregulation. Additionally, as *SFRP2* is a putative Wnt inhibitor and may be expressed by stroma, we were interested in examining the immunoexpression and clinical relevance of stromal and tumoral SFRP2 in our urothelial carcinoma cohorts containing 295 urinary bladder UC (UBUC) and 340 upper urinary tract UC (UTUC) patients. We observed that high SFRP2 expression in stroma but not in tumors is significantly linked to aggressive UC features, including high

tumor stage and histological grade, positive nodal metastasis, the presence of vascular and perineural invasion, and high mitotic activity in UBUC and UTUC. Moreover, high stromal SFRP2 expression significantly and independently predicted worse clinical outcomes in UBUC and UTUC. Utilizing bioinformatic analysis, we further noticed that stromal SFRP2 may link epithelial–mesenchymal transition (EMT) to UC progression.

Conclusion: Collectively, these results imply that stromal SFRP2 may exert oncogenic function beyond its Wnt antagonistic ability, and stromal SFRP2 expression can provide prognostic and therapeutic implications for UC patients.

Keywords: urothelial carcinoma, bladder cancer, upper urinary tract cancer, *SFRP2*, collagen, stroma

INTRODUCTION

Urothelial carcinoma (UC) is a malignancy derived from the transitional epithelium of the urinary tract, which is also known as transitional cell carcinoma. Although UC is mainly found in the urinary bladder (UBUC), the incidence of upper urinary tract UC (UTUC), including the ureter and renal pelvis, is increasing in Taiwan (1). UC patients often bear clinical and genetic heterogeneity, which may differ in management and prognosis. For UBUC, 70–80% of patients are non-muscle-invasive bladder cancer (NMIBC) at initial diagnosis, and the standard treatment is transurethral resection of bladder tumor (TURBT) with subsequent intravesical instillation (2). However, 50–70% of patients experience local recurrence, and 10–15% of patients progress to muscle-invasive or metastatic disease (3). In contrast, 20–30% of UBUC patients are initially diagnosed with muscle-invasive bladder cancer (MIBC) or metastatic disease, and radical cystectomy is indicated as the standard therapy (4). Nevertheless, recurrence and metastasis still occur in 15–50% of patients following radical surgery (4). For UTUC, curative nephroureterectomy with bladder cuff excision is recommended for most patients (5). In addition, cisplatin-based postoperative adjuvant chemotherapy is given for advanced/metastatic UBUC or UTUC patients, but the clinical outcomes remain disappointing due to chemoresistance (6). Since UBUC and UTUC are featured by clinical heterogeneity, the addition of genetic information may improve management and prognosis.

The Wingless-related integration site (Wnt)/β-catenin signaling pathway is involved in diverse physiological processes, including embryonic development, cell proliferation and differentiation, and tissue homeostasis and regeneration (7). The canonical Wnt/β-catenin signaling is triggered by the binding of Wnt ligands to the low density lipoprotein receptor-related protein 5/6 (LRP5/6) receptors and Frizzled (FZD) receptors on the cell surface. Subsequently, β-catenin is undegraded and increased in the cytosol and translocates to the nucleus and binds to T-cell factor (TCF)/lymphoid enhancer-binding factor (LEF) transcription factors, resulting in the upregulation of Wnt target genes (8). In addition to prominently described in colorectal cancer, the Wnt/β-catenin signaling is found to be highly activated in several cancers, including UC (9). This leads to the development of various Wnt/β-catenin inhibitors such as targeting Wnt ligand/receptor interface for cancer therapies (8). However, accumulated investigations have shown incompatible evidence between the Wnt/β-catenin signaling and UC carcinogenesis (10, 11). Additionally, the aberrant Wnt/β-catenin signaling is not only restricted to cancer cells but also implicated in dynamic interactions with the tumor microenvironment (TME) and immune system in UC (12). These observations further emphasize the molecular heterogeneity of UC, and a deeper understanding of the molecular characterization of UC may come up with more hints for how such pathways be therapeutically targeted.

The secreted Frizzled-related protein 2 (*SFRP2*) gene, which is located on chromosome 4q31.3 in humans, encodes a glycoprotein containing an Frizzled-like cysteine-rich domain. As this N-terminal cysteine-rich domain shares substantial sequence similarity with Wnt binding domain of FZD receptors, SFRP2 was initially considered to antagonize the Wnt signaling by preventing binding of Wnt ligands to FZD receptors, which may inhibit tumor development (13). However, recent study has indicated that SFRP2 can promote tumor angiogenesis *via* the noncanonical Wnt/Ca^{2+} signaling (14). Moreover, upon secreted to the extracellular matrix (ECM), SFRP2 has been linked to the fibronectin-integrin complex, which can promote cell adhesion and block apoptosis in canine mammary gland tumors (15). Also, high level of SFRP2 in serum has been correlated with a poor prognosis in breast cancer patients (16). A similar correlation between high SFRP2 protein expression and poor prognosis was observed in osteosarcoma, which usually develops in the osteoblast cells from bone (17). In addition, SFRP2 is also known as stromal cell-derived factor 5 (SDF5), which was identified by a cDNA screen for secreted proteins in bone marrow stromal cells (18). Impressively, it has been reported that SFRP2 expression in tumors may be conferred by stroma (19). These reflect the complicated regulation of SFRP2 in tumors and their microenvironment, which is composed of stromal cells, immune cells, and the ECM. The TME characteristics have also been comprehensively described in UC (20). Since *SFRP2* is specifically expressed in the urinary bladder and the contribution of stromal cell–tumor cell communication to UC progression remained to be determined, we were interested in exploring the role of SFRP2 in UBUC and UTUC, thereby improving prognosis and therapy.

PATIENTS AND METHODS

Transcriptomic Data Analysis

A transcriptome dataset (GSE31684), incorporating 93 bladder cancer patients who were managed by radical cystectomy, from the GEO database (NCBI) was used for data mining. The raw data of all probe sets were analyzed without preselection or filtering. To quantify the expression levels of all transcripts, we imported the raw CEL files into the statistical software Nexus Expression 3 (BioDiscovery, El Segundo, CA, USA). According to tumor invasion and metastasis determined by clinical assessment, a comparative analysis (invasive vs. noninvasive and metastatic vs. nonmetastatic) was conducted under supervision. We underscored differentially expressed genes with special interest to the Wnt signaling pathway (GO: 0016055) and further selected those with a log2-transformed expression fold change > 0.2 and a *p*-value less than 0.01 for further analysis.

Patient Eligibility and Enrollment

This study was approved by the Institutional Review Board of Chi Mei Medical Center (10501005). We enrolled 340 UTUC and 295 UBUC patients who had curative surgery from 1996 to 2004, and all specimens with the informed consents were procured from our biobank. Clinical data, pathological features, and clinical outcomes were retrospectively obtained from the patients' medical records. Patients with preoperative neoadjuvant chemotherapy, other malignancies, or missing clinical data were not included. With curative purpose, 10 UTUC patients received ureterectomy and 330 UTUC patients underwent nephroureterectomy with bladder cuff excision. Cisplatin-based postoperative adjuvant chemotherapy was given for 29 out of 106 UTUC patients with pT3 or pT4 status or nodal involvement. On the other hand, for patients with superficial UBUC (pTa or pT1), TURBT with or without intravesical Bacillus Calmette–Guérin (BCG) was performed. For those with tumor recurrence, radical cystectomy was further performed. Patients with muscle-invasive UBUC were subjected to radical cystectomy with bilateral pelvic lymph node dissection. Similarly, cisplatin-based postoperative adjuvant chemotherapy was given for UBUC patients with pT3 or pT4 stage disease or nodal metastasis. The median/mean follow-up duration was 38.9/44.7 and 23.1/30.8 months for UTUC and UBUC, respectively.

Histopathological and Immunohistochemical Assessments

Tumor stages and histological grades were appraised on hematoxylin and eosin (H&E) staining of all cases according to the 7th edition of the American Joint Committee on Cancer (AJCC) staging system (21) and the World Health Organization (WHO) classification criteria (22), respectively. Tumor location and multifocality were used to evaluate clinical outcomes in UTUC but not in UBUC. Vascular invasion and perineural invasion were determined by the presence of tumor emboli in the vascular channels and tumor nests surrounding the nerve bundles, respectively. The mitotic rate was determined by calculating mitotic figures per 10 high-power fields (HPFs; 400x light microscopic magnification). We defined the mitotic rate less than 10/10 HPFs as low mitotic activity and the mitotic rate equal to or beyond 10/10 HPFs as high mitotic activity. Immunohistochemistry was performed based on our previous study (23), and slides were stained with an anti-SFRP2 antibody. Two independent pathologists (Chien-Feng Li and Wan-Shan Li) appraised SFRP2 immunoreactivity by integrating the percentage of stained tumor cells and intensity of staining of UC cells to produce the H-score as previously described (24). The H-score was determined with the following equation: H-score = $\Sigma Pi\ (i + 1)$, where i is the intensity of stained tumor cells (0 to 3+) and Pi is the percentage of staining for each intensity, ranging from 0% to 100%. According to the H-score, SFRP2 expression levels were divided into low (less than the median) and high (above or equal to the median) groups.

Functional Annotation of The Cancer Genome Atlas (TCGA) Data

Utilizing the cBioPortal web platform (http://cbioportal.org), the correlations of the mRNA level of *SFRP2* with its coexpressed transcripts in the UTUC and UBUC datasets from the TCGA database were downloaded. To further realize the functional roles of SFRP2 in UC, the top 194 overlapping transcripts co-upregulated with *SFRP2* between UTUC and UBUC were examined utilizing the Gene Ontology (GO) classification system (http://geneontology.org/) according to three functional groups (biological processes, molecular functions, or cellular components) and were ranked by fold enrichment. To plot representative GO terms, an R script with ggplot2 package was used.

Statistical Analysis

All statistical analyses were executed in SPSS software version 22.0 (IBM Corporation, Armonk, NY, USA), and two-tailed tests with a *p*-value less than 0.05 were considered statistically significant. We analyzed three endpoints: disease-specific survival (DSS), metastasis-free survival (MeFS), and local recurrence-free survival (LRFS). DSS was measured from curative surgery to the time of cancer death, and MeFS and LRFS were measured from curative surgery to the first metastasis and local recurrence, respectively. Pearson's chi-square test was used to appraise the correlations of clinicopathological variables with SFRP2 expression. The Kaplan–Meier method with a log-rank test was employed to plot survival curves. All significant characteristics from the univariate analysis were entered into the Cox regression model for multivariate analysis to find independent prognostic factors.

RESULTS

SFRP2 Is the Most Significantly Upregulated Gene Related to the Wnt Signaling During UC Invasion and Metastasis

To identify promising genes related to UC progression, a public dataset (GSE31684), incorporating 93 bladder cancer patients who were managed by radical cystectomy, was used for data mining. Among these patients, 78 were diagnosed as muscle-invasive disease (pT2–pT4), and 15 were determined as having

superficial disease (pTa or pT1). We identified 10 probes covering 8 transcripts zooming in the Wnt signaling pathway (GO: 0016055) (**Table 1** and **Figure 1**). Phylogenetically, SFRP1, SFRP2, and SFRP5 belong to the same subfamily, whose members share homology in their cysteine-rich domain (25). In this study, we found that both the *SFRP1* and *SFRP2* transcripts are significantly increased in tumors with muscle invasiveness and distal metastasis, but the *SFRP2* level showed the most prominent upregulation among all identified transcripts. Nevertheless, using the Gene Expression Profiling Interactive Analysis (GEPIA) database (http://gepia.cancer-pku.cn/detail.php?gene=SFRP1) (http://gepia.cancer-pku.cn/detail.php?gene=SFRP2), which incorporates the TCGA data, we noticed that both the *SFRP1* and *SFRP2* transcripts significantly decrease in bladder urothelial carcinoma (n = 404) compared to their paired normal tissue (n = 28). Intriguingly, the violin plots showed that both the mRNA levels of *SFRP1* and *SFRP2* significantly increase with the progression of bladder cancer (from stage II to stage IV) (**Supplementary Figure 1A** and **Figure 2A**). However, only bladder tumors with high mRNA level of *SFRP2* (n = 101) significantly conferred inferior overall survival compared with those with low *SFRP2* mRNA level (n = 100) (p = 0.00052) (**Supplementary Figure 1B** and **Figure 2B**).

In the bladder, stromal cells have been reported to be crucial for urothelial proliferation (26), and some MIBC patients are also featured by stroma-rich (smooth muscle cells and fibroblasts) subtype (27). However, little attention was paid to the crosstalk between stromal cells and tumors in UC. Using the Tumor Immune Estimation Resource (TIMER) database version 2.0 (28), which integrates the TCGA data, we observed that both

TABLE 1 | Summary of 8 significantly altered genes associated with the Wnt signaling pathway (GO: 0016055) and UC invasion and metastasis (GSE31684).

Probe	MIBC vs. NMIBC		Distal Meta.[&] vs. No Meta.		Gene Symbol	Gene Title	Biological Process
	Log2 ratio	*p*-value	Log2 ratio	*p*-value			
202035_s_at	0.3856	0.0023	0.398	<0.0001	*SFRP1*	secreted frizzled-related protein 1	Wnt receptor signaling pathway, anatomical structure morphogenesis, anti-apoptosis, cell differentiation, multicellular organismal development, signal transduction
202036_s_at	0.668	0.0019	0.6812	<0.0001	*SFRP1*	secreted frizzled-related protein 1	Wnt receptor signaling pathway, anatomical structure morphogenesis, anti-apoptosis, cell differentiation, multicellular organismal development, signal transduction
202037_s_at	0.7204	0.0005	0.7285	<0.0001	*SFRP1*	secreted frizzled-related protein 1	Wnt receptor signaling pathway, anatomical structure morphogenesis, anti-apoptosis, cell differentiation, multicellular organismal development, signal transduction
205648_at	0.6169	0.0014	0.4056	0.0061	*WNT2*	wingless-type MMTV integration site family member 2	Wnt receptor signaling pathway, Wnt receptor signaling pathway; calcium modulating pathway, multicellular organismal development
206796_at	0.5217	<0.0001	0.2914	0.0025	*WISP1*	WNT1 inducible signaling pathway protein 1	Wnt receptor signaling pathway, cell adhesion, cell-cell signaling, regulation of cell growth, signal transduction
214724_at	0.8864	<0.0001	0.4693	0.0005	*DIXDC1*	DIX domain containing 1	Wnt receptor signaling pathway, multicellular organismal development
219179_at	0.8579	<0.0001	0.3414	0.0061	*DACT1*	dapper; antagonist of beta-catenin; homolog 1 (Xenopus laevis)	Wnt receptor signaling pathway, multicellular organismal development
221016_s_at	0.4905	0.0005	0.4551	<0.0001	*TCF7L1*	transcription factor 7-like 1 (T-cell specific; HMG-box)	Wnt receptor signaling pathway, axial mesoderm morphogenesis, determination of anterior/posterior axis; embryo, establishment and/or maintenance of chromatin architecture, positive regulation of transcription from RNA polymerase II promoter; mitotic, regulation of Wnt receptor signaling pathway, regulation of transcription; DNA-dependent, transcription
221029_s_at	0.3783	0.0034	0.277	0.0056	*WNT5B*	wingless-type MMTV integration site family; member 5B	Wnt receptor signaling pathway, Wnt receptor signaling pathway; calcium modulating pathway, multicellular organismal development
223121_s_at	2.1375	<0.0001	1.0374	0.0019	*SFRP2*	secreted frizzled-related protein 2	Wnt receptor signaling pathway, anterior/posterior pattern formation, cell differentiation, multicellular organismal development, somitogenesis

[&]*Development of subsequent metastasis.*

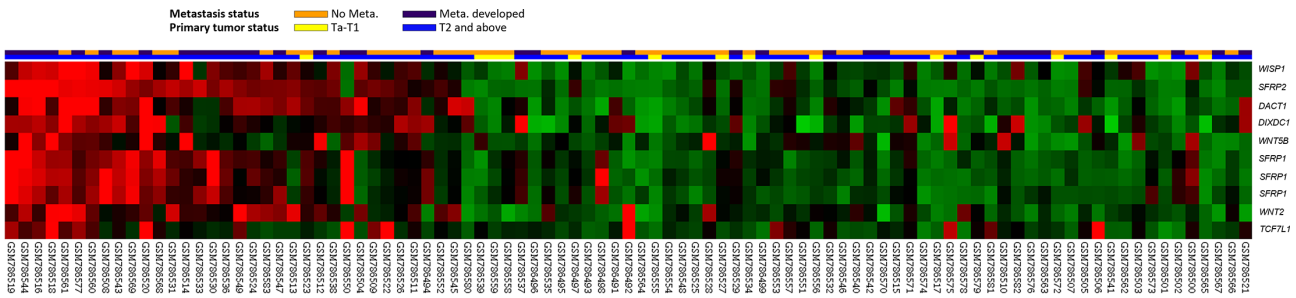

FIGURE 1 | Expression profiles of the top 8 genes correlated with the Wnt signaling pathway in advanced/metastatic bladder tumors. The expression levels of upregulated and downregulated genes are marked in red and green, respectively. A comparative analysis (invasive vs. noninvasive and metastatic vs. nonmetastatic) was conducted under supervision. We identified *SFRP2* as the most considerably upregulated gene related to the Wnt signaling pathway (GO: 0016055) among bladder cancer patients with advanced/metastatic disease.

the *SFRP1* and *SFRP2* transcripts are significantly negatively correlated with tumor purity (the percentage of cancer cells in a sample) and positively correlated with cancer-associated fibroblast (CAF) infiltration in bladder urothelial carcinoma, but the *SFRP2* gene showed a more distinguished correlation (**Supplementary Figure 2** and **Figure 2C**). These observations encouraged us to further survey the immunoexpression and clinical relevance of stromal and tumoral SFRP2 in our UTUC and UBUC cohorts.

Clinicopathological Characteristics of the UC Patients

We recruited 340 UTUC and 295 UBUC patients who had curative surgery from 1996 to 2004, and all samples were procured from our biobank (**Table 2**). In terms of UTUC, 62 (18.2%) patients showed multifocal tumors, and 49 (14.4%) patients had coexistent ureteral/renal pelvic tumors. There were 28 (8.2%) patients with lymph node metastasis, 159 (46.8%) patients with advanced stage disease, and 284 (83.5%) patients with high histological grade tumors. Perineural invasion was detected in 19 (5.6%) patients, and vascular invasion was found in 106 (31.2%) patients. Additionally, 167 (49.1%) samples were defined as high mitotic activity. In the context of UBUC, there were 29 (9.8%) patients with metastatic lymph nodes, 123 (41.7%) patients with muscle invasiveness, and 239 (81%) patients with high histological grade tumors. Vascular and perineural invasion were detected in 49 (16.6%) and 20 (6.8%) patients, respectively. Furthermore, 156 (52.9%) specimens were determined as having high mitotic activity.

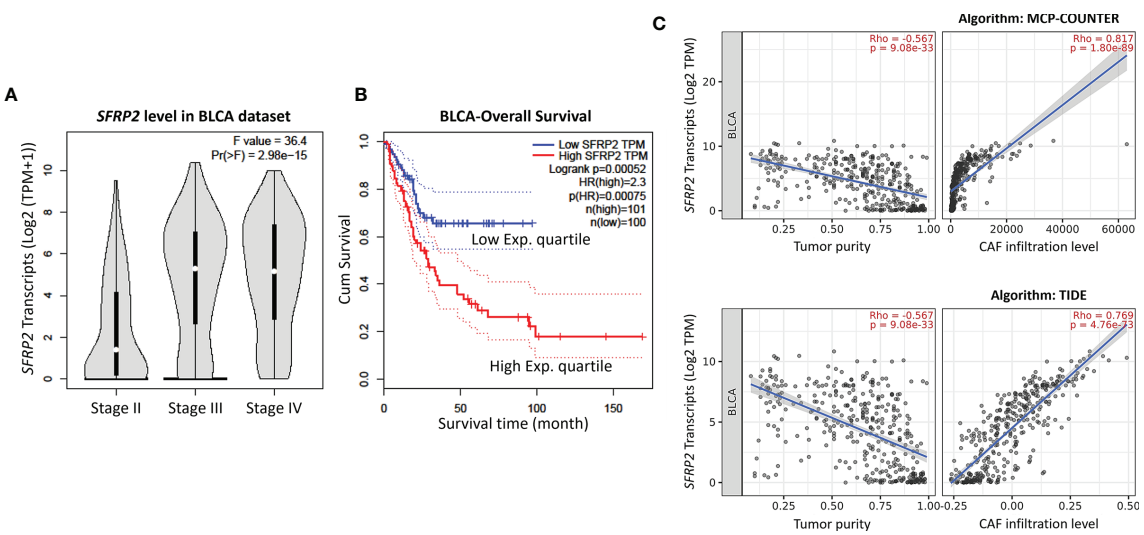

FIGURE 2 | High *SFRP2* mRNA level is correlated with advanced stage disease, inferior overall survival, and CAF infiltration. **(A)** The correlations between the mRNA levels of *SFRP2* and bladder cancer progression. **(B)** The impact of *SFRP2* mRNA levels on overall survival in bladder cancer. These data were acquired from the GEPIA database. **(C)** The correlations among the mRNA levels of *SFRP2*, tumor purity, and CAF infiltration in bladder cancer. These data were estimated using the MCP-COUNTER and TIDE algorithms from the TIMER2.0 database. BLCA, bladder urothelial carcinoma.

TABLE 2 | Correlations between stromal SFRP2 expression and other important clinicopathological parameters in urothelial carcinomas.

Parameter	Category	Upper Urinary Tract Urothelial Carcinoma				Urinary Bladder Urothelial Carcinoma			
		Case No.	Stromal SFRP2 Exp.		*p*-value	Case No.	Stromal SFRP2 Exp.		*p*-value
			Low	High			Low	High	
Gender	Male	158	76	82	0.514	216	103	113	0.223
	Female	182	94	88		79	44	35	
Age (years)	< 65	138	75	63	0.185	121	60	61	0.944
	≥ 65	202	95	107		174	87	87	
Tumor location	Renal pelvis	141	60	81	0.069	–	–	–	–
	Ureter	150	83	67		–	–	–	–
	Renal pelvis & ureter	49	27	22		–	–	–	–
Multifocality	Single	278	136	142	0.399	–	–	–	–
	Multifocal	62	34	28		–	–	–	–
Primary tumor (T)	Ta	89	64	25	**<0.001***	84	60	24	**<0.001***
	T1	92	55	37		88	39	49	
	T2-T4	159	51	108		123	48	75	
Nodal metastasis	Negative (N0)	312	165	147	**<0.001***	266	139	127	**0.012***
	Positive (N1-N2)	28	5	23		29	8	21	
Histological grade	Low grade	56	43	13	**<0.001***	56	39	17	**0.001***
	High grade	284	127	157		239	108	131	
Vascular invasion	Absent	234	144	90	**<0.001***	246	132	114	**0.003***
	Present	106	26	80		49	15	34	
Perineural invasion	Absent	321	165	156	**0.034***	275	143	132	**0.006***
	Present	19	5	14		20	4	16	
Mitotic rate (per 10 high power fields)	< 10	173	115	58	**<0.001***	139	89	50	**<0.001***
	>= 10	167	55	112		156	58	98	
Tumoral SFRP2 expression	High	170	115	55	**<0.001***	148	104	44	**<0.001***
	Low	170	55	115		147	43	104	

**Statistically significant.*

The bold values were considered statistically significant.

Correlations Among Stromal and Tumoral SFRP2 Immunoexpression and Clinicopathological Parameters

Immunohistochemical staining revealed that SFRP2 immunoreactivity in stroma was progressively increased from early stage to advanced stage UC (**Figures 3A, B**). **Table 2** displays stromal SFRP2 immunoexpression and its clinical significance in UTUC and UBUC. In the UTUC group, high stromal SFRP2 expression was remarkably linked to high tumor stage and histological grade (both $p < 0.001$), positive nodal metastasis ($p < 0.001$), the presence of vascular and perineural invasion ($p < 0.001$ and $p = 0.034$), high mitotic activity ($p < 0.001$), and low tumoral SFRP2 expression ($p < 0.001$). Likewise, in the UBUC group, we observed notable correlations between high stromal SFRP2 expression and high tumor stage and histological grade ($p < 0.001$ and $p = 0.001$), positive nodal metastasis ($p = 0.012$), the presence of vascular and perineural invasion ($p = 0.003$ and $p = 0.006$), high mitotic activity ($p < 0.001$), and low tumoral SFRP2 expression ($p < 0.001$).

In contrast, **Table 3** exhibits tumoral SFRP2 immunoexpression and its clinical significance in UTUC and UBUC. Interestingly, in the UTUC group, low tumoral SFRP2 expression was remarkably linked to high histological grade ($p = 0.041$) and positive nodal metastasis ($p = 0.006$). In the UBUC group, we detected remarkable correlations between low tumoral SFRP2 expression and high tumor stage ($p = 0.004$), the presence of vascular invasion ($p = 0.039$), and high mitotic activity ($p = 0.002$). Accordingly, the disparate roles of SFRP2 seem to be dependent on cell type-specific contexts.

Survival Analysis and Prognostic Impact of SFRP2 Expression in Stroma and Tumors

There were 113 deaths owing to UC, including 61 patients with UTUC and 52 patients with UBUC, in our cohorts. Additionally, a total of 146 patients, including 70 with UTUC and 76 with UBUC, had following distal metastasis. To appraise the prognostic implications of SFRP2 expression in patient death and distal metastasis in UC, univariate and multivariate analyses were utilized. In respect of UTUC, high SFRP2 expression in stroma but not in tumors was unfavorably prognostic for both disease-specific survival (DSS) and metastasis-free survival (MeFS) (both $p < 0.0001$) in the univariate analysis (**Table 4** and **Figures 4A–D**). Also, multifocal tumors, high tumor stage and histological grade, positive nodal metastasis, and vascular and perineural invasion significantly conferred poor outcomes in both DSS and MeFS (all $p < 0.0215$). Following multivariate analysis, stroma with high SFRP2 expression and multifocality, positive nodal metastasis, and perineural invasion remained independently prognostic for poor DSS and MeFS (all $p < 0.035$). These results imply that high SFRP2 expression in stroma instead of tumors can act as an adverse prognostic indicator for UTUC patients.

In terms of UBUC, high SFRP2 expression in stroma was unfavorably prognostic for both DSS and MeFS (both $p < 0.0001$) following univariate analysis (**Table 5** and **Figures 4E, F**).

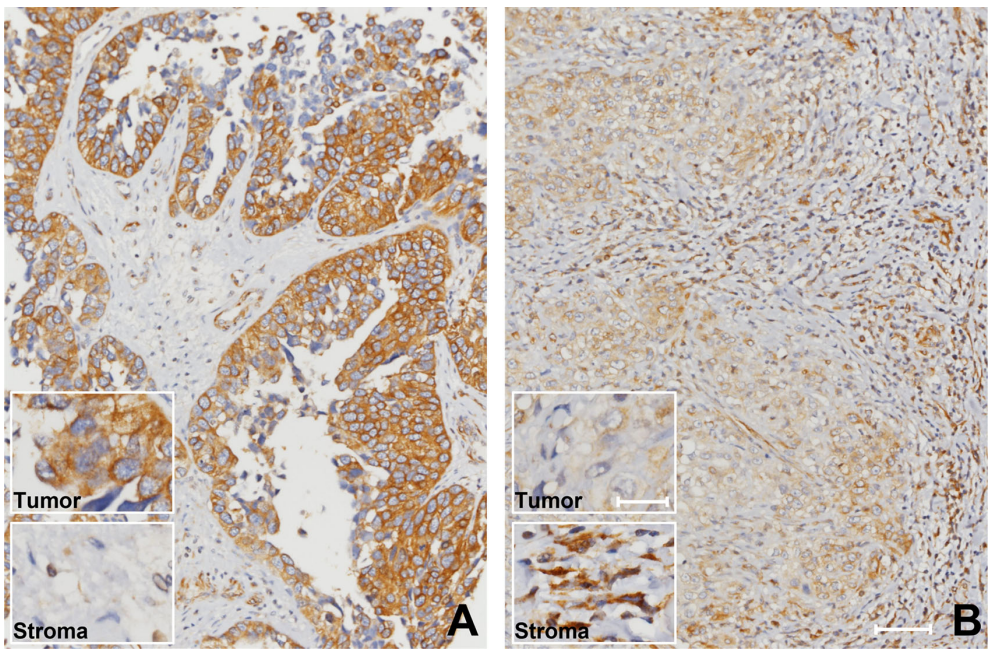

FIGURE 3 | High stromal SFRP2 immunoexpression was observed among bladder cancer patients with advanced stage disease. Immunohistochemistry was performed with an anti-SFRP2 antibody. SFRP2 immunoreactivity in stroma was gradually increased from **(A)** non-muscle-invasive to **(B)** muscle-invasive bladder cancer (200x, scale bar = 100 μm). Insect: 200x, scale bar = 25 μm.

TABLE 3 | Correlations between tumoral SFRP2 expression and other important clinicopathological parameters in urothelial carcinomas.

Parameter	Category	Upper Urinary Tract Urothelial Carcinoma				Urinary Bladder Urothelial Carcinoma			
		Case No.	Tumoral SFRP2 Exp.		*p*-value	Case No.	Tumoral SFRP2 Exp.		*p*-value
			Low	High			Low	High	
Gender	Male	158	74	84	0.277	216	112	104	0.251
	Female	182	96	86		79	35	44	
Age (years)	< 65	138	63	75	0.185	121	68	53	0.068
	≥ 65	202	107	95		174	79	95	
Tumor location	Renal pelvis	141	72	69	0.784	–	–	–	–
	Ureter	150	72	78		–	–	–	–
	Renal pelvis & ureter	49	26	23		–	–	–	–
Multifocality	Single	278	138	140	0.779	–	–	–	–
	Multifocal	62	32	30		–	–	–	–
Primary tumor (T)	Ta	89	37	52	0.083	84	31	53	**0.004***
	T1	92	44	48		88	42	46	
	T2-T4	159	89	70		123	74	49	
Nodal metastasis	Negative (N0)	312	149	163	**0.006***	266	130	136	0.319
	Positive (N1-N2)	28	21	7		29	17	12	
Histological grade	Low grade	56	21	35	**0.041***	56	23	33	0.145
	High grade	284	149	135		239	124	115	
Vascular invasion	Absent	234	113	121	0.349	246	116	130	**0.039***
	Present	106	57	49		49	31	18	
Perineural invasion	Absent	321	161	160	0.813	275	133	142	0.062
	Present	19	9	10		20	14	6	
Mitotic rate (per 10 high power fields)	< 10	173	81	92	0.233	139	56	83	**0.002***
	>= 10	167	89	78		156	91	65	
Stromal SFRP2 expression	Low	170	55	115	**<0.001***	147	43	104	**<0.001***
	High	170	115	55		148	104	44	

**Statistically significant.*
The bold values were considered statistically significant.

TABLE 4 | Univariate log-rank and multivariate analyses for disease-specific and metastasis-free survivals in upper urinary tract urothelial carcinoma.

Parameter	Category	Case No.	Disease-specific Survival					Metastasis-free Survival				
			Univariate analysis		Multivariate analysis			Univariate analysis		Multivariate analysis		
			No. of event	*p*-value	R.R.	95% C.I.	*p*-value	No. of event	*p*-value	R.R.	95% C.I.	*p*-value
Gender	Male	158	28	0.8286	–	–	–	32	0.7904	–	–	–
	Female	182	33		–	–	–	38		–	–	–
Age (years)	< 65	138	26	0.9943	–	–	–	30	0.8470	–	–	–
	≥ 65	202	35		–	–	–	40		–	–	–
Tumor side	Right	177	34	0.7366	–	–	–	38	0.3074	–	–	–
	Left	154	26		–	–	–	32		–	–	–
	Bilateral	9	1		–	–	–	0		–	–	–
Tumor location	Renal pelvis	141	24	**0.0079***	1	–	0.997	31	0.0659	–	–	–
	Ureter	150	22		0.888	0.480-1.645		25		–	–	–
	Renal pelvis & ureter	49	15		1.348	0.375-4.841		14		–	–	–
Multifocality	Single	273	48	**0.0026***	1	–	**0.011***	52	**0.0127***	1	–	**0.004***
	Multifocal	62	18		2.239	0.665-7.535		18		2.260	1.298-3.933	
Primary tumor (T)	Ta	89	2	**<0.0001***	1	–	0.051	4	**<0.0001***	1	–	0.110
	T1	92	9		3.667	0.786-17.104		15		3.295	1.078-10.075	
	T2-T4	159	50		4.768	1.062-21.399		51		2.497	0.790-7.892	
Nodal metastasis	Negative (N0)	312	42	**<0.0001***	1	–	**<0.001***	**55**	**<0.0001***	1	–	**0.002***
	Positive (N1-N2)	28	19		4.937	2.662-9.156		**15**		2.627	1.411-4.891	
Histological grade	Low grade	56	4	**0.0215***	1	–	**0.009***	3	**0.0027***	1	–	0.080
	High grade	284	57		3.661	1.343-9.9775		67		2.023	0.919-4.454	
Vascular invasion	Absent	234	24	**<0.0001***	1	–	0.362	26	**<0.0001***	1	–	**0.012***
	Present	106	37		1.315	0.710-2.435		44		2.192	1.191-4.035	
Perineural invasion	Absent	321	50	**<0.0001***	1	–	**<0.001***	61	**<0.0001***	1	–	**0.011***
	Present	19	11		4.109	1.949-8.665		9		2.647	1.245-5.630	
Mitotic rate (per 10 high power fields)	< 10	173	27	0.167	–	–		30	0.0823	–	–	
	>= 10	167	34		–	–		40		–	–	
Stromal SFRP2 expression	Low	170	12	**<0.0001***	1	–	**0.035***	13	**<0.0001***	1	–	**0.001***
	High	170	49		2.361	1.205-4.627		57		3.039	1.597-5.785	
Tumoral SFRP2 expression	Low	170	36	0.1065	–	–		38	0.3132	–	–	
	High	170	25		–	–		32		–	–	

**Statistically significant.*

The bold values were considered statistically significant.

In contrast, high SFRP2 expression in tumors was a favorable prognostic indicator and its prognostic effect was only on MeFS (p = 0.0053) (**Figures 4G, H**). In addition, high tumor stage and histological grade, positive nodal metastasis, vascular and perineural invasion, and high mitotic activity also significantly conferred worse outcomes in both DSS and MeFS (all $p < 0.0024$). In the multivariate analysis, stroma with high SFRP2 expression and high tumor stage were significantly prognostic for inferior DSS and MeFS (all $p < 0.001$). If NMIBC patients receiving TURBT develop local recurrence, radical cystectomy will be further performed, which may reduce quality of life. Accordingly, we also found that high stromal SFRP2 expression, low tumoral SFRP2 expression, and high tumor stage and histological grade were significantly correlated with poor local recurrence-free survival (LRFS) (all $p < 0.0414$) in the univariate analysis (**Table 6** and **Figures 4I, J**). Furthermore, only stroma with high SFRP2 expression remained independently prognostic for inferior LRFS (p = 0.012) following multivariate analysis. Taken together, these results suggest that the prognostic effects of stromal and tumoral SFRP2 expression are distinct, and incorporation of these variables can more accurately guide management for UBUC patients.

SFRP2 Function Prediction and Its Link to UC Progression

UTUC and UBUC are featured by etiological and clinical heterogeneity, while we identified SFRP2 linked to similar prognosis among UTUC and UBUC patients. To understand the functional roles of SFRP2 in UC, a gene coexpression network was

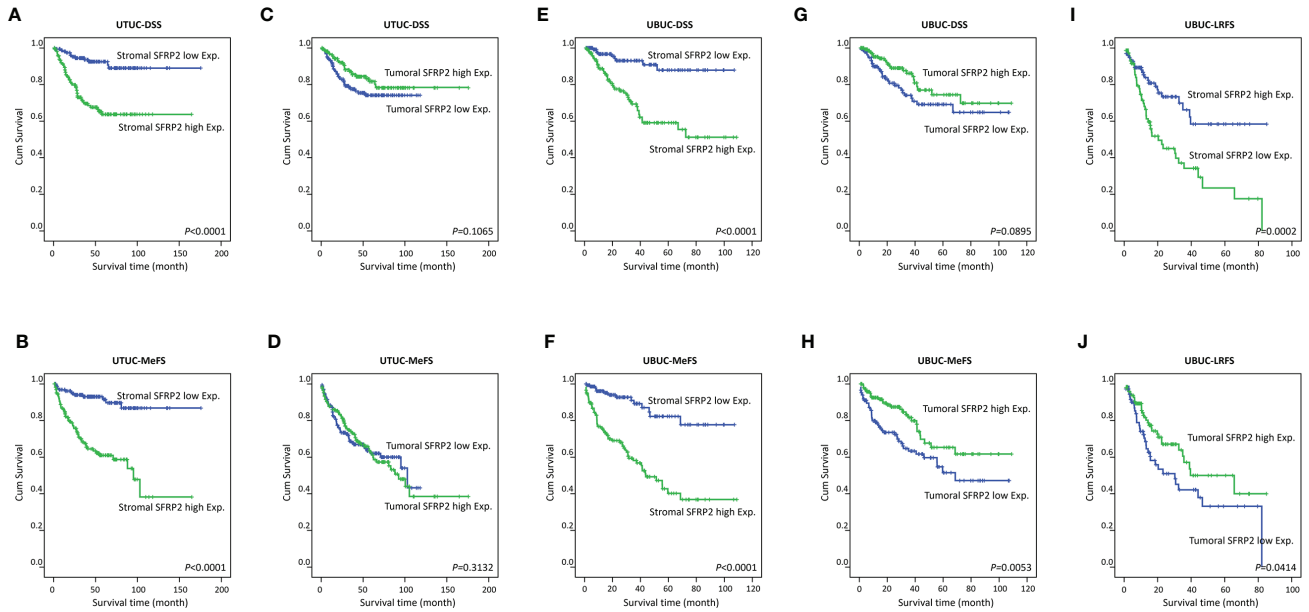

FIGURE 4 | Survival analysis. Kaplan–Meier curves show that high stromal SFRP2 immunoexpression conferred unfavorable prognostic effects on disease-specific survival and metastasis-free survival in **(A–D)** UTUC and **(E, F)** UBUC patients. Low tumoral SFRP2 expression was adversely prognostic only for metastasis-free survival in **(G, H)** UBUC patients. Also, high SFRP2 immunoexpression in stroma and low SFRP2 immunoexpression in tumors were significantly correlated with poor local recurrence-free survival in **(I, J)** UBUC patients.

examined. Employing the UTUC (n = 47) and UBUC (n = 411) datasets in the TCGA database, we appraised the top 194 overlapping transcripts (**Figure 5A**) that show positive correlations with *SFRP2* between UTUC (**Supplementary Table 1**) and UBUC (**Supplementary Table 2**). Subsequently, we utilized the GO classification system for functional annotation. With regard to molecular functions, we found that these overlapping genes are mainly implicated in the composition of the ECM (**Figure 5B**). In respect of cellular components, we observed that these overlapping genes are mostly involved in the collagen trimer assembly (**Figure 5C**). Moreover, the fibulin 2 (*FBLN2*) gene, one of the top 194 overlapping genes co-upregulated with *SFRP2* (**Supplementary Figure 3A**), has been identified as an unfavorable prognostic factor for UC in our previous study (29). Interestingly, the collagen family genes are also significantly positively correlated with *FBLN2* (29), further supporting the important role of collagen in UC development. As to biological processes, we detected that these overlapping genes are largely implicated in the immune cell regulation (**Figure 5D**). Furthermore, expressed by macrophages, the cathepsin K (*CTSK*) gene, one of the top 194 overlapping genes co-upregulated with *SFRP2* (**Supplementary Figure 3B**), has been suggested to be a promising therapeutic target for patients with high-risk MIBC (30). To connect key genes that were involved in the distinguished GO terms (fold enrichment > 50) of all three functional groups to each other, a weighted network was built using the GeneMANIA prediction server (31). The data showed that the top 2 predicted functions are mononuclear cell proliferation (false discovery rate: 1.85 x 10^{-7}) and lymphocyte proliferation (false discovery rate: 1.85 x 10^{-7}) (**Figure 6**). Additionally, annotated by the Molecular Signatures Database (MSigDB), several prominent pathways, including matrisome, epithelial–mesenchymal transition (EMT), and B lymphocyte, were identified. These observations further support the role of SFRP2 in the crosstalk among tumor cells, stromal cells, immune cells, and the ECM.

Furthermore, *SFRP4* was also identified as one of the overlapping genes considerably co-upregulated with *SFRP2* (**Supplementary Figure 3C**). It has been reported that *SFRP2* and *SFRP4* levels are tightly correlated with each other, which shares a common gene program across multiple cancers (19). Using the Human Protein Atlas database, in terms of single cell type specificity, we found that *SFRP2* is specifically expressed in the fibroblasts (https://www.proteinatlas.org/ENSG00000145423-SFRP2/celltype), but *SFRP4* is specifically expressed in the peritubular cells (https://www.proteinatlas.org/ENSG00000106483-SFRP4/celltype), suggesting that the contribution of tumor stroma to UC development is more likely to be mediated by SFRP2. We also identified fibroblast growth factor 7 (*FGF7*) and complement C1s (*C1S*) as the overlapping transcripts that are significantly positively correlated with *SFRP2* (**Supplementary Figures 3D, E**). In our previous investigations, high FGF7 (32) and C1S (33) expression have been correlated with worse clinical outcomes in UC patients. Altogether, although UTUC and UBUC are clinically managed as distinct entities, they share common genomic landscape with similar actionable drivers and prognostic factors to improve precision therapy.

DISCUSSION

Composed of five secreted glycoproteins (SFRP1–5), the SFRP family is approximately 300 amino acids in length, which fold

TABLE 5 | Univariate log-rank and multivariate analyses for disease-specific and metastasis-free survivals in urinary bladder urothelial carcinoma.

Parameter	Category	Case No.	Disease-specific Survival					Metastasis-free Survival				
			Univariate analysis		Multivariate analysis			Univariate analysis		Multivariate analysis		
			No. of event	*p*-value	R.R.	95% C.I.	*p*-value	No. of event	*p*-value	R.R.	95% C.I.	*p*-value
Gender	Male	216	41	0.4446	–	-	-	60	0.2720	–	–	–
	Female	79	11		–	-	-	16		–	–	–
Age (years)	< 65	121	17	0.1136	–	-	-	31	0.6875	–	–	–
	≥ 65	174	35		–	-	-	45		–	–	–
Primary tumor (T)	Ta	84	1	**<0.0001***	1	–	**<0.001***	4	**<0.0001***	1	–	**<0.001***
	T1	88	9		7.007	0.711-69.038		23		1.201	1.201-14.358	
	T2-T4	123	42		35.904	3.718-346.745		49		14.358	2.102-24.092	
Nodal metastasis	Negative (N0)	266	41	**0.0002***	1	–	0.743	61	**<0.0001***	1	–	0.177
	Positive (N1-N2)	29	11		1.124	0.559-2.260		15		1.521	0.827-2.796	
Histological grade	Low grade	56	2	**0.0013***	1	–	0.739	5	**0.0007***	1	–	1,000
	High grade	239	50		0.765	0.159-3.688		71		1.000	0.337-2.967	
Vascular invasion	Absent	246	37	**0.0024***	1	–	0.060	54	**0.0001***	1	–	0.543
	Present	49	15		0.513	0.26-1.029		22		0.832	0.459-1.507	
Perineural invasion	Absent	275	44	**0.0001***	1	–	0.173	66	**0.0007***	1	–	0.508
	Present	20	8		1.792	0.773-4.151		10		1.286	0.611-2.704	
Mitotic rate (per 10 high power fields)	< 10	139	12	**<0.0001***	1	–	0.066	23	**<0.0001***	1	–	0.106
	>= 10	156	40		1.888	0.959-3.719		53		1.539	0.912-2.598	
Stromal SFRP2 expression	Low	147	9	**<0.0001***	1	–	**0.001***	15	**<0.0001***	1	–	**<0.001***
	High	148	43		3.849	1.791-8.269		61		3.788	2.066-6.946	
Tumoral SFRP2 expression	Low	147	31	0.0895	–	–	-	48	**0.0053**	1	–	0.418
	High	148	21		–	–	-	28		0.819	0.505-1.328	

**Statistically significant.*

The bold values were considered statistically significant.

into two distinguishable domains: an N-terminal cysteine-rich domain and a C-terminal netrin domain (34). Because of their ability to antagonize the Wnt signaling and their frequent silencing by promoter methylation in many cancers, the SFRP proteins were initially described as tumor suppressors (35). Actually, one study found that the methylation level of *SFRP2* in gastric cancer is higher than that in adjacent normal tissue (36), whereas a recent report showed that the mRNA level of *SFRP2* is among the highest in advanced stages of gastric cancer and correlated with worse survival (37). Likewise, using the UALCAN platform (http://ualcan.path.uab.edu/cgi-bin/TCGA-methyl-Result.pl?genenam=SFRP1&ctype=BLCA) (http://ualcan.path.uab.edu/cgi-bin/TCGA-methyl-Result.pl?genenam=SFRP2&ctype=BLCA), we speculate that, compared to adjacent normal tissue, both the decreased *SFRP1* and *SFRP2* transcripts in bladder cancer may ascribe to their increased methylation levels, especially in patients with stage I disease. Interestingly, the violin plots showed that both the mRNA levels of *SFRP1* and *SFRP2* significantly increase with the progression of bladder cancer (from stage II to stage IV) (**Supplementary Figure 1A** and **Figure 2A**). These observed inconsistencies in the level of *SFRP2* might be owing to differences in the progressive stage. However, we observed that both the *SFRP1* and *SFRP2* mRNA levels are not inversely correlated with their methylation status using the TCGA bladder cancer database (n = 413) (**Supplementary Figures 4A, B**). This implies that alternative mechanisms may contribute to increased *SFRP1* and *SFRP2* transcripts in UC patients with advanced disease.

The dynamic interplays between tumors and their microenvironment comprising immune cells (macrophages and lymphocytes), stromal cells (fibroblasts), and the ECM, supporting or limiting tumor growth. To further dissect the molecular characterization of tumor–immune interactions, the TIMER2.0 database was used. The data revealed that high CAF infiltration was significantly correlated with poor cumulative survival in bladder urothelial carcinoma (**Supplementary Figures 5A, B**). Moreover, we observed that both the *SFRP1* and *SFRP2* transcripts are significantly negatively correlated with tumor purity and positively correlated with CAF infiltration in bladder urothelial carcinoma, but the *SFRP2* gene showed a more distinguished correlation (**Supplementary Figure 2** and **Figure 2C**). These observations suggest that stromal cells may at least in part result

TABLE 6 | Univariate log-rank and multivariate analyses for local recurrence-free survivals in NMIBC post TURBT.

Parameter	Category	Case No.	Local Recurrence-free Survival				
			Univariate analysis		Multivariate analysis		
			No. of event	*p*-value	R.R.	95% C.I.	*p*-value
Gender	Male	125	46	0.3370	–	-	-
	Female	47	19		–	-	-
Age (years)	< 65	70	30	0.3857	–	-	-
	≥ 65	102	35		–	-	-
Primary tumor (T)	Ta	84	27	**0.0193***	1	–	0.623
	T1	88	38		1.107	0.629-2.169	
Nodal metastasis	Negative (N0)	172	65	n.a.	–	–	–
	Positive (N1-N2)	0	0		–	–	–
Histological grade	Low grade	54	15	**0.0101***	1	–	0.165
	High grade	118	50		1.650	0.808-3.494	
Vascular invasion	Absent	171	65	0.6639	–	–	–
	Present	1	0		–	–	–
Perineural invasion	Absent	169	64	0.4725	–	–	–
	Present	3	1		–	–	–
Mitotic rate (per 10 high power fields)	< 10	94	35	0.1853	–	–	–
	>= 10	78	30		–	–	–
Stromal SFRP2 expression	Low	99	24	**0.0002***	1	–	**0.012***
	High	73	41		2.083	1.179-3.681	
Tumoral SFRP2 expression	Low	73	34	**0.0414***	1	–	0.558
	High	99	31		0.805	0.493-1.464	

**Statistically significant; n.a., not applicable.*
The bold values were considered statistically significant.

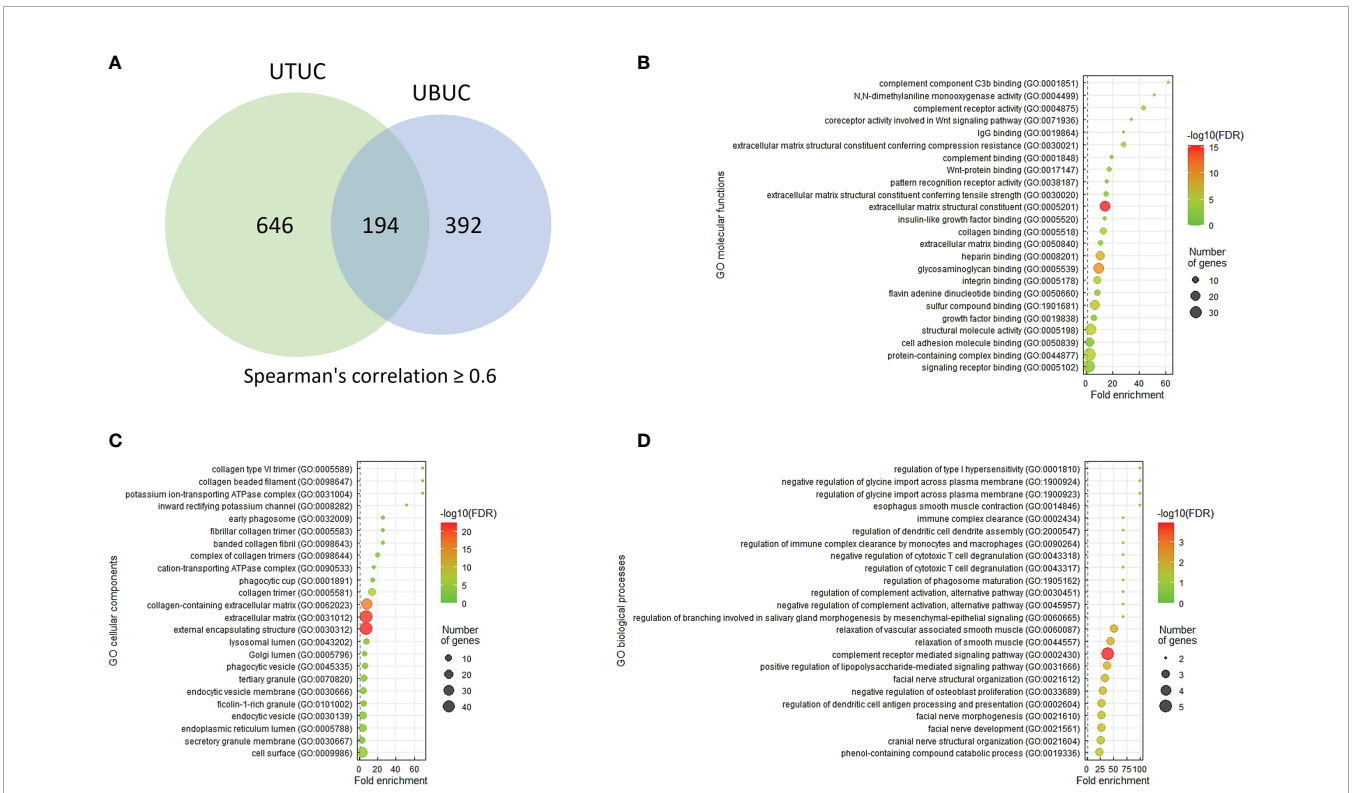

FIGURE 5 | The prominent GO terms enriched in *SFRP2* upregulation. **(A)** The top 194 overlapping genes (Spearman's correlation ≥ 0.6) co-upregulated with *SFRP2* between UTUC and UBUC were examined utilizing the GO classification system according to **(B)** molecular functions, **(C)** cellular components, or **(D)** biological processes and were ranked by fold enrichment for functional annotation. To plot representative GO terms, an R script with ggplot2 package was used.

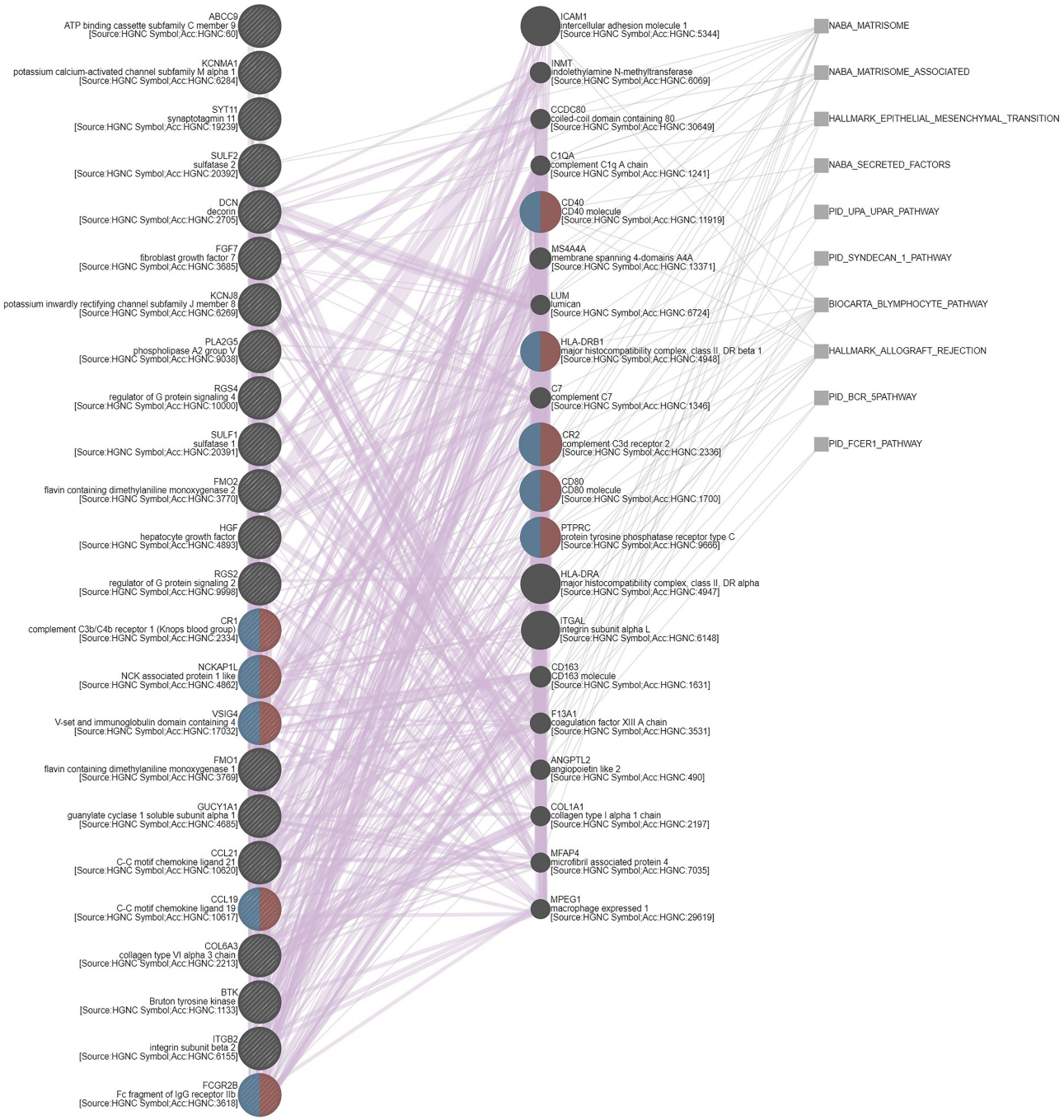

FIGURE 6 | Gene coexpression network. A weighted network that connects key genes to each other was built using the GeneMANIA prediction server. Red and blue semicircles represent genes that belong to mononuclear cell proliferation and lymphocyte proliferation, respectively. Purple and grey lines indicate coregulation and pathways, correspondingly.

in the increased *SFRP2* transcripts in urothelial carcinoma with advanced stage. We further validated that high stromal SFRP2 expression evaluated by immunohistochemistry is significantly linked to an aggressive clinical course and inferior survival in our urothelial carcinoma cohorts containing 340 UTUC and 295 UBUC patients, highlighting the promising prognostic utility of stromal SFRP2 expression.

Initially regarded as transcriptional noise, non-coding RNAs (ncRNAs) have attracted wide attention for their involvement in epigenetic regulation and multiple biological functions,

especially in cancer (38). Based on the length, ncRNAs can majorly be classified into microRNAs (miRNAs, about 22 nucleotides long) and long non-coding RNAs (lncRNAs, more than 200 nucleotides long) (39). miRNAs function by annealing to the three prime untranslated region (3′-UTR) of messenger RNA (mRNA) targets to negatively regulate gene expression. As competitive endogenous RNAs (ceRNAs) or miRNA sponges, lncRNAs with miRNA-complementary sites, which are also presented on mRNA targets, can compete with mRNA targets to bind to miRNAs, thereby reducing the availability of miRNAs. Accordingly, we aligned GSE31684 probe sequences with human lncRNA sequences from the LNCipedia database (https://lncipedia.org/) and created a lncRNA list. Utilizing the miRTarBase database (40), the regulatory networks among miRNAs, upstream regulators (lncRNA list), and downstream targets (gene list from **Table 1**) were analyzed, and the ZNF585B-6:1/miRNAs/SFRP2 network was identified (**Supplementary Figure 6**). Of these miRNAs, miR-218 has been reported to be downregulated in bladder cancer (41), which suggests that increased *SFRP2* transcripts may attribute to miR-218 downregulation in UC. Consequently, we do not rule out the possibility that ncRNAs may contribute to increased *SFRP2* transcripts in UC, and further analysis is needed.

A gene coexpression analysis was used to predict the functional roles of SFRP2 in UC, and we found that the collagen family genes, including collagen type I alpha 2 chain (*COL1A2*), *COL3A1*, *COL6A3*, *COL8A1*, *COL10A1*, and *COL14A1*, are significantly co-upregulated with *SFRP2* (**Supplementary Figures 7A–F**). These collagen genes, such as *COL1A2* and *COL6A3*, have been demonstrated to promote NMIBC progression to MIBC through EMT (42). We also found that EMT markers twist family basic helix-loop-helix (bHLH) transcription factor 1 (*TWIST1*) and zinc finger E-box binding homeobox 2 (*ZEB2*) are significantly co-upregulated with *SFRP2* (**Supplementary Figures 8A, B**). However, whether SFRP2 promotes UC progression through EMT regulated by the above-mentioned collagen genes needs further confirmation. On the other hand, although the use of immunotherapy has improved outcomes in the management of UC, only approximately 20% of patients benefit from it (43), which warrants a better understanding of the mechanisms underlying immunotherapy resistance. It has been reported that the transforming growth factor beta (TGFβ) signaling from fibroblasts and collagen enriched in peritumoral stroma promote cytotoxic T cell exclusion and confer immunotherapy resistance among patients with metastatic urothelial cancer (44). Additionally, we also observed that *TGFBI* and CAF marker fibroblast activation protein (*FAP*) are significantly co-upregulated with *SFRP2* (**Supplementary Figures 9A, B**). Accordingly, these observations suggest that SFRP2, a putative Wnt inhibitor, may function at the interactions between tumor cells and fibroblasts in UC development. Nevertheless, the Wnt/β-catenin signaling has also been suggested to drive cytotoxic T cell exclusion by modulating the crosstalk between tumor cells and tumor-associated macrophages (TAMs) and lead to immunotherapy resistance in UC treatment (12). These further highlight the complexity of the TME that creates a favorable niche to reduce treatment efficacy. Accordingly, SFRP2 may trigger immunotherapy resistance beyond its Wnt antagonistic ability, providing therapeutic implications for precisely selecting patients who can benefit from immunotherapy.

Increased deposition of fibrous collagen is the most common feature of ECM remodeling in the primary tumor (45). Despite the fact that the collagen family genes are significantly positively correlated with *SFRP2*, it is unclear how SFRP2 regulates collagen homeostasis. Using structure prediction analysis, it has been showed that the C-terminal netrin domains of SFRP proteins and procollagen C-endopeptidase enhancer 1 (PCPE1 or PCOLCE) share sequence similarity with the N-terminal netrin domains of tissue inhibitor of metalloproteinases (TIMPs) (46). PCPE1 is suggested to be highly specific to collagen synthesis and fibrosis, and its upregulation is observed at sites of high collagen deposition (47). Moreover, TIMPs are considered to inhibit matrix metalloproteinases (MMPs)-induced collagen degradation (48). However, whether SFRP2 can promote collagen synthesis and prevent collagen degradation through its C-terminal netrin domain requires further analysis. Otherwise, due to its sensitivity to inflammatory perturbations, variation of collagen stainability may be of little utility in respect of the prognosis of UC (49). Consequently, SFRP2, a supposed upstream regulator of collagen homeostasis, may act as a reliable prognostic factor for UC.

Metastatic UC is an aggressive disease and generally has a poor prognosis with a median overall survival of 12–14 months (4). Following lymph nodes (69%), bone (47%) has been reported to be the second most common site of metastatic bladder cancer (50). Bone metastasis may be correlated with pain, bone loss, and functional impairment. Accordingly, recent study has reported that UC patients with bone as the only metastatic site are less likely to receive systemic chemotherapy owing to their lower Eastern Cooperative Oncology Group (ECOG) performance status (51). The current European Association of Urology (EAU) guideline recommends anti-osteoporotic drugs (zoledronic acid or denosumab) for supportive treatment in case of bone metastasis, but patients should be aware of potential side effects, such as osteonecrosis of the jaw and hypocalcaemia (4). As a result, these patients deserve a valuable prognostic factor and a specific therapeutic target. Using gene coexpression analysis, we found that *CTSK* is significantly co-upregulated with *SFRP2* (**Supplementary Figure 3B**). Generally, CTSK, a lysosomal cysteine protease, is implicated in osteoclast-mediated bone degradation (52). Moreover, CTSK has also been described to be expressed by breast cancer (53) and prostate cancer (54) that metastasize to bone, where it functions in osteolysis that contributes to tumor invasiveness. Nevertheless, the correlations among the expression of SFRP2 and CTSK and metastatic bone disease in UC need further examination.

In this study, we identified that high stromal SFRP2 expression has a more significant impact on UC patient survival compared with that of low tumoral SFRP2 expression. This suggests that the distinct roles of SFRP2 seem to be dependent on cell type-specific contexts, and incorporation of these variables can more accurately

guide management for UC patients. The current study has some limitations. First, further experiments are needed to validate the role of fibroblast SFRP2 in UC development and immunotherapy resistance. Second, in this study, UC patients who had curative surgery were analyzed retrospectively at a single institution; accordingly, the value of stromal SFRP2 expression should be prospectively verified by multi-center studies.

CONCLUSION

Because of their Wnt antagonistic ability and their frequent epigenetic silencing in many cancers, the SFRP proteins were initially described as tumor suppressors. In the current study, we validated that high stromal SFRP2 expression is considerably correlated with an aggressive clinical course and serves as an independent prognostic factor for worse survival in our well-characterized UBUC and UTUC cohorts. Utilizing bioinformatic analysis, we further observed that stromal SFRP2 may link EMT to UC progression. Collectively, stromal SFRP2 may exert oncogenic function beyond its Wnt antagonistic ability, and stromal SFRP2 expression evaluation can add value to guiding management more precisely for UC patients.

DATA AVAILABILITY STATEMENT

The datasets presented in this study can be found in online repositories. The names of the repository/repositories and accession number(s) can be found in the article/**Supplementary Material**.

ETHICS STATEMENT

The studies involving human participants were reviewed and approved by Institutional Review Board of Chi Mei Medical Center (10501005). The patients/participants provided their written informed consent to participate in this study.

AUTHOR CONTRIBUTIONS

Conceptualization: H-YL and C-FL. Methodology: C-CC, Y-HK, H-HT, L-CW, W-HT, C-LL, and C-HH. Investigation: H-YL, C-CC, SH, and C-FL. Formal analysis: H-YL, C-CC, Y-HK, H-HT, and L-CW. Resources: W-HT, C-LL, and C-HH. Validation: Y-HK, H-HT, L-CW, W-HT, C-LL, and C-HH. Visualization: H-YL and C-CC. Writing - original draft: H-YL. Writing - review and editing: H-YL. Funding acquisition: SH and C-FL. Supervision: SH and C-FL. All authors contributed to the article and approved the submitted version.

SUPPLEMENTARY MATERIAL

The Supplementary Material for this article can be found online at: https://www.frontiersin.org/articles/10.3389/fonc.2022.834249/full#supplementary-material

Supplementary Figure 1 | High *SFRP1* mRNA level is correlated with advanced stage disease but not with inferior overall survival. **(A)** The correlations between the mRNA levels of *SFRP1* and bladder cancer progression. **(B)** The impact of *SFRP1* mRNA levels on overall survival in bladder cancer. These data were acquired from the GEPIA database. BLCA: bladder urothelial carcinoma.

Supplementary Figure 2 | *SFRP1* transcripts are moderately negatively correlated with tumor purity and positively correlated with CAF infiltration. The correlations among the mRNA levels of *SFRP1*, tumor purity, and CAF infiltration in bladder cancer. These data were estimated using the MCP-COUNTER and TIDE algorithms from the TIMER2.0 database. BLCA, bladder urothelial carcinoma.

Supplementary Figure 3 | Correlations between the expression levels of *SFRP2* and its co-upregulated genes. **(A–E)** Utilizing the cBioPortal web platform, these data were obtained from the TCGA database (n = 411).

Supplementary Figure 4 | Both the mRNA levels of *SFRP1* and *SFRP2* are not negatively correlated with their methylation status. **(A)** The correlations between the mRNA levels of *SFRP1* and their methylation status. **(B)** The correlations between the mRNA levels of *SFRP2* and their methylation status. Utilizing the cBioPortal web platform, these data were obtained from the TCGA database (n = 413).

Supplementary Figure 5 | High CAF infiltration is significantly correlated with poor cumulative survival. **(A, B)** The impact of CAF infiltration on cumulative survival in bladder cancer. These data were estimated using the MCP-COUNTER and TIDE algorithms from the TIMER2.0 database.

Supplementary Figure 6 | Regulatory networks among *ZNF585B-6:1*, miRNAs, and *SFRP2*. These data were obtained from the miRTarBase database.

Supplementary Figure 7 | Correlations between the expression levels of *SFRP2* and collagen family genes. **(A–F)** Utilizing the cBioPortal web platform, these data were obtained from the TCGA database (n = 411).

Supplementary Figure 8 | Correlations between the expression levels of *SFRP2* and EMT markers. **(A, B)** Utilizing the cBioPortal web platform, these data were obtained from the TCGA database (n = 411).

Supplementary Figure 9 | Correlations between the expression levels of *SFRP2* and *TGFB1* and CAF marker. **(A, B)** Utilizing the cBioPortal web platform, these data were obtained from the TCGA database (n = 411).

REFERENCES

1. Yang MH, Chen KK, Yen CC, Wang WS, Chang YH, Huang WJ, et al. Unusually High Incidence of Upper Urinary Tract Urothelial Carcinoma in Taiwan. *Urology* (2002) 59(5):681–7. doi: 10.1016/S0090-4295(02)01529-7
2. Babjuk M, Burger M, Compérat EM, Gontero P, Mostafid AH, Palou J, et al. European Association of Urology Guidelines on Non-Muscle-Invasive Bladder Cancer (TaT1 and Carcinoma In Situ) - 2019 Update. *Eur Urol* (2019) 76(5):639–57. doi: 10.1016/j.eururo.2019.08.016
3. Taylor J, Becher E, Steinberg GD. Update on the Guideline of Guidelines: non-Muscle-Invasive Bladder Cancer. *BJU Int* (2020) 125(2):197–205. doi: 10.1111/bju.14915
4. Witjes JA, Bruins HM, Cathomas R, Compérat EM, Cowan NC, Gakis G, et al. European Association of Urology Guidelines on Muscle-Invasive and Metastatic Bladder Cancer: Summary of the 2020 Guidelines. *Eur Urol* (2021) 79(1):82–104. doi: 10.1016/j.eururo.2020.03.055
5. Rouprêt M, Babjuk M, Compérat E, Zigeuner R, Sylvester RJ, Burger M, et al. European Association of Urology Guidelines on Upper Urinary Tract Urothelial Carcinoma: 2017 Update. *Eur Urol* (2018) 73(1):111–22. doi: 10.1016/j.eururo.2017.07.036

6. Kobayashi T, Ito K, Kojima T, Kato M, Kanda S, Hatakeyama S, et al. Risk Stratification for the Prognosis of Patients With Chemoresistant Urothelial Cancer Treated With Pembrolizumab. *Cancer Sci* (2021) 112(2):760–73. doi: 10.1111/cas.14762
7. MacDonald BT, Tamai K, He X. Wnt/beta-Catenin Signaling: Components, Mechanisms, and Diseases. *Dev Cell* (2009) 17(1):9–26. doi: 10.1016/j.devcel.2009.06.016
8. Zhang Y, Wang X. Targeting the Wnt/β-Catenin Signaling Pathway in Cancer. *J Hematol Oncol* (2020) 13(1):165. doi: 10.1186/s13045-020-00990-3
9. Garg M, Maurya N. WNT/β-Catenin Signaling in Urothelial Carcinoma of Bladder. *World J Nephrol* (2019) 8(5):83–94. doi: 10.5527/wjn.v8.i5.83
10. Ren J, Yang Y, Peng T, Xu D. Predictive Value of β-Catenin in Bladder Cancer: A Systematic Review and Meta-Analysis. *Biosci Rep* (2020) 40(9): BSR20202127. doi: 10.1042/BSR20202127
11. Zhu X, Kanai Y, Saito A, Kondo Y, Hirohashi S. Aberrant Expression of Beta-Catenin and Mutation of Exon 3 of the Beta-Catenin Gene in Renal and Urothelial Carcinomas. *Pathol Int* (2000) 50(12):945–52. doi: 10.1046/j.1440-1827.2000.01139.x
12. Chehrazi-Raffle A, Dorff TB, Pal SK, Lyou Y. Wnt/β-Catenin Signaling and Immunotherapy Resistance: Lessons for the Treatment of Urothelial Carcinoma. *Cancers (Basel)* (2021) 13(4):889. doi: 10.3390/cancers13040889
13. Chung MT, Lai HC, Sytwu HK, Yan MD, Shih YL, Chang CC, et al. SFRP1 and SFRP2 Suppress the Transformation and Invasion Abilities of Cervical Cancer Cells Through Wnt Signal Pathway. *Gynecol Oncol* (2009) 112(3):646–53. doi: 10.1016/j.ygyno.2008.10.026
14. van Loon K, Huijbers EJM, Griffioen AW. Secreted Frizzled-Related Protein 2: A Key Player in Noncanonical Wnt Signaling and Tumor Angiogenesis. *Cancer Metastasis Rev* (2021) 40(1):191–203. doi: 10.1007/s10555-020-09941-3
15. Lee JL, Lin CT, Chueh LL, Chang CJ. Autocrine/paracrine Secreted Frizzled-Related Protein 2 Induces Cellular Resistance to Apoptosis: A Possible Mechanism of Mammary Tumorigenesis. *J Biol Chem* (2004) 279 (15):14602–9. doi: 10.1074/jbc.M309008200
16. Huang C, Ye Z, Wan J, Liang J, Liu M, Xu X, et al. Secreted Frizzled-Related Protein 2 Is Associated With Disease Progression and Poor Prognosis in Breast Cancer. *Dis Markers* (2019) 2019:6149381. doi: 10.1155/2019/6149381
17. Kim H, Yoo S, Zhou R, Xu A, Bernitz JM, Yuan Y, et al. Oncogenic Role of SFRP2 in P53-Mutant Osteosarcoma Development *via* Autocrine and Paracrine Mechanism. *Proc Natl Acad Sci U S A* (2018) 115(47):E11128–e37. doi: 10.1073/pnas.1814044115
18. Shirozu M, Tada H, Tashiro K, Nakamura T, Lopez ND, Nazarea M, et al. Characterization of Novel Secreted and Membrane Proteins Isolated by the Signal Sequence Trap Method. *Genomics* (1996) 37(3):273–80. doi: 10.1006/geno.1996.0560
19. Vincent KM, Postovit LM. A Pan-Cancer Analysis of Secreted Frizzled-Related Proteins: Re-Examining Their Proposed Tumour Suppressive Function. *Sci Rep* (2017) 7:42719. doi: 10.1038/srep42719
20. Meng J, Lu X, Zhou Y, Zhang M, Ge Q, Zhou J, et al. Tumor Immune Microenvironment-Based Classifications of Bladder Cancer for Enhancing the Response Rate of Immunotherapy. *Mol Ther Oncolytics* (2021) 20:410–21. doi: 10.1016/j.omto.2021.02.001
21. Edge SB, Compton CC. The American Joint Committee on Cancer: The 7th Edition of the AJCC Cancer Staging Manual and the Future of TNM. *Ann Surg Oncol* (2010) 17(6):1471–4. doi: 10.1245/s10434-010-0985-4
22. Humphrey PA, Moch H, Cubilla AL, Ulbright TM, Reuter VE. The 2016 WHO Classification of Tumours of the Urinary System and Male Genital Organs-Part B: Prostate and Bladder Tumours. *Eur Urol* (2016) 70(1):106–19. doi: 10.1016/j.eururo.2016.02.028
23. Chen TJ, Chou CL, Tian YF, Yeh CF, Chan TC, He HL, et al. High FRMD3 Expression is Prognostic for Worse Survival in Rectal Cancer Patients Treated With CCRT. *Int J Clin Oncol* (2021) 26(9):1689–97. doi: 10.1007/s10147-021-01944-6
24. Chou CL, Chen TJ, Tian YF, Chan TC, Yeh CF, Li WS, et al. Upregulated MUC2 Is an Unfavorable Prognostic Indicator for Rectal Cancer Patients Undergoing Preoperative CCRT. *J Clin Med* (2021) 10(14):3030. doi: 10.3390/jcm10143030
25. Jones SE, Jomary C. Secreted Frizzled-Related Proteins: Searching for Relationships and Patterns. *BioEssays* (2002) 24(9):811–20. doi: 10.1002/bies.10136
26. Shin K, Lee J, Guo N, Kim J, Lim A, Qu L, et al. Hedgehog/Wnt Feedback Supports Regenerative Proliferation of Epithelial Stem Cells in Bladder. *Nature* (2011) 472(7341):110–4. doi: 10.1038/nature09851
27. Tran L, Xiao JF, Agarwal N, Duex JE, Theodorescu D. Advances in Bladder Cancer Biology and Therapy. *Nat Rev Cancer* (2021) 21(2):104–21. doi: 10.1038/s41568-020-00313-1
28. Li T, Fu J, Zeng Z, Cohen D, Li J, Chen Q, et al. TIMER2.0 for Analysis of Tumor-Infiltrating Immune Cells. *Nucleic Acids Res* (2020) 48(W1):W509–w14. doi: 10.1093/nar/gkaa407
29. Li WM, Chan TC, Huang SK, Wu WJ, Ke HL, Liang PI, et al. Prognostic Utility of FBLN2 Expression in Patients With Urothelial Carcinoma. *Front Oncol* (2020) 10:570340. doi: 10.3389/fonc.2020.570340
30. Zhang PB, Huang ZL, Xu YH, Huang J, Huang XY, Huang XY. Systematic Analysis of Gene Expression Profiles Reveals Prognostic Stratification and Underlying Mechanisms for Muscle-Invasive Bladder Cancer. *Cancer Cell Int* (2019) 19:337. doi: 10.1186/s12935-019-1056-y
31. Franz M, Rodriguez H, Lopes C, Zuberi K, Montojo J, Bader GD, et al. GeneMANIA Update 2018. *Nucleic Acids Res* (2018) 46(W1):W60–w4. doi: 10.1093/nar/gky311
32. Fan EW, Li CC, Wu WJ, Huang CN, Li WM, Ke HL, et al. FGF7 Over Expression is an Independent Prognosticator in Patients With Urothelial Carcinoma of the Upper Urinary Tract and Bladder. *J Urol* (2015) 194(1):223–9. doi: 10.1016/j.juro.2015.01.073
33. Chang IW, Lin VC, Wu WJ, Liang PI, Li WM, Yeh BW, et al. Complement Component 1, s Subcomponent Overexpression is an Independent Poor Prognostic Indicator in Patients With Urothelial Carcinomas of the Upper Urinary Tract and Urinary Bladder. *J Cancer* (2016) 7(11):1396–405. doi: 10.7150/jca.15339
34. Chong JM, Uren A, Rubin JS, Speicher DW. Disulfide Bond Assignments of Secreted Frizzled-Related Protein-1 Provide Insights About Frizzled Homology and Netrin Modules. *J Biol Chem* (2002) 277(7):5134–44. doi: 10.1074/jbc.M108533200
35. Surana R, Sikka S, Cai W, Shin EM, Warrier SR, Tan HJ, et al. Secreted Frizzled Related Proteins: Implications in Cancers. *Biochim Biophys Acta* (2014) 1845(1):53–65. doi: 10.1016/j.bbcan.2013.11.004
36. Liu Y, Zhou Q, Zhou D, Huang C, Meng X, Li J. Secreted Frizzled-Related Protein 2-Mediated Cancer Events: Friend or Foe? *Pharmacol Rep* (2017) 69 (3):403–8. doi: 10.1016/j.pharep.2017.01.001
37. Liu D, Sun C, Kim N, Bhan C, Tuason JPW, Chen Y, et al. Comprehensive Analysis of SFRP Family Members Prognostic Value and Immune Infiltration in Gastric Cancer. *Life (Basel Switzerland)* (2021) 11(6):522. doi: 10.3390/life11060522
38. Anastasiadou E, Jacob LS, Slack FJ. Non-Coding RNA Networks in Cancer. *Nat Rev Cancer* (2018) 18(1):5–18. doi: 10.1038/nrc.2017.99
39. Statello L, Guo CJ, Chen LL, Huarte M. Gene Regulation by Long Non-Coding RNAs and Its Biological Functions. *Nat Rev Mol Cell Biol* (2021) 22(2):96–118. doi: 10.1038/s41580-020-00315-9
40. Huang HY, Lin YC, Li J, Huang KY, Shrestha S, Hong HC, et al. miRTarBase 2020: Updates to the Experimentally Validated microRNA-Target Interaction Database. *Nucleic Acids Res* (2020) 48(D1):D148–54. doi: 10.1093/nar/gkz896
41. Yoshino H, Seki N, Itesako T, Chiyomaru T, Nakagawa M, Enokida H. Aberrant Expression of microRNAs in Bladder Cancer. *Nat Rev Urol* (2013) 10(7):396–404. doi: 10.1038/nrurol.2013.113
42. Zhu H, Chen H, Wang J, Zhou L, Liu S. Collagen Stiffness Promoted Non-Muscle-Invasive Bladder Cancer Progression to Muscle-Invasive Bladder Cancer. *Onco Targets Ther* (2019) 12:3441–57. doi: 10.2147/OTT.S194568
43. Bellmunt J, de Wit R, Vaughn DJ, Fradet Y, Lee JL, Fong L, et al. Pembrolizumab as Second-Line Therapy for Advanced Urothelial Carcinoma. *N Engl J Med* (2017) 376(11):1015–26. doi: 10.1056/NEJMoa1613683
44. Mariathasan S, Turley SJ, Nickles D, Castiglioni A, Yuen K, Wang Y, et al. TGFβ Attenuates Tumour Response to PD-L1 Blockade by Contributing to Exclusion of T Cells. *Nature* (2018) 554(7693):544–8. doi: 10.1038/nature25501
45. Winkler J, Abisoye-Ogunniyan A, Metcalf KJ, Werb Z. Concepts of Extracellular Matrix Remodelling in Tumour Progression and Metastasis. *Nat Commun* (2020) 11(1):5120. doi: 10.1038/s41467-020-18794-x
46. Bányai L, Patthy L. The NTR Module: Domains of Netrins, Secreted Frizzled Related Proteins, and Type I Procollagen C-Proteinase Enhancer Protein are

Homologous With Tissue Inhibitors of Metalloproteases. *Protein Sci* (1999) 8 (8):1636–42. doi: 10.1110/ps.8.8.1636
47. Lagoutte P, Bettler E, Vadon-Le Goff S, Moali C. Procollagen C-Proteinase Enhancer-1 (PCPE-1), a Potential Biomarker and Therapeutic Target for Fibrosis. *Matrix Biol Plus* (2021) 11:100062. doi: 10.1016/j.mbplus.2021.100062
48. Brew K, Nagase H. The Tissue Inhibitors of Metalloproteinases (TIMPs): An Ancient Family With Structural and Functional Diversity. *Biochim Biophys Acta* (2010) 1803(1):55–71. doi: 10.1016/j.bbamcr.2010.01.003
49. Brunner A, Tzankov A. The Role of Structural Extracellular Matrix Proteins in Urothelial Bladder Cancer (Review). *Biomark Insights* (2007) 2:418–27. doi: 10.4137/BMI.S294
50. Shinagare AB, Ramaiya NH, Jagannathan JP, Fennessy FM, Taplin ME, Van den Abbeele AD. Metastatic Pattern of Bladder Cancer: Correlation With the Characteristics of the Primary Tumor. *AJR Am J Roentgenol* (2011) 196 (1):117–22. doi: 10.2214/AJR.10.5036
51. Necchi A, Pond GR, Pal SK, Agarwal N, Bowles DW, Plimack ER, et al. Bone Metastases as the Only Metastatic Site in Patients With Urothelial Carcinoma: Focus on a Special Patient Population. *Clin Genitourin Cancer* (2018) 16(2): e483–e90. doi: 10.1016/j.clgc.2017.10.012
52. Troen BR. The Regulation of Cathepsin K Gene Expression. *Ann N Y Acad Sci* (2006) 1068:165–72. doi: 10.1196/annals.1346.018
53. Littlewood-Evans AJ, Bilbe G, Bowler WB, Farley D, Wlodarski B, Kokubo T, et al. The Osteoclast-Associated Protease Cathepsin K is Expressed in Human Breast Carcinoma. *Cancer Res* (1997) 57(23):5386–90.
54. Brubaker KD, Vessella RL, True LD, Thomas R, Corey E, Cathepsin K. mRNA and Protein Expression in Prostate Cancer Progression. *J Bone Miner Res* (2003) 18(2):222–30. doi: 10.1359/jbmr.2003.18.2.222

Conflict of Interest: Author C-CC is employed by Genetics Generation Advancement Corp.

The remaining authors declare that the research was conducted in the absence of any commercial or financial relationships that could be construed as a potential conflict of interest.

Publisher's Note: All claims expressed in this article are solely those of the authors and do not necessarily represent those of their affiliated organizations, or those of the publisher, the editors and the reviewers. Any product that may be evaluated in this article, or claim that may be made by its manufacturer, is not guaranteed or endorsed by the publisher.

frontiers | Frontiers in Oncology

ORIGINAL RESEARCH
published: 05 April 2022
doi: 10.3389/fonc.2022.833305

Preoperative Metabolic Syndrome and HDL-C Level Predict the Prognosis of Patients Following Radical Cystectomy: A Propensity Score Matching Study

Zenan Liu[1†], Hai Bi[1†], Wei He[1], Xuehua Zhu[1], Jide He[1], Min Lu[2] and Jian Lu[1,3*]*

[1] Department of Urology, Peking University Third Hospital, Beijing, China, [2] Department of Pathology, Peking University Third Hospital, Beijing, China, [3] NHC Key Laboratory of Metabolic Cardiovascular Diseases Research, Ningxia Medical University, Yinchuan, China

OPEN ACCESS

Edited by:
Matteo Ferro,
European Institute of Oncology (IEO), Italy

Reviewed by:
Simona Di Francesco,
Federiciana People's University, Italy
Francesco Del Giudice,
Sapienza University of Rome, Italy
Daniela Terracciano,
University of Naples Federico II, Italy

****Correspondence:***
Jian Lu
lujian@bjmu.edu.cn
Min Lu
lumin@bjmu.edu.cn

[†]These authors have contributed equally to this work and share first authorship

Specialty section:
This article was submitted to Genitourinary Oncology, a section of the journal Frontiers in Oncology

Received: *11 December 2021*
Accepted: *07 March 2022*
Published: *05 April 2022*

Citation:
Liu Z, Bi H, He W, Zhu X, He J, Lu M and Lu J (2022) Preoperative Metabolic Syndrome and HDL-C Level Predict the Prognosis of Patients Following Radical Cystectomy: A Propensity Score Matching Study. Front. Oncol. 12:833305. doi: 10.3389/fonc.2022.833305

Objective: To investigate the prognostic significance of metabolic syndrome (MetS) and its components in patients with bladder cancer (BCa) treated with radical cystectomy (RC).

Methods: A total of 335 BCa patients who underwent RC between 2004 and 2019 at Peking University Third Hospital (PUTH) were analyzed retrospectively. The Kaplan-Meier method with the log-rank test was performed to assess overall survival (OS) and progression-free survival (PFS). Univariate and multivariate Cox proportional hazard models were conducted to identify the prognostic factors of OS and PFS before and after propensity score matching (PSM).

Results: Enrolled patients were allocated into two groups according to the presence or absence of MetS (n=84 MetS vs n=251 non-MetS), and 82 new matched pairs were identified to balance the baseline characteristics after 1:1 PSM. In the Kaplan-Meier analysis, MetS was associated with better OS (P=0.031) than the group without MetS. In addition, a body mass index (BMI) ≥ 25 was associated with better OS (P=0.011) and PFS (P=0.031), while low high-density lipoprotein cholesterol (HDL-C) was associated with worse OS (P=0.033) and PFS (P=0.010). In all patients, multivariate Cox analysis showed that hemoglobin, pathologic tumor stage and lymph node status were identified as independent prognostic factors for both OS and PFS, while age, MetS and HDL-C were independent prognostic factors only for OS. Reproducible results of multivariate analysis can still be observed in propensity matched patients. The results of further subgroup analysis revealed that the association of MetS with increased OS (P=0.043) and BMI ≥25 with increased OS (P=0.015) and PFS (P=0.029) was observed in non-muscle invasive bladder cancer (NMIBC) patients.

Conclusions: MetS was independently associated with better OS in BCa patients after RC, and HDL-C was the only component of MetS that was independently associated with

worse OS. MetS and HDL-C may become reliable prognostic biomarkers of OS in BCa patients after RC to provide individualized prognostication and assist in the formulation of clinical treatment strategies.

Keywords: bladder cancer, radical cystectomy, metabolic syndrome, high-density lipoprotein cholesterol (HDL-C), survival outcome, propensity score matching

INTRODUCTION

Bladder cancer (BCa) is one of the most common malignancies of the genitourinary system and is a significant cause of morbidity and mortality worldwide. It was estimated that BCa accounted for 83,730 new cases of cancer and 17,200 cancer-related deaths in 2021 (1). Urothelial carcinoma (UC) is the most common histologic type, approximately 75% of patients present with non-muscle invasive bladder cancer (NMIBC)while 25% with muscle invasive bladder cancer (MIBC), and 10-20% of cases of NMIBC will progress to MIBC at diagnosis (2). Radical cystectomy (RC) remains the standard treatment for non-metastatic MIBC (3) and high risk NMIBC (4). Despite significant advancement in surgical techniques and increasing application of multimodal treatment approaches, the long-term survival outcome of BCa patients after RC is not satisfactory, and the 5-year disease-specific survival after RC is consistently 50-60% (5, 6). To improve the survival outcome, the assessment of reliable prognostic factors could be conducive to guiding clinical decision-making and patient consultation, such as tumor stage, lymph node status, lymphovascular invasion (LVI), pathologic grade (7), lymphocyte-to-monocyte (LMR) (8) and Vesical Imaging-Reporting and Data System (VI-RADS) score (9). Among them, tumor stage and lymph node status remain the dominant pathologic predictors for recurrence and survival. However, BCa with similar stage and grade may present significantly different clinical outcomes after RC unexpectedly (10). Therefore, it is necessary to identify additional appropriate prognostic factors to help in preoperative risk stratification and survival prediction.

Recently, there is increasing interest in describing the extent of the impact of metabolic changes on cancer development and progression, particularly with regard to metabolic syndrome (MetS) (11–14). MetS is a complex disorder characterized by a series of metabolic disturbances including abdominal obesity, hyperglycemia, high blood pressure, hypertriglyceridemia, and low high-density lipoprotein cholesterol (HDL-C) (15), all of which are independently associated with an increased risk of cancer (16–18), and their influence on survival outcome has been confirmed in a variety of cancers as well, such as liver cancer (19), gastric cancer (20), breast cancer (21) and colon cancer (11). In addition, MetS is closely associated with a variety of genitourinary diseases as well (22, 23). As for BCa, current studies focus more on the potential association between MetS and an increased risk of BCa (24). In contrast, data on the association between MetS and survival outcomes in BCa, such as overall survival, cancer-specific survival and disease recurrence, are extremely limited and unproven (25). Similarly, only a few studies have evaluated the relationship between each MetS component and the survival outcomes of BCa in detail (26, 27).

Thus, in view of the significant role of MetS in tumor prognosis, this study was designed to explore the prognostic significance of MetS and its components in BCa patients treated with RC.

MATERIALS AND METHODS

Study Population

After obtaining the approval of the Institutional Review Board for the Protection of Human Subjects, we used the BCa database from the Department of Urology at Peking University Third Hospital (PUTH)for our analysis. A total of 470 consecutive BCa patients treated with RC between 2004 and 2019 at PUTH were included in the study. Comprehensive clinicopathological information was reviewed and collected for each patient. Patients were excluded from the study based on the following criteria: pathologic diagnosis other than urothelial carcinoma (n=12), distant metastatic disease at the time of RC (n=28), unavailable information on any of the MetS components (n=62), postoperative 30-day death (n=8) or less than 1 month of follow-

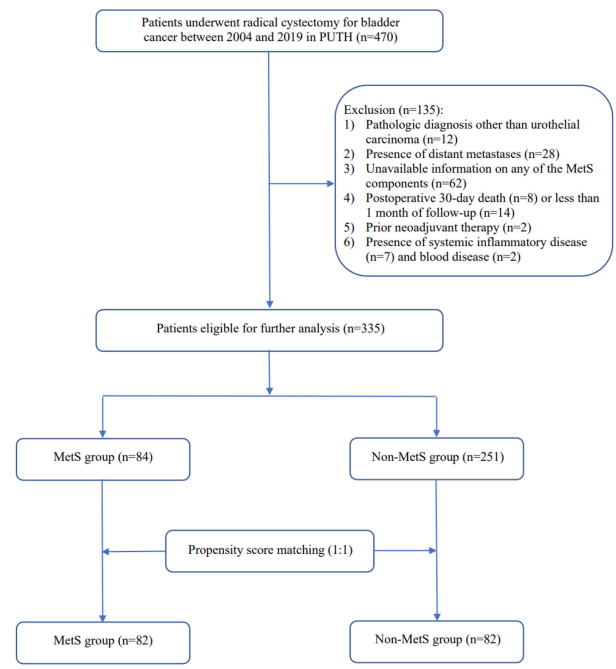

FIGURE 1 | Flow chart of patient selection.

up (n=14), prior neoadjuvant therapy (n=2), and presence of systemic inflammatory disease (n=7) and blood disease (n=2). This resulted in 335 BCa patients eligible for further analysis, the process of patient selection is shown in **Figure 1**.

Data Collection

The clinical and pathological variables of the enrolled patients were retrospectively collected from the database, including: age, gender, body mass index (BMI), hypertension, hyperglycemia, hypertriglyceridemia, high-density lipoprotein cholesterol (HDL-C), current smoking, hemoglobin (Hg), pathologic tumor stage (pT), lymph node status (pN), pathologic grade, concomitant carcinoma *in situ* (CIS), variation and adjuvant therapy. All surgical specimens after RC were processed according to standard pathological procedures. Genitourinary pathologists assigned tumor pathologic grade and clinical stage according to the 2004 WHO/International Society of Urologic Pathologists classification of bladder urothelial cancer and the 2017 TNM staging system of the AJCC, respectively.

Metabolic Syndrome Criteria

Patients were classified as MetS according to the diagnostic criteria from Chinese Medical Association Diabetes Society in 2004 (28) with at least three of the following four components: (i) overweight and/or obesity: body mass index (BMI) ≥ 25kg/m^2; (ii) hyperglycemia: fasting plasma glucose ≥6.1mmol/L (110 mg/dL) and/or 2-hr postprandial plasma glucose ≥7.8mmol/L (140 mg/dL), or drug treatment for diagnosed diabetes mellitus; (iii) hypertension: blood pressure ≥140/90 mmHg or drug treatment for diagnosed hypertension; (iv) dyslipidemia: fasting serum triglyceride (TG) level ≥1.7mmol/L (150 mg/dL) and/or fasting serum high-density lipoprotein cholesterol (HDL-C) <0.9mmol/L (35 mg/dL) in male and <1.0mmol/L (39 mg/dL) in female.

Follow-Up

In general, the patient underwent postoperative clinical and radiological follow-up following conventional institutional protocols, included quarterly sessions for the first two years, semiannually sessions for the next two years, and then annual follow-up thereafter. The primary study outcomes included overall survival (OS) and progression-free survival (PFS). OS was defined as the time from the day of surgery to the last follow-up or death due to any cause. PFS was defined as the time from the beginning of treatment to the observation of disease progression or death due to any cause.

Statistical Analysis

According to the data distribution, continuous variables are presented as medians and interquartile ranges (IQRs), and categorical variables are expressed as counts and frequencies. Comparisons of the differences between MetS patients and non-MetS patients were performed using Student's t test for continuous variables and the χ^2 test or Fisher's test for categorical variables. We reduced the influence of data deviation and confounding variables between the patients in the MetS and non-MetS groups by using the method of propensity score matching (PSM) to obtain matched data. Matching was conducted at a 1:1 fixed ratio with a caliper value of 0.05 by using the variables of age, gender, current smoking, hemoglobin, pT stage, pN status, pathologic grade, CIS, variation and adjuvant therapy. OS and PFS were estimated using standard Kaplan-Meier methods. The log-rank test was applied for the statistical comparison between survival curves. Univariate and multivariate analyses were performed using the Cox proportional hazards model to assess the correlation between MetS and individual components and survival outcomes, and the results were presented as hazards ratios (HRs) and 95% confidence intervals (95% CIs). All significant variables with a P value < 0.10 in the univariate analysis were incorporated into the subsequent multivariate analysis to identify the independent prognostic factors. All statistical analyses were performed using IBM SPSS Statistics 26.0. Two-sided P values <0.05 were considered statistically significant.

RESULTS

Patient Characteristics

A total of 335 patients treated with RC were included in the study and they were divided into two groups based on the presence or absence of MetS (n=84 MetS vs n=251 non-MetS). The overall prevalence of each of the various MetS components was 38.2% for obesity, 39.1% for hypertension, 34.9% for hyperglycemia, 30.4% for hypertriglyceridemia and 27.5% for low HDL-C. To balance the baseline and reduce the impact of potential confounding factors, PSM was performed at a 1:1 fixed ratio, and finally we obtained 82 new matched pairs. After matching, the clinicopathologic characteristics between patients in the MetS and non-MetS groups were well-balanced except for individual components of MetS (BMI, P <0.001; hypertension, P <0.001; hyperglycemia, P <0.001; hypertriglyceridemia, P <0.001; low HDL-C, P <0.001). The clinicopathologic characteristics of the all patients and propensity matched patients are shown in **Table 1**.

Survival Outcomes of OS and PFS

In total, the median follow-up period was 34.0 months (interquartile range: 13.0-64.0 months), with a total of 27 (32.1%) patients who died and 34 (40.5%) who developed disease progression in the MetS group, and 106 (42.2%) who died and 118 (47.0%) who developed disease progression in the non-MetS group. The median OS time was 46.4 months, and the 5-year OS probabilities for the MetS group and non-MetS group were 70.2% and 60.2%, respectively. The median PFS time weas 36.9 months, and the 5-year PFS probabilities for the MetS group and non-MetS group were 63.1% and 55.8%, respectively.

Univariate and Multivariate Analyses for OS and PFS in All Patients

Univariate analyses revealed that age, BMI, hemoglobin, pathologic tumor stage and lymph node status were associated with OS; age, HDL-C, hemoglobin, pathologic tumor stage, lymph node status and adjuvant therapy were associated with

TABLE 1 | Clinicopathological characteristics of the all patients and propensity matched patients.

Characteristics	All patients (n=335)			Propensity matched patients (n=164)		
	MetS (n=84)	Non-MetS (n=251)	P value	MetS (n=82)	Non-MetS (n=82)	P value
Age (years), median (IQR)	68 (59-73)	68 (60-75)	0.895	68.5 (59-73.3)	69 (61.8-76.3)	0.497
Gender, n (%)			0.044			0.319
Male	64 (76.2%)	215 (85.7%)		64 (78.0%)	69 (84.1%)	
Female	20 (23.8%)	36 (14.3%)		18 (22.0%)	13 (15.9%)	
BMI (kg/m2), n (%)			<0.001			<0.001
<25	16 (19.0%)	191 (76.1%)		16 (19.5%)	61 (74.4%)	
≥25	68 (81.0%)	60 (23.9%)		66 (80.5%)	21 (25.6%)	
Hypertension, n (%)			<0.001			<0.001
No	20 (23.8%)	184 (73.3%)		20 (24.4%)	60 (73.2%)	
Yes	64 (76.2%)	67 (26.7%)		62 (75.6%)	22 (26.8%)	
Hyperglycemia, n (%)			<0.001			<0.001
No	20 (23.8%)	198 (78.9%)		19 (23.2%)	69 (84.1%)	
Yes	64 (76.2%)	53 (21.1%)		63 (76.8%)	13 (15.9%)	
Hypertriglyceridemia, n (%)			<0.001			<0.001
No	31 (36.9%)	202 (80.5%)		30 (36.6%)	64 (78.0%)	
Yes	53 (63.1%)	49 (19.5%)		52 (63.4%)	18 (22.0%)	
Low HDL-C, n (%)			<0.001			<0.001
No	42 (50.0%)	201 (80.1%)		41 (50%)	64 (78.0%)	
Yes	42 (50.0%)	50 (19.9%)		41 (50%)	18 (22.0%)	
Current Smoking, n (%)			0.514			0.724
No	63 (75.0%)	179 (71.3%)		61 (74.4%)	59 (72.0%)	
Yes	21 (25.0%)	72 (28.7%)		21 (25.6%)	23 (28.0%)	
Hg (g/L), median (IQR)	137 (124-148)	132 (117-145)	0.150	137 (123-149)	134 (118-149)	0.588
pT Stage, n (%)			0.663			0.510
≤T2	52 (61.9%)	162 (64.5%)		52 (63.4%)	56 (68.3%)	
T3-4	32 (38.1%)	89 (35.5%)		30 (36.6%)	26 (31.7%)	
pN Status, n (%)			0.452			0.277
Negative	68 (81.0%)	212 (84.5%)		67 (81.7%)	72 (87.8%)	
Positive	16 (19.0%)	39 (15.5%)		15 (18.3%)	10 (12.2%)	
Pathologic Grade, n (%)			0.559			0.755
LG	5 (6.0%)	11 (4.4%)		5 (6.1%)	6 (7.3%)	
HG	79 (94.0%)	240 (95.6%)		77 (93.9%)	76 (92.7%)	
Variation, n (%)			0.993			0.717
Absent	78 (92.9%)	233 (92.8%)		77 (93.9%)	79 (96.3%)	
Present	6 (7.1%)	18 (7.2%)		5 (6.1%)	3 (3.7%)	
Concomitant CIS, n (%)			0.425			0.711
Absent	64 (76.2%)	180 (71.7%)		62 (75.6%)	64 (78.0%)	
Present	20 (23.8%)	71 (28.3%)		20 (24.4%)	18 (22.0%)	
Adjuvant Therapy*, n (%)			0.328			0.292
No	74 (88.1%)	210 (83.7%)		72 (87.8%)	76 (92.7%)	
Yes	10 (11.9%)	41 (16.3%)		10 (12.2%)	6 (7.3%)	

BCa, bladder cancer; BMI, body mass index; CIS, carcinoma in situ; HDL-C, high density lipoprotein cholesterol; Hg, hemoglobin; HG, high grade; IQR, interquartile range; LG, low grade; MetS, metabolic syndrome; pN, pathologic node stage; pT, pathologic tumor stage; RC, radical cystectomy.

**Adjuvant radiotherapy and/or adjuvant chemotherapy.*

PFS (**Table 2**). After adjusting for potential confounders by multivariate Cox regression analysis, age (P=0.011), MetS (P=0.005), HDL-C (P=0.006), hemoglobin (P<0.001), pathologic tumor stage (P<0.001) and lymph node status (P=0.001) were identified as independent prognostic factors for OS; hemoglobin (P<0.001), pathologic tumor stage (P=0.001) and lymph node status (P<0.001) were identified as independent prognostic factors for PFS (**Table 2**).

The Effect of MetS and Its Components on OS and PFS in Propensity Matched Patients

The Kaplan-Meier analysis and log-rank test revealed that there was statistical significance in both OS and PFS curves for BMI and HDL-C, and statistical significance in only OS curves for MetS. BMI ≥25 was associated with better OS (P=0.011; **Figure 2B**) and PFS (P=0.031; **Figure 3B**) while low HDL-C was associated with worse OS (P=0.033; **Figure 2F**) and PFS (P=0.010; **Figure 3F**). In addition, MetS was also associated with better OS (P=0.031) compared with non-MetS (**Figure 2A**). There was no statistical significance for other individual components of MetS in the OS (**Figures 2C–E**) and PFS (**Figures 3A, C–E**) curves.

Univariate analyses revealed that age, BMI, HDL-C, hemoglobin, pathologic tumor stage and lymph node status were all associated with OS and PFS while MetS was only associated with OS (**Table 3**). In order to ensure the assessment values of prognostic factors was consistent with that before PSM, we also performed multivariate Cox

TABLE 2 | Univariate and multivariate analysis of prognostic factors using the Cox proportional hazards model for OS and PFS in all patients.

Variables	OS				PFS			
	Univariate analysis		Multivariate analysis		Univariate analysis		Multivariate analysis	
	HR (95% CI)	P value	HR (95% CI)	P value	HR (95% CI)	P value	HR (95% CI)	P value
Age (years)	1.033 (1.014-1.052)	0.001	1.026 (1.006-1.046)	0.011	1.022 (1.006-1.040)	0.009	1.009 (0.991-1.027)	0.317
Gender								
Male	Ref				Ref			
Female	0.975 (0.612-1.556)	0.917			0.962 (0.622-1.489)	0.862		
Metabolic Syndrome								
No	Ref		Ref		Ref			
Yes	0.677 (0.441-1.041)	0.076	0.466 (0.272-0.798)	0.005	0.776 (0.527-1.143)	0.199		
BMI								
<25	Ref		Ref		Ref		Ref	
≥25	0.676 (0.470-0.974)	0.035	1.273 (0.809-2.004)	0.297	0.731 (0.523-1.023)	0.068	0.854 (0.601-1.214)	0.380
Hypertension								
No	Ref				Ref			
Yes	0.837 (0.587-1.194)	0.327			0.897 (0.645-1.247)	0.516		
Hyperglycemia								
No	Ref				Ref			
Yes	1.035 (0.723-1.481)	0.852			1.005 (0.718-1.406)	0.978		
Hypertriglyceridemia								
No	Ref				Ref			
Yes	0.854 (0.578-1.263)	0.430			0.953 (0.667-1.360)	0.789		
Low HDL-C								
No	Ref		Ref		Ref		Ref	
Yes	1.412 (0.981-2.033)	0.064	1.719 (1.165-2.537)	0.006	1.504 (1.073-2.107)	0.018	1.410 (0.999-1.990)	0.051
Current Smoking								
No	Ref				Ref			
Yes	0.980 (0.670-1.433)	0.916			0.916 (0.639-1.312)	0.633		
Hg (g/L)	0.976 (0.968-0.983)	<0.001	0.980 (0.971-0.988)	<0.001	0.977 (0.970-0.984)	<0.001	0.980 (0.972-0.988)	<0.001
pT Stage								
≤T2	Ref		Ref		Ref		Ref	
T3-4	2.927 (2.066-4.147)	<0.001	2.055 (1.406-3.005)	<0.001	2.935 (2.119-4.065)	<0.001	1.896 (1.322-2.718)	0.001
pN Status								
Negative	Ref		Ref		Ref		Ref	
Positive	2.689 (1.786-4.049)	<0.001	2.147 (1.381-3.336)	0.001	3.402 (2.345-4.937)	<0.001	2.685 (1.765-4.084)	<0.001
Pathologic Grade								
LG	Ref		Ref		Ref		Ref	
HG	2.346 (0.861-6.387)	0.095	1.057 (0.372-3.004)	0.917	2.182 (0.888-5.360)	0.089	1.182 (0.464-3.009)	0.726
Variation								
Absent	Ref				Ref			
Present	0.715 (0.315-1.624)	0.422			0.599 (0.264-1.356)	0.219		
Concomitant CIS								
Absent	Ref				Ref			
Present	0.770 (0.501-1.184)	0.233			0.816 (0.554-1.202)	0.304		
Adjuvant Therapy*								
No	Ref				Ref		Ref	
Yes	0.814 (0.495-1.341)	0.419			1.520 (1.011-2.286)	0.044	0.929 (0.599-1.441)	0.742

BCa, bladder cancer; BMI, body mass index; CI, confidence interval; CIS, carcinoma in situ; HDL-C, high density lipoprotein cholesterol; Hg, hemoglobin; HG, high grade; HR, hazard ratio; IQR, interquartile ranges; LG, low grade; OS, overall survival; PFS, progression-free survival; pN, pathologic node stage; pT, pathologic tumor stage; Ref, reference.
**Adjuvant radiotherapy and/or adjuvant chemotherapy.*

regression analysis after PSM. As a result, age (P=0.019), MetS (P=0.001), HDL-C (P=0.011), hemoglobin (P<0.001), pathologic tumor stage (P=0.001) and lymph node status (P=0.017) were identified as independent prognostic factors for OS. Hemoglobin (P=0.004), pathologic tumor stage (P=0.002) and lymph node status (P=0.007) were identified as independent prognostic factors for PFS (**Table 3**).

Further subgroup analyses were performed stratified by T stage (NMIBC vs MIBC). The results revealed that the association of MetS with increased OS (P=0.043) and BMI ≥25 with increased OS (P=0.015) and PFS (P=0.029) were observed in NMIBC patients. In contrast, there were no significant differences in MetS and its individual components in the OS and PFS curves of MIBC patients (**Supplementary Figures 1–4**).

DISCUSSION

In the present single-center study, we investigated the impact of MetS and its components on the prognosis of BCa patients who

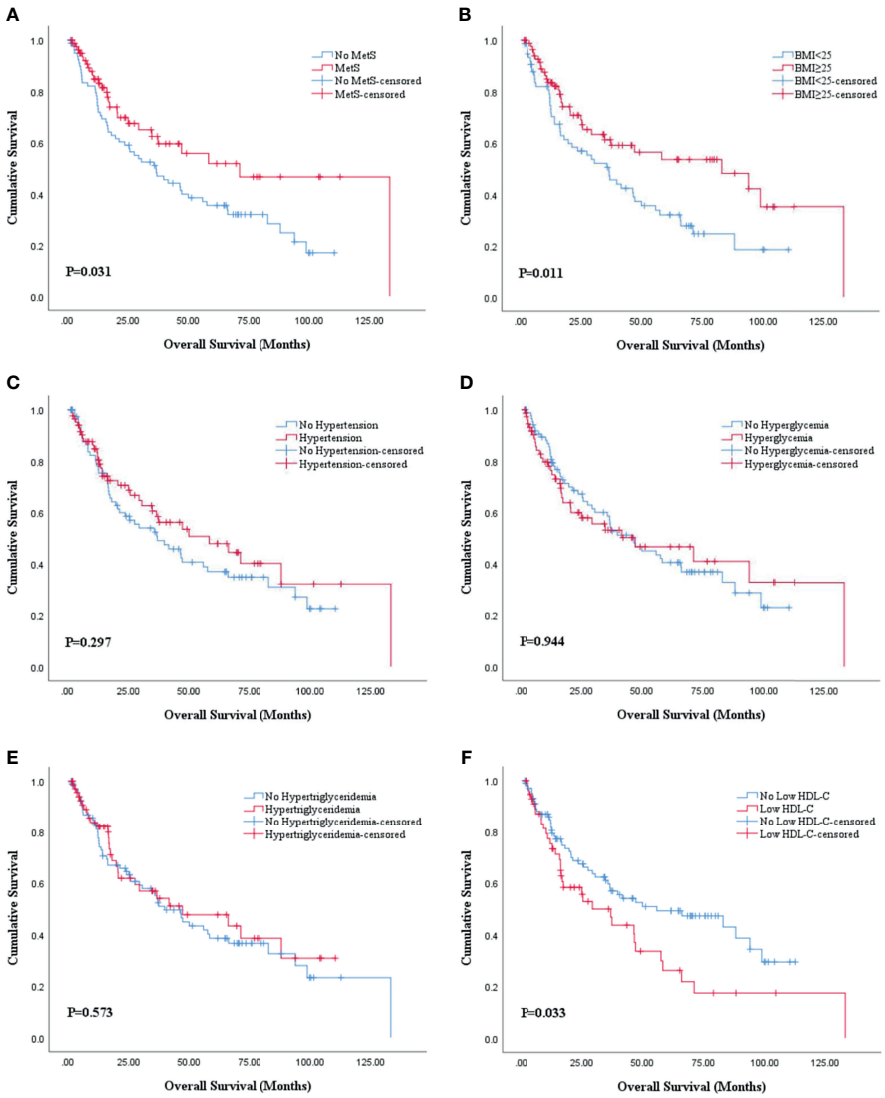

FIGURE 2 | Kaplan-Meier survival analysis of OS stratified by MetS and its components after PSM. **(A)** MetS and non-MetS; **(B)** BMI <25 and BMI ≥25; **(C)** hypertension and no hypertension; **(D)** hyperglycemia and no hyperglycemia; **(E)** hypertriglyceridemia and no hypertriglyceridemia; **(F)** low HDL-C and no low HDL-C. BMI, body mass index; HDL-C, high density lipoprotein cholesterol; MetS, metabolic syndrome; OS, overall survival; PSM, propensity score match.

underwent RC. We balanced out differences in clinicopathological characteristics between MetS and non-MetS patients and explored the influence of other potential risk factors by using PSM and multivariate Cox regression analysis. Our study found that MetS was independently associated with better OS in BCa patients after RC, and HDL-C was the only component of MetS that was independently associated with worse OS. We further performed detailed subgroup analyses stratified by tumor stage, and the results revealed that the presence of MetS and BMI ≥ 25 were protective factors for the survival of NMIBC patients. To the best of our knowledge, this is the first study to explore whether MetS or its components influence survival outcomes in BCa patients treated with RC, which might provide preliminary evidence and direction for future research in this area.

Our results highlight the necessary for more investigation into the potential molecular mechanisms underlying our findings. A variety of mechanisms have been proposed to explain the role of MetS in cancers including regulation of the insulin-like growth factor-1 (IGF-1) pathway, existence of hyperinsulinemia and insulin resistance, process of adipokine production, angiogenesis promotion, glucose malutilization, and oxidative stress/DNA damage, which can synergistically increase the cancer risk rather than just individual components (29, 30). Insulin can bind and activate the IGF-1 receptor and promote mitosis by triggering downstream pathways to act as a growth factor (31). Increased levels of insulin and IGF-1 can would promote tumors growth and progression by binding to the overexpressed insulin receptor in many cancers (32). At the same time, insulin resistance in patients

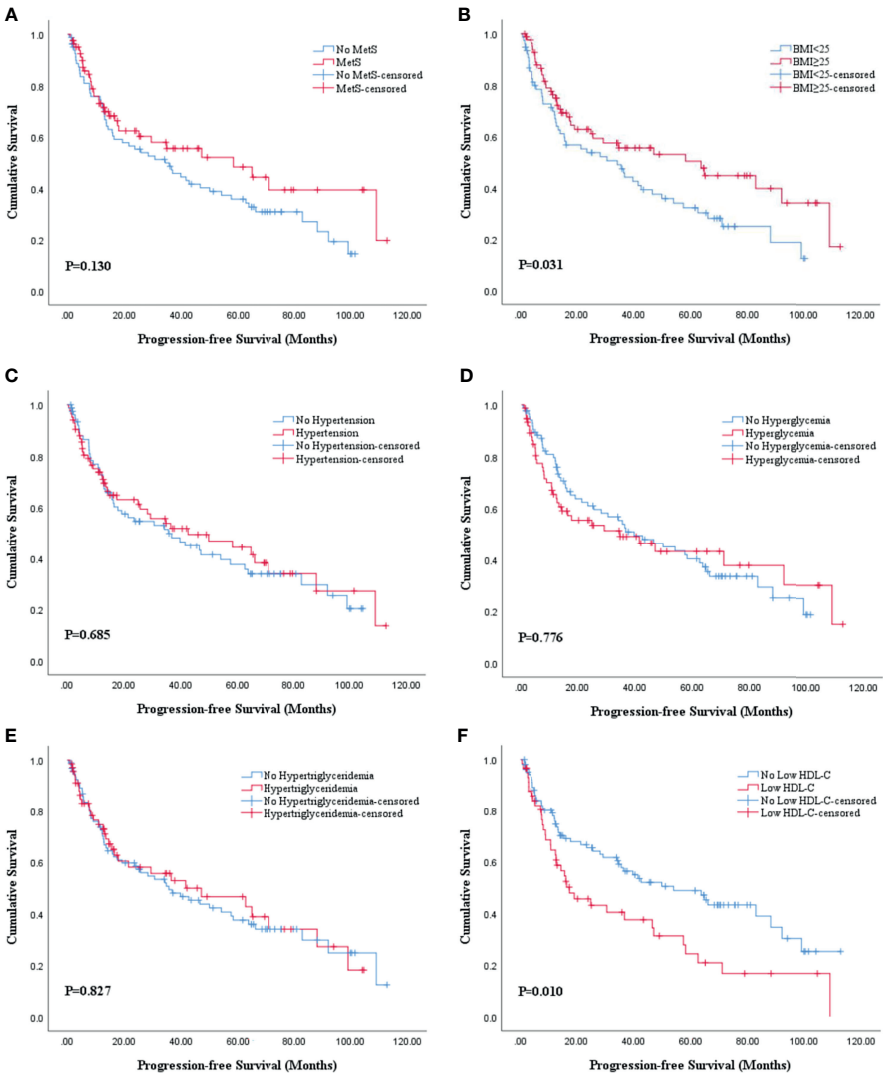

FIGURE 3 | Kaplan-Meier survival analysis of PFS stratified by MetS and its components after PSM. **(A)** MetS and non-MetS; **(B)** BMI <25 and BMI ≥25; **(C)** hypertension and no hypertension; **(D)** hyperglycemia and no hyperglycemia; **(E)** hypertriglyceridemia and no hypertriglyceridemia; **(F)** low HDL-C and no low HDL-C. BMI, body mass index; HDL-C, high density lipoprotein cholesterol; MetS, metabolic syndrome; PFS, progression-free survival; PSM, propensity score match.

with MetS can contribute to hyperinsulinemia, which enhances the activity of IGF by inhibiting the synthesis of IGF binding proteins (33). In addition to endocrine disorders, immuno-inflammatory responses such as adipose tissue releases proinflammatory cytokines such as TNF-α or IL-6, which promote angiogenesis and cell proliferation leading to rapid tumor growth (34). Besides, hyperglycemia is associated with mitochondrial malfunction, which leads to insufficient DNA repair and increases the production of reactive oxygen species (ROS) to raise oxidative stress damage (35). Therefore, there are complex prognostic effects in cancer patients due to the complex mechanisms between MetS and cancer.

The impact of MetS on cancer patient prognosis, including BCa, remains controversial. Several studies have illustrated that MetS is negatively associated with the survival outcomes of cancers. For instance, Hu D et al. discovered that the median survival time for MetS patients was significantly shorter than for non-MetS patients in a prospective study of 3012 gastric cancer patients (20). The result of Xu H et al. study also showed that MetS was an independent factor for decreased cancer-specific survival (CSS) in upper tract urothelial carcinoma (UTUC) patients (36). In contrast, Yang Y et al. (37) and Silva A et al. (11) both concluded that MetS was not a prognostic factor for OS or recurrence-free survival (RFS) in patients with colon cancer. Garg T et al. also found that there was no association between MetS and time to recurrence in a large, multi-institutional cohort of older patients with NMIBC (38). Interestingly, our results revealed that MetS was a favorable prognostic factor that was associated with better OS in patients with BCa after RC. Similar results have been seen in other cancer studies. Wen YS et al. also

TABLE 3 | Univariate and multivariate analysis of prognostic factors using the Cox proportional hazards model for OS and PFS in propensity matched patients.

Variables	OS				PFS			
	Univariate analysis		Multivariate analysis		Univariate analysis		Multivariate analysis	
	HR (95% CI)	P value	HR (95% CI)	P value	HR (95% CI)	P value	HR (95% CI)	P value
Age (years)	1.046 (1.020-1.073)	0.001	1.035 (1.006-1.065)	0.019	1.038 (1.013-1.063)	0.002	1.019 (0.993-1.046)	0.148
Gender								
Male	Ref				Ref			
Female	0.904 (0.499-1.636)	0.738			0.958 (0.550-1.670)	0.881		
Metabolic Syndrome								
No	Ref		Ref		Ref			
Yes	0.600 (0.375-0.959)	0.033	0.361 (0.195-0.669)	0.001	0.717 (0.465-1.105)	0.132		
BMI								
<25	Ref		Ref		Ref		Ref	
≥25	0.566 (0.362-0.885)	0.013	1.225 (0.684-2.195)	0.494	0.631 (0.414-0.961)	0.032	0.698 (0.451-1.081)	0.107
Hypertension								
No	Ref				Ref			
Yes	0.791 (0.508-1.231)	0.299			0.917 (0.604-1.393)	0.685		
Hyperglycemia								
No	Ref				Ref			
Yes	1.016 (0.649-1.590)	0.944			1.063 (0.696-1.624)	0.776		
Hypertriglyceridemia								
No	Ref				Ref			
Yes	0.877 (0.554-1.387)	0.574			0.953 (0.619-1.467)	0.827		
Low HDL-C								
No	Ref		Ref		Ref		Ref	
Yes	1.617 (1.035-2.527)	0.035	1.861 (1.150-3.013)	0.011	1.733 (1.137-2.642)	0.011	1.522 (0.985-2.350)	0.058
Current Smoking								
No	Ref				Ref			
Yes	0.983 (0.606-1.594)	0.943	Ref		0.877 (0.549-1.403)	0.585		
Hg (g/L)	0.974 (0.964-0.984)	<0.001	0.978 (0.966-0.990)	<0.001	0.976 (0.967-0.986)	<0.001	0.984 (0.973-0.995)	0.004
pT Stage								
≤T2	Ref		Ref		Ref		Ref	
T3-4	2.938 (1.885-4.579)	<0.001	2.312 (1.432-3.734)	0.001	3.037 (1.990-4.636)	<0.001	2.079 (1.319-3.278)	0.002
pN Status								
Negative	Ref		Ref		Ref		Ref	
Positive	3.263 (1.874-5.683)	<0.001	2.043 (1.138-3.668)	0.017	3.502 (2.089-5.872)	<0.001	2.147 (1.227-3.756)	0.007
Pathologic Grade								
LG	Ref		Ref		Ref			
HG	2.684 (0.842-8.560)	0.095	1.160 (0.343-3.921)	0.811	2.251 (0.819-6.184)	0.116		
Variation								
Absent	Ref				Ref			
Present	0.238 (0.033-1.710)	0.154			0.450 (0.111-1.831)	0.265		
Concomitant CIS								
Absent	Ref				Ref			
Present	0.985 (0.569-1.704)	0.957			1.005 (0.604-1.672)	0.985		
Adjuvant Therapy*								
No	Ref				Ref			
Yes	0.877 (0.422-1.825)	0.726			1.443 (0.765-2.724)	0.257		

BCa, bladder cancer; BMI, body mass index; CI, confidence interval; CIS, carcinoma in situ; HDL-C, high density lipoprotein cholesterol; Hg, hemoglobin; HG, high grade; HR, hazard ratio; IQR, interquartile ranges; LG, low grade; OS, overall survival; PFS, progression-free survival; pN, pathologic node stage; PSM, propensity score match; pT, pathologic tumor stage; Ref, reference.
**Adjuvant radiotherapy and/or adjuvant chemotherapy.*

discovered that MetS was associated with improved survival in patients with resectable esophageal squamous cell carcinoma independently and significantly (39). Furthermore, Liu Z et al. found MetS to be an independent favorable prognostic factor of CSS in patients with localized renal cell carcinoma (RCC) (33). These results could be explained by the fact that patients with MetS were generally accompanied by a better nutrition status, which could reduce the risk of mortality caused by malnutrition. Good nutritional status could improve survival by enhancing immunity and providing high tolerance for long-term treatment (40). In addition, there are studies suggesting that the better survival outcomes of RC patients with MetS in our study might be the result of a beneficial role played by obesity, which is a vital constituent of MetS. Patients with higher BMI might have better nutritional status and a potential survival advantage (41).

Obesity is a major component of MetS and was considered to be associated with worse outcomes in BCa patients treated with RC. Dabi Y et al. showed that obesity increased the risk of recurrence and cancer-specific mortality in patients with NMIBC and MIBC (26). Chromecki TF et al. found that BMI ≥30 kg/m^2

was an independent predictor of cancer recurrence, cancer-specific mortality and OS in patients treated with RC for UC of the bladder (42). However, inconsistent with previous observational studies, Kaplan-Meier analysis and log-rank test in the present study revealed that overweight and obese patients (BMI ≥ 25) showed a significantly more favorable survival outcome (OS: p = 0.011; PFS: p = 0.031) compared with normal weight patients (BMI < 25). Similar results were observed in NMIBC patients in further subgroup analysis. Other studies have reached similar conclusions to support our findings. Kwon T et al. reported that overweight patients who underwent RC had a better prognosis with decreased recurrence and cancer-specific mortality compared with normal BMI values in 714 Korean patients with both NMIBC and MIBC (43). At the same time, the result of univariate analysis in Xu X et al. study also noted that a significantly favorable decreased all-cause mortality in the higher BMI group (≥ 31.2 kg/m2) compared with a low BMI group (< 31.2 kg/m^2) (44). These results suggest that, contrary to the popular viewpoint, obesity might confer a survival benefit in BCa patients treated with RC. However, the specific mechanism of obesity related to a protective function in BCa remains insufficiently clear. The potential protective mechanisms resulting from overweight may be due to the elevated levels of proinflammatory molecules (45) such as adiponectin, cytokines and leptin, which are produced by adipose tissue. Leptin plays an anti-tumor role by promoting the proliferation and activation of natural killer cells (46). In addition, in MIBC patients, lymphocytes exert effect of tumor suppression by combining with adipocytes to contribute to immune regulation, antigen recognition, and elimination of malignant cells. Periprostatic mature adipocytes could also release TGFβ1 upregulated connective tissue growth factor (CTGF) expression in prostate cancer cells favoring migration (47). Therefore, BMI may be a potential reliable predictor of prognosis in RC patients, but further well-controlled clinical research with large sample sizes regarding this topic are still warranted.

Similar to obesity, diabetes mellitus (DM) is also a strong single risk factor for MetS components, and was potentially positively associated with adverse survival outcomes in patients with BCa (48). One retrospective study based on 1,502 patients who underwent RC for MIBC and high-risk NMIBC showed that compared with nondiabetic patients, there a significantly increased risk of disease recurrence, cancer-specific mortality, and any-cause mortality in diabetic patients without metformin therapy (49). Ferro M et al. concluded that type 2 diabetes mellitus (T2DM) was a predictor of an increased risk of recurrence and progression in patients with primary T1HG/G3 NMIBC in a large multi-institutional cohort (50). Hwang EC et al. also reported that DM seems to be an independent predictor of RFS and PFS in NMIBC patients (51). In contrast, our results did not show a significant relationship between DM and the prognosis of RC patients. This inconsistency might be explained by the effect of DM medication (metformin or insulin) on the ultimate survival outcome. Metformin has been discovered to play effective antineolastic effect by inhibiting the mammalian target of AMP-activated protein kinase (AMPK)-dependent and liver kinase B1 (LKB1)-dependent rapamycin (mTOR) pathway (52). Several studies found that the use of metformin seems to be associated with better RFS or CSS in patients with BCa (27, 53). Furthermore, the results from Rieken M et al. also showed that DM patients who used metformin had similar oncological outcomes after RC compared with non-DM patients (49). Therefore, future researches are supposed to consider the drug treatment of DM and further explore the impact of DM on the prognosis of RC patients.

Unlike obesity and DM, the role of hypertension in development and progression of BCa has not been well investigated. No unified conclusion has been reached in existing studies concerning hypertension and the prognosis of BCa. In the study of Stocks T et al. (54), elevated blood pressure increased the incidence and mortality rate of BCa in men, whereas there is no significant association between hypertension and BCa has been found in other studies (48). The results of Anceschi U et al. showed that hypertension was not significantly associated with OS in patients treated with robot assisted radical cystectomy (55), which was consistent with our findings. Abnormal proliferation in vascular smooth muscle cells might be the important link between hypertension and cancer. However, more evidence is needed to clarify the correlation between hypertension and BCa, as well as the underlying mechanism.

In the process of analyzing the impact of dyslipidemia on the outcomes of BCa patients treated with RC, we found that preoperative low HDL- C was independent predictors of worse OS while hypertriglyceridemia was not associated with both in OS and PFS in RC patients, suggesting that low HDL-C might be the primary component contributing to the associations between MetS and adverse prognosis of RC patients. Existing evidence suggests that HDL-C represent cancer cell renewal and epiphenomenon of cancer-related inflammation, which is closely associated with cancer-related mortality and incidence. Low HDL-C might play a vital role in cancer progression by promoting proinflammatory cytokine production, inhibiting antioxidation and inducing apoptosis (56). In addition, the associations between low HDL-C and cancer prognosis in other studies have also drawn meaningful result echoing the above mechanism. The result of Li X et al. study illustrated that breast cancer patients with lower HDL-C levels [≤ 1.02 mmol/L (40 mg/dl)] had worse OS and disease-free survival (DFS) compared with those with higher HDL-C levels (57). Xu H et al. also found the potential connection between low HDL-C and worse OS, CSS and RFS in patients with UTUC (36). Therefore, HDL-C may be a favorable marker for prognostic prediction for RC patients, and further studies are still required to elucidate the role and investigate whether HDL-C targeted therapy would improve the survival outcomes of BCa patients after RC.

There are several limitations of the study that need to be acknowledged. First of all, this study is a single-center retrospective study, which has the inherent shortcoming of limited sample size and inevitable selection bias. Second, this study mainly focused on the Chinese population, which might

result in ethnicity bias and affect the generalization of our results. The role of MetS and its components in BCa patients after RC in other races or ethnicities still remains to be explored. Third, we adopted BMI ≥ 25 kg/m^2 to define obesity instead of the commonly used BMI ≥ 30 kg/m^{2}or waist circumferences considering the particularity of Chinese population, which might lead to misclassification and affected the final results. Last but not least, we did not obtain relevant drug treatment concerning MetS components such as stains or metformin due to the lack of information. This may be an important source of bias, as these drugs might have an impact on survival outcomes.

CONCLUSION

In conclusion, we found that MetS was independently associated with better OS in patients with BCa treated with RC, and HDL-C was the only component of MetS that was independently associated with worse OS. MetS and HDL-C may become reliable prognostic biomarkers of OS in BCa patients after RC to provide individualized prognostication and assist in the formulation of clinical treatment strategies. However, given the inherent limitations of this study, these results need to be further confirmed by adequately designed prospective studies with larger populations to provide a better conclusion.

DATA AVAILABILITY STATEMENT

The raw data supporting the conclusions of this article will be made available by the authors, without undue reservation.

ETHICS STATEMENT

The studies involving human participants were reviewed and approved by the Peking University Third Hospital Medical Science Research Ethics Committee (No. M2018183). The patients/participants provided their written informed consent to participate in this study.

AUTHOR CONTRIBUTIONS

JL designed the research and controlled the structure and quality of the manuscript. ZL collected and analyzed the data and wrote this manuscript. HB, WH, XZ, and JH collected the data and helped in designing the study. ML was responsible for pathology data. All authors contributed to the article and approved the submitted version.

FUNDING

This work was supported by grants from Beijing Natural Science Foundation (Z200027) and the National Natural Science Foundation of China (No.61871004).

SUPPLEMENTARY MATERIAL

The Supplementary Material for this article can be found online at: https://www.frontiersin.org/articles/10.3389/fonc.2022.833305/full#supplementary-material

REFERENCES

1. Siegel RL, Miller KD, Fuchs HE, Jemal A. Cancer Statistics, 2021. *CA Cancer J Clin* (2021) 71(1):7–33. doi: 10.3322/caac.21654
2. Cumberbatch MGK, Jubber I, Black PC, Esperto F, Figueroa JD, Kamat AM, et al. Epidemiology of Bladder Cancer: A Systematic Review and Contemporary Update of Risk Factors in 2018. *Eur Urol* (2018) 74(6):784–95. doi: 10.1016/j.eururo.2018.09.001
3. Alfred Witjes J, Lebret T, Comperat EM, Cowan NC, De Santis M, Bruins HM, et al. Updated 2016 EAU Guidelines on Muscle-Invasive and Metastatic Bladder Cancer. *Eur Urol* (2017) 71(3):462–75. doi: 10.1016/j.eururo.2016.06.020
4. Chang SS, Boorjian SA, Chou R, Clark PE, Daneshmand S, Konety BR, et al. Diagnosis and Treatment of non-Muscle Invasive Bladder Cancer: AUA/SUO Guideline. *J Urol* (2016) 196(4):1021–9. doi: 10.1016/j.juro.2016.06.049
5. Stein JP, Lieskovsky G, Cote R, Groshen S, Feng AC, Boyd S, et al. Radical Cystectomy in the Treatment of Invasive Bladder Cancer: Long-Term Results in 1054 Patients. *J Clin Oncol* (2001) 19(3):666–75. doi: 10.1200/JCO.2001.19.3.666
6. Shariat SF, Karakiewicz PI, Palapattu GS, Lotan Y, Rogers CG, Amiel GE, et al. Outcomes of Radical Cystectomy for Transitional Cell Carcinoma of the Bladder: A Contemporary Series From the Bladder Cancer Research Consortium. *J Urol* (2006) 176(6 Pt 1):2414–22. doi: 10.1016/j.juro.2006.08.004
7. Margulis V, Lotan Y, Montorsi F, Shariat SF. Predicting Survival After Radical Cystectomy for Bladder Cancer. *BJU Int* (2008) 102(1):15–22. doi: 10.1111/j.1464-410X.2008.07594.x
8. Bi H, Yan Y, Wang D, Qin Z, Wang G, Ma L, et al. Predictive Value of Preoperative Lymphocyte-to-Monocyte Ratio on Survival Outcomes in Bladder Cancer Patients After Radical Cystectomy. *J Cancer* (2021) 12(2):305–15. doi: 10.7150/jca.50603
9. Del Giudice F, Leonardo C, Simone G, Pecoraro M, De Berardinis E, Cipollari S, et al. Preoperative Detection of Vesical Imaging-Reporting and Data System (VI-RADS) Score 5 Reliably Identifies Extravesical Extension of Urothelial Carcinoma of the Urinary Bladder and Predicts Significant Delayed Time to Cystectomy: Time to Reconsider the Need for Primary Deep Transurethral Resection of Bladder Tumour in Cases of Locally Advanced Disease? *BJU Int* (2020) 126(5):610–9. doi: 10.1111/bju.15188
10. Xylinas E, Rink M, Robinson BD, Lotan Y, Babjuk M, Brisuda A, et al. Impact of Histological Variants on Oncological Outcomes of Patients With Urothelial Carcinoma of the Bladder Treated With Radical Cystectomy. *Eur J Cancer* (2013) 49(8):1889–97. doi: 10.1016/j.ejca.2013.02.001
11. Silva A, Pereira SS, Monteiro MP, Araújo A, Faria G. Effect of Metabolic Syndrome and Individual Components on Colon Cancer Characteristics and Prognosis. *Front Oncol* (2021) 11:631257. doi: 10.3389/fonc.2021.631257
12. Di Francesco S, Tenaglia RL. Metabolic Syndrome and Aggressive Prostate Cancer at Initial Diagnosis. *Horm Metab Res* (2017) 49(7):507–9. doi: 10.1055/s-0043-109866
13. Zhang Q, Chen P, Tian R, He J, Han Q, Fan L. Metabolic Syndrome is an Independent Risk Factor for Fuhrman Grade and TNM Stage of Renal Clear Cell Carcinoma. *Int J Gen Med* (2022) 15:143–50. doi: 10.2147/IJGM.S346972
14. Mili N, Paschou SA, Goulis DG, Dimopoulos MA, Lambrinoudaki I, Psaltopoulou T. Obesity, Metabolic Syndrome, and Cancer: Pathophysiological and Therapeutic Associations. *Endocrine* (2021) 74(3):478–97. doi: 10.1007/s12020-021-02884-x
15. Eckel RH, Grundy SM, Zimmet PZ. The Metabolic Syndrome. *Lancet* (2005) 365(9468):1415–28. doi: 10.1016/S0140-6736(05)66378-7

16. Bardou M, Barkun AN, Martel M. Obesity and Colorectal Cancer. *Gut* (2013) 62(6):933–47. doi: 10.1136/gutjnl-2013-304701
17. Kocher NJ, Rjepaj C, Robyak H, Lehman E, Raman JD. Hypertension is the Primary Component of Metabolic Syndrome Associated With Pathologic Features of Kidney Cancer. *World J Urol* (2017) 35(1):67–72. doi: 10.1007/s00345-016-1850-2
18. Choi YJ, Lee DH, Han KD, Shin CM, Kim N. Abdominal Obesity, Glucose Intolerance and Decreased High-Density Lipoprotein Cholesterol as Components of the Metabolic Syndrome are Associated With the Development of Colorectal Cancer. *Eur J Epidemiol* (2018) 33(11):1077–85. doi: 10.1007/s10654-018-0440-6
19. Cauchy F, Zalinski S, Dokmak S, Fuks D, Farges O, Castera L, et al. Surgical Treatment of Hepatocellular Carcinoma Associated With the Metabolic Syndrome. *Br J Surg* (2013) 100(1):113–21. doi: 10.1002/bjs.8963
20. Hu D, Peng F, Lin X, Chen G, Zhang H, Liang B, et al. Preoperative Metabolic Syndrome is Predictive of Significant Gastric Cancer Mortality After Gastrectomy: The Fujian Prospective Investigation of Cancer (FIESTA) Study. *EBioMedicine* (2017) 15:73–80. doi: 10.1016/j.ebiom.2016.12.004
21. Kennard K, Buckley ME, Sizer LM, Larson S, Carter WB, Frazier TG, et al. Metabolic Syndrome: Does This Influence Breast Cancer Outcomes in the Triple-Negative Population? *Breast Cancer Res Treat* (2021) 186(1):53–63. doi: 10.1007/s10549-020-06034-1
22. Colicchia M, Morlacco A, Rangel LJ, Carlson RE, Dal Moro F, Karnes RJ. Role of Metabolic Syndrome on Perioperative and Oncological Outcomes at Radical Prostatectomy in a Low-Risk Prostate Cancer Cohort Potentially Eligible for Active Surveillance. *Eur Urol Focus* (2019) 5(3):425–32. doi: 10.1016/j.euf.2017.12.005
23. Giovannone R, Busetto GM, Antonini G, De Cobelli O, Ferro M, Tricarico S, et al. Hyperhomocysteinemia as an Early Predictor of Erectile Dysfunction: International Index of Erectile Function (IIEF) and Penile Doppler Ultrasound Correlation With Plasma Levels of Homocysteine. *Med (Baltimore)* (2015) 94(39):e1556. doi: 10.1097/MD.0000000000001556
24. Häggström C, Stocks T, Rapp K, Bjørge T, Lindkvist B, Concin H, et al. Metabolic Syndrome and Risk of Bladder Cancer: Prospective Cohort Study in the Metabolic Syndrome and Cancer Project (Me-can). *Int J Cancer* (2011) 128(8):1890–8. doi: 10.1002/ijc.25521
25. Cantiello F, Cicione A, Salonia A, Autorino R, De Nunzio C, Briganti A, et al. Association Between Metabolic Syndrome, Obesity, Diabetes Mellitus and Oncological Outcomes of Bladder Cancer: A Systematic Review. *Int J Urol* (2015) 22(1):22–32. doi: 10.1111/iju.12644
26. Dabi Y, Rouscoff Y, Anract J, Delongchamps NB, Sibony M, Saighi D, et al. Impact of Body Mass Index on the Oncological Outcomes of Patients Treated With Radical Cystectomy for Muscle-Invasive Bladder Cancer. *World J Urol* (2017) 35(2):229–35. doi: 10.1111/iju.12644
27. Rieken M, Xylinas E, Kluth L, Crivelli JJ, Chrystal J, Faison T, et al. Association of Diabetes Mellitus and Metformin Use With Oncological Outcomes of Patients With Nonmuscle-Invasive Bladder Cancer. *BJU Int* (2013) 112 (8):1105–12. doi: 10.1111/bju.12448
28. Group Cmadsmss. Chinese Medical Association Diabetes Society Recommendations for Metabolic Syndrome. *Chin J Diabetes* (2004) 12 (3):156–61. doi: 10.3321/j.issn:1006-6187.2004.03.002
29. Extermann M. Metabolic Syndrome, Aging, and Cancer. *Crit Rev Oncog* (2013) 18(6):515–29. doi: 10.1615/critrevoncog.2014010612
30. Ryan AM, Duong M, Healy L, Ryan SA, Parekh N, Reynolds JV, et al. Obesity, Metabolic Syndrome and Esophageal Adenocarcinoma: Epidemiology, Etiology and New Targets. *Cancer Epidemiol* (2011) 35(4):309–19. doi: 10.1016/j.canep.2011.03.001
31. Kaaks R, Lukanova A. Energy Balance and Cancer: The Role of Insulin and Insulin-Like Growth Factor-I. *Proc Nutr Soc* (2001) 60(1):91–106. doi: 10.1079/pns200070
32. Frasca F, Pandini G, Scalia P, Sciacca L, Mineo R, Costantino A, et al. Insulin Receptor Isoform a, a Newly Recognized, High-Affinity Insulin-Like Growth Factor II Receptor in Fetal and Cancer Cells. *Mol Cell Biol* (1999) 19(5):3278–88. doi: 10.1128/MCB.19.5.3278
33. Liu Z, Wang H, Zhang L, Li S, Fan Y, Meng Y, et al. Metabolic Syndrome is Associated With Improved Cancer-Specific Survival in Patients With Localized Clear Cell Renal Cell Carcinoma. *Transl Androl Urol* (2019) 8 (5):507–18. doi: 10.21037/tau.2019.10.04
34. Micucci C, Valli D, Matacchione G, Catalano A. Current Perspectives Between Metabolic Syndrome and Cancer. *Oncotarget* (2016) 7(25):38959–72. doi: 10.18632/oncotarget.8341
35. Federico A, Morgillo F, Tuccillo C, Ciardiello F, Loguercio C. Chronic Inflammation and Oxidative Stress in Human Carcinogenesis. *Int J Cancer* (2007) 121(11):2381–6. doi: 10.1002/ijc.23192
36. Xu H, Tan P, Zheng X, Ai J, Lin T, Jin X, et al. Metabolic Syndrome and Upper Tract Urothelial Carcinoma: A Retrospective Analysis From a Large Chinese Cohort. *Urol Oncol* (2019) 37(4):291.e19–291.e28. doi: 10.1016/j.urolonc.2018.12.005
37. Yang Y, Mauldin PD, Ebeling M, Hulsey TC, Liu B, Thomas MB, et al. Effect of Metabolic Syndrome and its Components on Recurrence and Survival in Colon Cancer Patients. *Cancer* (2013) 119(8):1512–20. doi: 10.1002/cncr.27923
38. Garg T, Young AJ, O'Keeffe-Rosetti M, McMullen CK, Nielsen ME, Murphy TE, et al. Association Between Metabolic Syndrome and Recurrence of Nonmuscle-Invasive Bladder Cancer in Older Adults. *Urol Oncol* (2020) 38 (9):737.e17–737.e23. doi: 10.1016/j.urolonc.2020.04.010
39. Wen YS, Huang C, Zhang X, Qin R, Lin P, Rong T, et al. Impact of Metabolic Syndrome on the Survival of Chinese Patients With Resectable Esophageal Squamous Cell Carcinoma. *Dis Esophagus* (2016) 29(6):607–13. doi: 10.1111/dote.12376
40. Zou L, Liu TR, Yang AK. Metabolic Syndrome is Associated With Better Prognosis in Patients With Tongue Squamous Cell Carcinoma. *Chin J Cancer* (2015) 34(4):184–8. doi: 10.1186/s40880-015-0009-7
41. Choi Y, Park B, Jeong BC, Seo SI, Jeon SS, Choi HY, et al. Body Mass Index and Survival in Patients With Renal Cell Carcinoma: A Clinical-Based Cohort and Meta-Analysis. *Int J Cancer* (2013) 132(3):625–34. doi: 10.1002/ijc.27639
42. Chromecki TF, Cha EK, Fajkovic H, Rink M, Ehdaie B, Svatek RS, et al. Obesity is Associated With Worse Oncological Outcomes in Patients Treated With Radical Cystectomy. *BJU Int* (2013) 111(2):249–55. doi: 10.1111/j.1464-410X.2012.11322.x
43. Kwon T, Jeong IG, You D, Han KS, Hong S, Hong B, et al. Obesity and Prognosis in Muscle-Invasive Bladder Cancer: The Continuing Controversy. *Int J Urol* (2014) 21(11):1106–12. doi: 10.1111/iju.12530
44. Xu X, Zhou L, Miao R, Chen W, Zhou Y, Pang Q, et al. Association of Cancer Mortality With Postdiagnosis Overweight and Obesity Using Body Mass Index. *Oncotarget* (2016) 7(4):5023–9. doi: 10.18632/oncotarget.6517
45. Navarro-Díaz M, Serra A, López D, Granada M, Bayés B, Romero R. Obesity, Inflammation, and Kidney Disease. *Kidney Int Suppl* (2008) 10(111):S15–8. doi: 10.1038/ki.2008.518
46. Hu X, Juneja SC, Maihle NJ, Cleary MP. Leptin—A Growth Factor in Normal and Malignant Breast Cells and for Normal Mammary Gland Development. *J Natl Cancer Inst* (2002) 94(22):1704–11. doi: 10.1093/jnci/94.22.1704
47. La Civita E, Liotti A, Cennamo M, Crocetto F, Ferro M, Liguoro P, et al. Peri-Prostatic Adipocyte-Released Tgfβ Enhances Prostate Cancer Cell Motility by Upregulation of Connective Tissue Growth Factor. *Biomedicines* (2021) 9 (11):1692. doi: 10.3390/biomedicines9111692
48. Peng XF, Meng XY, Wei C, Xing ZH, Huang JB, Fang ZF, et al. The Association Between Metabolic Syndrome and Bladder Cancer Susceptibility and Prognosis: An Updated Comprehensive Evidence Synthesis of 95 Observational Studies Involving 97,795,299 Subjects. *Cancer Manag Res* (2018) 10:6263–74. doi: 10.2147/CMAR.S181178
49. Rieken M, Xylinas E, Kluth L, Crivelli JJ, Chrystal J, Faison T, et al. Effect of Diabetes Mellitus and Metformin Use on Oncologic Outcomes of Patients Treated With Radical Cystectomy for Urothelial Carcinoma. *Urol Oncol* (2014) 32(1):e7–e14. doi: 10.1016/j.urolonc.2013.07.006
50. Ferro M, Katalin MO, Buonerba C, Marian R, Cantiello F, Musi G, et al. Type 2 Diabetes Mellitus Predicts Worse Outcomes in Patients With High-Grade T1 Bladder Cancer Receiving Bacillus Calmette-Guérin After Transurethral Resection of the Bladder Tumor. *Urol Oncol* (2020) 38(5):459–64. doi: 10.1016/j.urolonc.2020.02.016
51. Hwang EC, Kim YJ, Hwang IS, Hwang JE, Jung SI, Kwon DD, et al. Impact of Diabetes Mellitus on Recurrence and Progression in Patients With Nonmuscle Invasive Bladder Carcinoma: A Retrospective Cohort Study. *Int J Urol* (2011) 18(11):769–76. doi: 10.1111/j.1442-2042.2011.02845.x

52. Pernicova I, Korbonits M. Metformin–Mode of Action and Clinical Implications for Diabetes and Cancer. *Nat Rev Endocrinol* (2014) 10 (3):143–56. doi: 10.1038/nrendo.2013.256
53. Nayan M, Bhindi B, Yu JL, Hermanns T, Mohammed A, Hamilton RJ, et al. The Effect of Metformin on Cancer-Specific Survival Outcomes in Diabetic Patients Undergoing Radical Cystectomy for Urothelial Carcinoma of the Bladder. *Urol Oncol* (2015) 33(9):386.e7–13. doi: 10.1016/j.urolonc.2015.05.024
54. Stocks T, van Hemelrijck M, Manjer J, Bjørge T, Ulmer H, Hallmans G, et al. Blood Pressure and Risk of Cancer Incidence and Mortality in the Metabolic Syndrome and Cancer Project. *Hypertension* (2012) 59(4):802–10. doi: 10.1161/HYPERTENSIONAHA
55. Anceschi U, Brassetti A, Tuderti G, Ferriero MC, Costantini M, Bove AM, et al. Impact of Clinical Response to Neoadjuvant Chemotherapy in the Era of Robot Assisted Radical Cystectomy: Results of a Single-Center Experience. *J Clin Med* (2020) 9(9):2736. doi: 10.3390/jcm9092736
56. Pirro M, Ricciuti B, Rader DJ, Catapano AL, Sahebkar A, Banach M. High Density Lipoprotein Cholesterol and Cancer: Marker or Causative? *Prog Lipid Res* (2018) 71:54–69. doi: 10.1016/j.plipres.2018.06.001
57. Li X, Tang H, Wang J, Xie X, Liu P, Kong Y, et al. The Effect of Preoperative Serum Triglycerides and High-Density Lipoprotein-Cholesterol Levels on the Prognosis of Breast Cancer. *Breast* (2017) 32:1–6. doi: 10.1016/j.breast.2016.11.024

Conflict of Interest: The authors declare that the research was conducted in the absence of any commercial or financial relationships that could be construed as a potential conflict of interest.

Publisher's Note: All claims expressed in this article are solely those of the authors and do not necessarily represent those of their affiliated organizations, or those of the publisher, the editors and the reviewers. Any product that may be evaluated in this article, or claim that may be made by its manufacturer, is not guaranteed or endorsed by the publisher.

Advantages of publishing in Frontiers

OPEN ACCESS
Articles are free to read for greatest visibility and readership

FAST PUBLICATION
Around 90 days from submission to decision

HIGH QUALITY PEER-REVIEW
Rigorous, collaborative, and constructive peer-review

TRANSPARENT PEER-REVIEW
Editors and reviewers acknowledged by name on published articles

Frontiers
Avenue du Tribunal-Fédéral 34
1005 Lausanne | Switzerland

Visit us: www.frontiersin.org
Contact us: frontiersin.org/about/contact

REPRODUCIBILITY OF RESEARCH
Support open data and methods to enhance research reproducibility

DIGITAL PUBLISHING
Articles designed for optimal readership across devices

FOLLOW US
@frontiersin

IMPACT METRICS
Advanced article metrics track visibility across digital media

EXTENSIVE PROMOTION
Marketing and promotion of impactful research

LOOP RESEARCH NETWORK
Our network increases your article's readership